PROGRAMA INTERINSTITUCIONAL DE PÓS-GRADUAÇÃO

EM CIÊNCIAS FISIOLÓGICAS - UFSCar/UNESP

MARIANE CRISTINE VICENTE

ALTERAÇÕES NEUROANATÔMICAS E FUNCIONAIS DO SISTEMA RESPIRATÓRIO NO SONO E NA VIGÍLIA EM UM MODELO EXPERIMENTAL PARA DOENÇA DE ALZHEIMER

"Neuroanatomical and functional alterations of the respiratory system during sleep and wakefulness in an experimental model for Alzheimer's disease"

Jaboticabal - 2021

PROGRAMA INTERINSTITUCIONAL DE PÓS-GRADUAÇÃO

EM CIÊNCIAS FISIOLÓGICAS - UFSCar/UNESP

ALTERAÇÕES NEUROANATÔMICAS E FUNCIONAIS DO SISTEMA RESPIRATÓRIO NO SONO E NA VIGÍLIA EM UM MODELO EXPERIMENTAL PARA DOENÇA DE ALZHEIMER

"Neuroanatomical and functional alterations of the respiratory system during sleep and wakefulness in an experimental model for Alzheimer's disease"

Tese de doutorado apresentada ao Programa Interinstitucional de Pós-graduação em Ciências Fisiológicas da Universidade Federal de São Carlos/Universidade Estadual Paulista "Júlio de Mesquita Filho" (UFSCar/UNESP) como parte dos requisitos para obtenção do título de Doutora em Ciências Fisiológicas.

Orientadora: Profa. Dra. Luciane Helena Gargaglioni Batalhão

Jaboticabal - 2021

JOINT GRADUATE PROGRAM IN PHYSIOLOGICAL SCIENCES

PIPGCF - UFSCar/UNESP

ALTERAÇÕES NEUROANATÔMICAS E FUNCIONAIS DO SISTEMA RESPIRATÓRIO NO SONO E NA VIGÍLIA EM UM MODELO EXPERIMENTAL PARA DOENÇA DE ALZHEIMER

"Neuroanatomical and functional alterations of the respiratory system during sleep and wakefulness in an experimental model for Alzheimer's disease"

Thesis submitted to the Joint Graduate Program in Physiological Sciences PIPGCF - UFSCar/UNESP in partial fulfillment of the requirements for the degree of "Doctor in Physiological Sciences".

Supervisor: Dra. Luciane Helena Gargaglioni Batalhão

Jaboticabal - 2021

UNIVERSIDADE FEDERAL DE SÃO CARLOS

Centro de Ciências Biológicas e da Saúde
Programa Interinstitucional de Pós-Graduação em Ciências Fisiológicas

Folha de Aprovação

Defesa de Tese de Doutorado da candidata Mariane Cristine Vicente, realizada em 23/04/2021.

Comissão Julgadora:

Profa. Dra. Luciane Helena Gargaglioni Batalhao (UNESP)

Profa. Dra. Elaine Aparecida Del Bel Belluz Guimaraes (USP)

Prof. Dr. Hélio Zangrossi Junior (USP)

Profa. Dra. Debora Simões de Almeida Colombari (UNESP)

Profa. Dra. Mirela Barros Dias (UNESP)

O presente trabalho foi realizado com apoio da Coordenação de Aperfeiçoamento de Pessoal de Nível Superior - Brasil (CAPES) - Código de Financiamento 001.
O Relatório de Defesa assinado pelos membros da Comissão Julgadora encontra-se arquivado junto ao Programa Interinstitucional de Pós-Graduação em Ciências Fisiológicas.

Dedicatória

Eu dedico este trabalho a minha mãe Suely que do seu pouco fez se o meu tudo.

"Sonhos determinam o que você quer. Ação determina o que você conquista."

Aldo Novak

Início meus agradecimentos ao campo espiritual que compõe toda minha trajetória existencial. Sou grata à vida, a Deus, ao universo por permitirem a realização de um sonho de infância. O almejado título de doutora sempre permeou meus desejos e conduziu minhas escolhas. Sou grata às forças surreais que emergiram de Deus para chegada desse dia. Só as pessoas muito próximas sentiriam o peso emocional, profissional e existencial deste capitulo da minha vida.

Agradeço a minha amada orientadora Profa. Dra. Luciane H. G Batalhão pela oportunidade iniciada em 2010 em compor o time do seu laboratório. Foram 11 anos de trajetória ao seu lado (quase metade da minha vida). Eu agradeço imensamente todo aprendizado acadêmico e pessoal adquirido nessa jornada. Agradeço a vida por ter me proporcionado você como "minha chefe". E, nos momentos mais difíceis, principalmente financeiros em minha vida, o seu olhar de oportunidade e auxilio permitiram a minha permanência no universo acadêmico. Hoje, através de tudo que me ensinara eu realizo um sonho que não só meu, mas também da minha família. Eu praticamente cresci e amadureci fazendo ciência. Eu espero que por ter me inspirado em uma profissional com uma infinidade de qualidade eu possa compor o campo da ciência tendo-a como minha referência. A verbalização em palavras não expressaria a gratidão pela oportunidade, então, eu espero que meu trabalho ao longo desses anos possa expressar meu muito obrigada e admiração.

Agradeço ao time de fisiologia da UNESP de Jaboticabal, liderado pela Profa. Luciane e Profa. Kênia Bícego. Semelhante a minha orientadora, eu tive a oportunidade de trabalhar por 11 anos ao lado da professora Kênia. Muitíssimo obrigada por ser inspiração na minha carreira acadêmica, por auxílios e muitos aprendizados com seu time. Agradeço

imensamente ao técnico Euclides por todo auxilio direto e indireto com meus animais tratando-os como seus “babys” (11 anos do meu rei). A Dona Ângela (minha rainha) e minha paixão Damares. Agradeço aos veterinários que auxiliaram os protocolos experimentais do presente estudo: Virginia, Rafael e Isabela. Imensamente grata pelo conhecimento de vocês proporcionarem a nossa pesquisa qualidade e reprodução garantindo aos animais o melhor tratamento possível.

Agradeço a todos os colegas de laboratório de fisiologia e bancada. Individualmente cada um proporcionou diretamente e indiretamente o resultado dessa pesquisa. Agradeço por tornarem o ambiente cientifico um “lar” e uma família, já que, passamos a maior parte do tempo juntos. Agradeço por toda a ajuda, compreensão pelos meus surtos e apoio nessa jornada. Um agradecimento especial a Júlia de Lima Paneghini por toda contribuição direta na terceira parte da pesquisa que culminou na finalização a tempos de todos os protocolos experimentais. Além disso, por ter me dado à oportunidade de ensinar e orientar nessa etapa final da sua graduação. Foi um aprendizado enriquecedor para minha jornada e vida, obrigada. Agradeço imensamente a Danuzia por todo auxilio direto nos protocolos experimentais que compõem o ultimo capitulo desta pesquisa, não seria possível a execução e analise sem sua ajuda. Obrigada Danuzia, por toda ajuda pessoal e profissional que resultou neste estudo. Agradeço imensamente também, o Luís Gustavo (Lango), pela ajuda direta nos protocolos neuroanatômicos da pesquisa e por toda ajuda pessoal e profissional neste tempo.

Agradeço demasiadamente os professores e nossos colaboradores Camila Almeida e Daniel Carrettiero da Universidade Federal do ABC pelos aprendizados, auxílios, risadas, e momentos de ciência. Agradeço ao time da época dos seus respectivos laboratórios (Giovana, Carol, Ana Regina, Talita, Larissa e Núbia) pelos ensinamentos, acolhimento e

parceria. Foi uma época que carrego com grande amorosidade e inspiração para colaborações.

Agradeço ao Prof. Dr. Tim D. Ostrowski pela colaboração internacional que realizamos com nossos estudos in vitro. Obrigada por toda paciência com inglês e minha cultura. Obrigada pelos aprendizados adquiridos no tempo que trabalhos juntos. Meu agradecimento aos meus amados John, Raella e Jan que tornavam meus dias especiais em Kirksville. Obrigada às pessoas que conheci e contribuíram diretamente na minha vida naquele período e hoje carrego com muita amorosidade, admiração, respeito e muita saudade, Carissa, Ludmila, Daiana, Gean, Helena e Shara.

Agradeço imensamente e de forma muita especial aos amigos que da bancada que se tornaram amigos da vida: Elisa, Lucas, Naiara, Carol e Carlos. O suporte emocional que a amizades de vocês proporcionaram está refletido em todo esse trabalho. Obrigada especial a Elisa e o Lucas por acompanharem minha vida, meus sonhos e me resgatarem de mim mesma inúmeras vezes nesse tempo. Obrigada por serem meus olhos, meu coração e meus sonhos quando não fui capaz de ser. Obrigada por lembrarem do meu potencial todos os dias. Obrigada pela amizade profissional e pessoal. Meu eu te amo refletido em obrigada.

Obrigada aos meus pais Maximiliano e Suely, especial a minha mãe por todo suporte para execução desse trabalho e jornada acadêmica. Foram inúmeras dificuldades nesse caminho acadêmico que por sua ajuda pode ser executado. Um agradecimento especial a minha prima Débora por ser apoio e incentivo desde o início dessa caminhada. Muitas vezes a crença de alguém em nós mesmo é alimento que nos impulsiona a tornar um sonho em realidade. Meu agradecimento por estar ao meu redor e da minha mãe. Agradecimento a minha família pela torcida e por terem contribuído indiretamente e diretamente para este

momento. A vida não teria graça se não pudéssemos compartilhar vitórias. A conquista não é só minha.

Obrigada a todos os animais que compõem os resultados dessa pesquisa. Deixo minha homenagem e profundo respeito. Um dia eu espero que a humanidade seja grata ao reconhecer a importância cientifica resultante de suas vidas.

Agradeço minha psicóloga Zezé e psicanalista Kátia, por atuarem nos bastidores da minha vida que resultam nessa pesquisa e na minha vida.

Agradeço ao programa de pós-graduação em Ciência Fisiológicas (PIPGCF), Capes e FAPESP que proporcionaram a realização dessa pesquisa e de um sonho.

Agradeço a todos que cruzaram minha vida.

Aos outros, dou o direito de ser como são. A mim, dou o dever de ser cada dia melhor.

(Chico Xavier)

APOIO FINANCEIRO

Agradecemos imensamente ao apoio financeiro fornecido pela FAPESP (Processo: 2016/04412-0), CAPES e ao CNPq que permitiram a realização deste projeto de pesquisa com sucesso, e a FAPESP (Processo FAPESP: 2017/21750-9) que permitiu a realização do doutorado sanduíche na universidade de medicina A.T Still University, Kirksville-Missouri, EUA.

FINANCIAL SUPPORT

We greatly appreciate the financial support provided by FAPESP (São Paulo Research Foundation, Process: 2016 / 04412-0), CAPES (Coordination for the Improvement of Higher Education Personnel) and CNPq (National Council for Scientific and Technological Development) that allowed the realization of this successful research project. And FAPESP (Process Fapesp: 2017/21750-9) that allowed the realization of the sandwich doctorate at A.T Still University, Kirksville-Missouri, USA.

SUMÁRIO

SÍNTESE GERAL

CHAPTER 1

CHAPTER 2

Figura 1. Ilustração do controle da respiração em mamíferos.

Figura 2. RAMIREZ; ANDERSON, 2017. **Ilustração da geração do ritmo respiratório em mamíferos por três osciladores**. Em repouso, o complexo preBötzinger (preBötC) e o complexo pós-inspiratório (PiCo) alteram a atividade para gerar um ritmo bifásico, inspiração e pós-inspiração. Em períodos de alta demanda metabólica, por exemplo, durante o exercício, um terceiro oscilador é incorporado para criar um ritmo trifásico. Propõe-se que cada uma das três fases - inspiração, pós-inspiração e expiração ativa - seja controlada por osciladores independentes: o preBötC, PiCo e o núcleo parafacial lateral (pF L), respectivamente.

Figura 3. Células de micróglia com o fenótipo ramificado (esquerda) para o fenótipo ameboide (direita). Figura adaptada de Kim e de Vellis, (2005).

CHAPTER 1

Figure 1. Barnes Maze platform layout (adapted by Sunyer et al., 2007). The holes numbered from +1 to +9 (on the right side of the target hole), from -1 to -9 (on the left side of the target hole) and a hole opposite the target hole.

Figure 2. Photo of the Barnes Maze platform (adapted from Sunyer et al., 2007) with geometrical space cues.

Figure 3. Photo of the body plethysmography experiment in a closed system in which it is possible to observe the animal in the plethysmography chamber.

Figure 4. Effect of icv STZ (2 mg/kg) on spatial learning and memory retention in the Barnes maze test. A) Time to reach the target hole in seconds of the control and STZ groups in the 4 training sessions per day (1st to 4th day). B) Number of attempts to enter into the holes in the platform test pattern in the control and STZ group. Values are expressed as mean ± SEM. * indicates a significant difference between the control and STZ groups.

Figure 5. **The icv injection of STZ (2 mg/kg) increased sensitivity to CO_2 during wakefulness.** Effect of icv STZ (2 mg/kg) on ventilation (V_E), tidal volume (V_T) and respiratory frequency (fR) during hypercapnic exposure (7% CO_2) during wakefulness (A) and NREM sleep (B). Values are expressed as mean ± SEM. ∗ indicates a significant difference between the control and STZ groups.

Figure 6. The icv injection of STZ (2 mg/kg) does not change the respiratory parameters during hypoxia. Effect of icv STZ (2 mg/kg) on ventilation ($\dot{V}_E$), tidal volume (V_T) and respiratory frequency (fR) during hypoxic exposure (10% O_2) during wakefulness (A) and NREM sleep (B). Values are expressed as mean ± SEM.

Figure 7. The icv injection of STZ does not change the temperature of the animals of rats during room air, hypercapnia and hypoxia. Values are expressed as mean ± SEM. # indicates a significant difference from room air and hypercapnia.

Figure 8. T**he icv injection of STZ (2 mg/kg) increased the total awake time under room air and hypercapnic conditions.** Effect of icv STZ (2 mg/kg) on the percentage (%) of time

spent in each state (A), the duration of episodes in seconds (B) and the number of episodes (C) in control and STZ groups during room air, hypercapnia and hypoxia. Values are expressed as mean ± SEM. ∗indicates a significant difference between the control and STZ groups.

Figure 9. The icv injection of STZ injection did not alter the levels of phosphorylation of tau protein. Effect of icv STZ (2 mg/kg) on the phosphorylation levels of tau protein ($Ser^{199/202}$) (A) and the phosphorylation levels of tau protein (Ser^{396}) (B). The graphs represent the mean radius of the phosphorylated tau protein (pTau) relative to total tau protein levels. The values are expressed as percentage values in relation to the control group (100%). Values are expressed as mean ± SEM.

Figure 10. The icv injection of STZ (2 mg/kg) increased the expression of the beta amyloid peptide in the Locus Coeruleus region. Effect of icv STZ (2 mg/kg) on the expression of Aβ protein. The values are expressed as percentage values in relation to the control group (100%). Values are expressed as mean ±SEM. ∗indicates a significant difference between the control and STZ groups.

CHAPTER 2

Table 1. Cell membrane properties during the baseline and 10% CO2 from the control and STZ-AD group.

Table 2. AP properties during our step depolarization protocol.

Figure 1. Representation of the Morris Water Maze (MWM). The pool was divided virtually into 4 quadrants and the yellow circle represents the platform position during the test.

Figure 2. Vibratome (7000smz-2, Campden Instruments, Lafayette, IN) used for brain slice preparation (250-μm thick) containing the LC.

Figure 3. Patch Clamp EPC 10 USB amplifier/AD converter (HEKA Instruments, Holliston, MA) used for electrophysiological recording.

Figure 4. Representation of the phases of the action potential (AP) analyzed in the present study.

Figure 5. Representative IV curves during baseline and 10% CO_2. Note the overall decrease in K+ currents with CO_2. The red lines describe the area for measurements of transient and steady-state currents to each voltage step.

Figure 6. Spatial learning and memory deficits in the sporadic Alzheimer's disease (AD) animal model. A) Escape latency to find the hidden platform (HP) in the Morris water maze for the control (CTL) and streptozotocin-induced Alzheimer's disease (STZ-AD) groups during the 3-day testing period with 15 training sessions per day. Cut off time was 60 seconds. B) Swim velocity as measure for locomotor function shows no impairment in the STZ-AD group. Data are reported as mean ± SEM. # $p \leq 0.05$; 2-way repeated measures ANOVA. n = 6-7 rats per group. VP = visible platform

Figure 7. Unaltered neuronal density in the locus coeruleus (LC) of the streptozotocin-induced Alzheimer's disease (STZ-AD) group. Three representative coronal sections (30 μm) of the LC with labeling of NeuN-identified neurons (red) and tyrosine hydroxylase (TH)

-positive cells (green). Brain schematics illustrate the location and extent of the pontine LC (green area) in relation to bregma. TH+ neurons were counted in a 200 × 200 μm box (yellow box) in the dorsal-most portion of the LC. Data are presented as mean ± SEM. n = 6 rats per group. 4V = 4th ventricle.

Fig 8. Response classes of locus coeruleus (LC) neurons to increased CO_2 exposure. A) Representative horizontal brainstem section (250 μm) illustrating the location of the LC during patch clamp experiments. B) Magnification of a LC neuron with attached glass electrode during the recording. C) Immunohistochemical staining of tyrosine hydroxylase (TH) (blue) in a horizontal brainstem slice subsequent to neuronal recordings in the region of the LC. D) Representative responses of a CO_2-inhibited LC neuron to step depolarization (10 pA steps, 100 ms) at baseline and during the CO_2 condition. Reponses are shown for -20 pA (gray trace) and +70 pA (black trace) only. The stimulus is shown underneath the traces. Note that CO_2 eliminates spontaneous spike activity (before and after the stimulus) and blunts action potential discharge to current injection. E) Response classes of LC neurons to hypercapnia in the control (CTL) group F) Response classes of LC neurons to hypercapnia in the streptozotocin-induced Alzheimer's disease (STZ-AD) group. G) Confocal images (40× oil) of electrophysiologically identified LC neurons that were loaded with Lucifer yellow (LY) (green fluorescence) and stained against tyrosine hydroxylase (TH) (blue). Note the overlap of LY and TH in the merged image, indicating the same LC-specific phenotype for cells that were excited and inhibited by CO_2. All images shown are merged z-stack images from five sections (0.5 μm apart). 4V = 4th ventricle, r = rostral, c = caudal, m = medial, l = lateral.

Figure 9. Spike discharge of locus coeruleus (LC) neurons to current injections at baseline and during increased CO_2. Action potential (AP) number in response to step depolarization during baseline and hypercapnia (10% CO_2) for cells that were inhibited by CO_2 in the control (CTL) group (A) and the streptozotocin-induced Alzheimer's disease (STZ-AD) group (B). Data are expressed as mean ± SEM. ** $p \leq 0.01$ and *** $p \leq 0.001$ indicated a difference between baseline and the hypercapnia condition. ## $p \leq 0.01$ indicated a difference between STZ-AD and CTL groups; 2-way repeated measures ANOVA.

Figure 10. Reduced locus coeruleus (LC) network activity with increased CO_2. A) Typical example for a reduced number of spontaneous postsynaptic currents (sPSC), representing LC network activity, with 10% CO_2. B) Group data for sPSCs at baseline (Bsl) and at 10% CO_2 for the control (CTL) and streptozotocin-induced Alzheimer's disease (STZ-AD) groups. Data are expressed as mean ± SEM. * $p \leq 0.05$; t-test. n = 8-9 rats per group.

Figure 11. Action potential waveform for locus coeruleus (LC) neurons at baseline and increased CO_2. A) Representative action potential (AP) with the corresponding phase plane plot. Phase plane plots for CO_2-inhibited LC cells in the control (CTL) group (B) and the streptozotocin-induced Alzheimer's disease (STZ-AD) group (C). Insets show a representative AP at baseline (Bsl) and increased CO_2. Red arrowheads indicate a significant change in spike threshold. Black arrowheads indicate significant changes to baseline (see Table 2). Data are expressed as mean ± SEM. V_m = membrane potential.

Figure 12. Current-voltage relationship for K^+ channels in locus coeruleus (LC) neurons at baseline and during 10% CO_2. A) Typical example of currents elicited by step changes of the membrane potential from -100 mV to +80 mV (20 mV step, 400 ms) in a

CO_2-inhibited LC neuron at baseline (Bsl) and CO_2. The blue lines describe the time points for measurements of the transient (beginning of stimulus) and steady-state current (end of stimulus) at each voltage step. B) Steady-state K^+ currents of cells inhibited by CO_2 in the control (CTL) and streptozotocin-induced Alzheimer's disease (STZ-AD) groups. C) Transient K^+ currents of cells inhibited by CO_2 in the CTL and STZ-AD groups. Data are expressed as mean ± SEM. * $p \leq 0.05$, ** $p \leq 0.01$, and *** $p \leq 0.001$ indicated a difference from the Bsl condition. # $p \leq 0.05$, ## $p \leq 0.01$ indicated a difference between the STZ-AD and CTL groups; 2-way repeated measures ANOVA. V_m = membrane potential.

CHAPTER 3

Figure 1. **Minocycline improves learning and memory in the STZ-AD model.** A) Minocycline treatment (30 mg/kg, i.p, 5 days) on time to reach the target hole in seconds of the Vehicle (control and STZ) vs Minocycline (control and STZ) groups in the 4 training sessions per day (1st to 4th day). B) The average time per day to find the target hole in seconds of the Vehicle (control and STZ) vs Minocycline (control and STZ) groups. C) Number of attempts to enter into the holes inthe platform test pattern in the control and STZ group. Values are expressed as mean ± SEM. * indicates a significant difference between the Vehicle-STZ vs Minocycline-STZ. + indicates a significant difference in the Vehicle (Vehicle vs STZ) groups. # indicates a significant difference between the Minocycline (Vehicle vs STZ) groups.

Figure 2. Minocycline treatment did not restore CO_2 sensitivity during awake state in the STZ-AD model. Minocycline treatment (30 mg/kg, i.p, 5 days) on (V_E), tidal volume (V_T) and respiratory frequency (fR) during wakefulness (A) and NREM sleep (B) under room air, hypercapnia (7% CO_2)) in vehicle vs STZ-AD groups. Values are expressed as mean ± SEM. + indicate a significant difference in the Vehicle (Vehicle vs STZ). # indicates a significant difference in the Minocycline (Vehicle vs STZ) groups.

Figure 3. **Minocycline treatment does not affect respiratory parameters during hypoxia.** Minocycline treatment (30 mg/kg, i.p, 5 days) on (V_E), tidal volume (V_T) and respiratory frequency (fR) during wakefulness (A) and NREM sleep (B) under room air and hypoxia (10% CO_2) in vehicle vs STZ-AD groups. Values are expressed as mean ± SEM. + indicate a significant difference in the Vehicle (Vehicle vs STZ) groups.

Figure 4. Body temperature (Tb) was not altered by treatment with minocycline. The effect of minocycline treatment (30 mg/kg, i.p, 5 days) on body temperature during room air, hypercapnia and hypoxia in the vehicle and STZ groups. € indicates significant difference between hypoxia and room air.

Figure 5. Minocycline treatment did not decrease the percentage of time spent in the awake state during room air in STZ-AD model. The effect of minocycline treatment (30 mg/kg, i.p, 5 days) on the percentage (%) of time spent in each state during room air (A), hypercapnia (B) and hypoxia (C). The duration of episodes in seconds during rooim air (A_1), hypercapnia (B_1) and hypoxia (C_1). The number of episodes during room air (A2), hypercapnia (B2) and hypoxia (C2) in Vehicle (Vehicle vs STZ) and Minocycline (Vehicle vs STZ) groups. Values are expressed as mean ± SEM. * indicates a significant difference

between the Vehicle-STZ vs Minocycline-STZ. + indicates a significant difference in the Vehicle (Vehicle vs STZ). # indicates a significant difference in the Minocycline (Vehicle vs STZ).

Figure 6. Minocycline treatment did not decrease the increase in beta amyloid peptide expression in the Locus coeruleus region. The effect of minocycline treatment (30 mg/kg, i.p, 5 days) on the expression of Aβ protein in the Locus coeruleus region. The values are expressed as percentage values in relation to the control group (100%). Values are expressed as mean ± SEM. + indicate a significant difference in the Vehicle (Vehicle vs STZ) groups . # indicates a significant difference in the Minocycline (Vehicle vs STZ) groups.

Figure 7. Minocycline treatment decreases the increased cell density and inactivated microglia cells of the Locus coeruleus region in the STZ-AD model. A) The effect of minocycline treatment (30 mg/kg, i.p, 5 days) on microglial cell densities (cells/μm^2); B) distance between microglia cells NND (μm); C) arborization area (μm^2); D) cell body (μm^2) and E) morphological index in Vehicle (Vehicle vs STZ) and Minocycline (Vehicle vs STZ) groups. Values are expressed as mean ± SEM. * indicates a significant difference between the Vehicle-STZ vs Minocycline-STZ. + indicates a significant difference in the Vehicle (Vehicle vs STZ). # indicates a significant difference in the Minocycline (Vehicle vs STZ).

Figure 8. Minocycline treatment inactivated microglia cells of the Locus coeruleus region in the STZ-AD model. A) Schematic representation of the Locus coeruleus (LC; Bregma −9.96; Paxinos and Watson, 2005), where Iba-1 staining was analyzed. Photomicrographs of Iba-1-immunopositive cells, obtained in sections from animals, are represented. B) In each panel, the high-magnification inset illustrates representative the

effect of minocycline treatment (30 mg/kg, i.p, 5 days) on morphology of microglia in animals in the Vehicle (vehicle and STZ-AD) and Minocycline (vehicle and STZ-AD) groups (40x, microscopic). Note that it is possible to observe that the cells of the microglia of the STZ-AD group have a cell body increased and arborization area decreased compared to the control group. After the treatment, it is possible to observe a decrease in the cell body and an increase in arborization area in the STZ-AD model. 4V = four ventricle, LC= locus coeruleus.

ABBREVIATIONS

AD = Alzheimer's Disease

aCSF = artificial cerebrospinal fluid

AP = action potential

$CaCl_2 \cdot 2H_2O$ = Calcium chloride dehydrate

CTL = control

fR = respiratory frequency

HEPES = hydroxyethyl piperazineethanesulfonic acid

HPC = hippocampus

LC = locus coeruleus

K^+ = potassium

KCL = potassium chloride

kDa = kilodaltons

K_{DR} = delayed-rectifying K+ channels

kHz = kilohertz

K_A = A-type K+ channels

K_{ir} = inwardly rectifying K+ channels

K_V = voltage-gated K+ channels

PreBotz/BotzC = pre-Botzinger/Botzinger complex

MHPG = 3-methoxy-4-hydroxyphenylglycol

mΩ = milliohm

$MgSO_4 \cdot 7H_2O$ = Magnesium sulfate heptahydrate

mOsm = miliosmol

ms = miliseconds

mV = millivolts

Na^+ = sodium

NaH_2PO_4 = Monosodium phosphate

$NaHCO_3$ = Sodium bicarbonate

N_2 = nitrogen

NFTs = tau neurofibrillary tangles

NMDG = oxygenated N-Methyl-D-glucamine

NE = noradrenaline

NREM = non-rapid eye movement sleep

PBS-Triton = Phosphate-buffered saline with Triton

pA = picoampere

Ri = input resistance

RMP = resting membrane potential

RTN = retrotrapezoid nucleus

Ser = serine amino acid

sPSC = Spontaneous postsynaptic currents

STZ = streptozotocin

Tb = body temperature

TBS = tris-buffered saline

TBS-T = tris-buffered saline with Tween 20 Detergent

TGF-β = Transforming growth factor beta

TNF-α = Tumor necrosis factor

TH = tyrosine hydroxylase

TP = platform test

THR = threshold

V_T = tidal volume

VE = ventilation

Aβ = beta-amyloid

ABREVIAÇÕES

AMS = atrofia de múltiplos sistemas

AOS = apneia obstrutiva do sono

ASC = apneias do sono central

CpreBöt = complexo pré Botzinger

CO_2 = dióxido de carbono

DA = doença de Alzheimer

DRS = distúrbios respiratórios noturnos

DAE = doença de Alzheimer Esporádica

EEG = eletroencefalograma

EMG = eletromiograma

ICV = intracerebroventricular

IL = interleucina

ip = intraperitoneal injection

LC = locus coeruleus

NF = núcleo fastigial

NTS = núcleo do trato solitário

NTSc = núcleo do trato solitário comissural

O_2 = oxigênio

pFRG/RTN = grupo respiratório parafacial/retrotrapezóide

PA = potencial de ação

PFA = paraformol

PPA = proteína precursora Amiloide

PRM = potencial de repouso de membrana

R_i = resistência de membrana

RB = rafe rostral bulbar

STZ = estreptozotocina

TGF-β = fator de crescimento transformador beta

TNF-α = fator de necrose tumoral

βA = beta amiloide

SÍNTESE GERAL

1 RESUMO GERAL

A disfunção do sistema respiratório é vista em várias doenças neurodegenerativas, entre elas o Alzheimer. Entretanto, as informações sobre como os mecanismos fisiopatológicos da doença estão relacionados ás alterações do sistema respiratório ainda permanecem insuficientemente documentados. Aqui, tratamos animais com estreptozotocina intracerebroventricular (STZ, 2 mg/kg). No capítulo 1, medimos a ventilação (V_E), eletroencefalografia e eletromiografia durante normocapnia, hipercapnia e hipóxia em ratos Wistar. Além disso, realizamos análises de western blot para tau fosforilada, tau total e peptídeo amiloide- (βA) no locus coeruleus (LC), núcleo retrotrapezóide (RTN), rafe medular, complexo pré-B¨otzinger/B¨otzinger e hipocampo, e avaliamos a aquisição de memória e aprendizagem usando o labirinto de Barnes. O modelo STZ-DA aumentou a resposta ventilarória na hipercapnia em 26% durante vigília devido o aumento do volume corrente, mas nenhuma alteração na ˙V_E foi observada no ar ambiente ou em condições de hipóxia. Observamos o aumento de 93% da porcentagem de tempo de vigília durante a normocapnia no modelo STZ. E, associamos os resultados ao aumento de 73% do peptídeo beta amiloide na região do LC.

Afim de, analisarmos a propriedades eletrofisiológicas e a sensibilidade dos neurônios do LC durante a hipercapnia (10% CO_2, pH=7) no modelo STZ-DA, nós realizamos a técnica de patch clamp no capítulo 2. Nós observamos que a maioria (~ 60%) dos neurônios noradrenérgicos do LC em ratos adultos foram inibidos após a exposição ao CO_2, conforme indicado por uma diminuição significativa do potencial de ação (PA). O modelo STZ-DA teve uma maior sensibilidade ao CO_2 de 57% comparado aos controles que foi em parte devido à hiperpolarização do potencial de membrana em repouso -52.2 mV. A

redução do PA em ambos os grupos foi geralmente acompanhada por menor atividade da rede do LC, limiar despolarizado de PA, aumento da repolarização de PA e aumento da corrente através de uma subpopulação de canais de K + dependentes de voltagem (K_V).

Em seguida, no capítulo 3, nós decidimos fazer um tratamento com o fármaco minociclina para revertermos as disfunções cognitivas, respiratórias, do ciclo sono-vigília, e moleculares encontradas anteriormente no capítulo 1 no modelo STZ. Para isso, realizamos as mesmas técnicas do capítulo 1. Adicionalmente os animais foram tratados por cinco dias com minociclina na dose de 30 mg/kg, analisamos as células da micrologia na região do LC por imunohistoquímica para IBA-1 e as citocinas pró-inflamatórias por PCR em tempo Real. O tratamento com minociclina melhorou o aprendizado e a memória, possivelmente devido à diminuição da densidade celular e inativação das células da microglia na região do LC, bem como, diminuição da citocina IL-B. No entanto, o tratamento não reverteu o aumento da sensibilidade ao CO_2 durante a vigília em ar ambiente. Da mesma forma, não observamos diminuição na expressão do peptídeo beta-amilóide na região LC após o tratamento.

Nosso estudo demonstra que a resposta ventilatória ao CO2 está aumentada no modelo de STZ devido às alterações nos neurônios noradrenérgicos do LC que estão com suas propriedades eletrofisiológicas alteradas possivelmente por um aumento na beta-amilóide. As alterações cognitivas e do sono observadas no modelo STZ são decorrentes da alteração na micróglia, uma vez que, o uso de minociclina foi capaz de atenuar.

Palavras chaves: estreptozotocina, ventilação, sono, minociclina, micróglia e Alzheimer.

2 **ABSTRACT**

The dysfunction of the respiratory system is seen in several neurodegenerative diseases such as Alzheimer's, but how the pathophysiology mechanisms of the disease are related to the respiratory system remains poorly documented. Here, we treat animals with intracerebroventricular streptozotocin (STZ, 2 mg / kg). In chapter 1, we measured ventilation (V_E), electroencephalography and electromyography during normocapnia, hypercapnia and hypoxia in Wistar rats. In addition, we performed western blot analyzes for phosphorylated tau, total tau and amyloid- (Aβ) peptide at the locus coeruleus (LC), retrotrapezoid nucleus (RTN), medullary raphe, pre-B¨otzinger / B¨otzinger complex and hippocampus, and we evaluated memory acquisition and learning using Barnes' maze. The STZ-DA model increased the ventilatory response in hypercapnia by 26% during wakefulness due to the increase in tidal volume, but no change in V_E was observed in room air or ihypoxia conditions. We observed an increase of 93% in the percentage of awake-state time during room air in the STZ model. And, we associate the results to the 73% increase in amyloid beta peptide in the LC region.

In order to analyze the electrophysiological properties and sensitivity of LC neurons during hypercapnia (10% CO_2, pH = 7) in the STZ-DA model, we performed the patch clamp technique in chapter 2. We observed that most (~ 60%) of the noradrenergic neurons of the LC in adult rats were inhibited after exposure to CO_2, as indicated by a significant decrease in the action potential (AP). The STZ-DA model had a 57% higher sensitivity to CO_2 compared to controls, which was partly due to the hyperpolarization of the resting membrane potential -52.2 mV. The reduction in AP in both groups was generally accompanied by lower activity of the LC network, depolarized AP threshold, increased AP

repolarization and increased current through a voltage-dependent sub-population of K + channels (KV).

Then, in chapter 3, we decided to take a treatment with the drug minocycline to reverse the cognitive, respiratory, sleep-awake cycle, and molecular disorders found earlier in chapter 1 in the STZ model. For that, we performed the same techniques as in chapter 1. Additionally, the animals were treated for five days with minocycline at a dose of 30 mg / kg, we analyzed the micrology cells in the LC region by immunohistochemistry for IBA-1 and the pro-inflammatory cytokines by real-time PCR. Minocycline treatment improved learning and memory, possibly due to decreased cell density and inactivation of microglia cells in the LC region, as well as decreased IL-B cytokine. However, the treatment did not reverse the increased sensitivity to CO_2 during awake state in room air. Likewise, we did not observe a decrease in the expression of beta-amyloid peptide in the LC region after treatment.

Our study demonstrates that the ventilatory response to CO_2 is increased in the STZ model due to changes in the noradrenergic neurons of the LC, which have their electrophysiological properties altered possibly by an increase in beta-amyloid. The cognitive and sleep changes observed in the STZ model are due to changes in microglia, since the use of minocycline was able to attenuate.

Keywords: streptozotocin, ventilation, sleep, minocycline, microglia and Alzheimer's.

3.1 Respiração e doenças neurodegenerativas

A ventilação é um processo rítmico que mantém o oxigênio (O_2) e dióxido de carbono (CO_2) no sangue arterial e nos tecidos dentro de concentrações adequadas para a sobrevivência. Trata-se de um processo altamente coordenado e complexo, dependente de três componentes: geradores e integradores centrais do ritmo/padrão respiratório, localizados no sistema nervoso central, especificamente no bulbo e na ponte; de sensores que enviam informações para o gerador e integrador central e finalmente uma distribuição motora sincrônica de respostas aos efetores (musculatura das vias áreas superiores, diafragma, abdominais e intercostais) que realizam os ajustes respiratórios necessários (Figura 1). (DEMPSEY; SMITH, 2014a).

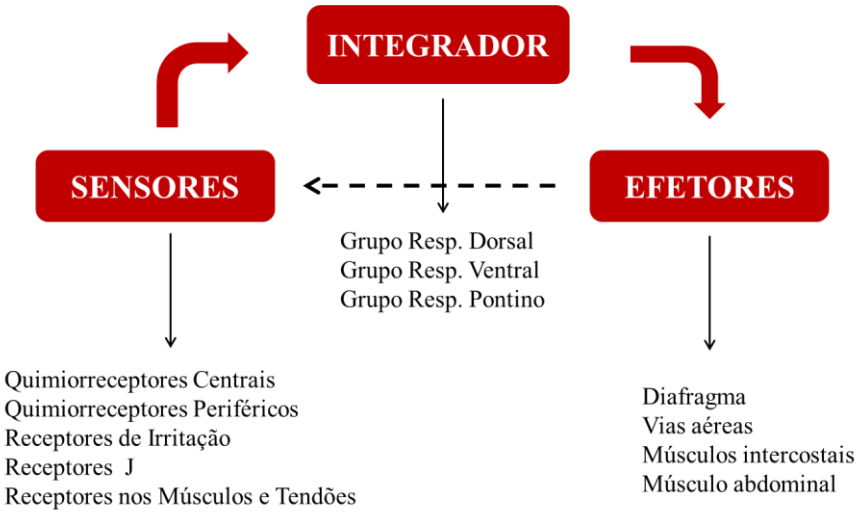

Figura 1. Ilustração do controle da respiração em mamíferos.

O automatismo respiratório se origina nos circuitos respiratórios bulbares e recebe modulação da ponte e regiões supra-pontinas (ALHEID; MCCRIMMON, 2008), sendo que,

a respiração em mamíferos resulta das interações entre três osciladores (FELDMAN; DEL NEGRO; GRAY, 2013; JANCZEWSKI; FELDMAN, 2006; MELLEN et al., 2003; RAMIREZ; ANDERSON, 2017) (Figura 2). Em repouso, a atividade para gerar um ritmo bifásico, inspiração e pós-inspiração é realizada pelo complexo pre-Bötzinger (preBötC). (SMITH et al., 1991; TAN et al., 2008) e o complexo pós-inspiratório (PiCo). (DEL NEGRO; FUNK; FELDMAN, 2018; RAMIREZ; ANDERSON, 2017). Em períodos de alta demanda metabólica, por exemplo, durante o exercício, um terceiro oscilador, o núcleo parafacial lateral (pF_L), uma subpopulação dentro do grupo respiratório parafacial do núcleo retrotrapezóide (RTN / pFRG), é ativada para criar um ritmo trifásico., responsável pela controle da expiração ativa (DEL NEGRO; FUNK; FELDMAN, 2018; RAMIREZ; ANDERSON, 2017).

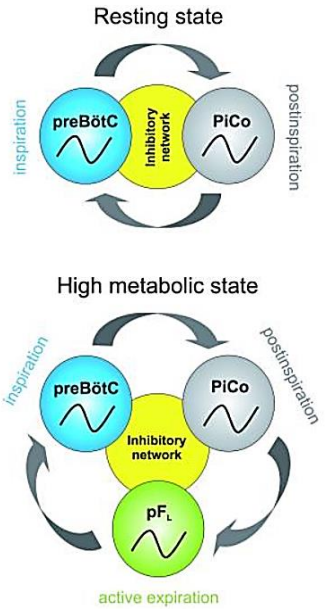

Figura 2. RAMIREZ; ANDERSON, 2017. Ilustração da geração do ritmo respiratório em mamíferos por três osciladores. Em repouso, o complexo preBötzinger (preBötC) e o complexo pós-inspiratório (PiCo) alteram a atividade para gerar um ritmo bifásico, inspiração e pós-inspiração. Em períodos de alta demanda metabólica, por exemplo, durante o exercício, um terceiro oscilador é incorporado para criar um ritmo trifásico. Propõe-se que cada uma das três fases - inspiração, pós-inspiração e expiração ativa - seja controlada por osciladores independentes: o preBötC, PiCo e o núcleo parafacial lateral (pF_L), respectivamente.

A circuitaria neural respiratória é estimulada quando sensores neurais especializados (quimiorreceptores) detectam baixa pressão parcial arterial de oxigênio (PaO_2) e/ou alta pressão parcial arterial de CO_2 ($PaCO_2$), e consequentemente queda no pH. Para detecção destas alterações são ativados quimiorreceptores periféricos e centrais. Os quimiorreceptores periféricos se localizam no corpo carotídeo, localizados no sistema nervoso periférico, próximo à bifurcação da artéria carótida, e no arco aórtico (ORTEGA-SÁENZ et al., 2013) e são sensíveis à alterações da PaO_2, PaO_2 e pH. Em relação aos quimiorreceptores centrais, estes estão espalhados em diferentes áreas do tronco encefálico, incluindo o núcleo do trato solitário (NTS), núcleo fastigial (NF), núcleo retrotrapezóide (RTN) (GUYENET et al., 2009; MULKEY et al., 2004), rafe rostral bulbar (RB), o locus coeruleus (LC) (BALLANTYNE; SCHEID, 2001; COATES; LI; NATTIE, 1993; E.E.; A., 2001; GARGAGLIONI; HARTZLER; PUTNAM, 2010; NATTIE, 1999; NATTIE; LI, 2010) e a região perifornical do hipotálamo lateral (LI; LI; NATTIE, 2013) e detectam alterações do CO_2/pH. Dessa forma, a respiração é regulada por mecanismos neurais envolvendo múltiplos neurotransmissores que promovem ajustes de acordo com a demanda metabólica e outros fatores, como estado de sono ou vigília (NATTIE; LI, 2010, 2012). Falhas nessas conexões, por drogas, por síndromes ou por doenças neurodegenerativas promovem distúrbios respiratórios que podem ocorrer durante o sono (NOGUÉS; RONCORONI; BENARROCH, 2002; SILVESTRELLI; LANARI; DROGHETTI, 2012).

Estudos revelam que os distúrbios respiratórios noturnos (DRS) podem preceder o estágio de demência em doenças neurodegenerativas, portanto, podem contribuir para a patogênese, além de ser uma importante ferramenta para diagnóstico pré-clínico (DEAK;

KIRSCH, 2014; FOLEY et al., 2001; J.R. et al., 2009; JAUSSENT et al., 2012; YAFFE et al., 2011). Recentemente, em um estudo com polissonografia em mulheres cognitivamente normais, os autores encontraram evidências diretas que essas mulheres com DRS estavam mais propensas a desenvolver comprometimento cognitivo leve ou demência (YAFFE et al., 2011). Ao passo que, outros estudos sugerem que a gravidade da demência pode ser positivamente correlacionada com a gravidade dos distúrbios respiratórios. Nesse contexto, as estimativas da prevalência de DRS nas demências são elevadas e mais de 70% dos pacientes diagnosticados com demência (Doença de Alzheimer, Doença de Parkinson, esclerose múltipla, apoplexia, epilepsia ou atrofia de múltiplos sistemas) apresentam problemas respiratórios (BOEVE, 2008; DEAK; KIRSCH, 2014; FLEMING; POLLAK, 2005; GAIG; IRANZO, 2012; SCHWARZACHER; RÜB; DELLER, 2011; YAFFE et al., 2011).

3.2 Doença de Alzheimer e distúrbios respiratórios

A DA descrita pelo neuropatologista alemão Alois Alzheimer em 1907, é uma enfermidade neurodegenerativa mais frequentemente associada à idade, cujas manifestações cognitivas e neuropsiquiátricas resultam em uma deficiência progressiva e uma eventual incapacitação do paciente (HARMAN, 2000; PIERCE; BULLAIN; KAWAS, 2017). À medida que a expectativa de vida torna-se mais elevada, especialmente em países desenvolvidos, tem-se observado um aumento da prevalência da DA (HARMAN, 2006; SMITH, 1999). A DA é causa mais comum de demência, atingindo mais de 20 milhões de pessoas no mundo. No Brasil, estima-se que número de pessoas que desenvolverão Alzheimer até o ano de 2025 seja de 1 milhão e 200 mil casos (OMS, 2019).

Os casos de DA podem ser classificados em dois grupos em função da idade: a DA de acometimento tardio ao redor de 60 anos de idade (99 % dos casos), ocorre de forma esporádica, e a DA de acometimento precoce, de incidência ao redor de 40 anos que mostra recorrência familiar (HARMAN, 2000; KAR et al., 2004). De acordo com os critérios de diagnóstico, a DA pode ser classificada em estágios de gravidade, como estágio leve, moderado e grave (SADOWSKY; GALVIN, 2012). O primeiro aspecto clínico é a deficiência da memória recente, enquanto as lembranças remotas são preservadas até certo estágio da doença (CALABRÒ et al., 2021; REITZ; BRAYNE; MAYEUX, 2011). Além das dificuldades de atenção e fluência verbal, outras funções cognitivas deterioram à medida que a doença evolui, como a orientação geográfica, raciocínio lógico, complicações motoras, o grau de vigília e lucidez (LINDEBOOM; WEINSTEIN, 2004). Acompanhado desses sintomas estão os distúrbios comportamentais, como agressividade, alucinações, hiperatividade, irritabilidade e depressão (CALABRÒ et al., 2021).

As características histopatológicas da DA incluem o acúmulo extracelular das placas senis e de emaranhados neurofibrilares intracelulares, que promovem a diminuição da densidade sináptica, neuroinflamação crônica que eventualmente leva à neurodegeneração generalizada, perda de sinapses e falência de neurotransmissores (MINTER; TAYLOR; CRACK, 2016; QUERFURTH; LAFERLA, 2010). O processamento anormal da proteína precursora Amiloide (PPA), uma proteína transmembranar expressa em tecidos neuronais, promove o acúmulo extracelular do peptídeo beta-amiloide (βA1-42) (HEPPNER; RANSOHOFF; BECHER, 2015; SERRANO-POZO et al., 2011). O peptídeo βA tende a se agregar em oligômeros e protofibrilas que posteriormente se agregam dando origem as fibrilas, as quais compõem as placas senis (HEPPNER; RANSOHOFF; BECHER, 2015;

LASAGNA-REEVES; GLABE; KAYED, 2011; SERRANO-POZO et al., 2011). Enquanto que os emaranhados neurofibrilares surgem do colapso do citoesqueleto neuronal, decorrente da hiperfosforilação da proteína associada à microtúbulo tau (HEPPNER; RANSOHOFF; BECHER, 2015; IQBAL et al., 2010; ŠERÝ et al., 2013).

A neurodegeneração ocorre em múltiplas regiões do encéfalo incluindo hipocampo, córtex, amígdala, neocortex, regiões subcorticais e regiões envolvidas na quimiossensibilidade central e na manutenção do estado de vigília, como o lócus coerules, rafe dorsal e hipotálamo (BEKDASH, 2021; KLUCKEN et al., 2003; MATCHETT et al., 2021; SPIRES; HYMAN, 2004; THEOFILAS et al., 2017). Estudos recentes enfatizam a possibilidade do envolvimento precoce do tronco encefálico na DA área em que se localizam as principais regiões envolvidas no controle da respiração (DEMPSEY; SMITH, 2014b; ESER et al., 2018; SIMIC et al., 2009). Embora muitas pesquisas reportem neurodegeneração no tronco encefálico, o papel dessa região nessa enfermidade não está bem elucidado (SIMIC et al., 2009). Os neurônios que permanecem na DA passam por mudanças morfológicas entre elas: distrofia neurítica, remodelação axônica e alteração na densidade dendrítica (SPIRES; HYMAN, 2004). Segundo(TERRY et al., 1991), essas mudanças alteram as conectividades entre os neurônios sendo responsável por vários sintomas da doença. De fato, além dos sintomas cognitivos clássicos da doença, pacientes com DA apresentam sintomas não cognitivos: como distúrbios do humor, do apetite, depressão, distúrbios do sono de caráter multifatorial (exibindo insônia, distúrbio do ritmo circadiano, agitação noturna), hiperatividade e problemas respiratórios (BOEVE, 2008; DEAK; KIRSCH, 2014; GAIG; IRANZO, 2012; LEE et al., 2019; OSORIO et al., 2014).

A doença DA começa cerca de 20 anos antes que os sintomas cognitivos apareçam e este período de ausência do declínio cognitivo é determinado como DA pré-clínica ou pré-sintomática (MORRIS, 2005; SPERLING; KARLAWISH; JOHNSON, 2013). A pesquisa clínica tem como base biomarcadores específicos para o diagnóstico da DA e/ou condições relacionadas a um estágio inicial (JU et al., 2013; SPERLING; KARLAWISH; JOHNSON, 2013). Apesar da intensa investigação, mecanismos fisiopatológicos subjacentes permanecem insuficientemente documentados para proposital descoberta. Neste cenário, o uso de animais como modelos são válidos e essenciais na investigação relacionada com a DA, pois permitem a apreciação de processos fisiopatológicos iniciais que muitas vezes não são acessíveis em pacientes e/ou em processos tardios que aliviam ou previnem tal condição neurodegenerativa (LAURIJSSENS; AUJARD; RAHMAN, 2013; VAN DAM; DE DEYN, 2011).

Os critérios clínicos atuais para diagnóstico da DA estão focados principalmente nos déficits cognitivos produzidos pela disfunção do hipocampo e de áreas neocorticais, ao passo que os sintomas não cognitivos, como distúrbios do sono ou do sistema respiratório são negligenciados e podem preceder a demência (LEE et al., 2019; LENG et al., 2017; LIGUORI et al., 2017; YAFFE et al., 2011). Estudos relataram que a prevalência da apneia do sono em pacientes com DA é alta, sendo que 70% a 80% dos pacientes apresentam cinco ou mais episódios de apneia por hora de sono, 38% a 48% com 20 ou mais episódios de apneia durante o sono (ANCOLI-ISRAEL; KRIPKE, 1991; DÍAZ-ROMÁN et al., 2021; GEHRMAN et al., 2003). De acordo com GAIG e IRANZO (2012), a apneia obstrutiva do sono (AOS) pode piorar ou causar prejuízo cognitivo na DA. Adicionalmente, parece existir uma forte associação que quanto maior os episódios de AOS maior é a probabilidade de se

desenvolver um transtorno cognitivo ou demência. De fato, LIGUORI et al. (2019) observaram que os pacientes com AOS sem demência, já expressam níveis aumentados do peptídeo βA, um dos principais biomarcadores da DA. Adicionalmente, tem se demonstrado que os tratamentos para distúrbios respiratórios noturnos melhoram o padrão respiratório dos pacientes com DA, e tem um efeito positivo sobre a cognição (BUBU et al., 2019; CHONG et al., 2006; LIGUORI et al., 2021; TSAI et al., 2020). Da mesma maneira, o tratamento por pressão positiva das vias aéreas em pacientes com DA exibem apneias do sono central (ASC), melhora a cognição e a qualidade de vida do paciente (TROUSSIÈRE et al., 2014). Provavelmente este cenário sintomático da área clínica é resultando da disfunção dos núcleos que modulam a respiração.

Diante desse cenário clínico, há poucos relatos na literatura, sobre a disfunção das redes de regulação da respiração, bem como, das respostas ventilatórias na progressão da DA. Portanto, para resultados cientificamente mais robustos, faz-se necessário extrapolar para estudos *in vivo* com uso de animais. Esse tipo de estudo é vantajoso, visto que a partir dos resultados, é possível transcender de forma mais confiável para sistemas fisiológicos humanos. Considerando que a DA esporádica representa mais de 95% dos casos de DA no mundo, acreditamos que modelos de DA esporádica sejam mais impactantes para a literatura científica.

A estreptozotocina (STZ), utilizada na criação do modelo animal deste estudo, é um agente químico derivado da bactéria *Streptomyces acromogenes*, com estrutura química semelhante à da glicose (SZKUDELSKI, 2001). A similaridade da estrutura química de STZ à da glicose permite que seja carreada para o interior das células através de GLUT-2, transportador de glicose já descrito no Sistema Nervoso (LENZEN, 2008; SZKUDELSKI,

2001). Seu uso promove alterações da sinalização de insulina e das enzimas envolvidas no metabolismo da glicose no encéfalo. Desta forma, ocorre redução no metabolismo da glicose e o desenvolvimento de um estado de resistência central à insulina, que pode ser a causa responsável pelo surgimento dos eventos neurodegenerativos da DA, visto que, esse dano ao metabolismo da glicose também é observado em pacientes com a DA (CORREIA et al., 2011; HOYER; LANNERT, 2007; SALKOVIC-PETRISIC et al., 2013). A administração intracerebroventricular (icv) de STZ em animais é capaz de mimetizar as alterações bioquímicas e estruturais encontradas no encéfalo de pacientes com DA, pelo acúmulo do peptídeo βA, aumento da fosforilação da proteína Tau, estresse oxidativo, com subsequente neuroinflamação levando à morte neuronal (GRÜNBLATT; HOYER; RIEDERER, 2004; KNEZOVIC et al., 2015; RAI et al., 2014). Além disso, este modelo também é caracterizado pela deterioração progressiva da função cognitiva (memória e aprendizado), juntamente com mudanças no metabolismo da glicose e energia, traços marcantes em pacientes com DA (DENG et al., 2009; GRÜNBLATT; HOYER; RIEDERER, 2004; LANNERT; HOYER, 1998a, 1998b). Estudos demonstram que 30 dias após a administração intracerebroventricular de STZ, os animais apresentaram déficit cognitivo (memória e aprendizado), aumento da Tau fosforilada e do peptídeo beta amiloide, acompanhado de morte neuronal e aumento do ventrículo (MOTZKO-SOARES et al., 2018; SANTOS et al., 2012). De tal maneira, que a janela de 30 dias após a indução da doença torna-se um modelo para estudos fisiopatológicos da DA neste modelo.

3.3 Neuroinflamação e minociclina na doença de Alzheimer

As micróglias são macrófagos que compreendem 10 a 15% das células do sistema nervoso central (CAI; HUSSAIN; YAN, 2014). Essas células quando ativadas atuam na

inflamação e nos mecanismos homeostáticos por meio da secreção de citocinas e outras moléculas de sinalização (HENEKA et al., 2015; TEJERA; T. HENEKA, 2016). Apesar de um amplo debate, a micróglia é geralmente classificada em, micróglia ameboide fagocitica, ramificada e ativada (CAI; HUSSAIN; YAN, 2014; GLENN; BOOTH; THOMAS, 1991; IMAMOTO, 1981) (Figura 3). As micróglias ramificadas estão envolvidas na manutenção de um ambiente imunologicamente estável por meio de reparos e eliminação de células mortas (BESSIS et al., 2007; MARÍN-TEVA et al., 2004; RANSOHOFF; PERRY, 2009). A micróglia ativada é um estado de transição da micróglia ramificada para um formato ameboide classificada no estado reativo em M1 e M2 dos macrófagos (GORDON; MARTINEZ, 2010; MARTINEZ; HELMING; GORDON, 2009; SICA; MANTOVANI, 2012). A ativação das células tipo M2 promovem ação de reparo e apoptose através da liberação de citocinas anti-inflamatórias, como as interleucinas IL-10, IL-4, IL-13 e o TGF-β (fator de crescimento transformador beta) (CAI; HUSSAIN; YAN, 2014; GOMOLIN et al., 2005; GORDON; MARTINEZ, 2010; MARTINEZ; HELMING; GORDON, 2009; WANG et al., 2015). Em contraste, a micróglia do tipo M1 induz inflamação e neurotoxicidade através da liberação de citocinas e quimiocinas pró-inflamatórias, como TNF-α (fator de necrose tumoral), as interleucinas IL-6, IL-1β, IL-12, bem como, espécies reativas de oxigênio e óxido nitríco (GORDON; MARTINEZ, 2010; MARTINEZ; HELMING; GORDON, 2009; SICA; MANTOVANI, 2012). Todos os mediadores inflamatórios podem atuar como a causa da neurodegeneração da DA (KAUR; SHARMA; DESHMUKH, 2019).

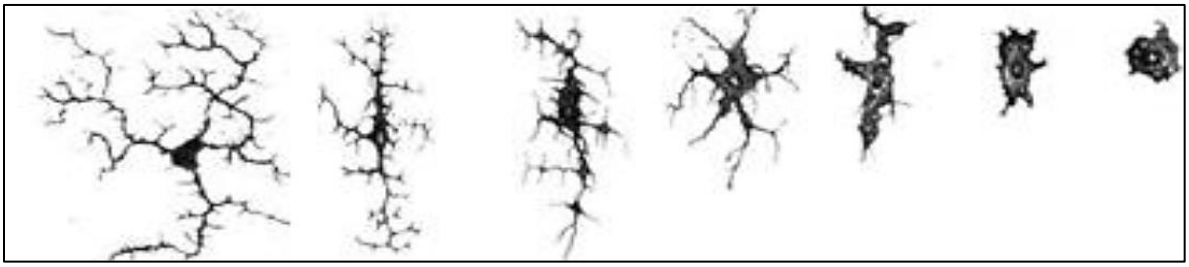

Figura 3. Células de micróglia com o fenótipo ramificado (esquerda) para o fenótipo ameboide (direita). Figura adaptada de Kim e de Vellis, (2005).

A inflamação crônica desempenha um papel importante na cascata de eventos moleculares no encéfalo subjacente à DA (BUDNI et al., 2016; HENEKA et al., 2015; KAUR; SHARMA; DESHMUKH, 2019; MINTER; TAYLOR; CRACK, 2016). Postula-se que a inflamação do SNC na DA é resultado da ativação das células da micróglia M1 em resposta a formação das placas amiloides (ou acúmulo extracelular do peptídeo βA1-42) e/ou da hiperfosforilação da proteína tau promovendo um estado crônico de neuroinflamação que piora e acelera a progressão da doença (HALLIDAY et al., 2000; MINTER; TAYLOR; CRACK, 2016; SCHWAB; MCGEER, 2017; THAMEEM DHEEN; KAUR; LING, 2007). Em circunstâncias normais, as micróglias ativadas exercem um papel neuroprotetor secretando várias citocinas pró-inflamatórias e quimiocinas que recrutam micróglias adicionais e astrócitos para o local inflamatório (GUERRIERO et al., 2017; SARDI et al., 2011; TEJERA; T. HENEKA, 2016). Contudo, na DA, a micróglia e os astrócitos recrutados na inflamação não eliminam o peptídeo βA ou emaranhados de Tau de forma eficaz, o que leva à excessiva produção de citocinas e quimiocinas pró-inflamatórias, que por sua vez, estimulam a proteína PPA na deposição de mais peptídeos βA que novamente ativam mais micróglias, desenvolvendo-se um ciclo vicioso neurotóxico (GUERRIERO et al., 2017; KAUR; SHARMA; DESHMUKH, 2019; MINTER; TAYLOR; CRACK, 2016; SHAMIM;

LASKOWSKI, 2017). Além disso, as citocinas liberadas aumentam a neurodegeneração dos neurônios adjacentes que se somam ao processo inflamatório desencadeando um quadro de deterioração celular (HENEKA et al., 2015; LATTA et al., 2015). Por conseguinte, este ciclo neuroinflamatório deletério permanece vicioso e auto-suficiente desencadeando mais perda neuronal na DA (HENEKA et al., 2015; LATTA et al., 2015; MINTER; TAYLOR; CRACK, 2016). Portanto, a supressão da neuroinflamação na DA por medicamentos com potenciais anti-inflamatórios podem representar um alvo terapêutico na minimização e/ou reversão dos eventos patológicos moleculares que se refletem nos problemas cognitivos e fisiológicos dos pacientes com DA (BISCARO et al., 2012; BUDNI et al., 2016; HENSLEY, 2010; MCGEER; MCGEER, 2013; NIZAMI et al., 2019; SHADFAR et al., 2015).

A minociclina é um derivado de segunda geração da tetraciclina com ação anti-microbiana bacteriostática (GARRIDO-MESA; ZARZUELO; GÁLVEZ, 2013a, 2013b; SHAMIM; LASKOWSKI, 2017). Trata-se de uma molécula altamente lipofílica que atravessa facilmente a barreira hematoencefálica possibilitando sua aplicação no tratamento de doenças que acometem o SNC (KIELIAN et al., 2007; KUANG et al., 2009). Além da sua ação antimicrobiana, estudos demonstram seu potente efeito anti-inflamatório exercido pela sua ação neuroprotetora através da inativação da microglia (GARRIDO-MESA; ZARZUELO; GÁLVEZ, 2013b). As propriedades anti-inflamatórias da minociclina são possivelmente fornecidas através de sua capacidade de inibir a proteína quinase p38 ativada por mitógeno (p38 MAPK) e a metaloproteinase de matriz-9 (MMP-9) (HUNTER et al., 2004; KIM; SUH, 2009; SCHIEVEN, 2009). Dado que, a proteína quinase p38 regula a produção de mediadores inflamatórios, sua inativação pela ação da minociclina pode reduzir citocinas liberadas em excesso fornecendo uma neuroproteção contra danos neuronais da

neuroinflamação (BUDNI et al., 2016; SCHIEVEN, 2005). De fato, em estudos pré-clínicos, a minociclina apresentou atividade neuroprotetora em várias doenças neurodegenerativas, tais como, doença de Parkinson (WU et al., 2002), esclerose lateral amiotrófica (ZHU et al., 2002), doença de Huntington (CHEN et al., 2000) e na DA (CHOI et al., 2007; PARACHIKOVA et al., 2010).

Até o momento, os estudos em modelos de animais e ensaios clínicos indicam que o efeito anti-inflamatório da minociclina resulta na minimização do declínio cognitivo, dos biomarcadores moleculares (beta amiloide e proteína tau) e da neuroinflamação na doença de Alzheimer. Neste contexto, NOBLE et al. (2009) demonstraram que a aplicação de minociclina em culturas de células expostas ao peptídeo βA impediu a ativação de caspases e à indução de morte celular. No mesmo estudo, os autores demonstraram que a administração de minociclina reduziu a fosforilação e agregação da proteína tau em camundongos. De maneira semelhante, (CAI; YAN; WANG, 2013) também observaram o decréscimo da fosforilação da proteína tau em modelo esporádico para DA após o tratamento oral com minociclina. Além disso, o tratamento crônico com minociclina em camundongos PPA (camundongos heterozigotos duplamente transgênicos que expressam o gene mutante da proteína precursora da proteína beta amiloide) reduziu a imunorreatividade da micróglia, com redução dos níveis hipocampais da proteína óxido nítrico sintase iNOS oriunda da inflamação e de citocinas pró-inflamatórias (BISCARO et al., 2012). Nessa linha, CUELLO et al. (2010) observaram que a administração de minociclina em camundongos transgênicos reverteu a deficiência comportamental e diminui também citocinas pro inflamatórias responsáveis pelo quadro crônico de neuroinflamação na DA.

Em relação a disfunção da proteína beta amiloide, FERRETTI et al. (2012) demostraram uma redução do PPA (proteína precursora amiloide), no tecido do hipocampo de camundongos tratados com injeções intraperitoneais de minociclina. Da mesma maneira, o uso de minociclina em ratos 3xTg-AD reduziu a formação de fibrilas da βA no córtex e no hipocampo (PARACHIKOVA et al., 2010), bem como, restaurou a cognição dos animais. Adicionalmente, a diminuição da proteína de βA (βA-42 e βA-40 insolúvel) na região do hipocampo também foi observada no modelo esporádico para DA (CAI; YAN; WANG, 2013). Tomado esse conjunto de informação, a minociclina tornar–se uma abordagem farmacológica promissora para prevenir ou retardar os eventos moleculares patológicos que se refletem nos problemas fisiológicos e cognitivos da doença.

Com base em todas as evidências apresentadas, o tratamento com a minociclina pode ter aplicações diretas nas disfunções moleculares que acometem as regiões envolvidas na respiração e no ciclo sono-vigília, tornando-se um fármaco promissor para reverter ou minimizar as disfunções respiratórias encontradas nos pacientes com DA. Dessa maneira, uma intervenção farmacológica pode minimizar e/ou reverter as disfunções encontradas no presente modelo. Com isso, o presente estudo tem como objetivo avaliar as alterações do sistema respiratório na DA e se essas alterações são dependentes do ciclo sono-vigília, bem como, a administração farmacológica de minociclina visando a melhora do quadro respiratório patológico da DA. O estudo foi realizado em ratos Wistar, induzidos por injeções intracerebroventriculares de estreptozotocina (STZ), modelo experimental da Doença de Alzheimer Esporádica (DAE).

4 **OBJETIVOS GERAIS**

Com base nas evidências apresentadas, o objetivo de nosso estudo foi avaliar:

Capítulo 1

Avaliar as alterações do sistema de controle respiratório e se as alterações são dependentes do ciclo sono-vigília em um modelo esporádico para DA (Publicado: Vicente et al., 2018)

Capítulo 2

Avaliar a excitabilidade dos neurônios LC em um modelo esporádico para DA (Publicado: Vicente et al., 2020).

Capítulo 3

Avaliar o efeito da administração farmacológica de minociclina nas disfunções respiratórias, cognitivas e moleculares de um modelo esporádico para Doença de Alzheimer. (em preparação).

5 MATERIAL E MÉTODOS GERAIS

Os experimentos referentes ao capítulo 1 e 3 foram realizados no Departamento de Morfologia e Fisiologia Animal da Faculdade de Ciências Agrárias e Veterinária da UNESP Campus Jaboticabal e conduzido de acordo com as diretrizes do Colégio Brasileiro de Experimentação Animal (CONCEA) e com a aprovação da Comissão de Ética e Bem-Estar Animal (CEUA) da FCAV/UNESP, protocolo n° 6.030/016. Os experimentos referente ao capítulo 2 (doutorado sanduíche) foram conduzidos de acordo com NIH ("Guide to the Care and Use of Laboratory Animals") e aprovados pelo comitê da universidade A.T. Still University's Animal Care and Usage Committee (protocolo A3058-01).

Capítulo 1

A avaliação das respostas respiratórias no modelo para DA no sono e na vigília foram realizados através da técnica de pletismografia de corpo inteiro e eletroencefalograma (EEG e EMG) em condições de normocapnia, hipercapnia e hipóxia em animais não anestesiados (in vivo). Da mesma maneira, nós utilizamos o eletroencefalograma para análise do tempo total de sono do modelo. As alterações moleculares dos principais biomarcadores da DA (proteína tau e peptídeo beta amiloide) nas regiões respiratórias (Locus Coeruleus, Rafe bulbar, Pré-Botzinger/Botzinger, Núcleo Retratropezóide) e na região do Hipocampo foram quantificados pela técnica de Western Blotting.

Capítulo 2

A avaliação da excitabilidade dos neurônios do LC no modelo para DA foi realizado através da técnica de patch clamp (in vitro), e o fenótipo dos neurônios da região pela técnica de imunohístoquimica.

Capítulo 3

Avaliação da administração do fármaco minociclina foram realizados pelas técnicas mencionadas no capitulo 1. Adicionalmente, avaliamos o efeito da minociclina nas células da microglia na região do LC pela técnica de imunohistoquimica para IBA-I.

6 PRINCIPAIS RESULTADOS ENCONTRADOS

Capítulo 1

Nós demonstramos que após a injeção i.c.v de estreptozotocina (STZ), os animais exibiram déficits de memória e aprendizado mimetizando sintomas clínicos encontrados em pacientes com DA. Nos testes respiratórios, nós demonstramos que o modelo STZ para DA apresenta um aumento na sensibilidade ao quimiorreflexo hipercápnico durante a vigília, bem como, o aumento do tempo no estado de vigília. Esse resultado pode estar associado ao aumento de 73% do peptídeo beta amiloide na região do LC.

Capítulo 2

Nós demonstramos que a maioria (~ 60%) dos neurônios noradrenérgicos do LC em ratos adultos foram inibidos pela exposição ao CO_2, conforme indicado por uma diminuição significativa no potencial de ação (PA). Os neurônios do LC no modelo STZ-DA apresentaram uma maior sensibilidade ao CO_2 que foi em parte devido à hiperpolarização do potencial de membrana em repouso e aumento do limiar para geração do PA.

Capítulo 3

Nós demonstramos que após o tratamento com minociclina o modelo STZ-DA melhorou a aprendizagem e memória e sugerimos que foi em decorrência da inativação das células da micróglia na região do LC. Não observamos alterações no aumento da sensibilidade CO_2, bem como, no aumento na porcentagem de tempo no estado de vigília. Acreditamos que esse resultado seja decorrente da não alteração da porcentagem de expressão do peptídeo beta amiloide na região do LC no modelo STZ-DA após o tratamento.

7 DISCUSSÃO GERAL

No presente estudo, a injeção intracerebroventricular de estreptozotocina na dose 2 mg/kg foi capaz de mimetizar aspectos cognitivos, moleculares e fisiológicos encontrados em pacientes com Alzheimer. Após 30 dias da injeção de STZ, não observamos hiperfosforilação da proteína Tau nos sítios (Ser^{396} e $Ser^{199/202}$) na janela temporal do presente trabalho nas regiões do LC, núcleo retrotrapezóide, rafe bulbar, complexo pré Botzinger/Botzinger e hipocampo. Apesar de não observamos alterações da proteína tau nos locais analisados, o presente estudo demonstrou aumento de 73% do peptídeo beta amiloide na região do LC, mas não no núcleo retrotrapezóide, rafe bulbar, complexo pré Botzinger/ Botzinger e hipocampo. Nesse cenário, alguns estudos revelam que o surgimento dos biomarcadores em pacientes com DA (hiperfosforilação da proteína TAU e placas beta amiloide) são cronológicos e hierárquicos, uma vez que, surgem primeiramente em algumas regiões do tronco encefálico, como o LC, se estendendo para regiões corticais e hipocampais e tardiamente se expressam em outras regiões como o cerebelo (BRAAK et al., 2011; P. et al., 2017; SIMIC et al., 2009; THEOFILAS et al., 2017). Nossos resultados se somam à literatura, em que um modelo STZ-DA, o surgimento histopatológicos dos biomarcadores para DA ocorram de forma hierárquica, cronológica e progressiva semelhante a relatos em pacientes (ALAFUZOFF et al., 2009; CORREIA et al., 2011; EHRENBERG et al., 2017; SALKOVIC-PETRISIC et al., 2013, 2015; WANG et al., 2017). Nossos resultados moleculares são primordiais para afirmarmos que possivelmente estamos trabalhando em uma janela inicial ou em uma transição molecular inicial para intermediaria na DA. Nós sugerimos este fato, em decorrência de observarmos alterações moleculares no LC, primeira região afetada na molecularmente na DA, mas não na região do hipocampo (ANDRÉS-

BENITO et al., 2017; BRAAK; BRAAK, 1991; BRAAK; DEL TREDICI, 2011a; THAL et al., 2002; THEOFILAS et al., 2018).

O modelo STZ apresentou um aumento de 28% na sensibilidade ao CO_2 durante a vigília, o que sugere que os núcleos quimiossensiveis que controlam a vigília estão alterados nessa janela temporal. De fato, nós observamos um aumento da expressão do peptídeo beta amiloide na região do LC, um importante núcleo quimiossensível do sistema nervoso central (BIANCARDI et al., 2008; FILOSA; PUTNAM, 2003; GARGAGLIONI; HARTZLER; PUTNAM, 2010; PUTNAM, 2010; VICENTE et al., 2016a). Além disso, os ratos com STZ permaneceram uma maior porcentagem de tempo no estado de vigília e consequentemente apresentaram uma diminuição dos episódios do sono NREM. O estado de alerta provavelmente é resultado de alterações das regiões reguladoras do ciclo sono-vigília como o córtex cerebral, rafe dorsal, núcleo tegmental dorso-lateral, pedúnculo pontino, área tegmental ventral e o lLC (BERRIDGE, 2008; PEYRON et al., 1998; SZYMUSIAK; MCGINTY, 2008). Uma vez que, o LC é necessário para manter as durações normais da vigília e promover transições sono-vigília é provável que o aumento da vigília no modelo STZ-DA decorra da alteração molecular deste núcleo. Tomado esse conjunto de resultados, nós acreditamos estarmos em uma janela temporal inicial da doença devido às alterações encontradas no LC e das respostas fisiológicas alteradas que observamos. Adicionalmente, não descartamos a possibilidade da participação de outras regiões como córtex, que não foram exploradas no presente estudo. Além disso, sugerimos por estarmos diante de uma janela temporal possivelmente inicial é importante elucidar os mecanismos que estão alterados já que fornecerão pistas para frear e minimizar os sintomas progressivo da doença.

Em virtude dos dados do mencionados acima do capítulo 1, nós decidimos explorar o possível envolvimento dos neurônios do LC no modelo para DA em condições normocápnicas e hipercápnicas (pH=7) *in vitro*. Nós observamos que o número de neurônios noradrenérgicos do LC no modelo para DA não estão alterados em relação ao controle. Sendo assim, possivelmente a resposta que encontramos sejam decorrentes da alteração da atividade dos neurônios no modelo STZ-DA. Além disso, ao expormos os neurônios do LC em condições hipercápnicas, nós observamos que aproximadamente 60% dos neurônios de ambos os grupos diminuíram a taxa de disparo, 20% aumentaram a taxa de disparo e 20% não responderam ao CO_2. Curiosamente, nossos dados se opõem aos estudos *in vitro* que revelaram que mais de 80% dos neurônios de neonatos em condições hipercápnicas aumentam a taxa de disparo (FILOSA; DEAN; PUTNAM, 2002; OYAMADA et al., 1998; RITUCCI; DEAN; PUTNAM, 2005; STUNDEN et al., 2001). Apesar da maioria dos estudos focarem na compreensão das células do LC que despolarizaram sob condições hipercápnicas, outros trabalhos, já relataram que animais com mais de 10 dias (P>10) os disparos dos neurônios do LC diminuíram (GARGAGLIONI; HARTZLER; PUTNAM, 2010; LOPES et al., 2016; NICHOLS et al., 2008). No presente estudo, sugerimos que a inibição das células do LC pelo CO_2 nos animais adultos ocorra em virtude do aumento: da voltagem para limiar do potencial de ação, da repolarização e das correntes de K^+ pelos canais dependentes de voltagem.

A taxa de disparo dos neurônios do LC dos animais STZ-DA foi menor comparados ao controle. Atribuímos esse achado à redução do potencial de repouso de membrana (PRM) e aumento da resistência de membrana (R_i) no modelo STZ-DA. Esta redução possivelmente ocorre por alteração nos canais para potássio retificadores de entrada responsáveis pelo

potencial de membrana. Além disso, a hiperpolarização de PRM em conjunto com o aumento do limiar de disparo do PA promoveu o aumento significativo da diferença de PRM para limiar e, portanto, a voltagem necessária para a geração de PA se torna maior. Sugerimos que essa diferença ocorra por aumento de correntes de K^+ do tipo A^+ o que dificultaria a voltagem para o limiar de disparo do PA. Tomado esse conjunto de informações acreditamos que esses fatores promovam a maior sensibilidade dos neurônios noradrenérgicos do modelo STZ-DA ao CO_2.

Diante dos achados *in vivo* e em *in vitro*, nós hipotetizamos que em condições hipercápnicas, os neurônios do LC inibidos pelo CO_2 poderiam se projetar para núcleos excitatórios da rede respiratória que, por sua vez, promovem aumento da ventilação em condições hipercápnicas. De fato, Lopes et al. (2016) mostraram que os neurônios do LC com projeções aferentes para o porção comissural do núcleo do trato solitário NTSc exibiram taxas de disparo que foram inibidas pela hipercapnia, sugerindo que a inibição dos neurônios do LC pode aumentar a atividade neuronal do NTSc. Desta forma, nós sugerimos que a diminuição acentuada da taxa de disparo dos neurônios do LC no modelo STZ-DA retiraria a inibição de núcleos excitatórios como NTS, que por sua vez, aumentaria a ventilação. Porém, com os dados atuais e os resultados da literatura, não é possível saber exatamente o papel desses neurônios do LC que são inibidos pelo CO_2 no controle ventilatório. Além disso, os animais STZ-AS apresentam células que despolarizaram na porção do LC em que realizamos os registros eletrofisiológicos. Adicionalmente, não podemos excluir que esse agrupamento celular também possa estar modulando o aumento da resposta ventilatória que encontramos em nossos estudos in vivo. Estudos futuros são necessários para esclarecer esta questão.

Seguindo nossos achados sobre os neurônios do LC no modelo STZ-DA, nós hipotetizamos que o aumento da expressão do peptídeo beta amiloide na região do LC pode estar provocando um estado de neuroinflamação. Nossa hipótese é suportada por inúmeros estudos da literatura que relataram que a presença da beta amiloide promove ativação e aglomeração das células da micróglia (BARGER; BASILE, 2001; D.; V.; R., 2019; HENEKA, 2017; WHITEN et al., 2020; YANG et al., 2011). A neuroinflamação juntamente com a beta amiloide provocaria os sintomas cognitivos, respiratórios e do ciclo sono-vigília relatados anteriormente no modelo STZ-DA. Dessa maneira, tratamos nossos animais durante 5 dias com o fármaco minociclina (30 mg/kg, ip).

Nós observamos que o tratamento com a minociclina melhorou a cognição no modelo STZ-DA possivelmente em decorrência da inativação e da diminuição da densidade celular das células da micróglia no modelo após o tratamento. Nossos dados se somam a literatura do efeito benéfico da minociclina na cognição (BISCARO et al., 2012; CAO et al., 2021; CHOI et al., 2007; CUELLO et al., 2010; FERRETTI et al., 2012; GARCEZ et al., 2017; HUNTER et al., 2004; PARACHIKOVA et al., 2010; WANG et al., 2016). Possivelmente, o efeito benéfico encontrado é decorrente da inativação das células da micróglia que provoca a redução de citocinas pro-inflamatórias, radicais livres ou óxido nítrico que causam danos nos neurônios e redução das sinapses (CURRAN; O'CONNOR, 2001; FRAYLING et al., 2007; PICKERING; O'CONNOR, 2007; RUBIO-PEREZ; MORILLAS-RUIZ, 2012; SHIN et al., 2014; TOBINICK, 2009; WEAVER et al., 2002).

O tratamento com o fármaco não alterou o aumento da sensibilidade aumentada ao CO_2 no modelo STZ e o aumento da porcentagem de tempo no estado de vigília. Desta forma, é possível que a microglia ativada não esteja envolvida com a modulação destas

respostas fisiológicas, pelo menos no modelo utilizado. Portanto, acreditamos que essas respostas fisiológicas possivelmente são decorrentes do aumento da expressão do peptídeo beta amiloide na região do LC. Semelhante a outros trabalhos, o tratamento com minociclina em nossos protocolos experimentais não alterou o aumento do peptídeo beta amiloide, mas a reduziu da ativação microglial (BISCARO et al., 2012; GARCIA-ALLOZA et al., 2007; SEABROOK et al., 2006). Em conjunto com os autores, nós sugerimos que o tratamento com o fármaco pode reduzir o acúmulo da proteína beta amiloide depositada pela ativação da excessiva da micróglia, mas não os dímeros, trímeros, oligômeros ou placas amiloides inicialmente existentes. Esses dados, nos orientam a afirmar que o modelo STZ-DA segue uma janela temporal de progressão na neurodegeneração, e que o momento da intervenção farmacológica é crucial para restauração de sintomas encontrado em pacientes acometidos com a DA.

8 **CONCLUSÃO GERAL**

O resultado do nosso estudo permite concluir que a injeção i.c.v de estreptozotocina na dose de (2mg/kg) mimetiza disfunções cognitivas, moleculares e fisiológicas que se enquadram em uma janela inicial/intermediária da doença de Alzheimer. O modelo é promissor para estudos da progressão da doença, pois permite selecionar janelas temporais para elucidar mecanismos moleculares, respostas fisiológicas ou comportamentais encontradas em pacientes com DA. A compreensão de aspectos intrínsecos da primeira região, locus coeuruleus, afetada molecularmente na DA fornecem evidências para posteriores tratamentos que minimizem ou interrompam a progressão da doença. O tratamento com fármaco minociclina é eficaz em melhorar aspectos cognitivos oriundos de um quadro neuroinflamatório da doença, mas não aspectos fisiológicos resultantes do surgimento inicial disfuncional da beta amiloide. Esse estudo nos direciona a intervenções que antecedam as disfunções moleculares que desencadeiam os sintomas subjacentes como a neuroinflamação. E, sintomas como insônia, apneias do sono, sensibilidade ao CO_2 (nunca testada em humanos) podem ser indicativos pré-clínicos para o diagnóstico da doença de Alzheimer.

CHAPTER 1

Hypercapnic and Hypoxic Respiratory Response During Wakefulness and Sleep in a Streptozotocin Model of Alzheimer's Disease in Rats - Journal of Alzheimer's Disease - 2018

9 **ABSTRACT**

Besides the typical cognitive decline, patients with Alzheimer's disease (AD) develop disorders of the respiratory system, such as sleep apnea, shortness of breath, and arrhythmias. These symptoms are aggravated with the progression of the disease. However, the cause and nature of these disturbances are not well understood. Here, we treated animals with intracerebroventricular streptozotocin (STZ, 2 mg/kg), a drug that has been described to cause Alzheimer-like behavioral and histopathological impairments. We measured ventilation (V_E), electroencephalography, and electromyography during normocapnia, hypercapnia, and hypoxia in Wistar rats. In addition, we performed western blot analyses for phosphorylated tau, total tau, and amyloid-(Aβ) peptide in the locus coeruleus (LC), retrotrapezoid nucleus, medullary raphe, pre-B¨otzinger/B¨otzinger complex, and hippocampus, and evaluated memory and learning acquisition using the Barnes maze. STZ treatment promoted memory and learning deficits and increased the percentage of total wakefulness during normocapnia and hypercapnia due to a reduction in the length of episodes of wakefulness. CO_2-drive to breathe during wakefulness was increased by 26% in STZ-treated rats due to an enhanced tidal volume, but no changes in ˙VE were observed in room air or hypoxic conditions. The STZ group also showed a 70% increase of Aβ in the LC and no change in tau protein phosphorylation. In addition, no alteration in body temperature was observed. Our findings suggest that AD animals present an increased sensitivity to CO_2 during wakefulness, enhanced Aβ in the LC, and sleep disruption.

Keywords: breathing, chemosensitivity, dementia, hypoxia, locus coeruleus, streptozotocin

10 **INTRODUCTION**

Alzheimer's disease (AD) is a neurodegenerative disorder, often associated with age, whose cognitive and neuropsychiatric manifestations result in a progressive impairment and eventual disability (HARMAN, 2000). AD is the most common cause of dementia, affecting more than 45 million people worldwide (Wimo et al., 2017). This disease is characterized by the accumulation of amyloid-(Aβ) plaques, intracellular neurofibrillary tangles (NFTs) of hyperphosphorylated tau protein, and decreased synaptic density, which eventually leads to widespread neurodegeneration and loss of neurotransmitters (KUMAR; OKELLO; HARRIS, 2012). The neurodegeneration occurs in multiple areas of the brain, including the hippocampus, cortex, amygdala, neocortex, and brainstem structures (BRAAK; BRAAK, 1991; HOF; MORRISON, 1990; KIELIAN et al., 2007; KLUCKEN et al., 2003; LIU et al., 2013; SIMIC et al., 2009; SPIRES; HYMAN, 2004).

AD is a multifactorial, neurodegenerative, age related disorder with multiple components involved in its progression (NIXON, 2017). Therefore, the establishment of animal models that reproduce human pathology becomes complex. Despite this, the use of animal models has been crucial in defining critical disease related mechanisms and has been at the forefront of evaluating novel therapeutic approaches (LAFERLA; GREEN, 2012). An animal model that replicates many behavioral and histological aspects of AD was created by the intracerebroventricular (icv) injection of streptozotocin (STZ) (GRÜNBLATT; HOYER; RIEDERER, 2004; HOYER; MULLER; PLASCHKE, 1994; SALKOVIC-PETRISIC et al., 2013, 2015). This drug promotes a decrement in brain glucose/energy metabolism (HOYER; MULLER; PLASCHKE, 1994), which is considered an incipient sign of AD (GRÜNBLATT; HOYER; RIEDERER, 2004; HOYER; MULLER; PLASCHKE, 1994;

SALKOVIC-PETRISIC et al., 2013, 2015), and have been used to induce AD-like neurodegeneration in rats, since the metabolic abnormalities found in this model resemble those found in sporadic AD. For instance, these animals display progressive loss of memory and learning, increased brain ventricular volume, abnormalities in mitochondrial function, increased tau phosphorylation and increased Aβ peptide in brain areas (LEE et al., 2014; RAVELLI et al., 2017; YEO et al., 2015). These morphological changes result in damage and loss of neuronal cells (CORREIA et al., 2011). Therefore, the use of the icv STZ model represents a viable experimental approach to explore changes involved in AD-like neurodegeneration in rats.

Aside from severe cognitive deficits, epidemiological studies have reported that up to 45% of patients with AD have sleep disturbances, such as increasing sleep fragmentation, nighttime awakenings, and a greater tendency for daytime sleep (MORAN et al., 2005; PETER-DEREX et al., 2015). These symptoms may occur at early stages of AD, but seem to be correlated with a more severe cognitive decline (MCCURRY et al., 2000; VITIELLO et al., 1990). In addition, it is known that over 70% of institutionalized patients with AD exhibit respiratory changes, and that these problems can contribute to cognitive decline (BOEVE, 2008; DEAK; KIRSCH, 2014; GAIG; IRANZO, 2012; OSORIO et al., 2014; S., 2010; SCHWARZACHER; RÜB; DELLER, 2011). According to GAIG e IRANZO (2012), obstructive sleep apnea may worsen or cause cognitive impairment in AD. Furthermore, there is a strong correlation of the severity of sleep-disordered breathing with the severity of AD (DEAK; KIRSCH, 2014). The late stages of clinica AD are accompanied by shortness of breath (S., 2010). This evidence shows that regions responsible for respiratory control are possibly changed.

There is a paucity of data in the literature on the study of respiratory control in AD progression. In this scenario, the use of animals as models are valid and essential in AD-related research, as they allow the assessment of early or late pathophysiological processes that are not accessible in human patients. Recently, (EBEL; TORKILSEN; OSTROWSKI, 2017) demonstrated that icv STZ induces increased respiration at rest and blunted peripheral chemoreflex responses and a small change in the CO_2-drive to breathe. However, the authors did not evaluate the respiratory pattern and ventilatory responses to hypoxic and hypercapnic stimuli during the different phases of the sleep/wake cycle, which was carried out in the present study. This is a crucial point, since the prevalence of sleep apnea in AD patients is high, with 70% to 80% of patients presenting five or more apnea-hypopnea episodes per hour of sleep, and 38% to 48% of individuals with 20 or more episodes of apnea during the sleep phase (ANCOLI-ISRAEL et al., 2008). Thus, it is quite likely that there is a difference in the chemosensitivity of patients with the AD-dependent phase of the sleep/wake cycle. Therefore, we used the STZ model in order to induce AD-like neurodegeneration in rats to determine the ventilatory response to hypoxia and hypercapnia during wakefulness and non-rapid eye movement (NREM) sleep. In addition, we performed western blot analyses for phosphorylated tau, total tau and amyloid-peptide (A) in locus coeruleus (LC), retrotrapezoid nucleus (RTN), medullary raphe (Raphe), pre-Bötzinger/Bötzinger complex (PreBötz/BötzC) and hippocampus (HPC), and evaluated memory and learning acquisition using the Barnes maze.

11.1 Animals

Male Wistar rats (3-4 months old; weight 300-350 g) were housed in a temperature-controlled chamber maintained at 24–26°C (ALE 9902001; Alesco Ltda., Monte Mor, SP, Brazil) with a 12:12-h light/dark cycle, and had free access to water and food. The experiments were performed between 08.00 a.m. and 17.00 p.m.

The study was conducted in compliance with the guidelines of the National Council for the Control of Animal Experimentation (CONCEA, MCT, Brazil) and with the approval of the Faculty of Agricultural and Veterinary Sciences and Animal Care and Use Committee (CEUA, FACV-UNESP, Jaboticabal campus; Protocol no. n° 6.030/016).

11.2 Surgical Procedures

All surgical procedures were performed under anesthesia with an intraperitoneal injection of 100 mg/kg of ketamine (Union National Pharmaceutical Chemistry S/A, Embu-Guaçu, SP, Brazil) and 10 mg/kg of xylazine (Laboratories Calier S/A Barcelona, Spain). Postoperatively, the animals were treated with antibiotic (enrofloxacin, 10 mg/kg, intramuscular) and analgesic (flunixin meglumine, 2.5 mg/kg, subcutaneous) agents.

11.2.1 Intracerebroventricular injection of streptozotocin

The head was shaved and the skin was sterilized with betadine solution and alcohol. The rats were fixed to a Kopf stereotaxic apparatus (David Kopf Instruments, Tujunga, CA, USA). The scalp was incised over the sagittal suture, the periosteum was excised, and two small bilateral orifices were made using a sterilized dental drill to access both lateral ventricles of the brain, where icv injections were to be applied. The following coordinates

were used: -0.8 mm posterior, ±1.4 mm lateral and -4.4 below bregma (SANTOS et al., 2012). Animals received bilateral icv injections of STZ (2 mg/kg dissolved in 0.05 mol/L citrate buffer, pH 4.5; Sigma, St. Louis, MO) or citrate buffer (2 µL/ventricle) (GRÜNBLATT et al., 2007). For the microinjection of drug and vehicle, a 5µL Hamilton syringe was used, linked to a PE 10 polyethylene tubing, connected to a gengival needle for the application. Thirty days after icv injection, rats were submitted to the behavioral, respiratory or molecular tests. The respiratory tests were performed in a different group of animals, whereas the behavioral and molecular tests were performed in the same group.

11.2.2 Electroencephalogram (EEG) and electromyogram (EMG) electrodes

Seven days before the beginning of the respiratory tests, EEG and EMG electrodes were implanted in the group that would undergo the respiratory tests. Three EEG electrodes were introduced: the frontal electrode, located 2 mm anterior to bregma and 2 mm lateral to the midline; the parietal electrode, positioned 4 mm anterior to the lambda and 2 mm lateral to the midline; and the electrode "ground" which was inserted between the frontal and parietal electrodes. For electromyogram (EMG) recordings, a pair of electrodes were inserted deep into the neck musculature of the rats. These electrodes allowed us to analyze ventilation in the different phases of the sleep/wake cycle.

11.2.3 Body temperature

On the same day as the EEG and EMG surgery, the rats underwent a second surgery for the implantation of a temperature datalogger (SubCue Dataloggers, Calgary, Canada) into the abdominal cavity through a midline laparotomy. The datalogger was programmed to acquire body temperature (Tb) data every 7 minutes.

11.3 Behavioral Analysis

11.3.1 Barnes maze

The Barnes maze test was used to assess spatial memory and learning to confirm the success and reliability of the model.

The Barnes maze test consists of a non-aquatic test for memory and spatial learning (SHARMA; RAKOCZY; BROWN-BORG, 2010; SUNYER et al., 2007). The protocol was adapted from (SUNYER et al., 2007). The maze was made from a circular, 13-mm thick, white PVC platform (110-cm diameter), which was maintained in the same position throughout the experiment. Twenty holes (10 cm in diameter, 7.5 cm between each hole) were made on the perimeter and the platform was mounted on top of a metal support, 105 cm above the ground. The maze was divided into target hole (T), opposite hole (OP), 9 holes clockwise (1 to 9, counting from T) and 9 holes counterclockwise (-1 to -9, counting from T) (Fig 1). The escape cage, below the T hole, had walls covered with black plastic to make the inside dark and attractive to the rats. The platform was also illuminated with a fluorescent white light and visual cues (colored geometric figures) were placed around the labyrinth as points of spatial reference for the animal to escape from the open platform to the "target hole" (Fig 2). These clues were not removed throughout the experiment. After testing each rat, as explained below, the whole maze was cleaned using 10% ethanol to avoid olfactory cues and the platform was rotated to avoid intra-maze odor or visual cues. All sessions were recorded by a video camera for further analysis. Prior to testing (probe day), training sessions

were performed over 5 days to familiarize the animals with the maze and to allow them learn the location of the escape zone.

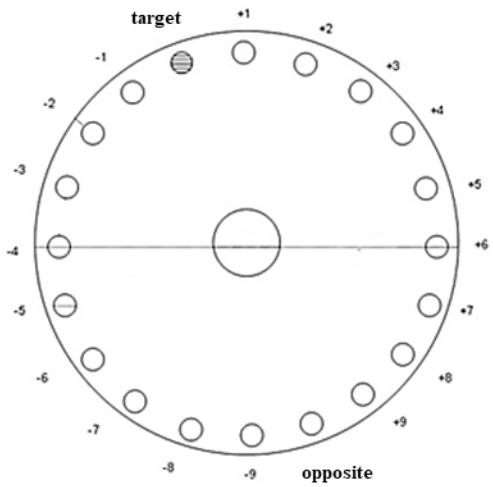

Figure 1. Barnes Maze platform layout (adapted by Sunyer et al., 2007). The holes numbered from +1 to +9 (on the right side of the target hole), from -1 to -9 (on the left side of the target hole) and a hole opposite the target hole.

Figure 2. Photo of the Barnes Maze platform (adapted from Sunyer et al., 2007) with geometrical space cues.

11.3.2 Acquisition phase

In this stage, spatial learning was evaluated through latency to enter the target hole. From days 1 to 4, each animal was placed in a square start chamber in the center of the maze. After 10 seconds, the chamber was removed and the animal was allowed to explore the maze for 3 minutes. The end of the trial was considered when the animal entered the target hole. Therefore, the animal was allowed to stay inside the dark cage for 1 minute and, after this period, was returned to its home cage. If the animal had not entered in the target hole after 3 minutes from the beginning of the test, it was gently coerced to the target hole. These steps were repeated for 4 trials per day with an intertrial interval of 15 minutes over 4 consecutive days.

11.3.3 Probe trial

On day 5, 24 hours after the last training day, the escape cage was removed, while the maze was maintained in the same position as training days. The animal was placed in the start chamber in the center of the maze and, after 10 seconds, it was removed and the animal was allowed to explore the maze for 90 seconds. The probe trial was performed in order to determine whether the animals remembered the location of the target hole. The number of times the animal searched for the "target hole" was used as a memory consolidation index (ADAMS et al., 2002; CHAWLA et al., 2017; DICKSON, 2011; SUNYER et al., 2007).

11.4 Respiration Test

11.4.1 Determination of pulmonary ventilation

We used the whole-body plethysmography method to measure of pulmonary ventilation ($\dot{V}_E$) (BARTLETT; TENNEY, 1970; DRORBAUGH; FENN, 1955), as is

commonly used in our laboratory (BIANCARDI et al., 2008; DE CARVALHO et al., 2014; VICENTE et al., 2016b). Freely-moving rats were kept in a 5-L chamber ventilated with room air or a hypercapnic gas mixture containing 7% CO_2 (White Martins, Sertãozinho, Brazil) or a hypoxia gas mixture containing 10% O_2 (White Martins, Sertãozinho, Brazil) in low ambient noise conditions (Fig 3). The flow rate of the inflow gas into the animal chamber was monitored by a flowmeter (model 822-13-OV1- PV2-V4, Sierra Instruments, Monterey, CA). During measurements, the flow was interrupted, and the chamber was sealed for short periods of time (approximately 2 min); the pressure oscillations due to respiration were monitored by a differential pressure transducer (TSD 160A, Biopac Systems, Santa Barbara, CA). The signals were fed into a differential pressure transducer (DA 100C, Biopac Systems), passed through an analog-to-digital converter, and digitized on a microcomputer equipped with data acquisition software (MP100A-CE, Biopac Systems). The sampling frequency was 1 kHz. The results were analyzed using the data analysis software Acqknowledge (v. 4.2.3 data acquisition system, Biopac Systems). Tidal volume (V_T) and respiratory frequency (fR) were calculated to estimate ventilation per breath.

V_T was calculated by using an appropriate formula [37]:

$$V_T = V_K \times (P_T / P_K) \times Tb \times (P_B - P_C) / Tb \times (P_B - P_C) - T_A \times (P_B - P_R)$$

where P_T is the pressure deflection associated with each V_T, P_K is the pressure deflection associated with the injection of the calibration volume (V_K), T_A is the air temperature in the animal chamber, P_B is the barometric pressure, P_C is the water vapor pressure in the animal chamber, Tb is the body temperature, and P_R is the vapor pressure of water at Tb. The $\dot{V}_E$ was calculated as the product of the f_R and the V_T. $\dot{V}_E$ and V_T are

presented under conditions of ambient barometric pressure, at Tb and saturated with water vapor (BTPS).

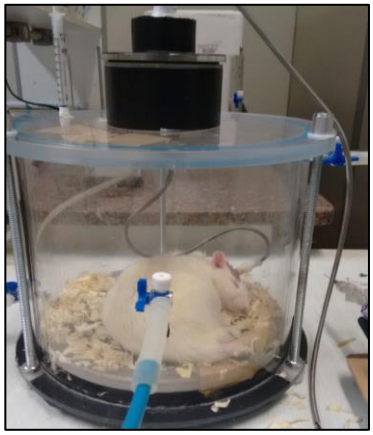

Figure 3. Photo of the body plethysmography experiment in a closed system in which it is possible to observe the animal in the plethysmographic chamber.

Tb was monitored by temperature datalogger (SubCue Dataloggers, Calgary, Canada) and the air temperature in the animal chamber was constantly monitored using a thermoprobe (model 8502-10, Cole Parmer, Chicago, IL, USA). The animal chamber was considered saturated because of a water lane in the bottom separated from the animal by a grid, and so the Pc was calculated indirectly using an appropriate table (BERNARDS, 1976). The calibration for volume was obtained during each experiment by injecting the animal chamber with 1 mL of room air.

11.5 EEG and EMG Signals

Similar to other previous studies, the arousal state was determined by analyzing the EEG and EMG records (E.E.; A., 2001; NATTIE; LI, 2002; VICENTE et al., 2016b). The signals from the EEG and EMG electrodes were sampled at 1 kHz, filtered at 0.3–50 and 0.1–100 Hz, respectively, and recorded on a computer. Both wakefulness and NREM sleep

states were observed consistently through the experiments, but periods of rapid eye movement (REM) sleep were short and were not present in every experiment; thus, REM sleep phases were excluded from the analysis (VICENTE et al., 2016b).

11.6 Experimental Protocol

Seven days after implantation of EEG and EMG electrodes, the animals were placed in a plethysmographic chamber and ventilation was continuously measured. The chamber was initially ventilated with moist atmospheric air (21% O_2) for an acclimation phase of at least 30 minutes. Ventilation control measures were then performed. Ventilation measurements were first made during normocapnia for 63 minutes. The animals were then submitted to hypercapnia for 63 minutes, where the chamber was ventilated with a gas mixture containing 7% CO_2, 21% O_2 and balanced with N_2 (White Martins Gases Industriais Ltda, Osasco, SP). After hypercapnia, the chamber was ventilated with atmospheric air again for recovery of baseline ventilation for 60 minutes. The animals were then submitted to hypoxia for 63 minutes, where the chamber was ventilated with a gas mixture containing 10% O_2 and equilibrated with N_2 (White Martins Gases Industriais Ltda, Osasco, SP). The order of exposure to hypercapnia and hypoxia was reversed randomly. The ventilatory measures were analyzed at 7, 14, 21, 28, 35, 42, 49, 56 and 63 minutes after gas exposure. Then, based on the sleep/wake cycle, for the $\dot{V}_E$ measurements, we selected the phases when the animals were either in wakefulness or in sleep.

11.7 Neurochemical Analysis

11.7.1 Brain area dissection

After each battery of behavioral tests, four rats were randomly selected out of each group and the animals' brains were removed quickly, frozen in liquid nitrogen and held at -80°C until dissection. In a cryostat at -22°C, the brains were coronary-sectioned to find target areas according to stereotaxic coordinates of the Atlas de Paxinos and Watson (PAXINOS; WATSON, 2007) as follow: locus coeruleus (LC - distance from bregma: -10.3 mm to -9.3 mm), retrotrapezoid nucleus (RTN, -11.3 mm to -10.3 mm), medullary raphe (-11.6 mm to -10.3 mm); pre-Bötzinger and Bötzinger complex (PreBötz/BötzC, -12.3 mm to -11.8 mm) and hippocampus (HPC, -4.16 mm to -3.16 mm). Samples of 0.7-mm thickness were removed with a 15-gauge needle.

11.7.2 Immunoblotting

Phosphorylated tau protein levels ($Ser^{199/202}$ and Ser^{396}) and β-amyloid peptide (Aβ) in LC, RTN, Raphe, PreBötzC/BötzC and HPC were evaluated.

After this procedure, a maceration of the tissue of each corresponding region was performed. This tissue sample was submitted to sonication to promote membrane lysis and eventual release of the intracellular material. The solution containing the lysed cells was collected and transferred to an Eppendorf tube. Then, the quantification of these proteins was performed by the Biochrom UV/Vis spectrophotometer, Biodrop Duo model, UV optical path.

Before running the gel, the samples were denatured at 100°C for 3 minutes and applied to a polyacrylamide gel (12%) for fractionation. As a control, 8 μL of a molecular

weight marker was applied to one well. The samples were applied to the gel, placed in a vial with running buffer and separated by applying 100 V for 2 hours. After the run, proteins were transferred to a nitrocellulose membrane (Bio-Rad) using ice-cold transfer buffer for 1 hour at 100 V. The membrane was then incubated with non-specific site blocking solution (5% milk in TBS-T) for 1 hour at room temperature. After this blocking, the membranes were cut and incubated with the respective primary antibodies, Anti-phospho-Tau (rabbit monoclonal $pSer^{199/202}$, cat. T6819, Sigma,-Aldrich, 1:1000 dilution and rabbit monoclonal $pSer^{396}$, cat. EPR2731-Ab109390, Abcam, 1:1000 dilution), anti-beta-actin (mouse monoclonal beta-actin antibody AC-15, cat. NB600-501, Novus Biological, 1:1000 dilution), anti-beta amyloid (mouse monoclonal B-amyloid B-4, cat. sc-28365, Santa Cruz Biotechnology, 1:500 dilution), and anti-Tau Total (rabbit polyclonal human tau, Ab-356, cat. GWB-ASC840, GenWay, 1:1000 dilution), diluted in the same blocking solution for 24 hours at 4°C under constant stirring. The beta-actin antibody was used to normalize the specific labeling values. After washing, the corresponding secondary (anti-mouse IgG and anti-rabbit, 1:1000 dilution, Jackson ImmunoResearch) antibodies were incubated for 2 hours at room temperature. The membranes were then washed twice with TBS-T and once with TBS for 10 minutes each, and the reaction was carried out by incubation with a chemiluminescent reagent for 1 minute. The membranes were immediately exposed to chemiluminescence-sensitive film for 30 seconds to 5 minutes, as instructed by the manufacturer.

The films were quantified through optical densitometry using a computerized image analysis system (NIH System, ImageJ developed at the US National Institute of Health, available at the website: http://www.rsb.info.nih.gov/nihimage/(ImageJ).

11.8 Statistical Analyses

Results were expressed as mean ± SEM. The Barnes maze results in the acquisition phase were evaluated by two-way ANOVA, followed by the Holm-Sidak post-test. The Barnes maze, on the day of the test, was evaluated by the two-way ANOVA. The results of ventilation, sleep/wake cycle and body temperature in normocapnic, hypercapnic and hypoxic conditions were evaluated by two-way ANOVA, followed by Bonferroni post-test. The quantification of phosphorylation of tau protein, total tau and Aβ were validated through the t-test (Student) for independent samples. The significance level adopted for all results was $p < 0.05$.

12.1 Behavioral Analysis for Model Validation

12.1.1 Barnes maze - acquisition phase

Figure 4A represents the latency value (s) to find the escape box in the target hole in training 4 for 4 days (acquisition phase). We observed that the control group decreased the latency (s) to escape through the target hole as a function of training (day 1: T1 134.3 ± 54.2 vs day 4: T4 29.0 ± 35.1 s, $p < 0.05$; two-way ANOVA). However, the STZ group required more time to find the escape hole compared to the control group on days 1, 2 and 3 ($p < 0.05$; two-way ANOVA). No difference between treatments was observed on the fourth day. On the same day, the STZ group decreased latency, thus improving performance on the platform to find the escape box (day 1: T1 165.8 ± 38.9 vs day 4: T4 39.8 ± 62.4 s, $p < 0.05$; two-way ANOVA).

12.1.2 Barnes maze - proof test

Figure 4B shows the number of attempts to enter the holes in the platform test pattern (TP). In the Barnes maze test, the STZ-treated group had a lower number of hits in the "target hole" compared to the control group (control: 4.5 ± 1.8 vs STZ: 2.0 ± 2.2, respectively, $p = 0.035$; two-way ANOVA). There was no significant difference between treatments in the other holes of the platform ($p > 0.05$; two-way ANOVA).

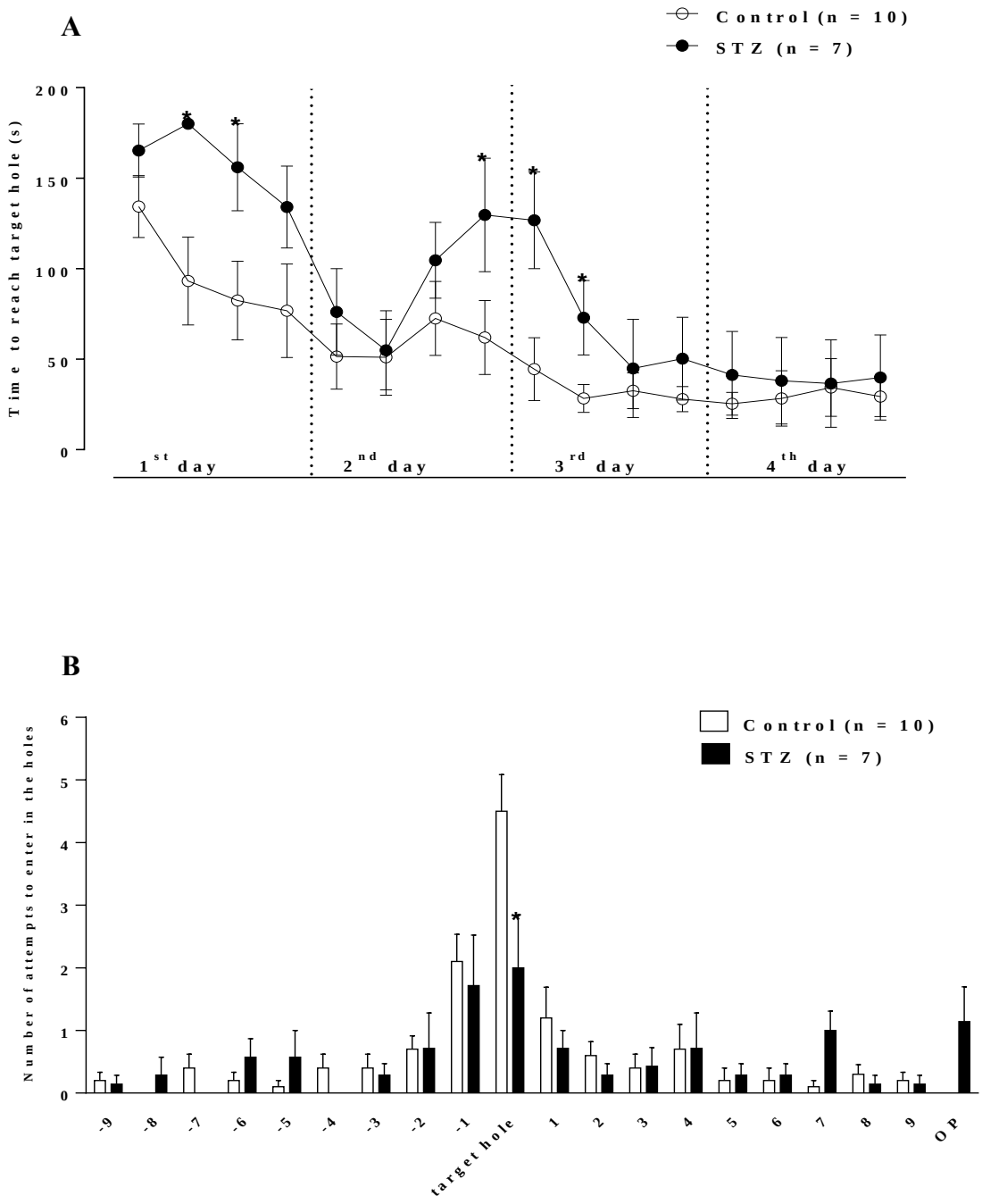

Figure 4. **Effect of icv STZ (2 mg/kg) on spatial learning and memory retention in the Barnes maze test**. A) Time to reach the target hole in seconds of the control and STZ groups in the 4 training sessions per day (1st to 4th day). B) Number of attempts to enter into the holes in the platform test pattern in the control and STZ group. Values are expressed as mean ± SEM. * indicates a significant difference between the control and STZ groups.

12.2 Respiration Test

During all experimental protocols, the mean chamber temperature was 25.7 ± 0.3°C, and the mean room temperature was 24.6 ± 0.2°C.

12.2.1 Respiration during wakefulness

We observed no difference in respiratory variables in room air conditions in the STZ-treated group compared to the control group during wakefulness (Fig. 5A and 6A). In hypercapnia and hypoxia, all groups showed a significant increase in ventilation when compared to room air conditions ($p < 0.0001$; two-way ANOVA) (Fig. 2A and 3A).

During hypercapnia (Fig. 5A), the increase in $\dot{V}_E$ of the STZ-treated animals was 26% higher compared to the control group (control: 1823.9 ± 457.5 vs STZ: 2481.3 ± 514.2 $mL.Kg^{-1}.min^{-1}$, $p < 0.05$; two-way ANOVA) due to a higher V_T (vehicle: 13.7 ± 2.9 vs STZ: 17.1 ± 2.7 $mL.Kg^{-1}$, $p < 0.05$; two-way ANOVA).

Hypoxia caused a similar increase in $\dot{V}_E$ in all groups due to an increase in fR (Fig. 6A). No difference was observed between treatments.

12.2.2 Respiration during NREM sleep

Figures 5B and 6B show the effects of STZ treatment on ventilatory parameters under room air and hypoxia conditions in rats during the sleep cycle. No difference was observed between the control and STZ groups. Both hypercapnia (Figure 5B) and hypoxia (Figure 6B) promoted a similar increase in ventilation in both groups, with no difference between them.

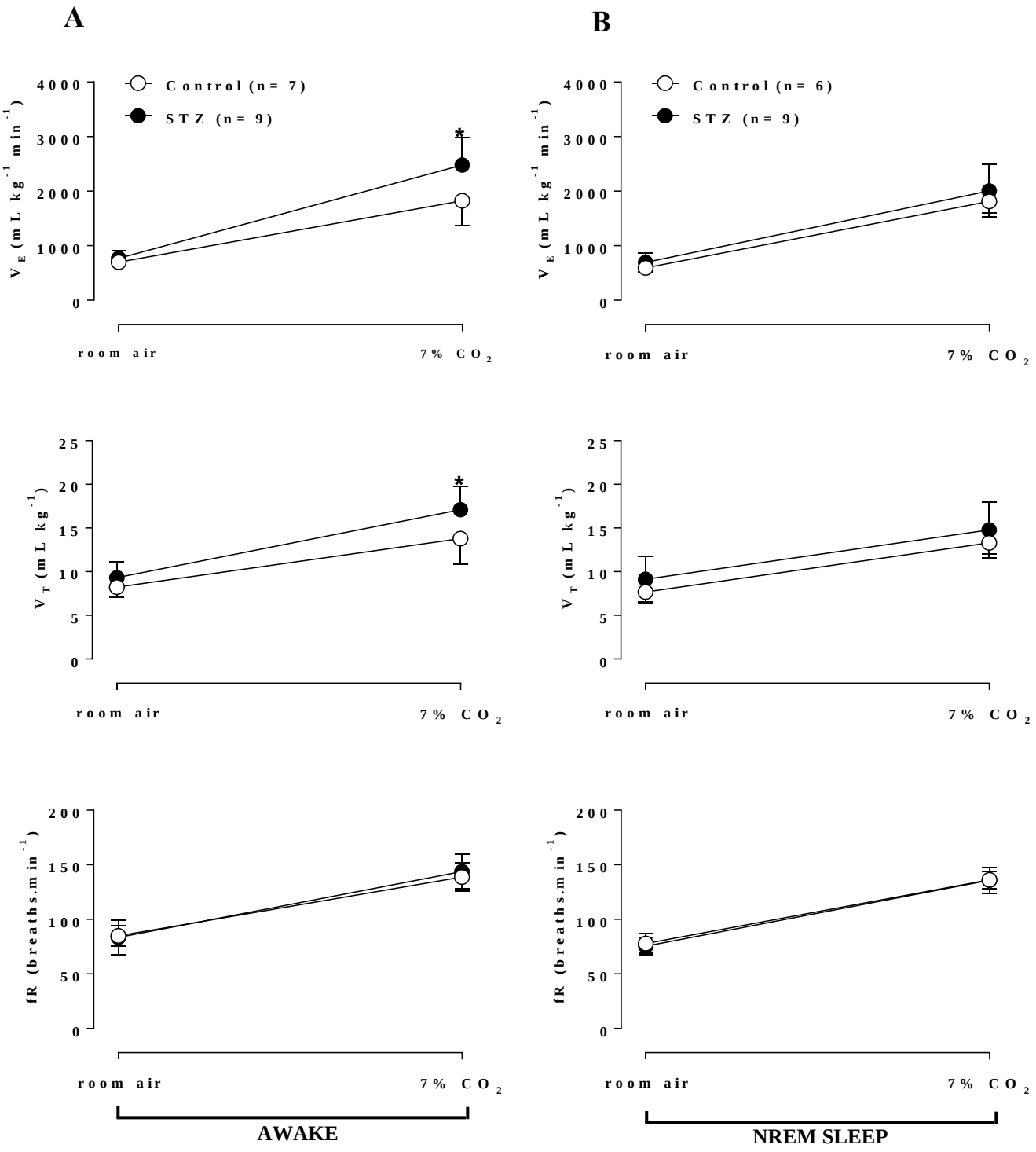

Figure 5. **The icv injection of STZ (2 mg/kg) increased sensitivity to CO_2 during wakefulness.** Effect of icv STZ (2 mg/kg) on ventilation (V_E), tidal volume (V_T) and respiratory frequency (fR) during hypercapnic exposure (7% CO_2) during wakefulness (A) and NREM sleep (B). Values are expressed as mean ± SEM. ∗ indicates a significant difference between the control and STZ groups.

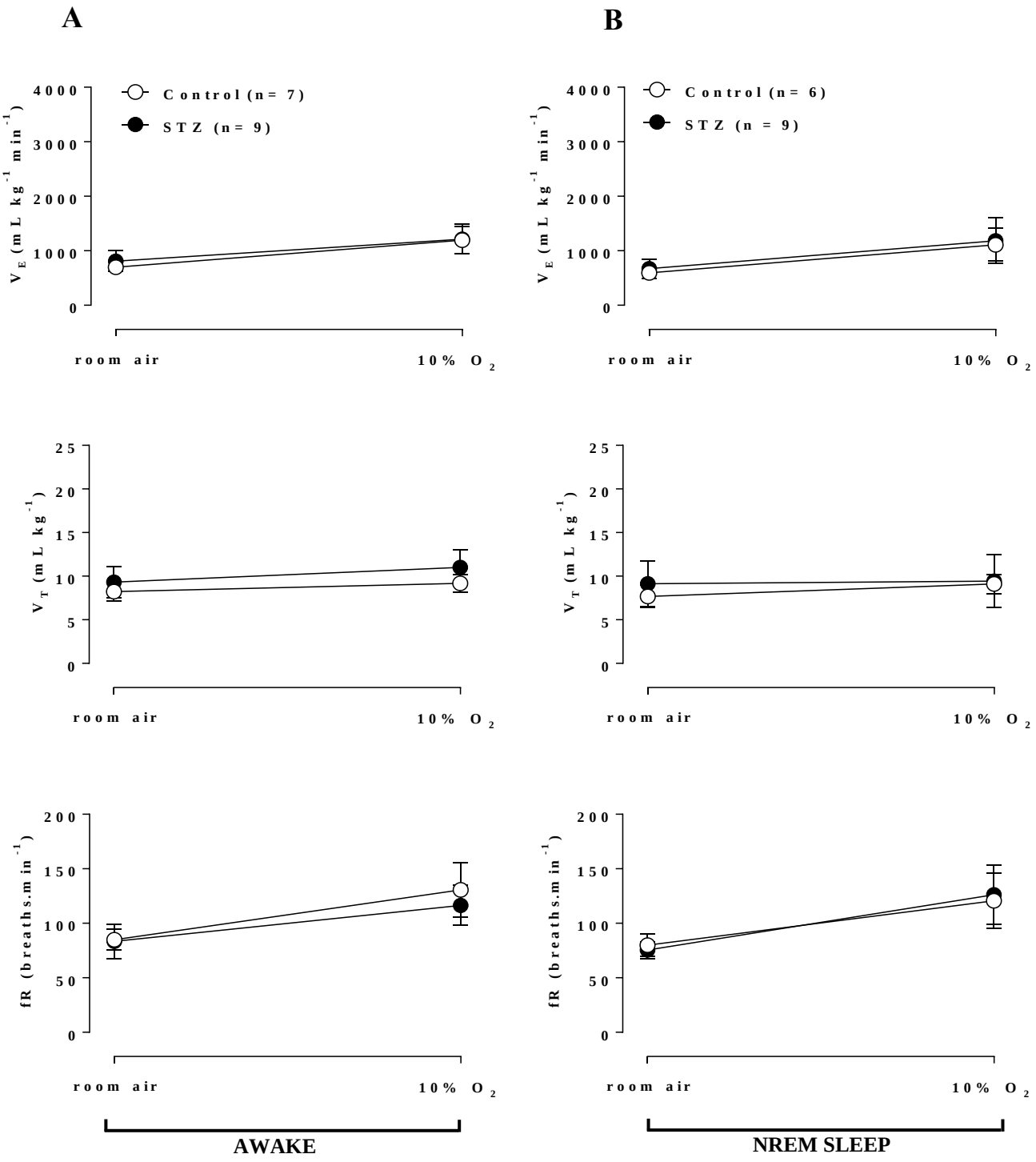

Figure 6. The icv injection of STZ (2 mg/kg) does not change the respiratory parameters during hypoxia. Effect of icv STZ (2 mg/kg) on ventilation ($\dot{V}_E$), tidal volume (V_T) and respiratory frequency (fR) during hypoxic exposure (10% O_2) during wakefulness (A) and NREM sleep (B). Values are expressed as mean ± SEM.

12.3 Body Temperature (Tb)

No significant difference was observed between treatments during room air conditions and hypercapnia (Fig. 7). Hypoxia caused a similar decrease in body temperature of both control and STZ groups.

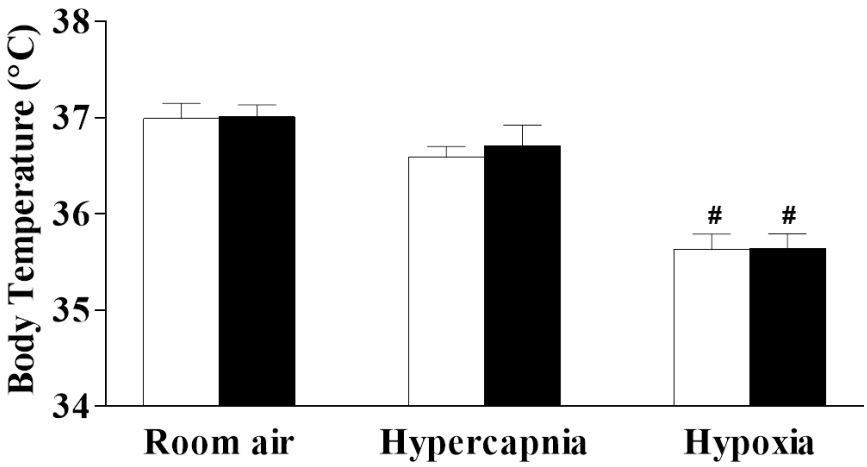

Figure 7. The icv injection of STZ does not change the temperature of the animals of rats during room air, hypercapnia and hypoxia. Values are expressed as mean ± SEM. # indicates a significant difference from room air and hypercapnia.

12.4 Sleep/Wakefulness

Under room air condition (Fig. 8A), the rats spent more time awake, but the STZ-treated rats increased the percentage of total wakefulness compared with the control group (control: 73.9 ± 4.0% vs STZ: 87.0 ± 3.0%, $p < 0.05$; two-way ANOVA). This effect was due to a significant reduction in the length of the episodes of wakefulness (Fig. 5B), while the number of episodes did not change (Fig. 8C). CO_2 exposure and hypoxia significantly increased the time the rats were awake (Fig. 8A), with no difference between treatments during hypoxia. However, under hypercapnic conditions, STZ treatment enhanced the time

that the animals spent awake (control: 81.0 ± 5.7% vs STZ: 93.5 ± 2.3%, $p < 0.05$; two-way ANOVA) due to an increase in episode duration (Fig. 8B) (control: 502.4 ± 179.6 vs STZ: 2096.8 ± 537.9 s, $p < 0.05$; two-way ANOVA) and a reduction in the number of episodes (Fig. 8C) (control: 5.2 ± 1.3 vs STZ: 2.5 ± 0.6, $p < 0.05$; two-way ANOVA).

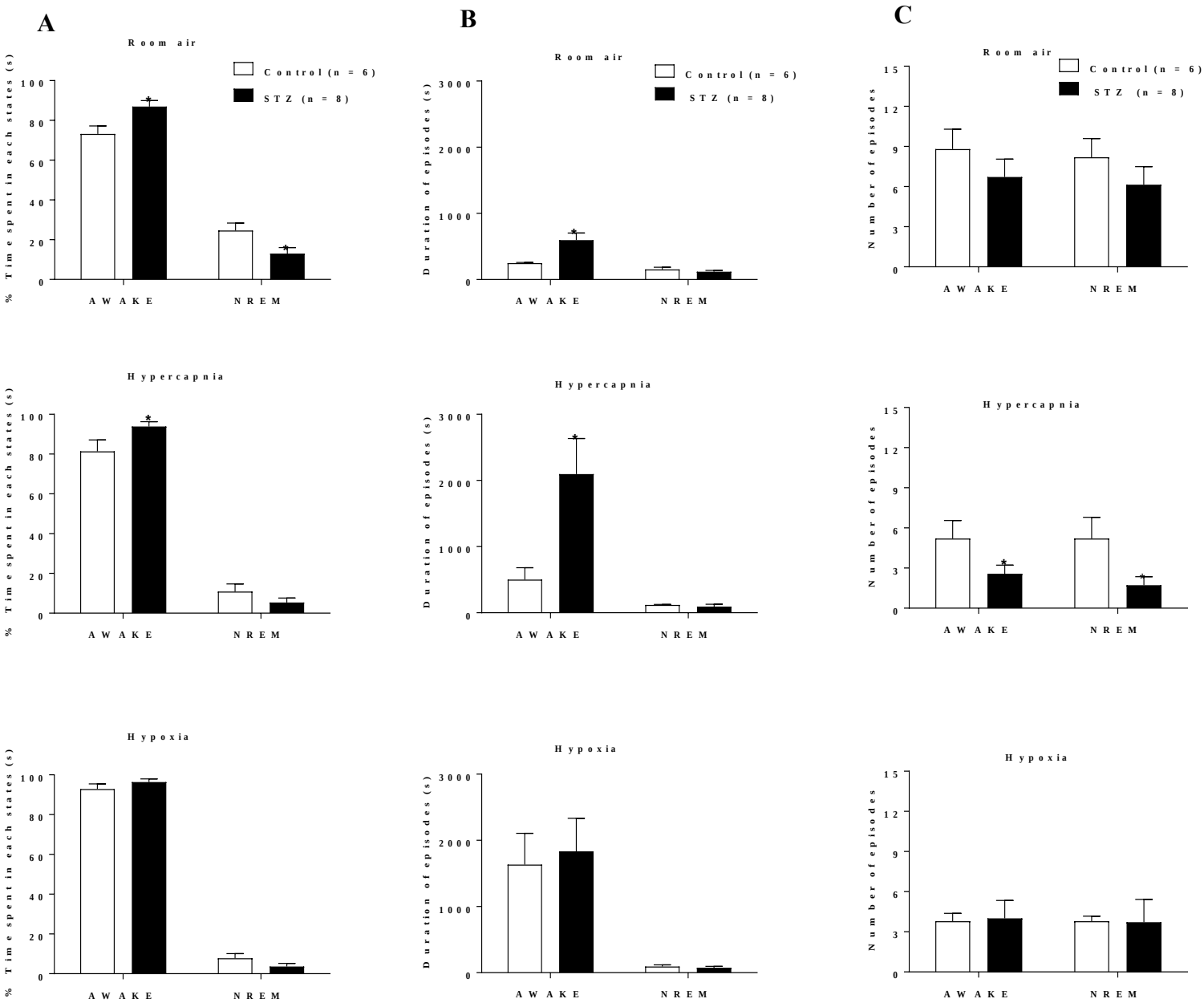

Figure 8. T**he icv injection of STZ (2 mg/kg) increased the total awake time under room air and hypercapnic conditions.** Effect of icv STZ (2 mg/kg) on the percentage (%) of time spent in each state (A), the duration of episodes in seconds (B) and the number of episodes (C) in control and STZ groups during room air, hypercapnia and hypoxia. Values are expressed as mean ± SEM. ∗indicates a significant difference between the control and STZ groups

12.5 Neurochemical Analysis

12.5.1 Tau protein phosphorylation

In the analysis of tau protein phosphorylation at the $Ser^{199/202}$ and Ser^{396} sites, we evaluated the ratio of phosphorylated tau protein (pTau) levels to total tau protein levels in the regions of interest: LC, RTN, Raphe, PreBötz/BötzC and HPC.

STZ injection did not alter the levels of phosphorylation of tau protein at $Ser^{199/202}$ site on LC, RTN, Raphe, PreBötz/BötzC and HPC (Figure 12). In addition, STZ injection did not alter the levels of phosphorylation of tau protein at the Ser^{396} site in the same regions (Fig. 9).

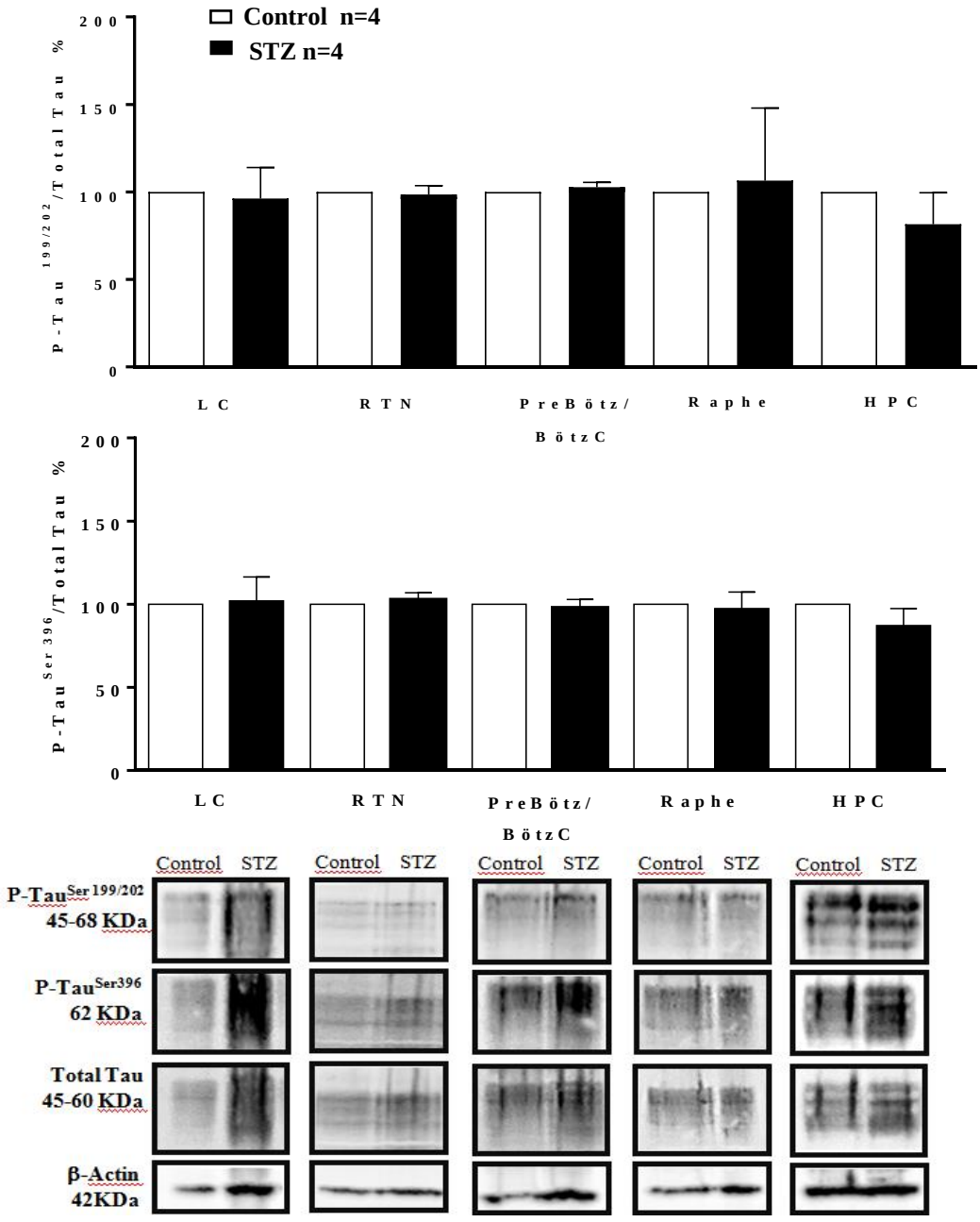

Figure 9. The icv injection of STZ injection did not alter the levels of phosphorylation of tau protein. Effect of icv STZ (2 mg/kg) on the phosphorylation levels of tau protein ($Ser^{199/202}$) (A) and the phosphorylation levels of tau protein (Ser^{396}) (B). The graphs represent the mean radius of the phosphorylated tau protein (pTau) relative to total tau protein levels. The values are expressed as percentage values in relation to the control group (100%). Values are expressed as mean ± SEM.

12.5.2 Aβ protein

Expression analysis of Aβ protein demonstrated a 73% increase in this protein in the LC of the STZ group compared to the control (p = 0.0325, Student's t-test) (Figure 10). The other structures did not present significant differences between the treatments.

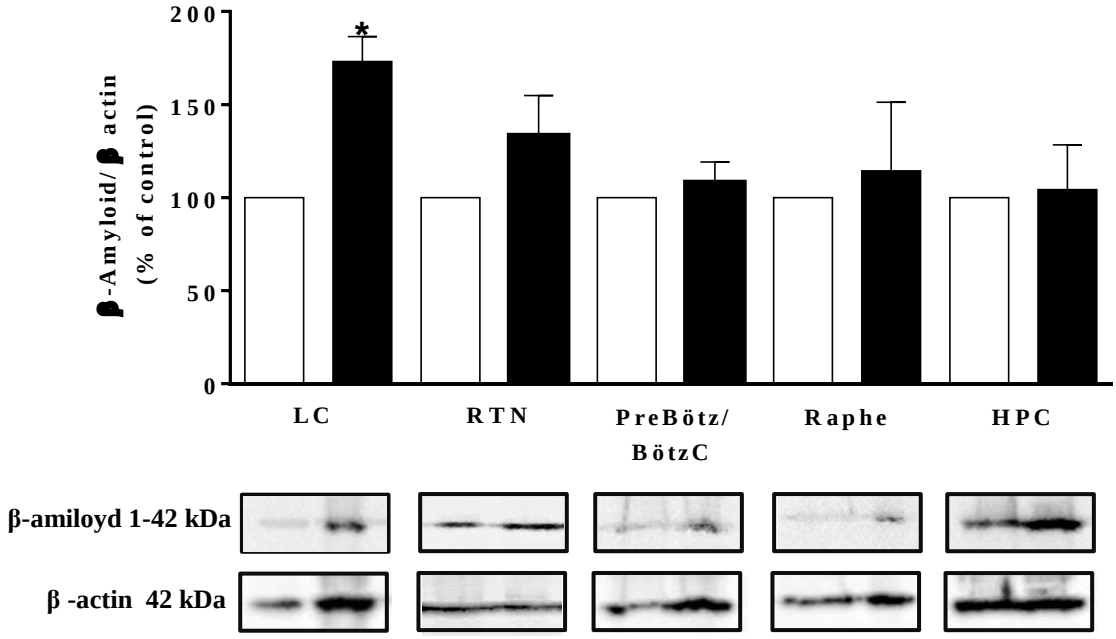

Figure 10. **The icv injection of STZ (2 mg/kg) increased the expression of the beta amyloid peptide in the Locus Coeruleus region.** Effect of icv STZ (2 mg/kg) on the expression of Aβ protein. The values are expressed as percentage values in relation to the control group (100%). Values are expressed as mean ± SEM. ∗indicates a significant difference between the control and STZ groups.

13 **DISCUSSION**

In the present study we successfully demonstrated that STZ-treated rats had learning and memory deficits, sleep disturbances, with increase time spent in awake state. Our main results were that STZ rats showed increased Aβ peptide in the LC region and increased ventilatory response to hypercapnia in wakefulness but not during sleep, with no changes in ventilation during room air conditions and hypoxia. Additionally, no changes were observed in body temperature.

In our study, we were able to reproduce the STZ-induced memory deficits. We showed an impairment in learning and retention of spatial memory (as assessed by a higher latency to find the escape box in the acquisition phase of the Barnes maze), as well as difficulty in maintaining spatial reference information (as assessed by the lower number of correct pokes into the target hole of the Barnes maze on the test day). Thus, our results confirm previous studies that have shown that STZ injection causes learning and memory deficits (GRÜNBLATT; HOYER; RIEDERER, 2004; LIU et al., 2014; MULLER et al., 2012; RAVELLI et al., 2017; SANTOS et al., 2012). These findings corroborate the use of STZ in neurodegeneration-induced dementia of the Alzheimer´s type in rats, since animals present one of the main cognitive characteristics found in patients with AD (HARMAN, 2006; QIU et al., 2019). Indeed, evidence that AD patients have problems with spatial orientation – one of the earliest cognitive symptoms – as well as progressive decline in memory, is reported in a number of different studies (E. et al., 2005; HENDERSON; MACK; WILLIAMS, 1989; KAR et al., 2004; MONACELLI et al., 2003; O'BRIEN et al., 2001).

AD is also characterized by the deposit of extracellular amyloid plaques, composed of Aβ peptide, and intracellular neurofibrillary tangles (NFTs) of hyperphosphorylated tau protein (P-Tau) (KUMAR; OKELLO; HARRIS, 2012). In the present study, we did not observe increased phosphorylation of tau protein (Ser^{396} and $Ser^{199/202}$) in the LC, RTN, Raphe, PreBötz/BötzC and HPC. The absence of increased P-Tau after STZ was also reported previously as P-Tau at $Ser^{199/202}$ in both rats (Santos et al., 2012) and mice (RAVELLI et al., 2017) were unaltered in the hippocampus after 30 and 21 days post-STZ, respectively. On the other hand, increases in P-Tau at Ser^{396} and $Ser^{199/202}$ in the hippocampus have been reported after STZ using higher doses (3 mg/kg) than the present study (DENG et al., 2009) and/or later evaluation (CHEN et al., 2013; SALKOVIC-PETRISIC et al., 2013). Besides, Grünblatt et al. (GRÜNBLATT et al., 2007), using lower doses of STZ (1 mg/kg), observed changes in P-Tau protein in the hippocampus, but did not perform a ratio analysis of phosphorylated/total tau; therefore, this may not be considered hyperphosphorylation. In fact, some studies have shown that the onset of NFTs is chronological and hierarchical, since it arises primarily in some regions and late in others (ARNOLD et al., 1991; BRAAK et al., 2011; THAL et al., 2002; THEOFILAS et al., 2017). In this sense, it is known that some phosphorylation sites of tau protein hyperphosphorylate at early stages, and other sites in late stages of AD (AUGUSTINACK et al., 2002; KIMURA et al., 1996), which would also explain the discrepancy in the literature regarding the effects of STZ in P-Tau.

The Aβ peptide in the brain of AD patient was initially considered to be a primary cause of AD dysfunction; however, later studies suggest that the presence of Aβ would be a consequence of early AD events, rather than the cause itself (DRACHMAN, 2014;

STRUBLE et al., 2010). Similar to what occurs with tau protein phosphorylation, the prevalence of Aβ results from the different stages of AD and different brain regions (ALAFUZOFF et al., 2009). In the present study, we observed a 73% increase of Aβ peptide expression in the LC after 30 days of icv administration of STZ. Our data corroborate previous studies showing that central injection of STZ promotes increases in the expression of Aβ peptide (RAVELLI et al., 2017; SALKOVIC-PETRISIC et al., 2015; SANTOS et al., 2012). In addition, it is well described that the LC region is affected in AD (CHAN-PALAY; ASAN, 1989; EHRENBERG et al., 2017; GANNON et al., 2015; THEOFILAS et al., 2017). In this context, we did not observe changes in Aβ peptide expression in the RTN region, Raphe, PreBötz/BötzC and HPC, which reinforces that the histopathological emergence of AD occurs in a hierarchical and chronological manner (ALAFUZOFF et al., 2009; EHRENBERG et al., 2017; WANG et al., 2017). Despite the fact that we did not find histopathological molecular evidence in the present temporal window (30 days after the icv STZ) in the HPC, we observed a cognitive deficit in the model. Therefore, it is possible that other cognitive regions in this temporal window may be affected.

Regarding breathing, STZ treatment did not cause alterations in ventilation under room air conditions and hypoxia during sleep and wakefulness. In the literature, there is a paucity of information on the study of the respiratory system in the progression of AD. MENUET et al. (2011), working on a model of taupatia, an important clinical aspect found in AD, observed alterations of the respiratory system, such as upper airway dysfunction, changes in respiratory pattern, and compromised ventilatory response to hypercapnia. However, the authors observed respiratory disfunction in late phases of the disease. In this context, EBEL et al. (2017), after 14 days of icv injection of STZ (3 mg/kg), observed

respiratory dysfunction in normocapnia, attenuation of the peripheral chemoreflex, as well as a small decrease in respiratory frequency during hypercapnia. Our results differ from those of EBEL et al. 2017, as we observed no changes in breathing during room air conditions or hypoxia, and a 26% increase of the ventilatory response to hypercapnia after 30 days of the icv STZ injection (2 mg/kg) only during wakefulness. We believe that these differences may reside in the fact that the authors performed the experiments using a higher dose (3 mg/kg) and a different time window (14 days after the icv injection), whereas in our study, we performed the experiments after 2 mg/kg at 30 days after STZ injection. According to GRIEB, 2016, the neurochemical changes triggered by icv STZ injection(s) follow a time-dependent pattern. Therefore, the effects observed by EBEL et al. (2017) may be due to impairment of other brain structures, since they observed a reduction in hypoxic ventilatory response, whereas we showed an exacerbation of the CO_2-drive to breathe. Moreover, higher doses may induce more severe and acute neurodegenerative lesions, which could be associated with inflammation and local oxidative stress, whereas lower doses may lead to less severe but more chronic and widespread effects (GRIEB, 2016). In this regard, KRASKA et al. (2012) stated that doses of 3 mg/kg and higher could be considered a model of very aggressive neurotoxic lesions, rather than subtle alterations due to small mechanistic alterations, as would be expected during the slowly evolving dementia processes or during aging. According to the authors, an intermediate dose, e.g. 2 mg/kg, is more relevant as a sporadic AD model.

The exacerbated CO_2 ventilatory response during wakefulness observed in the present study may result from changes in the central CO_2 chemosensitive areas. In fact, we observed an increase in Aβ peptide expression in the LC region, an important chemosensitive

nucleus of the central nervous system (BIANCARDI et al., 2008; GARGAGLIONI; HARTZLER; PUTNAM, 2010; IMBER et al., 2018; TAXINI et al., 2013; VICENTE et al., 2016b). We suggest that increased peptide expression may be deregulating the Ca^{2+} channels, increasing their influx within the neuron, which in turn would increase the release of neurotransmitters, such as noradrenaline (NE) (BOBICH; ZHENG; CAMPBELL, 2004). Increased NOR in the medullary respiratory neurons would trigger a more pronounced ventilatory response to CO_2. Previous studies have shown that LC/subcoeruleus neurons represent an early starting point for AD pathology, even preceding the occurrence of cortical lesions (ATTEMS; THAL; JELLINGER, 2012; BRAAK; DEL TREDICI, 2012; THEOFILAS et al., 2017). Measurements of 3-methoxy-4-hydroxyphenylglycol (MHPG), the principal metabolite of noradrenaline (NE), was found to be increased in postmortem brain tissue of AD patients (GOTTFRIES et al., 1983; HERREGODTS et al., 1989; HOOGENDIJK et al., 1999; PALMER et al., 1987). The authors also found an enhanced ratio of MHPG/NE, which indicates that NE metabolism is augmented in these patients, suggesting an increased activity of the remaining LC neurons to compensate for decreased cerebral NE levels in AD (GOTTFRIES et al., 1983; J.R. et al., 2009; RASKIND et al., 1999). As suggested previously (CHALERMPALANUPAP et al., 2018), enhanced LC activity may occur in the first stages of AD, prior to cell loss or significant reduction in NE neurotransmission, and this would be harmful due to the enhanced spread of P-Tau, whereas at late stages of AD, LC would be degenerating, and NE levels would be low, and tau pathology is already abundant in the forebrain. Therefore, the activity of LC neurons in AD may be dependent on the disease stage.

Around 45% of patients with AD are affected by sleep disturbances (MCCURRY et al., 2000; MORAN et al., 2005; PETER-DEREX et al., 2015) and rodent models of AD also show greater sleep fragmentation and shorter amounts of NREM and rapid eye movement sleep (ROH et al., 2012; SONG et al., 2018). Our data corroborate these previous studies, since STZ-treated rats spent more time in wakefulness than in NREM sleep during the experimental period in normocapnia and hypercapnia. During hypoxia, both groups increased their wakefulness similarly. In fact, high levels of Aβ correlate with sleep deficiencies (WINER; MANDER, 2018). In this context, immunization with Aβ prevents amyloid plaque formation in transgenic mice that develop Aβ aggregation and normalizes sleep/wake patterns (ROH et al., 2012). Since we found an increase in Aβ in the LC, and since this nucleus is necessary for maintaining normal durations of wakefulness and to promote immediate sleep-to-wake transitions (CARTER et al., 2010), it is likely that the increase in wakefulness in the STZ-treated rats is related to this fact.

Regarding Tb, the main risk factor for sporadic AD is age (HARPER, 2005). In fact, aging alone is associated with a decrease in Tb, a consequence of a deficit in thermoregulation and, in particular, in thermogenesis (GOMOLIN et al., 2005; WEINERT, 2010). However, studies have shown that patients with AD exhibit increased Tb (HARPER, 2005; KLEGERIS et al., 2006). Interestingly, rats with icv infusion of Aβ select a higher ambient temperature and show a lower heat tolerance compared to control animals (MATSUZAKI et al., 2015). Increased Tb was also shown in a 6 to 10-month-old 3xTg-AD mouse – a transgenic AD animal model (KNIGHT et al., 2013). Recently, the thermoregulatory profile of rats injected with 2 mg/kg of STZ was evaluated, and it was shown that STZ-treated rats presented a higher Tb when compared to controls from day 6 to

25 post-STZ injection (MOTZKO-SOARES et al., 2018). Although at later stages, (>30 days post-injection) STZ-treated animals present a cold-avoidance response, and their basal Tb is no longer different from controls (MOTZKO-SOARES et al., 2018). In accordance, in the present report, at 30 days post STZ treatment no differences in body temperature of animals treated with STZ under resting conditions were observed. Furthermore, treated animals seem to keep intact the thermal response to hypoxia, which is considered a regulated fall in temperature due to a drop in O_2 consumption during hypoxia (BICEGO; BARROS; BRANCO, 2007; BRANCO; GARGAGLIONI; BARROS, 2006; TATTERSALL; MILSOM, 2009). Therefore, we suggest that, in the temporal window analyzed in the present study, STZ treatment does not impair thermoregulation in rats.

14 **CONCLUSION**

Our study provides evidence that icv STZ-treated rats present an increased sensitivity to CO_2 during wakefulness, but have no changes in basal ventilation or the hypoxic chemoreflex. These changes in the CO_2-drive to breathe might be associated with enhanced Aβ in the LC, since this nucleus is highly involved in hypercapnic ventilatory response, mainly during the wake period (VICENTE et al., 2016). Furthermore, STZ animals showed an increase in the percentage of total wakefulness, which correlates with sleep disturbs observed in AD. Therefore, a better comprehension of respiratory alterations in different phases of the sleep/wake cycle, and the role of LC neurons in this modulation in AD models, is needed in order to target novel approaches for the treatment of this disorder.

Conflict interests

There is no conflict of interest for any of the authors.

Acknowledgments

This work was supported by Fundação de Amparo à Pesquisa do Estado de São Paulo (FAPESP – 2016/24577-3, 2015/02991-0 and 2015/23426-9) and Conselho Nacional de Desenvolvimento Científico e Tecnológico (CNPq - 442560/2014-1 and 449102/2014-9). The authors thank Euclides Seccato for his technical assistance.

CHAPTER 2

Decreased Excitability of Locus Coeruleus Neurons During Hypercapnia Is Exaggerated in the Streptozotocin-Model of Alzheimer's Disease – Experimental Neurology - 2020

15 **ABSTRACT**

The locus coeruleus (LC) is a pontine nucleus important for respiratory control and central chemoreception. It is affected in Alzheimer's disease (AD) and alteration of LC cell function may account for respiratory problems observed in AD patients. In the current study, we tested the electrophysiological properties and CO_2/pH sensitivity of LC neurons in a model for AD. Sporadic AD was induced in rats by intracerebroventricular injection of 2 mg/kg streptozotocin (STZ), which induces behavioral and molecular impairments found in AD. LC neurons were recorded using the patch clamp technique and tested for responses to CO_2 (10% CO_2, pH = 7.0). The majority (~60%) of noradrenergic LC neurons in adult rats were inhibited by CO_2 exposure as indicated by a significant decrease in action potential (AP) discharge to step depolarizations. The STZ-AD rat model had a greater sensitivity to CO_2 than controls. The increased CO_2-sensitivity was demonstrated by a significantly stronger inhibition of activity during hypercapnia that was in part due to hyperpolarization of the resting membrane potential. Reduction of AP discharge in both groups was generally accompanied by lower LC network activity, depolarized AP threshold, increased AP repolarization, and increased current through a subpopulation of voltage-gated K^+ channels (K_V). The latter was indicated by enhanced transient K_V currents particularly in the STZ-AD group. Interestingly, steady-state K_V currents were reduced under hypercapnia, a change that would favor enhanced AP discharge. However, the collective response of most LC neurons in adult rats, and particularly those in the STZ-AD group, was inhibited by CO_2.

Keywords: brainstem; STZ; intracerebroventricular; patch clamp; brain slice; CO_2; chemosensitivity; potassium currents; neurodegeneration.

1 INTRODUCTION

Alzheimer's disease (AD) is a neurodegenerative disease often associated with aging (FOLCH et al., 2016; WILSON et al., 2012). In addition to the typical decline in cognition and memory, patients with AD also present with respiratory problems (DEAK; KIRSCH, 2014; GAIG; IRANZO, 2012; LEE et al., 2019; LIGUORI et al., 2017). Over 70% of institutionalized AD patients have respiratory disturbances, such as insufficient ventilation during sleep, sleep apnea, and shortness of breath (DEAK; KIRSCH, 2014; GAIG; IRANZO, 2012; LENG et al., 2017). Recent studies show respiratory problems may lead to cognitive decline and may be a consequence of AD progression (LEE et al., 2019; LIGUORI et al., 2017; YAFFE et al., 2011). Therefore, respiratory impairment likely reflects alterations in brain areas that control breathing (DEAK; KIRSCH, 2014; SMITH et al., 2013).

The locus coeruleus (LC) is a noradrenergic nucleus of the central nervous system involved in a variety of functions, including wakefulness, learning and memory (ASTON-JONES; COHEN, 2005; ASTON-JONES; WATERHOUSE, 2016; BERRIDGE; WATERHOUSE, 2003), and respiratory function (BIANCARDI et al., 2008; GARGAGLIONI; HARTZLER; PUTNAM, 2010; HILAIRE et al., 2004; OYAMADA et al., 1998; PUTNAM; FILOSA; RITUCCI, 2004). Specifically, LC neurons have a vital role in central chemoreception (BIANCARDI et al., 2008; FILOSA; PUTNAM, 2003; GARGAGLIONI; HARTZLER; PUTNAM, 2010; VICENTE et al., 2016b). Previous studies in neonates (postnatal <10 days) showed CO_2 and pH sensitivity for a high percentage (80%) of LC neurons, thus, making this nucleus important for compensatory responses to CO_2

(FILOSA; DEAN; PUTNAM, 2002; JOHNSON; HAXHIU; RICHERSON, 2008; OYAMADA et al., 1998; PINEDA; AGHAJANIAN, 1997).

The LC of AD patients is severely affected (ANDRÉS-BENITO et al., 2017; ARENDT et al., 2015; SERRA et al., 2018; WILSON et al., 2013) and abnormalities in this chemosensitive area may have direct implications in the respiratory dysfunction with AD. The LC is one of the first regions that undergoes degeneration in the progression of human AD (ANDRÉS-BENITO et al., 2017; ARENDT et al., 2015; BRAAK; DEL TREDICI, 2011b; PETERSON; LI, 2018). Postmortem analysis of AD brains indicated cell loss in the LC as high as 50%, which correlated with high levels of hyperphosphorylated tau protein and amyloid beta in this nucleus (MATTHEWS et al., 2002; PAMPHLETT; KUM JEW, 2015; ŠIMIĆ et al., 2017; THAL et al., 2002; ZAROW et al., 2003). The reduced number of noradrenergic LC cells, in turn, may play a role in the declining level of noradrenaline in the hypothalamus and cortex, contributing to the severity of cognitive impairments. Interestingly, AD damage seems greater in the LC than in any other subcortical nuclei, including the nucleus basalis, that is typically implicated with cholinergic loss in patients with AD (ŠIMIĆ et al., 2017; ZAROW et al., 2003). The collective data suggest an early dysfunctional LC in AD, which may also have an underlying role in breathing dysfunction observed in patients.

To date, there is little data associating LC with respiratory dysfunctions in AD progression. Therefore, we started to focus on the respiratory deficits of the disease using the streptozotocin (STZ)-induced rat model of sporadic AD (BROWN et al., 2019; VICENTE et al., 2018). Besides progressive deterioration of learning and memory, intracerebroventricular administration of STZ mimics the biochemical and structural changes found in the brains of

AD patients. These changes include increased amyloid beta accumulation and tau protein phosphorylation, reduced glucose and energy metabolism, and the typical oxidative stress and neuroinflammation leading to neuronal death (DENG et al., 2009; GRÜNBLATT; HOYER; RIEDERER, 2004; JOHNSTON; FORSYTHE; KOPP-SCHEINPFLUG, 2010; KNEZOVIC et al., 2015; LANNERT; HOYER, 1998b; RAI et al., 2014; TOTA et al., 2010), all of which are prominent features of human AD (Ingelsson et al., 2004; Lyness et al., 2003; Milton, 2004; Sato and Morishita, 2015; Zhang et al., 2015). Furthermore, we previously showed that an increase in amyloid beta peptide in the LC region paralleled alterations in the ventilatory responses to hypercapnia. Thus, analyzing the intrinsic activity of LC neurons could provide mechanistic insight into respiratory alterations in this model and in patients with AD. In the current study, we used the patch clamp technique to evaluate the electrophysiological responses of LC neurons to CO_2 in the STZ-AD model.

2.1 Animals

The current study used male Sprague-Dawley rats (6-7 weeks; total of 39 rats) that were kept in an AAALAC accredited vivarium at A.T. Still University's Kirksville College of Osteopathic Medicine in Kirksville, Missouri, USA. Rats were maintained on a 12-hour day/night cycle at 24°C and 46% humidity with water and food available ad libitum. All experimental protocols were conducted in accordance with the guidelines of the NIH ("Guide to the Care and Use of Laboratory Animals") and were approved by A.T. Still University's Animal Care and Usage Committee.

2.2 Sporadic Alzheimer's Disease Model

Similar to our previous studies (BROWN et al., 2019; EBEL; TORKILSEN; OSTROWSKI, 2017; VICENTE et al., 2018), the typical symptoms of AD were induced by pressure injection of a subdiabetogenic dose of STZ (2 mg/kg, Alfa Aesar, Haverhill, MA) into both lateral ventricles of the brain (5 µL per side). Unlike STZ-AD rats, control (CTL) rats received vehicle only (0.9 mM citrate buffered saline, pH 4.5). For intracerebroventricular injections, rats were anesthetized using isoflurane (5% induction, 2% maintenance, Piramal, Bethlehem, PA) and positioned in a stereotaxic frame (type 68001, RWD Life Science, San Diego, CA). A sagittal midline incision was made on the scalp to expose the sagittal and coronal suture of the skull. Two holes were drilled into the skull with a rotating tool (Dremel 7300 with engraving cutter 105) to allow access to the lateral ventricles. Injection glass capillaries (type 1B120F-4, World Precision Instruments, Sarasota, FL) were drawn using a P-97 micropipette puller (Sutter Instruments, Novato, CA) and used

for intracerebroventricular injections at the following stereotaxic coordinates (PAXINOS; WATSON, 2007): -0.9 mm AP, ±1.5 mm ML, and 3.6 mm DV. After surgery, rats received high sugar supplements (Froot Loops, Kellogg's, Battle Creek, MI) in addition to normal rat chow to facilitate weight recovery.

Rats also received 2 mg/kg Dexamethasone (VetOne, Boise, ID) as an immunosuppressant before injections to avoid possible brain swelling. Postoperatively rats were treated with 50 µg/kg buprenorphine hydrochloride (Reckitt Benckiser, Slough, UK) for pain management, 7 mg/kg enrofloxacin (VetOne) for antibiotic treatment, and 3 mL of 0.9% sodium chloride solution (Hospira, Lake Forest, IL) for fluid reconstitution.

2.3 Behavioral Test

Eleven days after intracerebroventricular injections, we used the Morris water maze as a positive control to test spatial reference learning and memory in the STZ-AD model (BAO et al., 2017; BROMLEY-BRITS; DENG; SONG, 2011). The apparatus consisted of a 178-cm diameter cylindrical tank filled with water (~730 L, pH = 7.2, 22°C) that was made opaque with black nontoxic paint (DyeMond pond dye, Airmax, Romeo, MI). The pool was conceptually divided into four equal quadrants, and each quadrant was marked with a visual cue (i.e., yellow star, blue square, red circle, or green triangle) (Figure 14). A black platform (10-cm diameter) that was height adjustable was positioned close to the middle of the target quadrant (green triangle).

On day 1, animals were trained during five initial trials to find the raised escape platform (1 cm above water level). Then, the platform was submerged 1 cm below water level and rats were subjected to 15 consecutive trials per day for 3 days (each series was 24 hours apart). The rats were placed at randomized starting positions (except the target

quadrant) and given 60 seconds (cutoff time) to find the submerged platform. If the rat was unable to find the hidden escape platform within the cutoff time, it was manually guided to the platform. The time to reach the platform was noted as the escape latency. The swim velocity was recorded using a camera (AW615, Ausdom, City of Industry, CA) positioned above the tank and analyzed using the Animal Tracker plugin in Fiji software (version 1.52i, NIH).

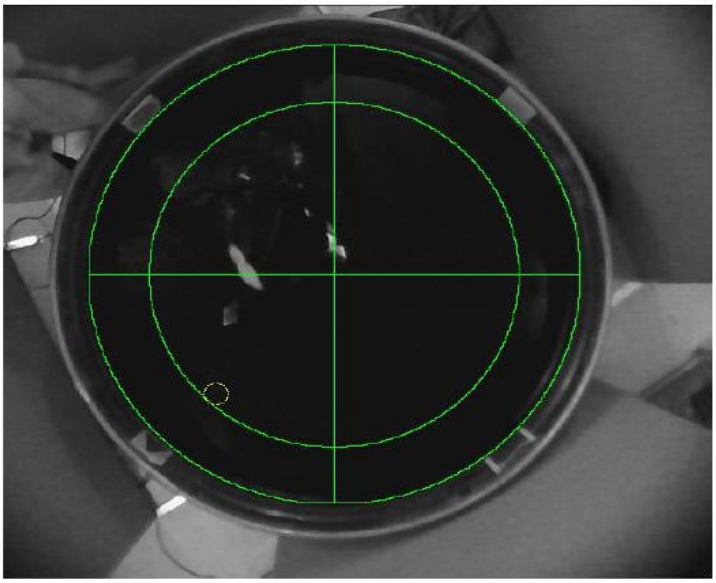

Figure 1. **Representation of the Morris Water Maze (MWM).** The pool was divided virtually into 4 quadrants and the yellow circle represents the platform position during the test.

2.4 Patch Clamp Recordings

2.4.1 In vitro brain slice preparation

Similar to Ting et al. (2014, 2018), rats were anesthetized with isoflurane and transcardially perfused with 60 mL of ice-cold oxygenated *N*-Methyl-D-glucamine (NMDG)-based artificial cerebrospinal fluid (aCSF) with the following composition (in

mM): 93 NMDG, 2.5 KCl, 1.2 NaH_2PO_4, 30 $NaHCO_3$, 20 HEPES, 25 glucose, 2 thiourea, 5 sodium ascorbate, 3 sodium pyruvate, 0.5 $CaCl_2 \cdot 2H_2O$, and 10 $MgSO_4 \cdot 7H_2O$, pH 7.4, 300-305 mOsm. NMDG-based solutions were used to better preserve the health of brain tissue from adult rats. Next, the brainstem was rapidly removed and horizontal brain slices (250-µm thick) containing the LC were obtained using a vibratome (7000smz-2, Campden Instruments, Lafayette, IN) (Bregma level: from – 7.34 mm) (Fig 2). Slices were then incubated for 20 minutes in warm (35°C) oxygenated (95% O_2–5% CO_2) NMDG aCSF. For patch clamp recordings, tissue sections were placed in a superfusion chamber, secured with a nylon mesh, and superfused at 2-3 mL/min with standard recording aCSF (in mM: 124 NaCl, 3 KCl, 1.2 NaH_2PO_4, 1.2 $MgSO_4$, 25 $NaHCO_3$, 11 D-glucose, and 2 $CaCl_2$, saturated with 95% O_2–5% CO_2, pH 7.4, 300 mOsm) at 35°C.

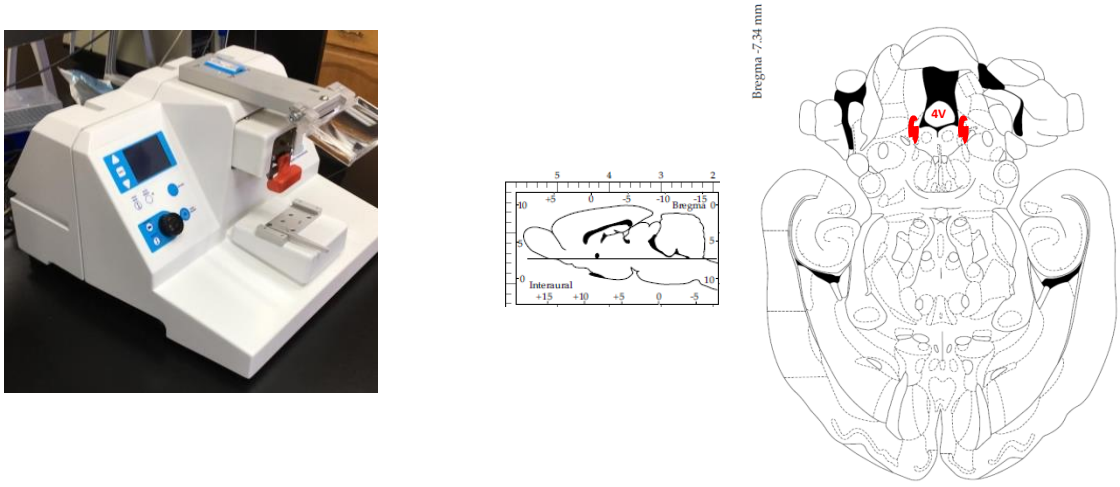

Figure 2. Vibratome (7000smz-2, Campden Instruments, Lafayette, IN) used for brain slice preparation (250-µm thick) containing the LC.

2.4.2 Electrophysiological recording

Similar to our previous studies (OSTROWSKI et al., 2014a, 2014b), LC cell somas were recorded to analyze the electrophysiological properties. Recordings were primarily obtained from neurons in the dorsal LC because of the greater number of healthy cells. Pipettes (8250, King Precision Glass, Claremont, CA) were made with a Flaming/Brown micropipette puller (Model P-97, Sutter Instruments) and had resistances of 4.5-5 MΩ when filled with standard recording solution (in mM: 130 potassium gluconate, 10 HEPES, 0.4 EGTA, 1 $MgCl_2$, 0.3 Na_2-GTP, and 2 Na_2-ATP, pH 7.45, 280 mOsm) (NICHOLS et al., 2008). Recording pipettes were guided with a motorized micromanipulator (MP-225, Sutter Instruments). Data were recorded (20 kHz sampling rate) and filtered at 2 kHz using a Patch Clamp EPC 10 USB amplifier/AD converter (HEKA Instruments, Holliston, MA) (Fig 3). The liquid junction potential was not corrected and the series resistance was not compensated.

The activity of LC neurons was recorded under normocapnia (baseline: standard 5% CO_2, balanced with O_2) and 5 minutes into perfusion of hypercapnic aCSF (10% CO_2, balanced with O_2). CO_2 concentrations were achieved by saturating the perfusate using mass flow controllers (MC-5SLPM-D, Alicat Scientific, Tucson, AZ). Increasing CO_2 content from 5% to 10% lowered the pH from an initial 7.4 to 7.0. This drop in pH is sufficient to study the CO_2-induced response of LC neurons (LI; PUTNAM, 2013; LOPES et al., 2016; OYAMADA et al., 1998).

All electrophysiological data were analyzed using Igor Pro 8 (WaveMetrics, Portland, OR), MiniAnalysis (Synaptosoft, Fort Lee, NJ), and Excel (Microsoft, Redmond, WA) software programs.

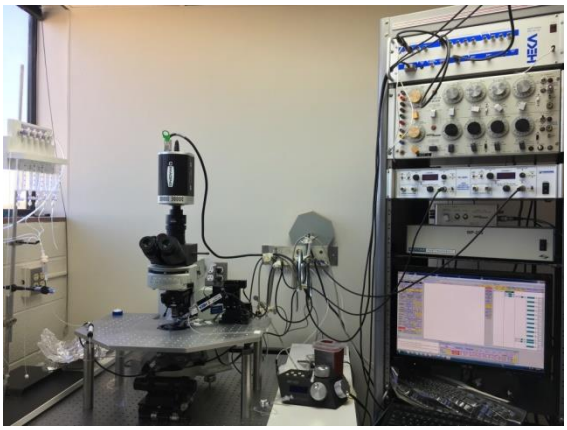

Figure 3. Patch Clamp EPC 10 USB amplifier/AD converter (HEKA Instruments, Holliston, MA) used for electrophysiological recording.

2.4.3 Current clamp protocol

Criteria for healthy LC neurons under baseline conditions (after establishing whole cell configuration) were a resting membrane potential (RMP) close to -45 to -50 mV and spontaneous spike activity. We used step depolarization (-20 to 100 pA, 10 pA steps, 100-ms duration) to induce action potential (AP) discharge (KLINE et al., 2010; OSTROWSKI et al., 2014a). Because of the heterogeneous response of LC neurons to CO_2 (LOPES et al., 2016; NICHOLS et al., 2008), we grouped cells according to their change in AP discharge from baseline to hypercapnia. Cells that increased spike activity by 5% (average over all current steps) were categorized as CO_2-activated, those that decreased by 5% as CO_2-inhibited, and those that did not change as non-responder. These classifications do not represent the intrinsic chemosensitivity of LC cells (see Discussion).

Phase plan plots (change of membrane voltage [mV/ms] against the membrane potential [mV]) were generated from an AP elicited during the step depolarizations protocol (first AP to lowest depolarizing current to exclude possible effects from repetitive spiking

with stronger stimulation). AP threshold (THR) was identified when the voltage change exceeded 10 mV/ms (GUDES et al., 2015). Other parameters analyzed were AP rising slope (maximal Na^+ conductance) (JENERICK, 1963), AP peak (overshoot), AP falling slope, AP half-width (measured at 50% AP amplitude from RMP), and the afterhyperpolarization (measured from THR) (Fig 4). The delay to the first AP in response to 100 pA current is the time from stimulus begin until AP peak. RMP was recorded in the absence of current induction (I=0).

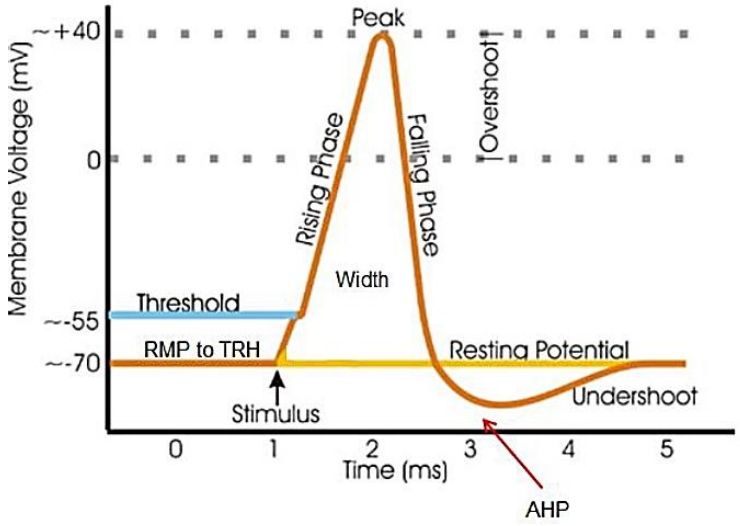

Figure 4. Representation of the phases of the action potential (AP) analyzed in the present study.

2.4.4 Voltage clamp protocol

All cells were clamped at -60 mV (at the calculated reversal potential for chloride), and the membrane resistance (i.e., input resistance, R_i) was determined from a 5-mV hyperpolarizing step. K^+ conductances were measured using a step protocol between -100 and +80 mV (+20 mV per step, 400 ms step). Cell capacitance was equal between cells from control and STZ-AD groups (CTL, 104.0 ± 11.0 pF vs STZ-AD, 111.5 ± 7.6; p = 0.58; n =

13 in each group). The transient K^+ current was examined by subtracting the steady-state current (near the end of the voltage step) from the initial current to the voltage step (KLINE et al., 2010; OSTROWSKI et al., 2014a) (Fig 5). Spontaneous postsynaptic currents (sPSC) were recorded for 1 minute in the absence of stimulation and constitute network activity (FORTIN; CHAMPAGNAT, 1993) within the LC.

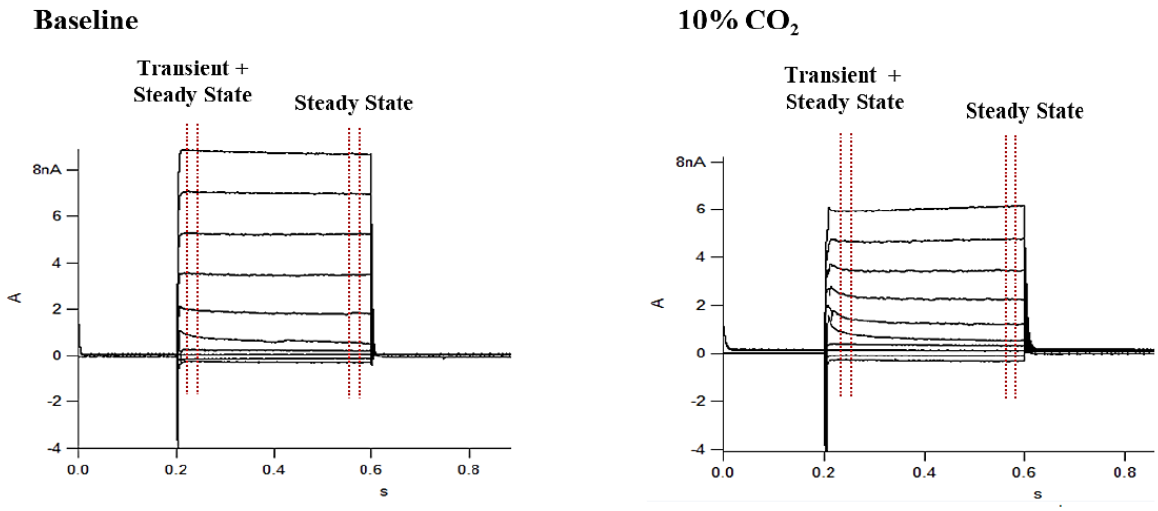

Figure 5. Representative IV curves during baseline and 10% CO2. Note the overall decrease in K+ currents with CO_2. The red lines describe the area for measurements of transient and steady-state currents to each voltage step.

2.5 Immunohistochemistry

Similar to our previous studies (BROWN et al., 2019; EBEL; TORKILSEN; OSTROWSKI, 2017), slices containing the LC (30 µm thick; if previously used for patch clamp recordings, slice thickness was 250 µm) were washed in phosphate buffered saline (PBS) and blocked for 30 minutes in 10% normal donkey serum (MilliporeSigma, Burlington, MA) with 0.3% Triton-PBS. Next, slices were incubated overnight in 1% normal donkey serum with 0.3% Triton-PBS and primary antibody against tyrosine hydroxylase

(TH) (chicken, 1:1000, ab76442, Abcam, Cambridge, MA) and, in some applications, additionally with NeuN (mouse, 1:500, MAB377, MilliporeSigma). The next day, slices were washed and incubated for 2 hours in secondary antibody using Alexa Fluor 647 (donkey anti-chicken, 1:200, 703-605-155, Jackson ImmunoResearch, West Grove, PA) or Alexa Fluor 488 (donkey anti-chicken, 1:200, 703-545-155, Jackson ImmunoResearch) and, in some applications, with Alexa Fluor 594 (donkey anti-mouse, 1:200, 715-585-151, Jackson ImmunoResearch). After a final wash, slices were mounted on gelatin-coated glass slides, dried, and cover-slipped using ProLong Diamond (Thermo Fisher Scientific, Waltham, MA). All immunohistochemical steps were performed at room temperature. In a subset of experiments, the patch pipette solution contained 3% Lucifer yellow (LY) (L0259, Sigma-Aldrich, St. Louis, MO) that was ionophoretically injected (negative current for approximately 20 minutes) into LC neurons after electrophysiological characterization. Patch-slices were then fixed in 4% paraformaldehyde for later immunohistochemical identification of TH. Immunoreactivity was examined on a conventional epifluorescent microscope (Eclipse 80i, Nikon, Tokyo, Japan) with a digital monochrome camera (DS-Qi1Mc, Nikon) and appropriate filter sets or on a confocal microscope (DMI6000 B, Leica, Wetzlar, Germany) using lasers (Argon, HeNe 633) with fluorophore-specific excitation and emission wave length and appropriate filter sets. Confocal images were collected in z-stacks (0.5 μm optical slices). Post-processing of the images (adjustment of contrast and brightness for clarity) was done using the software Fiji.

Schematics of the LC were created with the Inkscape program (version 0.91, http://www.inkscape.org/), and nuclei were identified using Paxinos and Watson's rat brain atlas (PAXINOS; WATSON, 2007). Analysis of neuron number was completed in

representative sections of the LC (Bregma level: from -9.96 to -9.60) and counted blindly by 3 independent persons using Fiji software. Neurons were counted in a 200 × 200 μm box in the dorsal-most portion of the LC excluding spaces that are devoid of cells (e.g., blood vessels). Results of all counters were averaged and compared between groups

2.6 Statistical Analysis

Behavioral, electrophysiological, and immunohistochemical data were analyzed using the *t* test or two-way repeated measures ANOVA followed by Newman-Keuls post-hoc test where appropriate. All results were considered statistically significantly different at $p \leq 0.05$. Group data are presented as mean ± SEM.

3.1 Diminished Memory Performance in the Streptozotocin-Induced Alzheimer's disease (STZ-AD) Model

Previous research has shown the STZ-AD rat model results in reduced memory performance (LANNERT; HOYER, 1998b; SALKOVIC-PETRISIC et al., 2013). To verify memory dysfunction in our study, we used the Morris water maze. Trial-to-trial performance was compared between groups as measure of spatial memory. Figure 6A shows the escape latencies for 15 trials on each of the consecutive testing days. During the initial trials (with the visible platform), escape latency of all animals was typically near the cut off time of 60 seconds, indicating a similar performance for both groups in the new environment. With an increasing number of trials (and a hidden platform), STZ-AD rats spent significantly more time finding the platform than the control group, demonstrating impairment in learning and retention of spatial memory. Both groups had comparable swim velocity (Fig. 6B), indicating motor function of STZ-AD rats was not affected.

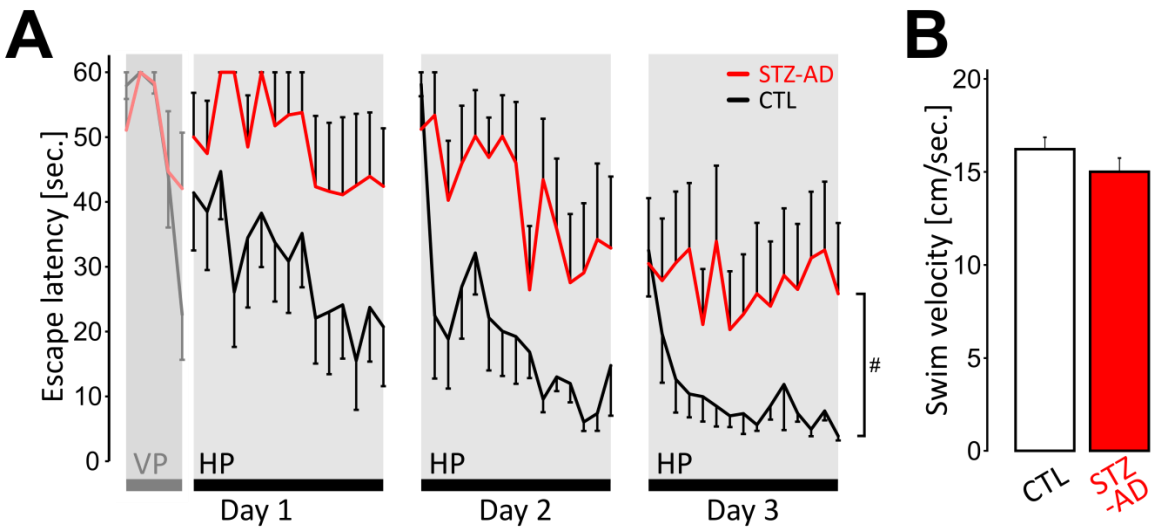

Figure 6. Spatial learning and memory deficits in the sporadic Alzheimer's disease (AD) animal model. A) Escape latency to find the hidden platform (HP) in the Morris water maze for the control (CTL) and streptozotocin-induced Alzheimer's disease (STZ-AD) groups during the 3-day testing period with 15 training sessions per day. Cut off time was 60 seconds. B) Swim velocity as measure for locomotor function shows no impairment in the STZ-AD group. Data are reported as mean ± SEM. # $p \leq 0.05$; 2-way repeated measures ANOVA. n = 6-7 rats per group. VP = visible platform

3.2 No Change in Locus Coeruleus (LC) Neuron Number in the STZ-AD Model

Because of neurodegeneration of the LC in advanced human AD, we analyzed neuronal number in our STZ-AD model (Fig. 7). We concentrated on three representative regions for the caudal-rostral extent of the LC and immunohistochemically stained for NeuN (neuronal marker) and tyrosine hydroxylase (TH) (typically found in the LC). The numbers of neurons that co-stained for TH and NeuN were compared between the STZ-AD and control group. No difference was found between groups, likely indicating that the AD model of the current study represents an early time point in disease progression (two weeks after AD induction) and that morphological changes in the LC are not (yet) present.

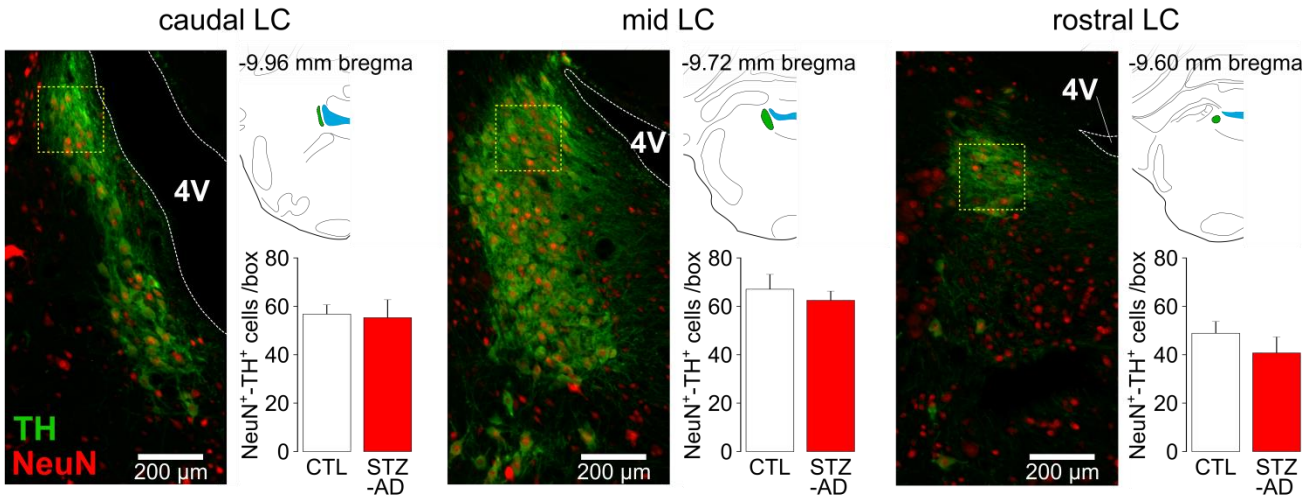

Figure 7. Unaltered neuronal density in the locus coeruleus (LC) of the streptozotocin-induced Alzheimer's disease (STZ-AD) group. Three representative coronal sections (30 µm) of the LC with labeling of NeuN-identified neurons (red) and tyrosine hydroxylase (TH) -positive cells (green). Brain schematics illustrate the location and extent of the pontine LC (green area) in relation to bregma. TH^+ neurons were counted in a 200 × 200 µm box (yellow box) in the dorsal-most portion of the LC. Data are presented as mean ± SEM. n = 6 rats per group. 4V = 4th ventricle.

3.3 Spike Response of LC Neurons During Hypercapnia

The LC is located adjacent to the 4th ventricle in the dorsal aspect of the pons. Figure 8A shows an example of the LC (white dashed line) in a horizontal brainstem slice used for patch clamp recordings. A 40× magnification from a typical cell in the LC with attached patch pipette is shown in Figure 8B. In a subset of rats and after completion of electrophysiological recordings, we immunohistochemically stained for TH (Fig. 8C). Dense TH is found in the noradrenergic LC (GRZANNA; MOLLIVER, 1980) and verified correct placement of our patch pipettes.

The LC is a chemosensitive nucleus with a population of neurons having different response patterns to increased CO_2 conditions. Neurons may show an increase, decrease, or no alteration of activity when exposed to CO_2 (LOPES et al., 2016; NICHOLS et al., 2008).

To test this heterogeneity of neuronal responses to CO_2, we performed a step depolarization protocol (100 ms steps with increasing current, +10 pA/step) to evoke action potential (AP) discharge (Figs. 8D and 9). In the control group (data from 6 rats), the majority of LC neurons (57%, 8 cells from 5 rats) were inhibited by CO_2 (i.e., reduced current-evoked AP discharge) (Fig. 3E). Only a few cells were either activated (increased spiking, 21%, 3 cells from 3 rats) by CO_2 or did not respond (21%, 3 cells from 3 rats). A similar result was obtained for the STZ-AD group (data 6 rats). The majority of cells (64%, 9 cells from 6 rats) were inhibited by CO_2, only 14% (3 cells from 2 rats) showed activation, and 21% (2 cells from 2 rats) did not change spike discharge to current injections under hypercapnic conditions (Fig. 8F).

Given previous studies that found over 50% of noradrenergic LC neurons in neonatal rats increased firing rate to CO_2 exposure (BERRIDGE; WATERHOUSE, 2003; FILOSA; DEAN; PUTNAM, 2002; JOHNSON; HAXHIU; RICHERSON, 2008), we wanted to confirm the phenotype of LC cells in our preparation using adult rats. A subset of cells (5 cells in uninjected control rats) were loaded with the fluorescent dye Lucifer yellow (LY) during and after electrophysiological characterization. We later co-stained against TH and visualized LY-labeled cells using confocal microscopy (Fig. 8G). Cells that were excited or inhibited by CO_2 expressed the same phenotype for TH. This result furthermore suggests that all neurons recorded in the current study are noradrenergic (see also Fig. 8C). In the following analysis, we concentrated on the majority of LC neurons that were inhibited by CO_2.

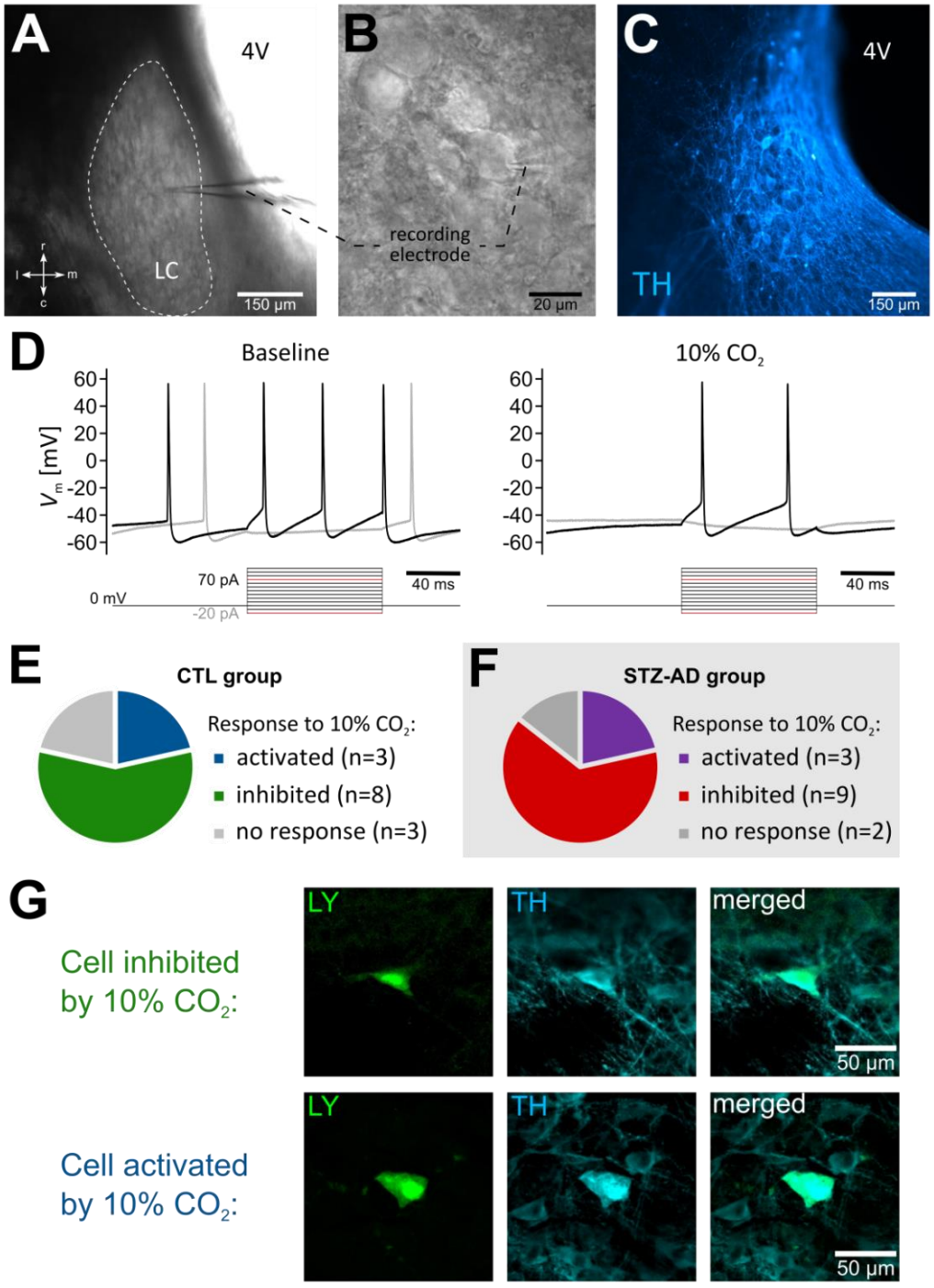

Fig 8. Response classes of locus coeruleus (LC) neurons to increased CO_2 exposure. A) Representative horizontal brainstem section (250 µm) illustrating the location of the LC during patch clamp experiments. B) Magnification of a LC neuron with attached glass electrode during the recording. C) Immunohistochemical staining of tyrosine hydroxylase (TH) (blue) in a horizontal brainstem slice subsequent to neuronal recordings in the region of the LC. D) Representative responses of a CO_2-inhibited LC neuron to step depolarization (10 pA steps, 100 ms) at baseline and during the CO_2 condition. Reponses are shown for -20 pA (gray trace) and +70 pA (black trace) only. The stimulus is shown underneath the traces. Note that CO_2 eliminates spontaneous

spike activity (before and after the stimulus) and blunts action potential discharge to current injection. E) Response classes of LC neurons to hypercapnia in the control (CTL) group F) Response classes of LC neurons to hypercapnia in the streptozotocin-induced Alzheimer's disease (STZ-AD) group. G) Confocal images (40× oil) of electrophysiologically identified LC neurons that were loaded with Lucifer yellow (LY) (green fluorescence) and stained against tyrosine hydroxylase (TH) (blue). Note the overlap of LY and TH in the merged image, indicating the same LC-specific phenotype for cells that were excited and inhibited by CO_2. All images shown are merged z-stack images from five sections (0.5 µm apart). 4V = 4th ventricle, r = rostral, c = caudal, m = medial, l = lateral.

3.4 Decreased Excitability of LC Neurons During Hypercapnia Is Exaggerated in the STZ-AD Model

Group data for current-evoked spike discharge in LC neurons that responded to CO_2 is shown in Figure 9. In the control group, spike discharge of cells inhibited by hypercapnia (Fig. 9A) decreased significantly across all current steps when compared with their baseline response. Spike discharge in the STZ-AD group was also significantly blunted by CO_2 at all current steps (Fig. 9B). This hypercapnic inhibition on discharge was exaggerated in the STZ-AD group when compared with the control group (% change at 100 pA: CTL, 16.7 ± 8.3% vs STZ-AD, 57.4 ± 11.8; $p \leq 0.01$; n = 8-9). Notably, the baseline discharge of both groups reached similar magnitudes. A closer look at the spike discharge in the absence of depolarizing current (-20 to 0 pA in Fig. 9) showed the spontaneous activity of LC cells. Hypercapnia also reduced the spontaneous activity of CO_2-inhibited cells in both groups (Figs. 9A and 9B), indicating the inhibitory effect of CO_2 was independent of neuronal activity. Together, these data suggest that CO_2 is able to depress activity in a large subgroup of LC cells and that the STZ-AD rat model exhibits an impaired response to hypercapnic conditions.

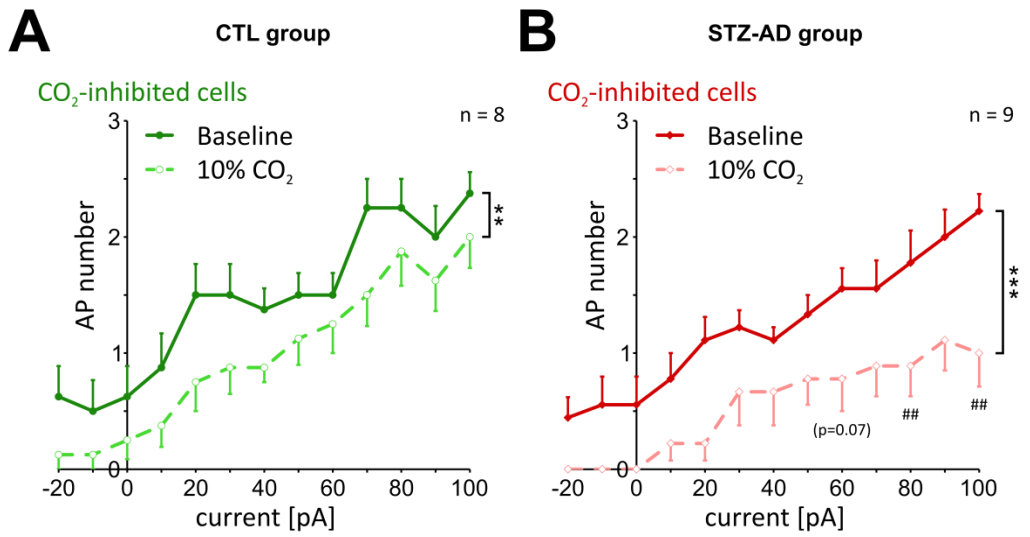

Figure 9. Spike discharge of locus coeruleus (LC) neurons to current injections at baseline and during increased CO_2. Action potential (AP) number in response to step depolarization during baseline and hypercapnia (10% CO_2) for cells that were inhibited by CO_2 in the control (CTL) group (A) and the streptozotocin-induced Alzheimer's disease (STZ-AD) group (B). Data are expressed as mean ± SEM. ** $p \leq 0.01$ and *** $p \leq 0.001$ indicated a difference between baseline and the hypercapnia condition. ## $p \leq 0.01$ indicated a difference between STZ-AD and CTL groups; 2-way repeated measures ANOVA.

3.5 CO_2 Exposure Decreases Overall LC Network Activity

Network activity in the LC can be assessed by analyzing the spontaneous postsynaptic currents (sPSCs) in the absence of stimulation. All cells were clamped at -60 mV (the calculated equilibrium potential for chloride) and sPSCs recorded in this configuration likely represent excitatory inputs. Figure 10A is a representative example of LC network activity during baseline and at 10% CO_2. CO_2 exposure significantly decreased the number of sPSCs as shown for CO_2-inhibited cells in both groups (Fig. 10B). The magnitude of this reduction was similar between groups (CO_2-induced change in network activity: CTL, -34.3 ± 12.3% vs STZ-AD, -32.1 ± 13.2%; $p > 0.05$; n = 8-9). The amplitude of sPSCs did not change with exposure to hypercapnia in the control group (baseline, 25.3 ±

3.4 pA vs CO_2, 26.3 ± 2.1 pA; p > 0.05; n = 8) or STZ-AD group (baseline, 27.5 ± 1.9 pA vs CO_2, 26.4 ± 2.8 pA; p > 0.05; n = 9).

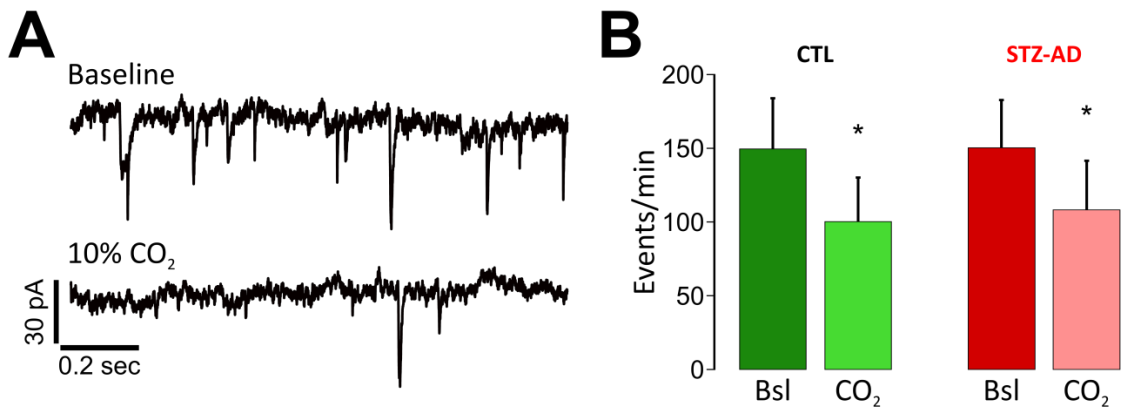

Figure 10. Reduced locus coeruleus (LC) network activity with increased CO_2. A) Typical example for a reduced number of spontaneous postsynaptic currents (sPSC), representing LC network activity, with 10% CO_2. B) Group data for sPSCs at baseline (Bsl) and at 10% CO_2 for the control (CTL) and streptozotocin-induced Alzheimer's disease (STZ-AD) groups. Data are expressed as mean ± SEM. * p ≤ 0.05; t-test. n = 8-9 rats per group.

3.6 CO_2 Decreases Resting Membrane Potential (RMP) in the STZ-AD Model

To determine whether CO_2 alters basic cell membrane properties, we initially analyzed input resistance (R_i) (resistance across the cell membrane) from a 5 mV step (-60 to -65 mV) in voltage clamp configuration. There was no difference in R_i between groups at baseline and during hypercapnia. However, within the STZ-AD group R_i decrease significantly from baseline to hypercapnia in CO_2-inhibited cells (Table 1). This decrease of R_i is indicative of membrane channel opening. Consistent with this reduction of R_i, RMP was significantly hyperpolarized to more negative potentials in CO_2-inhibited cells from the STZ-

AD group. This change indicates alterations of K^+ currents that are important for RMP generation and may contribute to the hypercapnia-induced reduction of AP discharge in the STZ-AD rat model. RMP of CO_2-inhibited cells in the control group did not change.

CO_2-inhibited LC neurons			CTL / STZ-AD
Parameter	**Baseline (bsl)**	**10% CO_2**	***p***, bsl vs. CO_2
Membrane resistance (R_i) [MΩ]	116.1 ± 19.5	113.5 ± 18.7	0.693
	126.5 ± 14.9	98.4 ± 8.2	**0.006**
Resting membrane potential (RMP) [mV]	-46.4 ± 1.4	-47.7 ± 2.1	0.393
	-49.0 ± 1.6	-52.2 ± 1.7	**0.030**

Table 1. Cell membrane properties during the baseline and 10% CO_2 from the control and STZ-AD group.

3.7 CO_2 Depolarizes Spike Threshold (THR) and Increases AP Repolarization in LC Neurons

To identify additional mechanisms for CO_2-induced inhibition of AP discharge in the majority of LC neurons, we closely examined AP properties during our step depolarization protocol. The delay to the first AP in response to 100 pA step depolarization is given in Table 2 and serves as an indicator of neuronal excitation. CO_2-inhibited cells in the STZ-AD group comprised a strong increase in delay of AP discharge, which is consisted with hypercapnia-induced inhibition of the response. This increase in delay is underestimated since three cells (STZ-AD group only) did not elicit spikes at 100 pA under hypercapnia and a higher current step needed to be evaluated. AP delay of CO_2-inhibited cells from the CTL group only showed a small and non-significant increase.

As detailed in Figure 11A, main AP properties include THR, upstroke, AP peak amplitude, and downstroke. To reliably quantify these parameters, we generated phase plane plots that show the first derivative of membrane voltage against the change in membrane potential. A complete list of all parameters, their changes, and statistical analysis is provided in Table 2. In CO_2-inhibited cells of the CTL and STZ-AD groups, THR increased significantly with hypercapnia (Figs. 11B and 11C, Table 2). The CO_2-induced change in THR also increased the voltage difference from RMP to THR in both groups, making it harder to overcome this voltage difference by a depolarizing stimulus and eliciting AP discharge. The significant hyperpolarization of RMP in the STZ-AD group (Table 1) added to this difference. The STZ-AD group also had a hypercapnia-induced increase in rising slope and peak amplitude of the AP, suggesting alteration of Na^+-dependent inward currents. A prominent change in both groups was the CO_2-induced reduction of half-width resulting from a significantly steeper falling slope of the AP (Figs. 11B and 11C, Table 2). Faster AP repolarization is indicative of increased K^+-dependent outward currents that may contribute to the inhibitory effects of CO_2 observed in the majority of LC neurons.

CO_2-inhibited LC neurons			CTL / STZ-AD
Parameter	**Baseline (bsl)**	**10% CO_2**	***p***, bsl vs. CO_2
Delay to first AP [ms]	15.1 ± 4.3	18.4 ± 4.0	0.164
	18.6 ± 3.7	49.5 ± 10.2†	**0.004**
AP threshold (THR) [mV]	-36.2 ± 3.1	-33.8 ± 3.4	**0.040**
	-38.7 ± 2.7	-34.8 ± 3.4	**0.010**
RMP to THR [mV]	-10.1 ± 1.9	-13.9 ± 2.4	**0.012**
	-10.3 ± 1.9	-17.4 ± 3.3	**0.003**
AP peak [mV]	50.3 ± 2.7	51.0 ± 3.5	0.589
	49.2 ± 1.9	52.2 ± 1.8	**0.038**
Max. AP rising slope [mV/ms]	276.0 ± 24.4	280.1 ± 30.0	0.692
	274.7 ± 15.7	298.9 ± 12.8	**0.049**
Max. AP falling slope [mV/ms]	-83.7 ± 8.4	-107.4 ± 12.4	**0.017**
	-92.2 ± 7.2	-118.8 ± 4.8	**0.001**
AP half-width [ms]	1.19 ± 0.16	0.92 ± 0.12	**0.015**
	1.03 ± 0.08	0.87 ± 0.06	**0.011**
Afterhyperpolarization [mV] from THR	-20.0 ± 3.0	-21.9 ± 2.7	0.142
	-17.4 ± 2.6	-19.1 ± 3.5	0.304

†, vs. CTL

Table 2. AP properties during our step depolarization protocol.

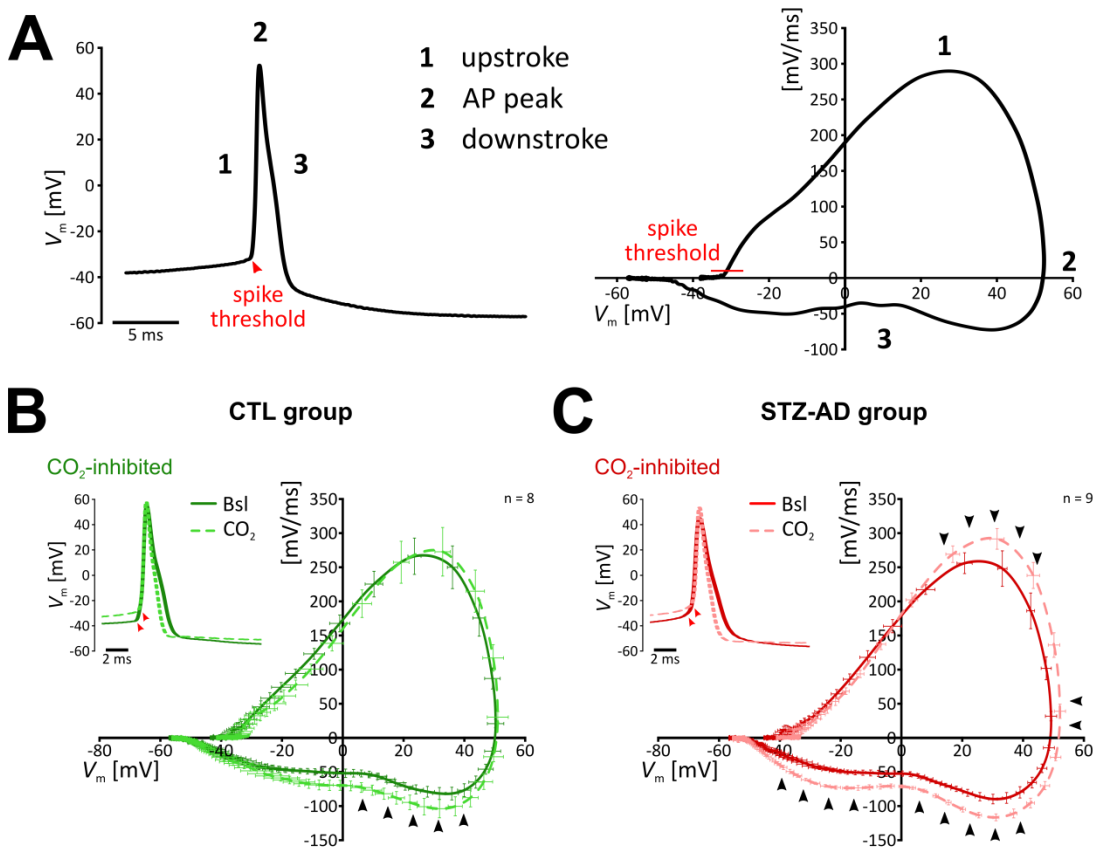

Figure 11. Action potential waveform for locus coeruleus (LC) neurons at baseline and increased CO_2. A) Representative action potential (AP) with the corresponding phase plane plot. Phase plane plots for CO_2-inhibited LC cells in the control (CTL) group (B) and the streptozotocin-induced Alzheimer's disease (STZ-AD) group (C). Insets show a representative AP at baseline (Bsl) and increased CO_2. Red arrowheads indicate a significant change in spike threshold. Black arrowheads indicate significant changes to baseline (see Table 2). Data are expressed as mean ± SEM. V_m = membrane potential.

3.8 CO_2 Modulates Currents Through Voltage-Gated K^+ (K_V) Channels

Because of the CO_2-induced increase of AP repolarization and the reduction of AP discharge in the majority of LC neurons, we analyzed the potential contribution of outward K^+ currents. We used step depolarization of the membrane from −100 to +80 mV (20 mV steps) to elicit outward K^+ currents in LC neurons. Figure 12A shows representative K^+ currents during baseline and at 10% CO_2 in a LC cell that was inhibited by CO_2. The blue

lines depict the time points used to measure the current-voltage (IV) relationship of transient (beginning of the stimulus) and steady-state (end) currents for each voltage step. Results for the steady-state current of CO_2-inhibited cells in the CTL and STZ-AD groups are shown in Figure 12B. The IV relationship of both groups comprised a significant reduction of steady-state K^+ current with perfusion of 10% CO_2. This decrease of outward K^+ currents occurred at membrane potentials greater than +20 mV, a range that is typically associated with activity of K_V channels (JOHNSTON; FORSYTHE; KOPP-SCHEINPFLUG, 2010; MATHIE; WOOLTORTON; WATKINS, 1998). Interestingly, a reduced steady-state K^+ current with depolarization would facilitate AP discharge. Enhanced AP discharge to CO_2 was not observed in this group of LC neurons, likely indicating a minor role of steady-state K^+ currents on overall neuronal spike activity. While steady-state IV curves at baseline were similar between groups, CO_2 induced a significantly greater reduction of steady-state current in STZ-AD rats than in control animals.

A reliable increase in transient K^+ current (calculated by subtracting the steady-state current from the initial current at the beginning of the voltage step) was seen for CO_2-inhibited cells between -40 to +40 mV under baseline conditions (Fig. 12C), which is consistent with the response typical for A-type K^+ channels (K_A) channels (SONNER; STERN, 2007). Responses of K_A channels became variable at membrane potentials of +40 mV and higher. The transient current increased in CO_2-inhibited cells when exposed to hypercapnia. While this change was only a strong trend in the control group at 0 mV membrane potential and amounted to an increase of ~135% (baseline, 0.142 ± 0.033 nA vs CO_2, 0.337 ± 0.078 nA; $p = 0.059$; $n = 8$), cells of the STZ-AD group were significantly increased by ~170% (baseline, 0.153 ± 0.054 nA vs CO_2, 0.417 ± 0.045 nA; $p \leq 0.05$; $n = 9$).

The CO_2-dependent increase of K_A current in CO_2-inhibited cells can antagonize AP generation (LI; PUTNAM, 2013) and may in part explain the observed decrease in AP discharge.

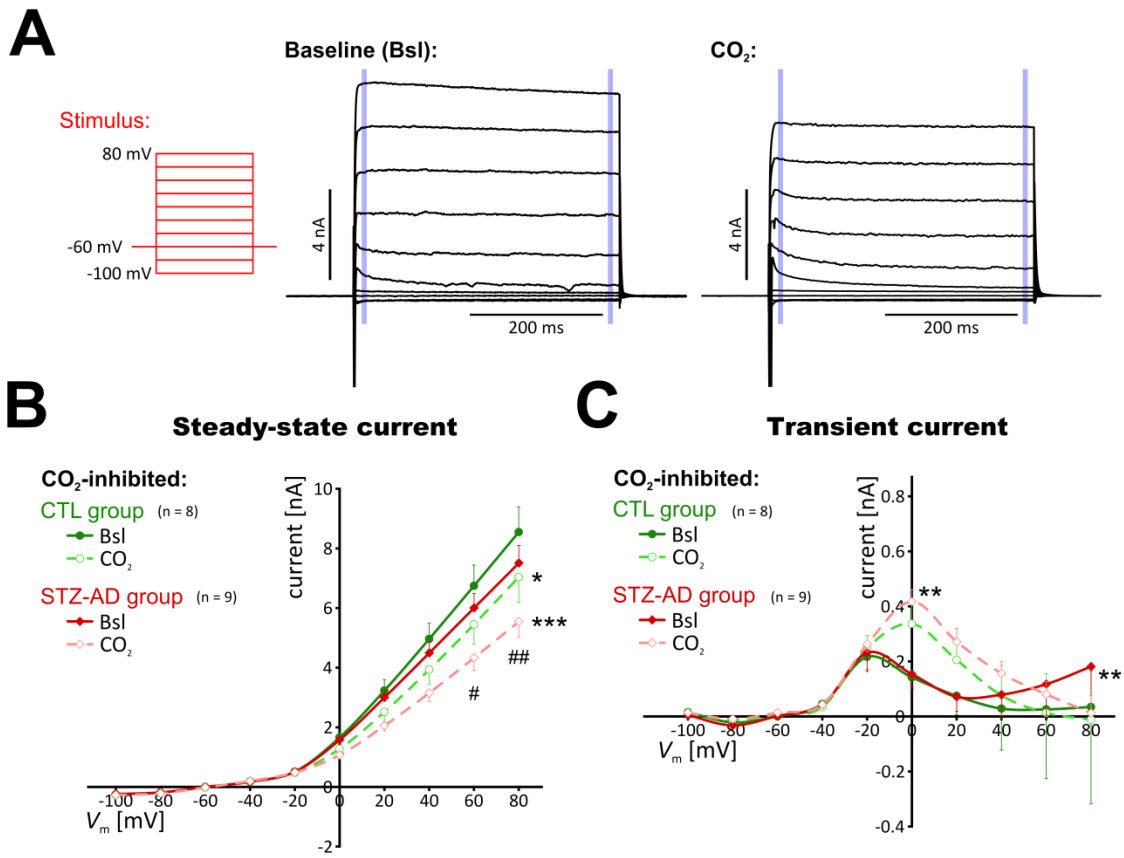

Figure 12. Current-voltage relationship for K^+ channels in locus coeruleus (LC) neurons at baseline and during 10% CO_2. A) Typical example of currents elicited by step changes of the membrane potential from -100 mV to +80 mV (20 mV step, 400 ms) in a CO_2-inhibited LC neuron at baseline (Bsl) and CO_2. The blue lines describe the time points for measurements of the transient (beginning of stimulus) and steady-state current (end of stimulus) at each voltage step. B) Steady-state K^+ currents of cells inhibited by CO_2 in the control (CTL) and streptozotocin-induced Alzheimer's disease (STZ-AD) groups. C) Transient K^+ currents of cells inhibited by CO_2 in the CTL and STZ-AD groups. Data are expressed as mean ± SEM. * $p \leq 0.05$, ** $p \leq 0.01$, and *** $p \leq 0.001$ indicated a difference from the Bsl condition. # $p \leq 0.05$, ## $p \leq 0.01$ indicated a difference between the STZ-AD and CTL groups; 2-way repeated measures ANOVA. V_m = membrane potential.

The current study showed that the majority of noradrenergic LC neurons in adult rats (64% in the STZ-AD group and 57% in the CTL group) were inhibited by CO_2 as indicated by a significant decrease in AP discharge to current injections. The remainder of cells either increased AP discharge (~20%) or did not respond (~20%). The STZ-AD group also had a greater sensitivity to CO_2 than controls as demonstrated by a significantly stronger inhibition of spike discharge during hypercapnia, which was in part from hyperpolarization of the RMP. Reduction of AP discharge in both groups was generally accompanied by lower LC network activity, depolarized AP threshold, increased AP repolarization, and increased current through a subpopulation of K_V channels. The latter result was indicated by enhanced transient K_V currents (strong trend in the control group and significant change in the STZ-AD group). Interestingly, steady-state K_V currents were reduced under hypercapnia, a change that would favor enhanced AP discharge. However, the collective response of most LC neurons in adult rats was inhibited by CO_2.

In the current study, STZ-AD rats had impairment in learning and retention of spatial memory when tested in the Morris water maze. These data corroborate previous studies demonstrating learning and memory deficits with brain-injection of STZ (Ebel et al., 2017; Motzko-Soares et al., 2018; Salkovic-Petrisic et al., 2013; Vicente et al., 2018) and therefore, we were able to reproduce the cognitive alterations found in patients with AD (Kumar et al., 2015; Qiu et al., 2019). It is well known that LC is involved in regulating a broad range of higher cognitive functions, such as working memory, learning and attention (Aston-Jones and Cohen, 2005; Benarroch, 2009; Mather and Harley, 2016; Robbins, 1984), as well as memory consolidation and retrieval (Sara, 2009; Sterpenich et al., 2006). We have

previously observed an increase of amyloid beta peptide in the LC of STZ-AD animals (Vicente et al., 2018). In fact, selective lesions of LC neurons exacerbate AD neuropathology and cognitive deficits in both amyloid-based transgenic mouse models and mouse models of tauopathy (Hammerschmidt et al., 2013; Heneka et al., 2010). Therefore, decreased cognitive function in STZ-treated rats may be related to neuronal alterations occurring in the LC–noradrenergic system.

The majority of studies analyzing LC neuron responses to CO_2 were done in neonatal rodents (FILOSA; DEAN; PUTNAM, 2002; OYAMADA et al., 1998; RITUCCI; DEAN; PUTNAM, 2005; STUNDEN et al., 2001). In these studies, up to 80% of LC neurons in neonates (postnatal <10 days) were activated/depolarized by CO_2 in the presence of synaptic blockage (i.e., neurons were intrinsically chemosensitive to CO_2). Studies in older neonates (postnatal >10 days) showed only 20%–40% of LC neurons were activated/depolarized by hypercapnia (GARGAGLIONI; HARTZLER; PUTNAM, 2010; NICHOLS et al., 2008), indicating that the number of CO_2-activated LC neurons is dependent on the age of the animal. Although no synaptic blocker was used in the current study, meaning changes may not exclusively arise from intrinsic chemosensitivity, we also found a low number of activated LC neurons (up to 21%) in 8-9 week old rats (Figs. 3E and 3F). The majority of neurons (more than 57% of cells independent of group) were inhibited by CO_2 exposure as indicated by reduced current-evoked spike discharge (Fig. 4) and overall lower network activity (Fig. 5). These results, in conjunction with the above mentioned previous studies, indicate that inhibition by CO_2 may be unique to LC neurons in adult animals only. Similarly, Lopes et al. (2016) showed a hypercapnia-induced decrease in firing rate of LC neurons projecting to the commissural nucleus tractus solitarii, a brainstem area heavily

involved in respiratory control. According to Imber et al. (2018), blunted CO_2-responses of LC neurons in older animals is related to a developmental increase in Ca^{2+}-activated BK channel current. Hypercapnic acidosis raised intracellular Ca^{2+} content and led to BK channel-dependent lowering of spike discharge to CO_2. This process is known as brake phenomenon and appears to be minimally active in the LC neurons of newborn rats, but develops over the first two weeks of life. The influence of such a limiting mechanism may increase with advanced age and result in a general inhibition to hypercapnia as observed in the current study. Additional changes, such as the hypercapnia-induced increase in transient K_V currents (this study), may further contribute to the developmental brake mechanism, ultimately lowering output of LC neurons in adult animals in response to CO_2.

Hypercapnic exposure significantly altered currents through K_V channels. Steady-state K^+ currents, presumably from delayed-rectifying K^+ channels (K_{DR}) (Mathie et al., 1998), were significantly reduced under CO_2 in all LC neurons in the current study. CO_2-sensitivity of K_{DR} in LC neurons has been previously reported in neonates (FILOSA; PUTNAM, 2003; LI; PUTNAM, 2013). Similar to our data, these studies showed hypercapnia-induced inhibition of K_{DR} currents. A reduction in K_{DR} current likely favors excitatory responses; however, spike discharge to CO_2 was reduced in the majority of LC neurons in our study, suggesting a minor role for decreased steady-state currents at least in adult rats. Conversely, transient K^+ currents from K_A channels (Mathie et al., 1998) may play a greater role whether LC neurons increase or decrease spike discharge in response to CO_2. The strong impact of K_A on spike discharge was previously reported in neonatal LC neurons, where blockade of K_A led to increased spike discharge (LI; PUTNAM, 2013). The opposite may then hold true for the response of LC cells from this study that increased K_A

current and decreased AP discharge. Similarly, K_A are well known to modulate AP delay (Dekin and Getting, 1987; Schild et al., 1993). Our data on the delay of the first AP (to 100 pA current injection) is consistent with CO_2-induced modulation of K_A. However, other channels (e.g. those controlling RMP or AP threshold) may change AP delay as well (Corbin-Leftwich et al., 2018; Noble, 1966). K_A also significantly influences AP waveforms (SONNER; STERN, 2007). Blocking K_A resulted in a lower THR and widened APs from delayed repolarization. Enhanced K_A current may then lead to increased THR and reduced AP width. These changes were observed in the majority of LC neurons from the current study and suggest an important role of K_A on the activity of LC neurons during hypercapnic conditions.

Few studies address the CO_2 response of LC neurons in adult rats. Elam et al. (1981) performed extracellular recordings in single LC neurons in intact anesthetized rats (200-300 g, ~7-9 weeks of age), where CO_2 was supplied through the inspired gas mixture. That study reported increased activity of LC neurons in response to hypercapnia, but there was no information about the percentage of cells that responded to activation with CO_2. Similar to our current-evoked AP discharge, increased activation of LC neurons may resemble external inputs that drive neuronal activity of LC neurons to CO_2. In intact animals, such input may stem from other chemosensitive brain regions like the retrotrapezoid nucleus, medullary raphe, and commissural nucleus tractus solitarii (LOPES et al., 2016; PUTNAM; FILOSA; RITUCCI, 2004). Thus, whether CO_2 modulates or attenuates spike discharge in LC cannot be concluded from experiments with intact connections to the LC. A study by Pineda and Aghajanian (1997) used slice preparations from adult rats (170-220 g, ~6-7 weeks) and found a depolarizing effect of CO_2 on LC neurons. Their slice thickness was 600 µm and cut

in coronal orientation; these two factors allow for intact tracts/inputs coming from more ventral chemosensitive regions in the same slice (e.g., retrotrapezoid nucleus, medullary raphe). Again, in this preparation it cannot be excluded that responses of LC neurons may be driven by input from other centers. We used 250-µm thick horizontal slices containing the dorsal portion of the LC. This preparation excludes respiratory centers that are situated more rostral, ventral, and caudal from the LC and therefore resembles a highly reduced preparation that may reveal responses of LC neurons to CO_2 with very limited external drive.

A direct comparison between our groups showed that the hypercapnia-induced inhibition of LC neurons was exaggerated in the STZ-AD group (Fig. 4B). Mechanisms contributing to this stronger inhibition may be the significantly reduced RMP and associated decrease in R_i (Table 1). Potential candidates for this change are two-pore-domain (GOLDSTEIN et al., 2001) and inwardly rectifying K^+ channels (XU et al., 2000), which have been previously shown to exhibit CO_2/pH-sensitive properties in LC neurons (FILOSA; PUTNAM, 2003; PINEDA; AGHAJANIAN, 1997) although with different consequences for the cell than observed in the current study. Hyperpolarization of RMP in conjunction with a depolarized THR significantly increased the difference from RMP to THR and, thus, the voltage required for spike generation. This difference in RMP to THR was more pronounced in the STZ-AD model than the CTL group (Table 2). Depolarized THR, reduced AP half-width, and enhanced AP repolarization under CO_2 can be attributed to the increase in K_A currents (see above). This change was significant in the STZ-AD group only (trend in the CTL group). Further, the hypercapnia-induced reduction of K_{DR} was more pronounced in the STZ-AD group than in the control group (Fig. 7B). Given the mainly inhibitory actions of CO_2, the impact of reduced K_{DR} on spike discharge seems minimal. The combined data from

the current study indicates an overall increased CO_2-sensitivity of LC neurons in the STZ-AD group, a change that ultimately led to pronounced inhibition of the LC during hypercapnic conditions. We also found a significant increase in AP peak and rising slope. These results (and potentially the changes to THR) may arise from altered voltage-gated Na^+ channels (GHOVANLOO; PETERS; RUBEN, 2018); however, specific involvement in the CO_2-response of LC neurons has not yet been reported.

Although responses of LC neurons in the control and STZ-AD groups differed considerably during hypercapnic conditions, baseline responses were similar between groups. These results agree with our previously published in vivo study about respiratory response to high CO_2 conditions (Vicente et al., 2018). In that study, the STZ-AD group had no changes in basal ventilation, but the ventilatory reflex to hypercapnia was significantly stronger than in the control group. Thus, the respiratory response of the STZ-AD rat model to CO_2 exhibited a higher sensitivity to CO_2, which is similar to the responses of LC neurons in the current study. Changes in respiratory function were also correlated with increased amyloid beta protein in the LC region. It has been previously shown that AD modulates K^+ channel expression in humans (Angulo et al., 2004). Amyloid beta also alters currents through K_A, K_{DR}, and voltage-gated Na^+ channels in cortical and hippocampal tissue of AD animal models (Chen, 2005; Pan et al., 2004; Verret et al., 2012; Yu et al., 1998). Although some results from these studies are inconsistent (possibly from tissue-specific effects), it is likely that amyloid beta in the STZ-AD rat model affects the function of K^+ and Na^+ channels in the LC. Furthermore, ion imbalance (increased [Na^+] and [K^+]) was shown in the cerebrospinal fluid of AD patients (VITVITSKY et al., 2012). Increased extracellular [Na^+] could also account for the observed increase in AP rising slope and peak in the current study.

Previous studies of AD patients and AD animal models have mainly concentrated on the cortex and hippocampus. AD patients have also been shown to exhibit a high prevalence of breathing problems (BOEVE, 2008; GAIG; IRANZO, 2012; LEE et al., 2019; OSORIO et al., 2014), but currently there is no information on changes of neuronal activity associated with respiratory dysfunction in AD. To our knowledge, our study reports the first data on neuronal changes in the LC of the brainstem with abnormal response properties under respiratory stress conditions in an animal model for sporadic AD. We did not observe any changes in LC neuron number in the STZ-AD group, suggesting we were analyzing an early stage of the disease as shown in human patients with successive loss of LC neurons in the course of AD (KELLY et al., 2017; THEOFILAS et al., 2017). This finding also indicates that AD-induced changes of LC output are not necessarily due to lower neuron number; they may rather be the result of altered intrinsic neuronal properties.

5 CONCLUSION

In summary, our study shows that the responses of LC neurons to CO_2 in the STZ-induced model for sporadic Alzheimer's disease is enhanced and potentially involves AD-induced changes in voltage-gated K^+ and Na^+ channels. The exaggerated inhibitory response of the LC to hypercapnia may be an underlying mechanism for the breathing disturbances observed in patients with AD.

AUTHOR CONTRIBUTIONS

MCV, LHGB, and TDO designed the study. MCV performed all experiments. MCV and CMH prepared and analyzed immunohistochemical data. MCV and TDO analyzed the data, prepared figures, and drafted the manuscript. MCV, LHGB, and TDO interpreted the data and edited the manuscript. All authors approved the final manuscript version.

ACKNOWLEDGEMENTS

We thank Dr. D. S. Middlemas (A.T. Still University) for provision of his microscope, Jeong Sook Kim-Han (A.T. Still University) for her help and expertise using the confocal microscope in the university's imaging core, and Deborah Goggin (A.T. Still University) for improving the grammar of the manuscript. This work was supported with the FAPESP stipend 2017/21750-9 to MCV and seed money from A.T. Still University's Kirksville College of Osteopathic Medicine to TDO.

CHAPTER 3

Inactivation of microglia cells improves cognitive, but not respiratory, sleep-wake and β-amyloid dysfunction in a sporadic model for Alzheimer's Diseases.

IN PREPARATION

1 ABSTRACT

Neuroinflammation in Alzheimer's disease (AD) can occur due to excessive activation of microglia cells in response to the accumulation of amyloid beta peptide. In our previous study, we demonstrated an increased expression of beta amyloid peptide in the Locus coeruleus region (LC) in a sporadic model for Alzheimer's disease (icv, streptozoticin, STZ, 2 mg/kg). We hypothesized that the STZ-AD model exhibits a condition of neuroinflammation and treatment with a microglia inhibitor (minocycline) reverse the cognitive, respiratory, sleep and molecular disorders of this model. To this end, we treated control and STZ rats for five consecutive days with minocycline (30 mg/kg, ip) and evaluated cognitive performance (Barnes maze), chemoreflex response to hypercapnia (7% CO_2) and hypoxia (10% O_2) and total sleep time. In addition, quantification of beta amyloid peptide in the LC region was performed by Wester Blotting technique and analysis of microglia cells by immunohistochemistry for IBA-1. Minocycline treatment improved learning and memory, possibly due to the decrease in cell density and inactivation of microglia cells in the LC region. However, the treatment did not reverse the increased sensitivity to CO_2 during wakefulness in room air. Similarly, we did not observe a decrease in the expression of beta-amyloid peptide in the LC region after treatment. Our finding suggests that minocycline effectively reduced cognitive impairment, which is possibly associated with LC microglia inhibition but failed to suppress beta amyloid expression and normalize CO_2 ventilatory response.

Keywords: microglia, minocycline, locus coeruleus, streptozotocin, Alzheimer

2 **INTRODUCTION**

Alzheimer's disease (AD) is characterized by the extracellular accumulation of beta-amyloid peptide (βA_{1-42}) that forms the senile plaques (BLENNOW et al., 2015) and by formation of intracellular neurofibrillar tangles (NFTs), which arise from the collapse of the neuronal cytoskeleton, resulting from the hyperphosphorylation of the Tau protein associated with the microtubule (JACK et al., 2018; VILLEMAGNE et al., 2015). In the progression of AD these biomarkers promote reduction in synaptic density, neuronal and axonal damage and neuroinflammation (ARENDT, 2009; BOS et al., 2019; MILÀ-ALOMÀ et al., 2020; NORDENGEN et al., 2019).

In fact, neuroinflammation in AD results from the activation of microglia cells in response to the formation of amyloid plaques and/or hyperphosphorylation of tau protein (CAGNIN et al., 2001; MAWUENYEGA et al., 2010; TEJERA; T. HENEKA, 2016). Under normal circumstances, activated microglia plays a neuroprotective role, secreting several pro-inflammatory cytokines and chemokines that recruit additional microglia and astrocytes to the inflammatory site (GUERRIERO et al., 2017; SARDI et al., 2011; TEJERA; T. HENEKA, 2016). In sporadic cases of AD, inefficient clearance of Aβ by microglia has been identified as a major pathogenic pathway (MAWUENYEGA et al., 2010). Furthermore, prolonged activation of proinflammatory cytokines affects the activity of the beta secretase enzyme, which is responsible for the cleavage of the beta-amyloid precursor protein (APP) in the formation of amyloid beta peptides (HICKMAN; ALLISON; EL KHOURY, 2008; MCGEER; MCGEER, 2013; SASTRE et al., 2006; SASTRE; WALTER; GENTLEMAN, 2008). This process results in elevation of Aβ burden which again activate more microglia, developing a vicious neurotoxic cycle (GRATHWOHL et al., 2009; STANDRIDGE, 2006).

The released cytokines increase the neurodegeneration of adjacent neurons that add to the inflammatory process, triggering a of cellular deterioration (Cai et al., 2011; Latta et al. 2015; Heneka et al. 2015, Salter & Stevens, 2017). Indeed, many observations supports that microglial activation triggered by Aβ is likely an early event in AD pathology (JANELSINS et al., 2005; STANDRIDGE, 2006).

In our previous study, we demonstrated that STZ rats showed increased Aβ peptide in the LC region that is possibly leading to an augmented sensitivity to CO_2, an increase in the percentage of time in the awake state and cognitive impairment (VICENTE et al., 2018). In addition, we found no evidence of increased expression of TAU and Aβ peptide in the hippocampus region. These molecular findings data lead us to suggest that STZ-rats are in the initial stage of the progression of AD (BRAAK; DEL TREDICI, 2011a; GRUDZIEN et al., 2007; P. et al., 2017). It has been shown that LC is one of the first regions affected in the progression of AD and clinical evidence suggests that aberrant tau accumulation in this region may be a critical early step in AD progression (BRAAK; DEL TREDICI, 2011a; RORABAUGH et al., 2017). Hence, the increased expression of the Aβ peptide in the LC region may cause an initial neuroinflammation that contributes to the cognitive and physiological deficits found in the model. Thus, interrupting the initial process of AD by drugs may represent a therapeutic target in minimizing and/or reversing the molecular pathological events that are reflected in the cognitive and physiological problems of patients with AD.

Minocycline has been demonstrated to be capable of preventing buildup of β-amyloid (Aβ) or tau accumulation and also reduces interleukin and tumor necrosis factor levels (FERRETTI et al., 2012; LI et al., 2018; PARACHIKOVA et al., 2010; XU et al., 2020).

Minocycline is a second generation derivative of tetracycline with strong anti-inflammatory and anti-apoptotic agent (BUDNI et al., 2016; GARRIDO-MESA; ZARZUELO; GÁLVEZ, 2013a). The anti-inflammatory properties of this drug are possibly due to its ability to inhibit mitogen-activated protein kinase p38 (p38 MAPK) and matrix-9 metalloproteinase (MMP-9) (HUNTER et al., 2004; KIM; SUH, 2009; SCHIEVEN, 2009). Since protein kinase p38 regulates the production of inflammatory mediators, its inactivation by the action of minocycline may reduce cytokines released in excess providing neuroprotection against neuronal damage from neuroinflammation (BUDNI et al., 2016; SCHIEVEN, 2009). In this scenario, the present study evaluated the treatment of minocycline on cognition, ventilation, sleep-wake cycle, expression of amyloid beta peptide and microglia morphology in the LC region in a sporadic model for AD.

3.1 Animals

We used Wistar rats 3-4 months old (weight 300–350 g). The animals were maintained in temperature-controlled chamber at 24–26° (ALE 9902001; Alesco Ltda., Monte Mor, SP, Brazil) with a 12:12- h light/dark cycle, and had free access to water and food. The experiments were performed between 08.00 a.m. and 17.00 p.m.

The study was conducted according to the guidelines of the Brazilian College of the National Council for the Control of Animal Experimentation (CONCEA, MCT, Brazil) and with the approval of-the Faculty of Agricultural and Veterinary Sciences and Animal Care, Use Committee (CEUA, FACV-UNESP, Jaboticabal campus; Protocol n◦ 05796/19).

3.2 Surgical procedures

All surgical procedures were performed under anesthesia with an intraperitoneal injection of 100 mg/kg of ketamine (Union National Pharmaceutical Chemistry S/A, Embu-Guacu, SP, Brazil) and 10 mg/kg of xylazine (Laboratories Calier S/A Barcelona, Spain). Postoperatively, the animals were treated with antibiotic (enrofloxacin, 10 mg/kg, intramuscular) and analgesic (flunixin meglumine, 2.5 mg/kg, subcutaneous) agents and 3mL of 0.9% sodium chloride solution for fluid reconstitution.

3.2.1 Sporadic Alzheimer's Disease Model

Similar to our previous studies (VICENTE et al., 2018, 2020) the model for sporadic model for AD was induced by pressure injection of a subdiabetogenic dose of STZ (2 mg/kg,) into both lateral ventricles of the brain (2μL per side). The control group received vehicle 0.05 mol/L citrate buffer, pH 4.5. The rats were fixed to a Kopf stereotaxic apparatus

(David Kopf Instruments, Tujunga, CA, USA). The scalp was incised over the sagittal suture, the periosteum was excised, and two small bilateral orifices were made using a sterilized dental drill to access both lateral ventricles of the brain, where icv injections were to be applied. The following coordinates were used: –0.8mm posterior, ±1.4mm lateral, and –4.4 below bregma (PAXINOS; WATSON, 2007). For the microinjection of drug and vehicle, a 5-µL Hamilton syringe was used, linked to a PE 10 polyethylene tubing, connected to a gengival needle for the application. Thirty days after icv injection, rats were submitted to the behavioral, respiratory, or molecular tests. The respiratory and microglia tests were performed in a same group of animals, whereas the behavioral and β- amyloid tests were performed in the same group.

3.2.2 Electroencephalogram (EEG) and electromyogram (EMG) electrodes

For analysis of ventilation and time spent in the different phases of the sleep-wake cycle, we performed the surgery to implant EEG and EMG electrodes (VICENTE et al., 2016a, 2018). Seven days before the experiments three EEG electrodes were introduced: the frontal electrode, located 2 mm anterior to bregma and 2 mm lateral to the midline; the parietal electrode, positioned 4 mm anterior to the lambda and 2 mm lateral to the midline; and the electrode "ground" which was inserted between the frontal and parietal electrodes. For EMG recordings, a pair of electrodes were inserted deep into the neck musculature of the rats.

3.3 Body temperature

For temperature measurements during experiments, on the same day as implantation of the electrodes, the rats underwent a second surgery for the implantation of a temperature

datalogger (SubCue Dataloggers, Calgary, Canada) into the abdominal cavity through a midline laparotomy. The datalogger was programmed to acquire body temperature (Tb) data every 5 min.

3.4 Minocycline treatment

We performed the treatment with minocycline (M9511, Sigma-Aldrich, St Louis, MO, USA) that started 5 days before the behavioral and/or respiratory experiments, at a dose of 30 mg / kg, via intraperitoneal injection (ip) (LIMA-SILVEIRA et al., 2019; MIYAMOTO et al., 2016; SILVA et al., 2018). Minocycline was daily prepared (30 mg minocycline for 1 mL vehicle / Vehicle, pH adjusted to 7.4) and the animals received a daily dose of the vehicle (50% saline + 50% distilled water) or minocycline for 5 days. Rats were randomly divided into 4 groups: Group 1- rats that received icv vehicle + ip Vehicle (Vehicle-Vehicle); Group 2- rats that received icv STZ + ip Vehicle (Vehicle-STZ); Group 3- rats that received icv vehicle + ip minocycline (Minocycline-Vehicle) and Group 4- rats that received icv STZ + ip minocycline (Minocycline-STZ).

3.5 Behavioral test

To assess the effect of minocycline treatment on cognition and spatial memory we used the Barnes maze. The Barnes maze test consists of a non-aquatic test for memory and spatial learning (SHARMA; RAKOCZY; BROWN-BORG, 2010). The maze was made from a circular, 13-mm thick, white PVC platform (110-cm diameter) with twenty holes (10 cm in diameter, 7.5 cm between each hole) and it was divided into target hole (T), opposite hole (OP), 9 holes clockwise (1 to 9, counting from T), and 9 holes counterclockwise (–1 to –9, counting from T). The escape cage, below the T hole, had walls covered with black plastic to

make the inside dark and attractive to the rats. The platform was also illuminated with a fluorescent white light and visual cues (colored geometric figures) were placed around the labyrinth as points of spatial reference for the animal to escape from the open platform to the "target hole" These clues were not removed throughout the experiment. After testing each rat, as explained below, the whole maze was cleaned using 10% ethanol to avoid olfactory cues and the platform was rotated to avoid intra-maze odor or visual cues. All sessions were recorded by a video camera for further analysis. Prior to testing (probe day), training sessions were performed over 5 days to familiarize the animals with the maze and to allow them learn the location of the escape zone. The learning (acquisition phase) and memory (probe test) protocol was used the same as that performed in our previous study (VICENTE et al., 2018).

3.5.1 Experimental Protocol Behavioral test

In acquisition phase, we evaluated spatial learning through latency to enter the target hole. These step consisted of 4 trials (T1-T4) per day with an inter-trial interval of 15 min for 4 consecutive days (D1-D4), during which a rat could explore the maze for 3 min in each trial. The end of the trial was considered when the animal entered the target hole. Therefore, the animal was allowed to stay inside the dark cage for 1 min and, after this period, was returned to its home cage. If the animal had not entered in the target hole after 3 min from the beginning of the test, it was gently coerced to the target hole.

In the probe trial, we evaluated memory consolidation. After the last training day, the escape cage was removed, while the maze was maintained in the same position as in the training days. The animal was allowed to explore the maze for 90 s. The probe trial was performed in order to determine whether the animals remembered the location of the target hole. The number of times (pokes) the animal searched for the "target hole" was used as a

memory consolidation index (ADAMS et al., 2002; SHARMA; RAKOCZY; BROWN-BORG, 2010; SUNYER et al., 2007).

3.6 Respiratory Test

3.6.1 Ventilation

To evaluate the effect of minocycline treatment in respiratory sensitivity to CO_2 and hypoxia, we used the whole-body plethysmography method to measure of pulmonary ventilation (V_E) (BARTLETT; TENNEY, 1970; DRORBAUGH; FENN, 1955). Briefly, the rats were kept in a 5-L chamber ventilated with room air or a hypercapnic gas mixture containing 7% CO_2 (White Martins, Sertãozinho, Brazil) or a hypoxia gas mixture containing 10% O_2 (White Martins, Sertãozinho, Brazil) in low ambient noise conditions (VICENTE et al., 2018). The flow rate of the inflow gas into the animal chamber was monitored by a flowmeter (model 822-13-OV1- PV2-V4, Sierra Instruments, Monterey, CA). During measurements, the flow was interrupted, and the chamber was sealed for short periods of time (approximately 2 min); the pressure oscillations due to respiration were monitored by a differential pressure transducer (TSD 160A, Biopac Systems, Santa Barbara, CA). The signals were fed into a differential pressure transducer (DA 100C, Biopac Systems), passed through an analog-to-digital converter, and digitized on a microcomputer equipped with data acquisition software (MP100ACE, Biopac Systems). The sampling frequency was 1 kHz. The results were analyzed using the data analysis software Acqknowledge (v. 4.2.3 data acquisition system, Biopac Systems). Tidal volume (V_T) and respiratory frequency (fR) were calculated to estimate ventilation per breath. Tidal volume (V_T) was calculated applying Drorbaugh & Fenn's formula (1955):

V_T = VK x (PT/PK) x TB x (PB - PC) / TB x (PB - PC) – TA x (PB – PR),

where PT is the pressure deflection associated with each V_T, PK is the pressure deflection associated with the injection of the calibration volume (VK), TA is the air temperature in the animal chamber, PB is the barometric pressure, PC is the water vapor pressure in the animal chamber, Tb is the body temperature, and PR is the vapor pressure of water at Tb. The VE was calculated as the product of the fR and the V_T. Ventilation and V_T are presented under conditions of ambient barometric pressure, at Tb and saturated with water vapor (BTPS). Body temperature was monitored by temperature datalogger (SubCue Dataloggers, Calgary, Canada) and the air temperature in the animal chamber was constantly monitored using a thermoprobe (model 8502-10, Cole Parmer, Chicago, IL, USA). The animal chamber was considered saturated because of a water lane in the bottom separated from the animal by a grid, and so the Pc was calculated indirectly using an appropriate table (BERNARDS, 1976). The calibration for volume was obtained during each experiment by injecting the animal chamber with 1mL of room air.

3.6.2 EEG and EMG signals

The effect of minocycline on ventilation in sleep and wakefulness and on sleep-wake cycle of animals was analyzed using EEG and EMG records. Similar to other previous studies, the signals from the EEG and EMG electrodes were sampled at 1 kHz, filtered at 0.3–50 and 0.1–100 Hz, respectively, and recorded on a computer (NATTIE; LI, 2002; VICENTE et al., 2016b). Both wakefulness and NREM sleep states were observed consistently through the experiments, but periods of rapid eye movement (REM) sleep were

short and were not present in every experiment; thus, REM sleep phases were excluded from the analysis (VICENTE et al., 2016b).

3.6.3 Experimental Protocol Respiratory Test

The animals were placed in a plethysmographic chamber and V_E was recorded. The chamber was initially ventilated with moist atmospheric air (21% O_2) for an acclimation phase of at least 30 min. Ventilation control measurements were first performed during normocapnia for 63 min. Then, the animals were submitted to hypercapnia for 63 min, where the chamber was ventilated with a gas mixture containing 7% CO_2, 21% O_2 and balanced with N_2 (White Martins Gases Industriais Ltda, Osasco, SP). After hypercapnia, the chamber was ventilated with atmospheric air again for recovery of baseline V_E for 60 min. Finally, the animals were submitted to hypoxia for 63 min, where the chamber was ventilated with a gas mixture containing 10% O_2 and equilibrated with N_2 (White Martins Gases Industriais Ltda, Osasco, SP). The order of exposure to hypercapnia and hypoxia was randomly reversed. The ventilatory measures were analyzed at 7, 14, 21, 28, 35, 42, 49, 56, and 63 min after gas exposure. Then, based on the sleep/wake cycle, for the $\dot{V}_E$ measurements, we selected the phases when the animals were either in wakefulness or in sleep.

3.7 Molecular Test

3.7. β-amyloid peptide expression in the Locus coeruleus

For the study of the effect of minocycline on the expression of amyloid beta peptide in the LC region, we used the western blotting technique similar to previous study (VICENTE et al., 2018). After behavioral experiments, rats were randomly selected out of each group and the animals' brains were quickly removed, frozen in liquid nitrogen, and held

at –80◦C until dissection. In a cryostat at –22◦C, the brains were coronary-sectioned to find stereotaxic coordinates to LC (distance from bregma: –10.3 mm to –9.3 mm) (PAXINOS; WATSON, 2007). Samples of 1.0 -mm thickness were removed with a 15-gauge needle. After homogenized, protein quantification in the tissue was performed using the Lowry method (FAIM et al., 2019). Samples with 15 μg of protein were mixed with the sample buffer and heated to 95º C for 5 minutes. The samples were submitted to SDS-PAGE on a 10% gradient bis-acrylamide gel, in a buffer, pH 8.3. After transfer, nonspecific sites on the membrane were blocked with TBS-T buffer plus 5% bovine serum albumin (BSA) by 1 hour at room temperature, under constant agitation. After washing the blocking solution with TBS-T, the membranes were incubated overnight at 4ºC, with the anti-beta amyloid (mouse monoclonal-amyloid B-4, cat. sc-28365, Santa Cruz Biotechnology, 1:1000 dilution) in TBS-T solution plus 3% BSA. The membranes were washed five times for 5 minutes with TBS-T before adding the second peroxidase-labeled antibody (Santa Cruz Biotechnology), diluted 1: 5.000 in TBS-T plus 5% BSA for 1 h at room temperature. Then the membranes were washed five times for 5 minutes with TBS-T and then the chemiluminescence enhancer (ECL) and the exposed film were added.

The bands were quantified using the ImageJ program, available for free download at https://imagej.nih.gov/ij/download.html. The bands of the β-amyloid protein were normalized by actin.

3.8. Microglia Analyses

3.8.1. Immunohistochemistry for microglia cells in Locus coeruleus region

To confirm the neuroinflammation and the effect of the minocycline treatment in the AD model, we performed the morphological analysis of the microglia cells of the LC. After the experiments, the animals were perfused through the left ventricle of the heart with 0.9% saline followed by the 4% paraformaldehyde solution (PFA) in 0.1 M sodium tetraborate buffer (PFA / borax; pH 9.5 at 4C). Then, the brains were collected and fixed for 24 hours in 4% PFA / borax and placed in 20% sucrose for 48 hours at 4ºC and finally they were frozen and stored at -80ºC. On the day of the immunohistochemistry, the brain was cut into a cryostat in 40 μm coronal sections containing the LC region and the free-floating methodology was used for microglia labelling (TENORIO-LOPES et al., 2017). Similar to other studies, the labeling of microglia cells was performed by using the binding-adapter-molecule 1 (Iba-1), a protein present in microglia cells (ANSORG et al., 2015; BALDY et al., 2018a; KORZHEVSKII; KIRIK, 2016; TENORIO-LOPES et al., 2017, MARQUES et al., 2021).

The tissue containing the LC region was washed with Tris-buffered saline solution (TBS) at pH 7.4 for 10 minutes. Then, the endogenous activity of peroxidase was blocked for 30 minutes with 1% H_2O_2 in TBS. The tissue sections was washed 3 times (5 minutes each) in TBS, then the sections was incubated in blocking solution (1% BSA / 0.4% Triton X-100 in TBS) for 2 hours. The sections was then incubated with the primary antibody rabbit monoclonal anti-Iba-1(1:750; Cell Signaling Technology, Cat # 17198) for 12-18 hours at 4ºC. Sections were then washed 3 times again (10 minutes each) in TBS before incubation with the secondary antibody goat anti-rabbit IgG biotinylated (1:200-Vector Laboratories,

Cat #BA-1000-1.5) for 3 hours at room temperature. After incubation with the secondary antibody, the slices were washed 3 times in TBS (5 minutes each) and the avidin-biotin-peroxidase complex method (ABC-Vector Laboratories) were used and the sections were incubated for 2 hours. The slices were incubated in 0.5% H_2O to decrease the endogenous peroxidase activity (and background signal) (Ansorg et al., 2015). A final wash was performed in TBS (3 times, 10 min each) and the nickel chloride diaminobenzidine peroxidase method was used to reveal biotinylated secondary antibody (SigmaFast™ DAB with metal enhancer; Sigma Aldrich, St. Louis, MO, USA).

3.8.2. Microglia morphology in LC

Similar procedures described previously were used to analyze *cell density, microglia morphology* (mean soma area, mean arborization area, mean width and height of the arborization) and *nearest neighbor distance* (NND) using the Image J (NIH software, U.S. National Institutes of Health System) (BALDY et al., 2018a). We used 20X magnification objective for microglial density analysis and 40X magnification objective for cell body and arborization area measurements. For all parameters, analysis was performed on the right and left side of the LC.

The values used to calculate the cell density were given by the ratio between the total number of cells in the total area analyzed (LAWSON et al., 1990; VERDONK et al., 2016). The increase in the number of cells was indicative that the microglia cells may be being recruited in response to a stimulus. Within each structure, microglia morphology was evaluated by delineating manually the arborizations and cell bodies of 10 microglial cells; these values were used to calculate the morphological index (soma area/arborization area) (BALDY et al., 2018b; VERDONK et al., 2016, MARQUES et al., 2021). The

morphological index allows us to state that the variables considered favor the activated form of microglia cells, in relation to the resting form (TREMBLAY et al., 2010; VERDONK et al., 2016). After analyzing the morphology of 10 cells (as mentioned before), we selected those cells and all microglial cells closely to them and performed a point with 14 pixels in each microglia soma to exclude artefacts for subsequent analyzes using the plugin NND developed by Y. Mao in the Image J software. So, we measured the nearest neighbor distance (NND) between microglia as an indicator of cell motility (STOWELL et al., 2018).

3.9 Quantitative real-time RT-PCR

After behavioral experiments, rats were randomly selected out of each group and the animals' brains were quickly removed, frozen in liquid nitrogen, and held at –80◦C until dissection. In a cryostat at –22◦C, the brains were coronary-sectioned to find stereotaxic coordinates to LC (distance from bregma: –10.3 mm to –9.3 mm) (PAXINOS; WATSON, 2007). Samples of 1.0 -mm thickness were removed with a 15-gauge needle and rapidly homogenized in 500 μl of TRI Reagent (SigmaAldrich) reagent at 4◦C. Total cellular RNA was purified from tissue according to the manufacturer's instruction. The purity of total RNA was measured with a spectrophotometer and the wavelength absorption ratio (260/280 nm) was between 1.8 and 2.0 for all preparations. Reverse transcription was performed with a reverse transcription reaction (Superscript II; Invitrogen, Thermo Fisher Scientific,Waltham, MA, USA). Real-time PCR was performed using primers specific for the rats genes TNF-α, IL-10 and IL-β the levels of each gene were normalized to the levels of the rats Gapdh gene. Reactions were conducted on the ABI Prism 7500 Sequence Detection System using the SYBR-green fluorescence system (Applied Biosystems, Thermo Fisher Scientific, Waltham, MA, USA). The results were analyzed by the method of quantitative relative expression

$2^{-\Delta\Delta Ct}$ as previously described.35 Primer pairs for murine Gapdh, TNF-α, IL-10 and IL-β were as follows:

IL-1β F	GAAGTCAAGACCAAAGTGG
IL-1β R	TGAAGTCAACTATGTCCCG
TNF-α F	CAAGGAGGAGAAGTTCCCA
TNF-α R	TTGGTGGTTTGCTACGACG
IL-10 F	TAAGGGTTACTTGGGTTGCC
IL-10 R	TATCCAGAGGGTCTTCAGC
GAPDH F	GTTTGTGATGGGTGTGAACC
GAPDH R	TCTTCTGAGTGGCAGTGATG

3.10 Statistical Analysis

Behavioral data were analyzed using two-way ANOVA followed by Holm-Sidak post-test. The results of ventilation, sleep/wake cycle and body temperature in room air, hypercapnic, and hypoxic conditions were evaluated by two-way ANOVA, followed by Bonferroni post-test. The quantification of Aβ peptide, microglia parameters and cytokines mRNA were validated through one-way ANOVA. The significance level adopted for all results was $p < 0.05$. Group data are presented as mean ± SEM.

4.1 Minocycline improves learning and memory in the STZ-AD model

Similar to VICENTE et al. (2018), in the acquisition phase, the latency of the STZ-AD model to find the target hole during trials was greater over the time compared to the control animals (Vehicle-STZ: Day 1:T1 166.4 ± 13.6 vs Day 4:T4 57.9 ± 21.1 seconds) vs (Vehicle-Vehicle: Day 1:T1 135.9 ± 10.4 vs Day 4:T4 5.6 ± 1.07 seconds) ($p < 0.05$; two way ANOVA) (Fig. 1B). This difference between Vehicle animals (STZ vs vehicle) remained at the average of trial per day (Fig. 1A). During the acquisition phase, minocycline treatment in STZ rats reduced the time to find the target hole in the platform during trials on days 1 and 2 compared to STZ group treated with Vehicle (Day 1- Minocycline-STZ: 106.3 ± 17.4 vs Vehicle-STZ: 159.0 ± 14 seconds) and 2 (Day 2- Minocycline-STZ: 54.3 ± 16.2 vs Vehicle-STZ: 117 ± 21.3; $p < 0.05$; two way ANOVA) (Fig. 1B). No difference between treatments was observed on days 3 and 4 (Fig. 1B). However, when analyzing the average training per day, we observed that minocycline treatment improved the performance on the platform over the days in STZ rats (Fig. 1A). In addition, treatment with minocycline in the vehicle did not alter the performance on the platform compared to the Vehicle-vehicle group.

On the test day, the average number of pokes of the in the target hole was lower in STZ rats compared to the vehicle (Vehicle-STZ: 2.2 ± 0.3 vs Vehicle-Vehicle 6.6 ± 2.9; $p < 0.05$, two-way ANOVA). After treatment with minocycline, STZ rats improved the performance on the platform due to the increased number of pokes compared to the Vehicle-STZ-group (Minocycline-STZ: 3.7 ± 0.9 vs Vehicle-STZ: 2.2 ± 0.3 $p < 0.05$, two-way ANOVA) (Fig. 1C). There was no significant difference between treatments in the other

holes of the platform. In addition, the performance on the platform was not different between Minocycline-Vehicle and Vehicle-Vehicle groups.

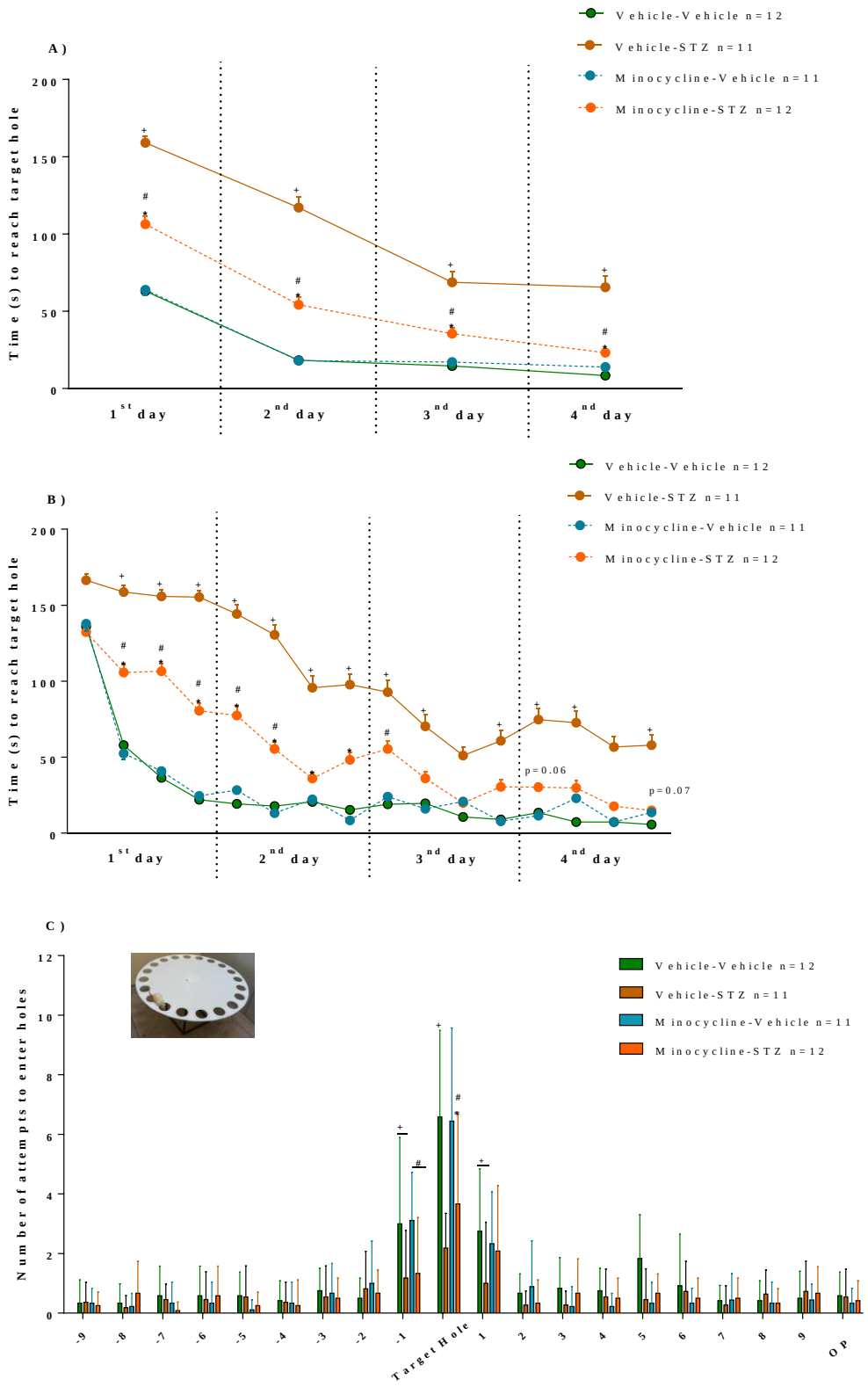

Figure 1. **Minocycline improves learning and memory in the STZ-AD model.** A) Minocycline treatment (30 mg/kg, i.p, 5 days) on time to reach the target hole in seconds of the Vehicle (control and STZ) vs Minocycline (control and STZ) groups in the 4 training sessions per day (1st to 4th day). B) The average time per day to find the target hole in seconds of the Vehicle (control and STZ) vs Minocycline (control and STZ) groups. C) Number of attempts to enter into the holes inthe platform test pattern in the control and STZ group. Values are expressed as mean ± SEM. * indicates a significant difference between the Vehicle-STZ vs Minocycline-STZ. + indicates a significant difference in the Vehicle (Vehicle vs STZ) groups. # indicates a significant difference between the Minocycline (Vehicle vs STZ) groups.

4.2 Minocycline treatment did not restore CO_2 sensitivity during wakefulness in the STZ-AD model

We did not observe differences between groups in respiratory variables in room air conditions during wakefulness (Figs. 2 and 3). In hypercapnia and hypoxia, all groups showed a significant increase in ventilation when compared to room air conditions ($p < 0.0001$; two-way ANOVA) (Figs. 2 and 3).

Similar to our previous study, under hypercapnia we observed that the Vehicle-STZ animals increased ventilation compared to vehicle animals during wakefulness (Vehicle-STZ: 2479.1 ± 125.5 vs Vehicle-Vehicle: 1930 ± 70.2 mL. Kg^{-1}. min^{-1}; $p < 0.05$; two-way ANOVA) and this effect was due to the increase in V_T (Vehicle-STZ: 17.9 ± 0.6 vs Vehicle-Vehicle: 13.4 ± 0.5 mL. Kg^{-1}; $p < 0.05$; two-way ANOVA). Minocycline treatment did not reverse the increase in ventilation under hypercapnia in the awake in the STZ animals (Minocycline-STZ: 2581.3 ± 92.2 vs Vehicle-STZ: 2479.1 ± 125.5 mL. Kg^{-1}). In addition, we observed no difference between Minocycline-Vehicle and Vehicle-Vehicle groups.

Hypoxia caused a similar increase in $\dot{V}_E$ in all groups due to an increase in fR (Fig. 3). No difference was observed between treatments.

Minocycline treatment did not change ventilatory parameters under normocapnia conditions in the groups during NREM sleep (Fig. 2). Both hypercapnia and hypoxia promoted a similar increase in ventilation in both groups, with no difference between them (Fig. 3).

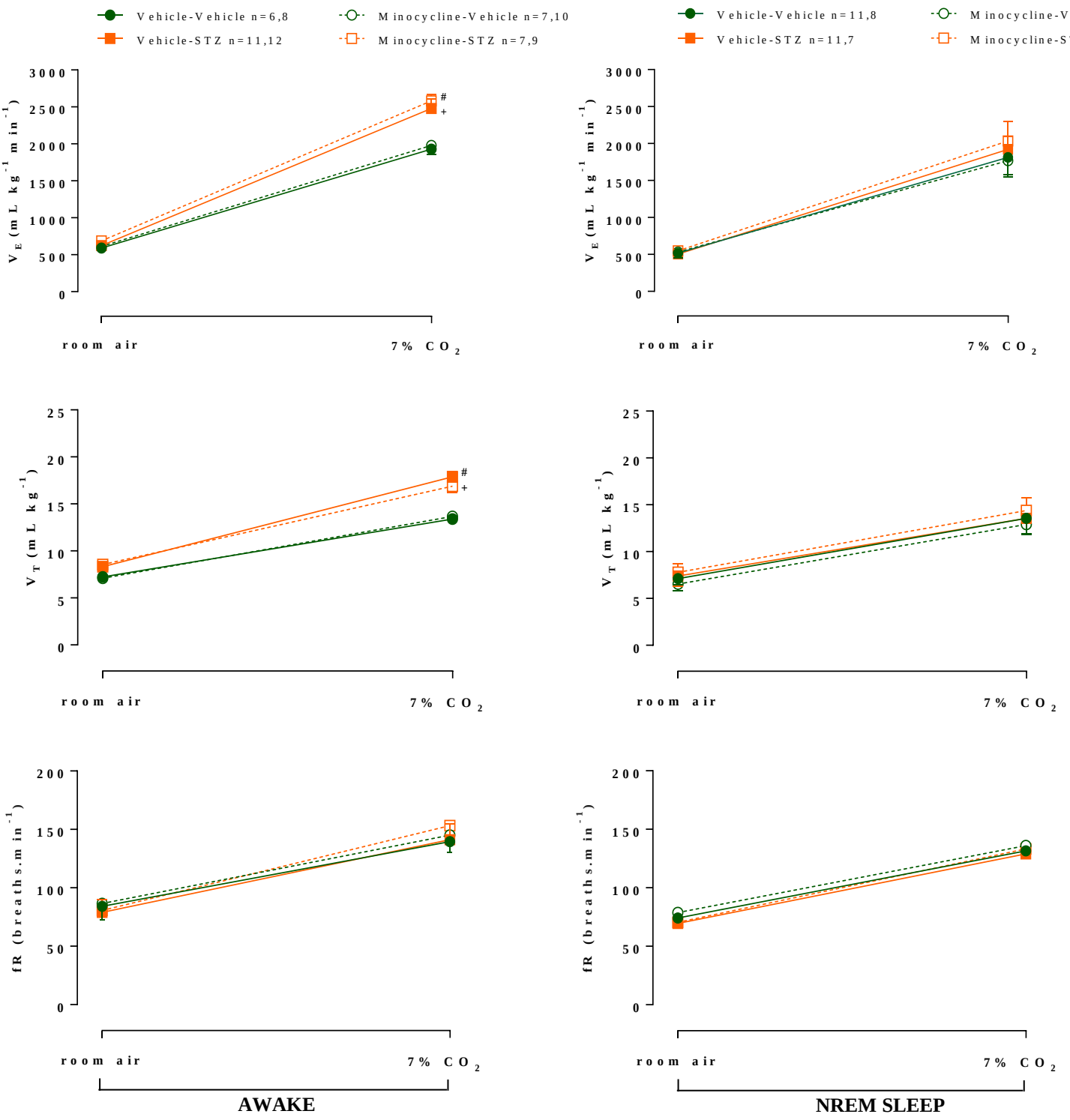

Figure 2. Minocycline treatment did not restore CO_2 sensitivity during awake state in the STZ-AD model. Effect of minocycline treatment (30 mg/kg, i.p, 5 days) on (V_E), tidal volume (V_T) and respiratory frequency (fR) during walkefuness (A) and NREM sleep (B) under room air, hypercapnia (7% CO_2) in vehicle vs STZ-AD groups. Values are expressed as mean ± SEM. + indicates a significant difference in the Vehicle (Vehicle vs STZ). # indicates a significant difference in the Minocycline (Vehicle vs STZ) groups.

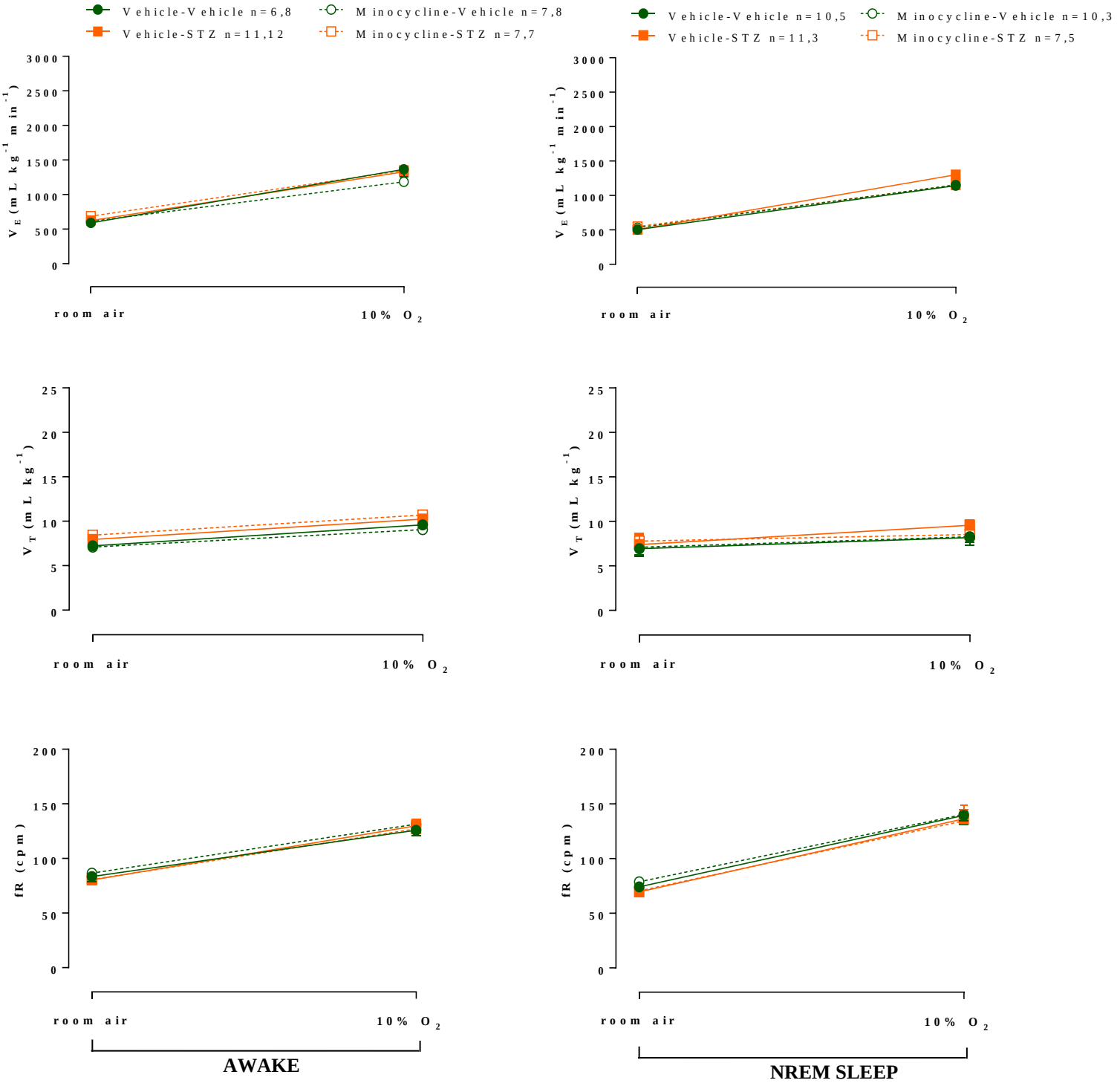

Figure 3. **Minocycline treatment does not affect respiratory parameters during hypoxia.** Minocycline treatment (30 mg/kg, i.p, 5 days) on (V_E), tidal volume (V_T) and respiratory frequency (fR) during walkefuness (A) and NREM sleep (B) under room air and hypoxia (10% CO_2) in vehicle vs STZ-AD groups. Values are expressed as mean ± SEM. + indicates a significant difference in the Vehicle (Vehicle vs STZ) groups.

4.3 Body temperature (Tb) was not altered by treatment with minocycline

Similar to Vicente et al (2018), no significant difference was observed between treatments during room air conditions and hypercapnia ($p > 0.05$; two way ANOVA) (Fig. 4). Hypoxia caused a similar decrease in body Tb in the groups (Fig. 4).

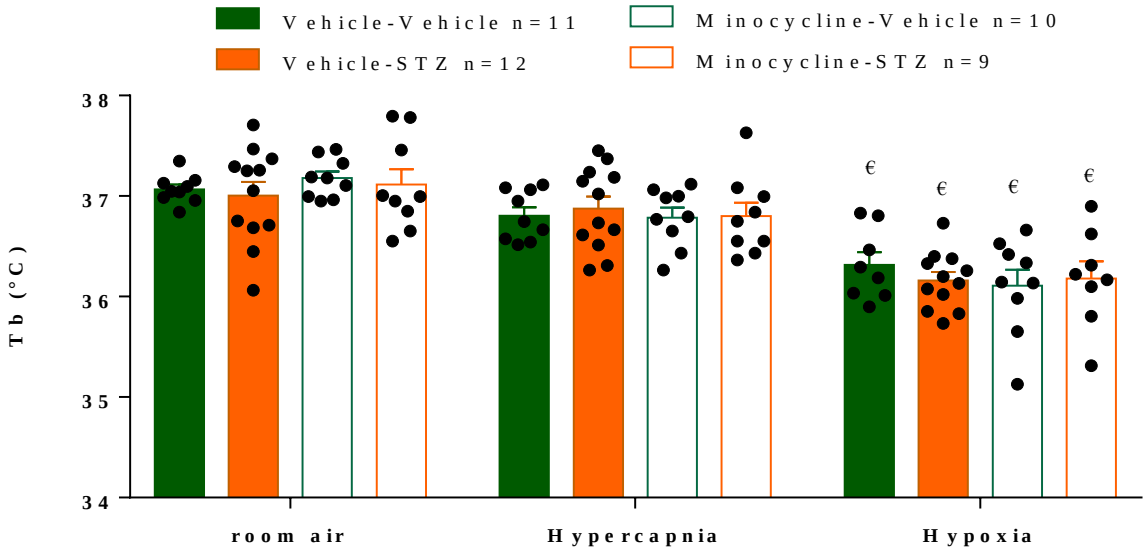

Figure 4. Body temperature (Tb) was not altered by treatment with minocycline. The effect of minocycline treatment (30 mg/kg, i.p, 5 days) on body temperature during room air, hypercapnia and hypoxia in the vehicle and STZ groups. € indicates significant difference between hypoxia and room air.

4.4 Minocycline treatment did not decrease the percentage of time spent in the awake state during room air, but changes the architecture of the sleep-wake during hypoxia and hypercapnia in the STZ-AD model

Similar to our previous study, the STZ group spends more time in the awake state compared to the Vehicle vehicle group during room air (Vehicle-STZ: 75.9 ± 4.8 % vs Vehicle-Vehicle: 53.9 ± 3.8 %, $p < 0.05$; One Way Anova) (Fig. 5A). The treatment with minocycline did not alter the increase in the percentage of time spent in awake state in the STZ model (Minocycline-STZ: 67.9 ± 3.3% vs Vehicle-STZ: 75.9 ± 4.8 %) (Fig. 5A).

Consequently, in room air conditions, the Vehicle STZ group spends less time on NREM sleep compared to the Vehicle vehicle (Vehicle-STZ: 22.7 ± 4.4% vs Vehicle-Vehicle: 40.5 ± 3.1%, $p < 0.05$; One Way Anova) (Fig. 5A). Also, minocycline treatment did not reverse the lowest percentage of sleep time in the STZ rats (Minocycline-STZ: 32.4 ± 3.5% vs Vehicle-STZ: 22.7 ± 4.4%). Likewise, treatment with minocycline did not change the mean duration of episodes of the wakefulness (Minocycline-STZ: 238.8 ± 36.0 vs Vehicle-STZ: 825.3 ± 364.8 seconds) and NREM sleep (Minocycline-STZ: 123 ± 16.0 s vs Vehicle-STZ: 92.5 ± 14.1 seconds) (Fig $5A_1$). In addition, minocycline treatment did not affect the number of episodes in wakefulness (Minocycline-STZ: 11.37 ± 1.94 vs Vehicle-STZ: 9.0 ± 1.5) and in NREM sleep (Minocycline-STZ: 11.5 ± 1.2 vs Vehicle-STZ: 8.8 ± 1.5) (Fig. $5A_2$).

During hypercapnia (Fig. 5B), we observed that treatment with minocycline restored the percentage of wakefulness (Vehicle-STZ: 91.0 ± 2.5% vs Minocycline-STZ: 76.5 ± 2.2%; $p < 0.05$; One Way Anova) and NREM sleep time (Vehicle-STZ: 8.0 ± 2.3% vs Minocycline-STZ: 22.8 ± 1.8%; $p < 0.05$; One Way Anova) in the STZ model. However, we did not observe any significant difference in the average duration of wakefulness (Vehicle-STZ: 2062.6 ± 452.9 vs Minocycline-STZ: 487.4 ± 55.2 seconds) and NREM sleep (Vehicle-STZ: 259.4 ± 81.1 vs Minocycline-STZ: 147.9 ± 14.7 seconds) (Fig. $5B_1$). Likewise, there was no significant difference after treatment in the STZ model in the number of episodes in each state wakefulness (Vehicle-STZ: 3.7 ± 0.9 vs Minocycline-STZ: 6.1 ± 0.7) and NREM sleep (Vehicle-STZ: 3.5 ± 0.9 vs Minocycline-STZ: 6.0 ± 0.6) (Fig. $5B_2$).

Similar to hypercapnia, treatment with minocycline under hypoxia in the STZ model restored the percentage of time spent wakefulness (Vehicle-STZ: 98.1 ± 0.9% vs Minocycline-STZ: 88.5 ± 1.6%; $p < 0.05$, One Way Anova) and NREM sleep (Vehicle-STZ:

2.2 ± 0.9% vs Minocycline-STZ: 12.3 ± 2.1%; p< 0.05 One Way Anova) (Fig. 5C). This effect occurred due to the reduction in the average duration of episodes of awake state (Vehicle-STZ: 2985.7 ± 384.9 vs Minocycline-STZ: 1081.6 ± 371.7 seconds, p <0.05; One Way Anova) (Fig. $5C_1$) and to the increase in the number of NREM sleep episode (Vehicle-STZ: 1.2 ± 0.4 vs Minocycline-STZ: 4.7 ± 0.2 seconds; p <0.05, One Way Anova) (Fig. $5C_2$).

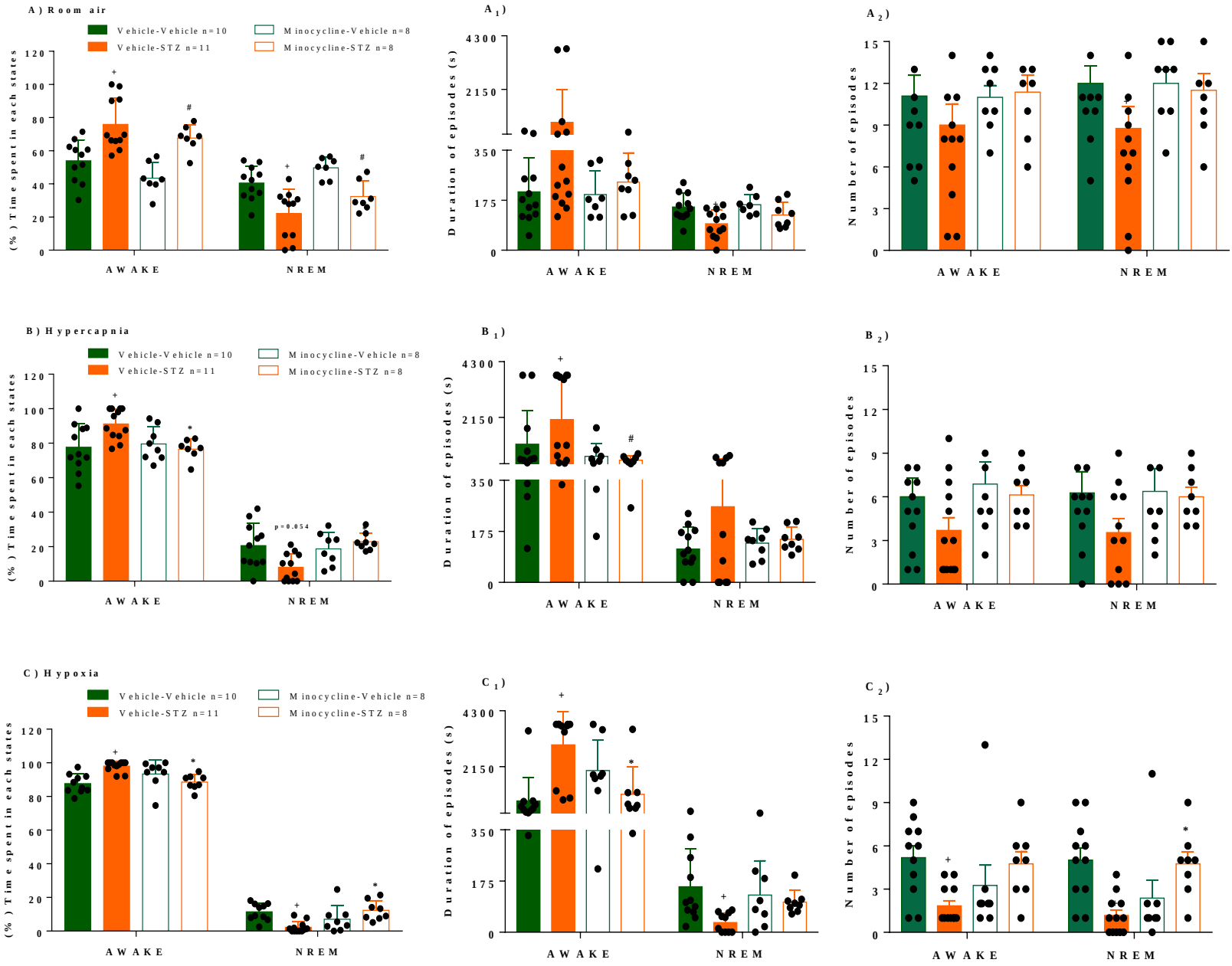

Figure 5. Minocycline treatment did not decrease the percentage of time spent in the awake state during room air in STZ-AD model. The effect of minocycline treatment (30 mg/kg, i.p, 5 days) on the percentage (%) of time spent in each state during room air (A), hypercapnia (B) and hypoxia (C). The duration of episodes in seconds during rooim air (A_1), hypercapnia (B_1) and hypoxia (C_1). The number of episodes during room air (A2), hypercapnia (B2) and hypoxia (C2) in Vehicle (Vehicle vs STZ) and Minocycline (Vehicle vs STZ) groups. Values are expressed as mean ± SEM. * indicates a significant difference between the Vehicle-STZ vs Minocycline-STZ. + indicates a significant difference in the Vehicle (Vehicle vs STZ). # indicates a significant difference in the Minocycline (Vehicle vs STZ).

4.5 Minocycline treatment did not attenuate the increase in beta amyloid peptide expression in the LC region in the STZ-AD model.

In the same way as our previous study (Vicente et al. 2018), the Vehicle STZ-AD rats showed a 70% increased expression of the amyloid beta peptide compared to the Vehicle vehicle in the LC region ($p < 0.05$, One Way ANOVA) (Fig. 6). Minocycline treatment did not affect the increased expression of beta amyloid peptide in the STZ model (% β-amyloid: 71%) (Fig. 6).

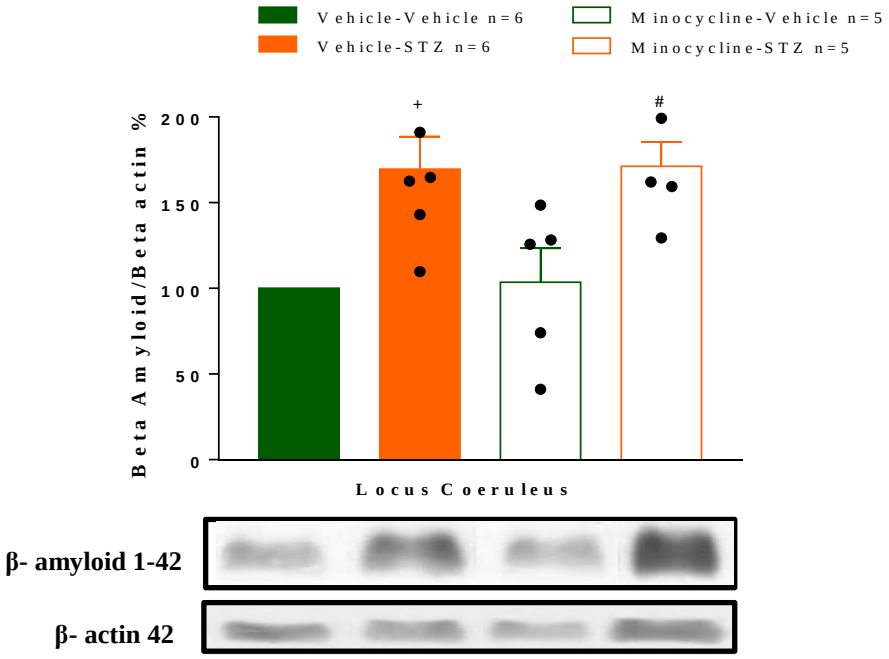

Figure 6. Minocycline treatment did not decrease the increase in beta amyloid peptide expression in the Locus coeruleus region. The effect of minocycline treatment (30 mg/kg, i.p, 5 days) on the expression of Aβ protein in the Locus coeruleus region. The values are expressed as percentage values in relation to the control group (100%). Values are expressed as mean ± SEM. + indicates a significant difference in the Vehicle (Vehicle vs STZ) groups . # indicates a significant difference in the Minocycline (Vehicle vs STZ) groups.

4.6 Minocycline treatment attenuates the increase in cell density and inactivated microglia cells of the LC region in the STZ-AD model.

Our STZ-AD model presented an increase in microglia cell density compared to the vehicle (Vehicle-Vehicle: 0.4 ± 0.05 vs Vehicle-STZ: 0.9 ± 0.06 cells/μm^2; $p<0.05$, One way ANOVA) as indicative of response to a stimulus (Fig 7A). Minocycline treatment partially attenuated the increase in cell density in the STZ-AD model (Vehicle-STZ: 0.9 ± 0.06 vs Minocycline-STZ: 0.7 ± 0.02 cells/μm^2; $p<0.05$, one way ANOVA) (Fig. 7A). Also, STZ-AD rats presented a decrease in arborization area (Vehicle-STZ: 264.8 ± 75.9 vs Vehicle-Vehicle: 647.7 ± 44.7 μm^2) (Fig. 7C) and an increase in the cell body (Vehicle-STZ: 4.64 ± 1.03 vs Vehicle-Vehicle: 2.57 ± 0.28 μm^2; $p<0.05$, one way ANOVA) of the microglia cells compared to the control group as indicative of the microglia activated state (Fig. 7D and 8B). Minocycline treatment was able to increase arborization area (431.7 ± 43.0 μm^2; $p <0.05$, one way ANOVA) (Fig. 7C) and decrease the cell body (2.9 ± 0.4 μm^2) of the microglia cells in the STZ-AD model, partially reverting the effect of STZ, indicating a shift to the resting state (Fig. 7D and 8B). The resting state can be confirmed by the morphological index, which decreased after treatment with minocycline in the STZ-AD model (Vehicle-STZ: 0.022 vs Minocycline-STZ: 0.008; $p <0.05$, one way ANOVA) compared to the control group (Vehicle-Vehicle 0.004; $p <0.05$, one way ANOVA) (Fig 7E). In addition, STZ-AD rats present an approximation of the microglia cells due to the shorter distance between them compared to the vehicle group (Vehicle-Vehicle: 27.4 ± 1.2 vs Vehicle-STZ: 17.6 ± 0.9 µm; $p <0.05$, one way ANOVA) (Fig. 7B), however, treatment with minocycline did not change the distance between the cells in STZ-AD group (Minocycline-STZ: 21.1 ± 0.8 vs Vehicle-STZ: 17.6 ± 0.9 µm) (Fig 7B and 8).

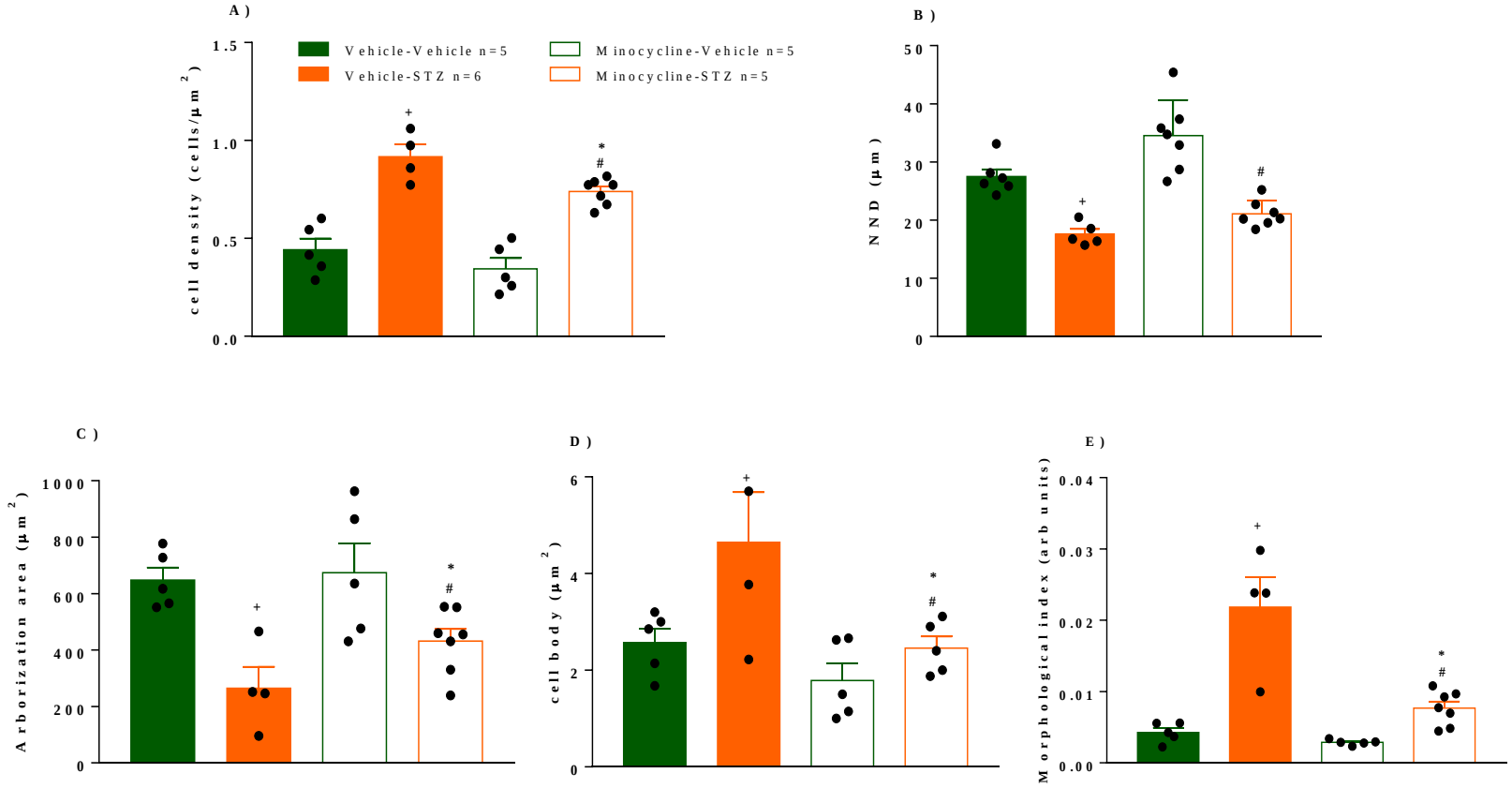

Figure 7. Minocycline treatment decreases the increased cell density and inactivated microglia cells of the Locus coeruleus region in the STZ-AD model. A) The effect of minocycline treatment (30 mg/kg, i.p, 5 days) on microglial cell densities (cells/µm^2); B) distance between microglia cells NND (µm); C) arborization area (µm^2); D) cell body (µm^2) and E) morphological index in Vehicle (Vehicle vs STZ) and Minocycline (Vehicle vs STZ) groups. Values are expressed as mean ± SEM. * indicates a significant difference between the Vehicle-STZ vs Minocycline-STZ. + indicates a significant difference in the Vehicle (Vehicle vs STZ). # indicates a significant difference in the Minocycline (Vehicle vs STZ).

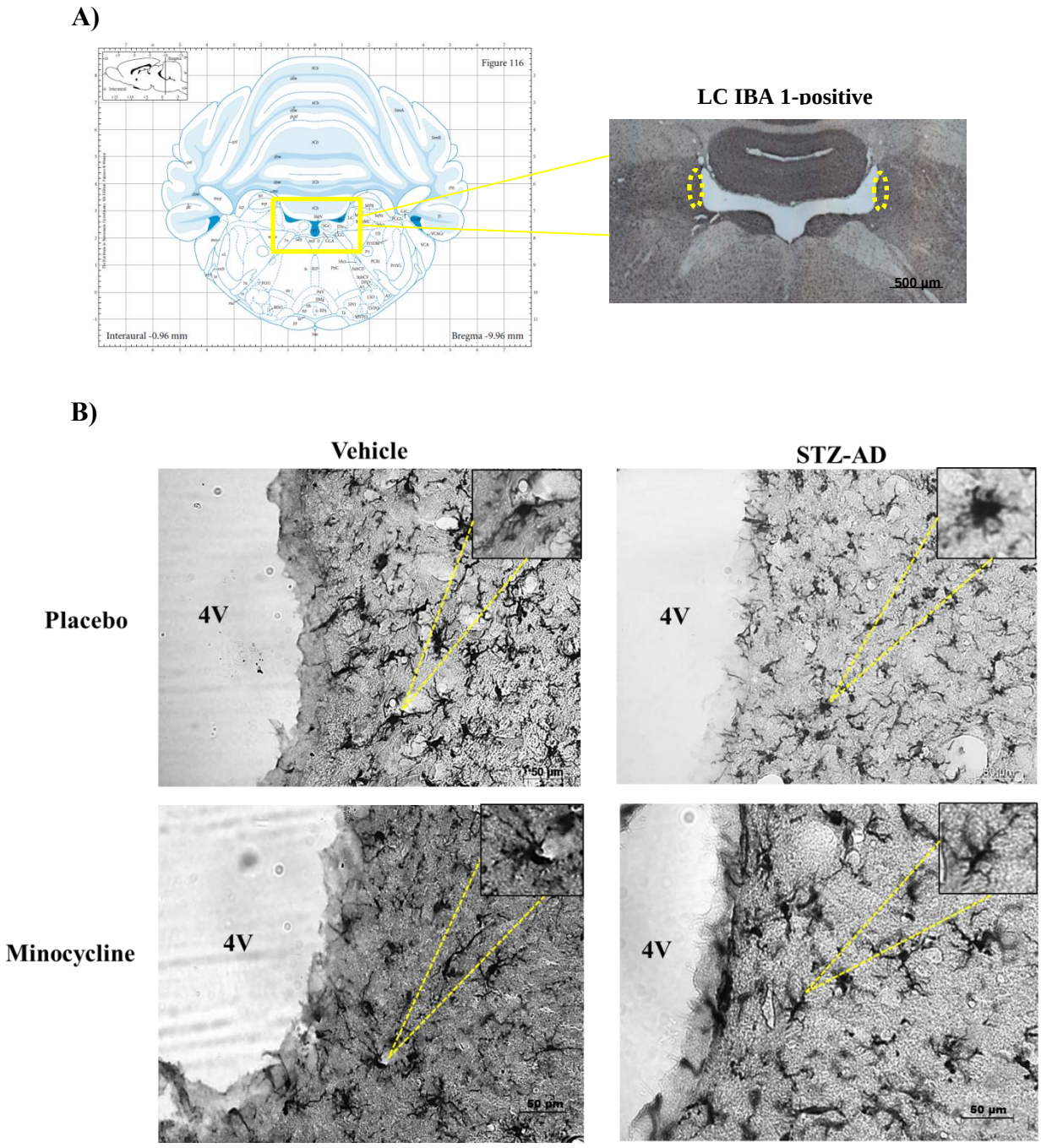

Figure 8. Minocycline treatment inactivated microglia cells of the Locus coeruleus region in the STZ-AD model. A) Schematic representation of the Locus coeruleus (LC; Bregma −9.96; Paxinos and Watson, 2005), where Iba-1 staining was analyzed. Photomicrographs of Iba-1-immunopositive cells, obtained in sections from animals, are represented. B) In each panel, the high-magnification inset illustrates representative the effect of minocycline treatment (30 mg/kg, i.p, 5 days) on morphology of microglia in animals in the Vehicle (vehicle and STZ-AD) and Minocycline (vehicle and STZ-AD) groups (40x, microscopic). Note that it is possible to observe that the cells of the microglia of the STZ-AD group have a cell body increased and arborization area decreased compared to the control group. After the treatment, it is possible to observe a decrease in the cell body and an increase in arborization area in the STZ-AD model. 4V = four ventricle, LC= locus coeruleus

4.7 Minocycline treatment did not alter TNF-α, Il-10, IL-β mRNA relative expression to GAPDH level in Locus coeruleus region.

We did not observe any difference in relative expression of TNF-α and IL-β mRNA between treatments. The relative expression of IL-10 mRNA is increased in the STZ-AD model compared to the vehicle (Vehicle-Vehicle: 0.08 ± 0.01 vs Vehicle-STZ: 1.43 ± 0.7; $p < 0.05$, one-way ANOVA). And minocycline treatment did not promote significant changes ($p > 0.05$, one-way ANOVA).

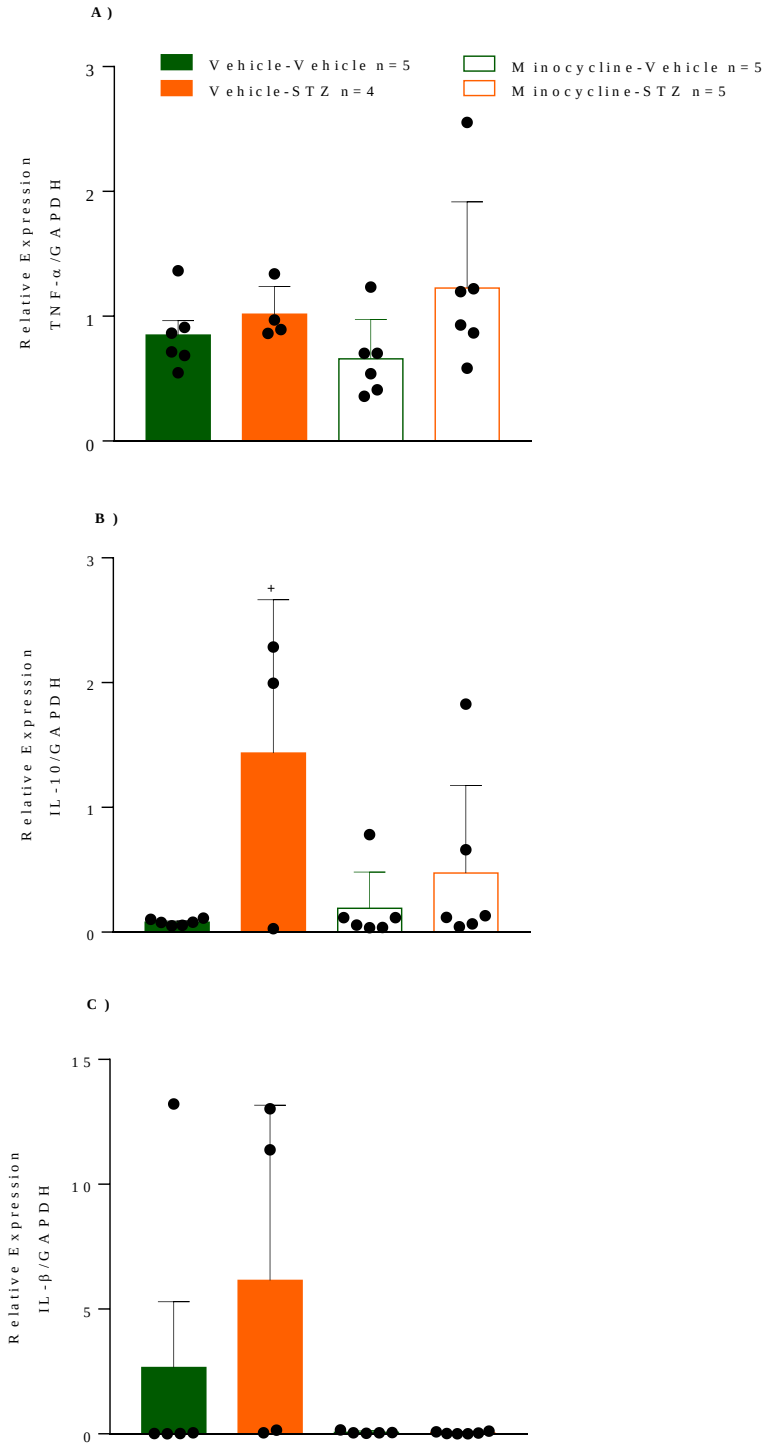

Figure 9. Minocycline treatment did not alter TNF-α, Il-10, IL-β mRNA expression relative to GAPDH level in Locus coeruleus. Values are expressed as mean ± SEM. + indicates a significant difference in the Vehicle (Vehicle vs STZ).

5 DISCUSSION

The present study demonstrated that treatment for five consecutive days with minocycline in the STA-AD model is capable of improving learning and memory as well as restoring the percentage of time spent on wakefulness and sleep during conditions of hypercapnia and hypoxia. These results might be related to change in microglia morphology in LC region, since the minocycline treatment attenuates the rise in morphological index, decreases the cell density and partially restored the mean arborization area. However, the treatment did not reverse the increased sensitivity to CO_2 during wakefulness and increase relative expression of IL-10 mRNA. Likewise, we did not observe a decrease in the expression of beta-amyloid peptide in the LC region after treatment. In addition, the drug does not affect body temperature in different gaseous conditions.

Similar to our previous study, our data demonstrated that the STZ-AD model shows increased expression of amyloid beta peptide in LC area (VICENTE et al., 2018) and an activation and agglomeration of microglia cells in the LC which is an indicative of a neuroinflammatory condition in the sporadic model of AD. Our hypothesis is supported by numerous studies that reported the activation and agglomeration of the microglial and release of pro-inflammatory cytokines due to the deposition of the amyloid beta peptide (BARGER; BASILE, 2001; D.; V.; R., 2019; HENEKA, 2017; WHITEN et al., 2020; YANG et al., 2011). In fact, we observed an increase in the relative expression of the IL-10 proinflammatory cytokine mRNA confirming neuroinflammation in our STZ-DA model. Reactive microglia is capable of producing inflammatory and toxic substances, such as reactive oxygen species, proteases and cytokines, which may trigger neuronal apoptosis. These responses are important for the defenses against pathogens and tumor cells, but can be

dangerous in uncontrolled situations, as in neurodegenerative diseases (Butovsky et al., 2006, Davies et al., 2017, Habib and Beyer, 2015, Luo and Chen, 2012).

Studies in animal models and patients with AD have shown that chronic glial activation stimulates neurodegenerative processes, such as cognitive dysfunction (CALSOLARO; EDISON, 2016; HAMMERSCHMIDT et al., 2013; HENEKA et al., 2015; HOOZEMANS et al., 2006). The release of pro-inflammatory cytokines by chronic activation of microglia promote damage to neurons, compromising synapses such as long-term potentiation (LTP) that are essential for neural plasticity in the formation of memory and learning (CURRAN; O'CONNOR, 2001; FRAYLING et al., 2007; PICKERING; O'CONNOR, 2007; RUBIO-PEREZ; MORILLAS-RUIZ, 2012; SHIN et al., 2014; TOBINICK, 2009; WEAVER et al., 2002). Other studies have also revealed that amyloid β protein dimers and trimers reduce neuron dendrites and LTP (KLYUBIN et al., 2005; SHANKAR et al., 2008; TOWNSEND et al., 2006; WALSH; SELKOE, 2007). Therefore, we suggest that microglial activation in the LC together with the increased expression of the amyloid β peptide is causing cognitive deficits in the STZ-AD model.

Along with the hippocampus and cortex, LC is a region recruited during memory and learning processing (HANSEN; MANAHAN-VAUGHAN, 2015; LEMON et al., 2009; NAKAHATA; YASUDA, 2018). Accordingly, failures in their connections, and / or molecular changes in neurons or glial cells directly affect cognition as observed in the present study in the STZ model (GANNON et al., 2015; GANNON; WANG, 2019; GHOSH et al., 2020). Our suggestion is supported because we showed cognitive improvements in STZ rats after minocycline administration corroborating other studies in rodents (BISCARO et al., 2012; CAO et al., 2021; CHOI et al., 2007; CUELLO et al., 2010; FERRETTI et al.,

2012; GARCEZ et al., 2017; HUNTER et al., 2004; PARACHIKOVA et al., 2010; WANG et al., 2016). Pre-clinical studies that evaluated the effect of minocycline on cognitive performance in AD models have associated the beneficial effect of the drug in reducing inflammatory processes mediated by microglia activation, and / or by reducing neuronal death, and / or by reducing main biomarkers (beta-amyloid protein (βA) and hyperphosphorylation of the Tau protein) of AD that enhance the neuroinflammatory condition present in AD (BISCARO et al., 2012; FAMILIAN et al., 2006; GARCEZ et al., 2017; HUNTER et al., 2004; PARACHIKOVA et al., 2010; RYU et al., 2004). However, in the present study, treatment with minocycline was not able to reduce the increased expression of beta amyloid peptide in the LC region. Other studies have also failed to observe a reduction in amyloid beta plaques after treatment with minocycline (BISCARO et al., 2012; GARCIA-ALLOZA et al., 2007; SEABROOK et al., 2006). The increased permanence of beta amyloid peptide expression would explain why the minocycline has improved but not restored cognition in the STZ-DA model. Similarly, GARCIA-ALLOZA et al. (2007), did not observe a reduction in beta amyloid plaques after treatment with minocycline, but observed a reduction in excessive microglial activation. In agreement, we suggest that the effect of minocycline may depend on the stages of AD. In such a way that, intermediate stages the intervention with the drug may only be able to stop the accumulation of the protein, but not the beta amyloid initially have changed.

There are few studies on the role of minocycline in respiratory parameters in AD models. In this scenario, we bring the first evidence of a pharmacological treatment with minocycline on respiratory symptoms in a model for AD. In relation to our STZ model, treatment with minocycline did not restore increased sensitivity to CO_2 during wakefulness.

These results suggest that microglial activation in LC may not be responsible for the increased sensitivity to CO_2. Similarly, STOKES et al. (2017) did not observe changes in ventilation during hypercapnia after seven-days of treatment with minocycline. Thus, the molecular results lead us to suggest that the increased expression of the beta amyloid peptide in the LC is possibly causing the higher sensitivity to the hypercapnic chemoreflex in STZ rats (Vicente et al. 2018) and since minocycline treatment did not reverse the molecular changes, the physiological response remained augmented.

Studies involving the role of minocycline in sleep arise from the idea that microglia release cytokines can regulate sleep (KRUEGER, 2008; NONAKA; NAKAZAWA; KOTORII, 1983; OBAL; KRUEGER, 2003; WISOR; SCHMIDT; CLEGERN, 2011a). In this regard, investigations in rabbits and rodents provided consistent evidence that pro-inflammatory cytokines like TNF and IL-1 increase NREM sleep (Krueger et al., 2007; Obal and Krueger, 2003). More recently, a study with humans found that reducing pro-inflammatory signaling by using minocycline (200 mg in one day) can act towards deepening NREM sleep and enhancing its memory forming efficacy (Besedovsky et al., 2016). However, in the present study, treatment with minocycline was not able to reverse the increase in time spent on awake state in the STZ-AD model under room air conditions. Drug treatment also did not change the percentage of sleep in the vehicle group. Thus, in our experimental protocol, our data suggest that microglia would not be responsible for the results of the sleep-wake cycle in room air or higher doses of this drug is needed to change sleep cycle. Different from our results, previous studies in humans and mice, observed that NREM sleep time decreased and awake time increased after minocycline administration (NONAKA; NAKAZAWA; KOTORII, 1983; WISOR; SCHMIDT; CLEGERN,

2011a)(WISOR; SCHMIDT; CLEGERN, 2011b). These discrepancies may be related to different doses and the treatment duration. In this regard, NONAKA et al. (1983) have used a single dose of 200 mg in humans and Wisor et al. (2011) administered 45 mg/kg in mice for 8 days. In view of the controversial data in the literature, we need to be cautious in our statements because our experiments were carried out within 1 hour of the light phase. In addition, due to the limitation of the technique, we did not analyze REM sleep.

Similar to the ventilation results, we can suggest that minocycline may not minimize the impact of beta-amyloid peptide expression in the LC region which is reflected in responses during wakefulness. In this context, it is known that the neurons of the LC promote the awake state through wide projections for the forebrain and neocortex (BERRIDGE, 2008; BERRIDGE; WATERHOUSE, 2003). The noradrenergic neurons in this region are active during wakefulness, reducing their firing rate during NREM sleep (no rapid yes movement) and silencing during REM sleep (ASTON-JONES; FOOTE; SEGAL, 1985; HOBSON; MCCARLEY; WYZINSKI, 1975; VICENTE et al., 2016b). Therefore, it is expected that respiratory and the sleep-awake changes resulting from the alteration of this nucleus are mainly in the awake as observed in this study. Nonetheless, we do not exclude the possibility that other regions such as cortex are altered.

Interestingly, we observed that minocycline treatment restored the percentage of total time spent awake and NREM sleep in gaseous stress conditions such as hypoxia and hypercapnia in the STZ-AD model. This result suggests a possible role of microglia in the modulation of sleep in the STZ animals during stress conditions. Since we observed the same effect during hypercapnia and hypoxia, the results indicate that this response might be related to stress condition and not to a specific gaseous condition. In addition, the inactivation of

microglia by minocycline only changed the total awake and NREM-sleep time in the STZ model, which exhibits a possible neuroinflammatory condition. Therefore, it is possible that this effect is due to the reduction of the cytokines release and pro-inflammatory chemokines or / and free radicals or / and nitric oxide or / and damage to neurons by the microglia.

In relation to the body temperature data, treatment with minocycline did not affect the body temperature of the animals in the gaseous condition. Likewise, we observed that hypoxia caused a similar drop in body temperature in all groups. Our findings are in agreement with the literature that during hypoxia regulated there is a drop in temperature due a fall in O_2 consumption (STEINER; ROCHA; BRANCO, 2002) and metabolic rate (MORTOLA; REZZONICO, 1988).

6. CONCLUSION

In summary, the present study demonstrated that acute treatment for five consecutive days with minocycline in the STA-AD model is capable improve cognitive dysfunction of as well as restoring the percentage of time spent on wakefulness and sleep during conditions of hypercapnia and hypoxia. These changes might be related to alteration in microglia morphology in LC region, since a minocycline treatment attenuates the rise in morphological index, decreases the cell density and partially restored the mean arborization Finally, the treatment with minocycline is promising to attenuate molecular dysfunctions resulting from the activation of the microglia that result in the physiological problems encountered in Alzheimer's patients.

Conflict interests

There is no conflict of interest for any of the authors.

Acknowledgments

This work was supported by Fundação de Amparo à Pesquisa do Estado de São Paulo (FAPESP – 2016/04412-0 to MCV and 2019/09469-8 to LHG) and Conselho Nacional de Desenvolvimento Científico e Tecnológico. The authors thank Euclides Seccato for his technical assistance and Danuzia Ambrozio Marques for helping to standardize and analyze the experimental protocol for microglia.

7. ATIVIDADES EXTRA-CURRICULARES (16/02/2020 a 15/04/2021)

Artigos completos submetidos em periódicos

1. ELISA M FONSECA , **MARIANE C VICENTE** , STEPHANIE FOURNIER , RICHARD KINKEAD , KÊNIA C BÍCEGO , LUCIANE H GARGAGLIONI. Influence of light/dark cycle and orexins on breathing control in green iguanas (Iguana iguana). SCI REP. Dec, v. 16; p. 22105, 2020. (Anexo I)

2. RIPAMONTE, GABRIEL C. ; BERNARDES-RIBEIRO, MARIANA ; PATRONE, LUIS GUSTAVO A. ; **VICENTE, MARIANE C**. ; BÍCEGO, KÊNIA C. ; GARGAGLIONI, LUCIANE H. . Functional role for preoptic CB1 receptors in breathing and thermal control. NEUROSCIENCE LETTERS, v. 732, p. 135021, 2020. (Anexo 2)

3. **VICENTE, MARIANE C.;** HUMPHREY, CHUMA M. ; GARGAGLIONI, LUCIANE H. ; OSTROWSKI, TIM D. . Decreased excitability of locus coeruleus neurons during hypercapnia is exaggerated in the streptozotocin-model of Alzheimer's disease. EXPERIMENTAL NEUROLOGY, v. 328, p. 113250, 2020. (Anexo 3)

Apresentação de trabalhos em reuniões internacionais

1. **Vicente, Mariane C**.; Paneghini, Julia L.; Almeida, Maria C.; Bícego, Kênia C.; Carrettiero, Daniel C.; Gargaglioni, Luciane H. Minocycline treatment effects on cognition, sleep, breathing and body temperature in a model for sporadic Alzheimer's diseases. In: Alzheimers Association International Conference, 2020, Amsterdã. Basic Science and Pathogenesis, Alzheimer's Imaging Consortium (AIC), and Technology and Dementia, 2020. - POSTER (Anexo 4)

2. Session: Sleep and Circadian Rhythms PIA. *Inactivation of microglia cells improves cognitive, but not respiratory and sleep-wake deficits in a sporadic model for Alzheimer's Diseases*. Virtual conference. **AAIC Neuroscience Next**, 2020. - ORAL (Anexo 5).

Apresentação de trabalho em congressos nacionais

1. Vicente, Mariane C.; Paneghini, Julia L.; Stabile Angelita M.; Almeida, Maria C.; Bícego, Kênia C.; Carrettiero, Daniel C.; Gargaglioni, Luciane H. Minocycline treatment improved cognition, but not respiratory, molecular and sleep-wake deficits in a sporadic model for Alzheimer's disease. In: 55° Congresso Anual da SBFIS, 2020, Ribeirão Preto. 54° Congresso Anual da SBFIS, 2020. (Anexo 6)

Participação em cursos ou reuniões cientificas

Curso de Neuroplasticidade - 40 horas. Centro educacional Sete de Setembro. 02 a 10 de novembro de 2020. (Anexo 7)

Orientações em projetos de pesquisas

Co-orientação no projeto de pesquisa bolsa PIBIC-2020, Julia de Lima Paneghini (Anexo 8).

A., W. et al. The worldwide costs of dementia 2015 and comparisons with 2010. **Alzheimer's and Dementia**, 2017.

ADAMS, B. et al. Altered performance characteristics in cognitive tasks: Comparison of the albino ICR and CD1 mouse strains. **Behavioural Brain Research**, 2002.

ALAFUZOFF, I. et al. Assessment of β-amyloid deposits in human brain: A study of the BrainNet Europe Consortium. **Acta Neuropathologica**, 2009.

ALHEID, G. F.; MCCRIMMON, D. R. **The chemical neuroanatomy of breathingRespiratory Physiology and Neurobiology**, 2008.

ANCOLI-ISRAEL, S. et al. Cognitive effects of treating obstructive sleep apnea in Alzheimer's disease: A randomized controlled study. **Journal of the American Geriatrics Society**, 2008.

ANCOLI-ISRAEL, S.; KRIPKE, D. F. Prevalent sleep problems in the aged. **Biofeedback and Self-Regulation**, 1991.

ANDRÉS-BENITO, P. et al. Locus coeruleus at asymptomatic early and middle Braak stages of neurofibrillary tangle pathology. **Neuropathology and Applied Neurobiology**, v. 43, n. 5, p. 373–392, 2017.

ANGULO, E. et al. Up-regulation of the Kv3.4 potassium channel subunit in early stages of Alzheimer's disease. **Journal of Neurochemistry**, 2004.

ANSORG, A. et al. Immunohistochemistry and multiple labeling with antibodies from the

same host species to study adult hippocampal neurogenesis. **Journal of Visualized Experiments**, 2015.

ARENDT, T. **Synaptic degeneration in Alzheimer's diseaseActa Neuropathologica**, 2009.

ARENDT, T. et al. Early neurone loss in Alzheimer's disease: cortical or subcortical? **Acta neuropathologica communications**, v. 3, p. 10, 2015.

ARNOLD, S. E. et al. The topographical and neuroanatomical distribution of neurofibrillary tangles and neuritic plaques in the cerebral cortex of patients with alzheimer's disease. **Cerebral Cortex**, 1991.

ASTON-JONES, G.; COHEN, J. D. AN INTEGRATIVE THEORY OF LOCUS COERULEUS-NOREPINEPHRINE FUNCTION: Adaptive Gain and Optimal Performance. **Annual Review of Neuroscience**, 2005.

ASTON-JONES, G.; FOOTE, S. L.; SEGAL, M. Impulse conduction properties of noradrenergic locus coeruleus axons projecting to monkey cerebrocortex. **Neuroscience**, 1985.

ASTON-JONES, G.; WATERHOUSE, B. **Locus coeruleus: From global projection system to adaptive regulation of behaviorBrain Research**, 2016.

ATTEMS, J.; THAL, D. R.; JELLINGER, K. A. **The relationship between subcortical tau pathology and Alzheimer's disease**. Biochemical Society Transactions. **Anais**...2012

AUGUSTINACK, J. C. et al. Specific tau phosphorylation sites correlate with severity of

neuronal cytopathology in Alzheimer's disease. **Acta Neuropathologica**, 2002.

BALDY, C. et al. The influence of sex and neonatal stress on medullary microglia in rat pups. **Experimental Physiology**, 2018a.

BALDY, C. et al. The influence of sex and neonatal stress on medullary microglia in rat pups. **Experimental Physiology**, v. 103, n. 9, p. 1192–1199, set. 2018b.

BALLANTYNE, D.; SCHEID, P. **Central chemosensitivity of respiration: A brief overview**. Respiration Physiology. **Anais**...2001

BAO, J. et al. Sex Differences in the cognitive and hippocampal effects of streptozotocin in an animal model of sporadic AD. **Frontiers in Aging Neuroscience**, 2017.

BARGER, S. W.; BASILE, A. S. Activation of microglia by secreted amyloid precursor protein evokes release of glutamate by cystine exchange and attenuates synaptic function. **Journal of Neurochemistry**, 2001.

BARTLETT, D.; TENNEY, S. M. Control of breathing in experimental anemia. **Respiration Physiology**, 1970.

BEKDASH, R. A. **The cholinergic system, the adrenergic system and the neuropathology of alzheimer's diseaseInternational Journal of Molecular Sciences**, 2021.

BERNARDS, J. A. Principles of comparative respiratory physiology. **European Journal of Obstetrics & Gynecology and Reproductive Biology**, 1976.

BERRIDGE, C. W. **Noradrenergic modulation of arousalBrain Research Reviews**, 2008.

BERRIDGE, C. W.; WATERHOUSE, B. D. **The locus coeruleus-noradrenergic system: Modulation of behavioral state and state-dependent cognitive processesBrain Research Reviews**, 2003.

BESSIS, A. et al. **Microglial control of neuronal death and synaptic propertiesGLIA**, 2007.

BIANCARDI, V. et al. Locus coeruleus noradrenergic neurons and CO2 drive to breathing. **Pflugers Archiv European Journal of Physiology**, 2008.

BICEGO, K. C.; BARROS, R. C. H.; BRANCO, L. G. S. **Physiology of temperature regulation: Comparative aspectsComparative Biochemistry and Physiology - A Molecular and Integrative Physiology**, 2007.

BISCARO, B. et al. Inhibition of microglial activation protects hippocampal neurogenesis and improves cognitive deficits in a transgenic mouse model for alzheimer's disease. **Neurodegenerative Diseases**, 2012.

BLENNOW, K. et al. Amyloid biomarkers in Alzheimer's disease. **Trends in Pharmacological Sciences**, 2015.

BOBICH, J. A.; ZHENG, Q.; CAMPBELL, A. Incubation of nerve endings with a physiological concentration of Aβ1-42 activates CaV2.2(N-Type)-voltage operated calcium channels and acutely increases glutamate and noradrenaline release. **Journal of Alzheimer's Disease**, 2004.

BOEVE, B. F. **Update on the Diagnosis and Management of Sleep Disturbances in DementiaSleep Medicine Clinics**, 2008.

BOS, I. et al. Cerebrospinal fluid biomarkers of neurodegeneration, synaptic integrity, and astroglial activation across the clinical Alzheimer's disease spectrum. **Alzheimer's and Dementia**, 2019.

BRAAK, H. et al. Stages of the pathologic process in alzheimer disease: Age categories from 1 to 100 years. **Journal of Neuropathology and Experimental Neurology**, 2011.

BRAAK, H.; BRAAK, E. **Neuropathological stageing of Alzheimer-related changesActa Neuropathologica**, 1991.

BRAAK, H.; DEL TREDICI, K. The pathological process underlying Alzheimer's disease in individuals under thirty. **Acta Neuropathologica**, v. 121, n. 2, p. 171–181, 2011a.

BRAAK, H.; DEL TREDICI, K. The pathological process underlying Alzheimer's disease in individuals under thirty. **Acta Neuropathologica**, 2011b.

BRAAK, H.; DEL TREDICI, K. **Where, when, and in what form does sporadic Alzheimer's disease begin?Current Opinion in Neurology**, 2012.

BRANCO, L. G. S.; GARGAGLIONI, L. H.; BARROS, R. C. H. **Anapyrexia during hypoxia**. Journal of Thermal Biology. **Anais**...2006

BROMLEY-BRITS, K.; DENG, Y.; SONG, W. Morris Water Maze test for learning and memory deficits in Alzheimer's disease model mice. **Journal of Visualized Experiments**, 2011.

BROWN, A. G. et al. Impaired chemoreflex correlates with decreased c-Fos in respiratory brainstem centers of the streptozotocin-induced Alzheimer's disease rat model.

Experimental Neurology, 2019.

BUBU, O. M. et al. Obstructive sleep apnea and longitudinal Alzheimer's disease biomarker changes. **Sleep**, 2019.

BUDNI, J. et al. The Anti-Inflammatory Role of Minocycline in Alzheimers Disease. **Current Alzheimer Research**, 2016.

CAGNIN, A. et al. In-vivo measurement of activated microglia in dementia. **Lancet**, 2001.

CAI, Z.; HUSSAIN, M. D.; YAN, L. J. **Microglia, neuroinflammation, and beta-amyloid protein in Alzheimer's diseaseInternational Journal of Neuroscience**, 2014.

CAI, Z.; YAN, Y.; WANG, Y. Minocycline alleviates beta-amyloid protein and tau pathology via restraining neuroinflammation induced by diabetic metabolic disorder. **Clinical Interventions in Aging**, 2013.

CALABRÒ, M. et al. The biological pathways of Alzheimer disease: a review. **AIMS Neuroscience**, 2021.

CALSOLARO, V.; EDISON, P. **Neuroinflammation in Alzheimer's disease: Current evidence and future directionsAlzheimer's and Dementia**, 2016.

CAO, S. et al. Comparisons of neuroinflammation, microglial activation, and degeneration of the locus coeruleus-norepinephrine system in APP/PS1 and aging mice. **Journal of Neuroinflammation**, 2021.

CARTER, M. E. et al. Tuning arousal with optogenetic modulation of locus coeruleus neurons. **Nature Neuroscience**, 2010.

CHALERMPALANUPAP, T. et al. Locus coeruleus ablation exacerbates cognitive deficits, neuropathology, and lethality in P301S tau transgenic mice. **Journal of Neuroscience**, 2018.

CHAN-PALAY, V.; ASAN, E. Alterations in catecholamine neurons of the locus coeruleus in senile dementia of the Alzheimer type and in Parkinson's disease with and without dementia and depression. **Journal of Comparative Neurology**, 1989.

CHAWLA, A. et al. Cognitive impairment and gene expression alterations in a rodent model of binge eating disorder. **Physiology and Behavior**, 2017.

CHEN, C. β-amyloid increases dendritic Ca2+ influx by inhibiting the A-type K+ current in hippocampal CA1 pyramidal neurons. **Biochemical and Biophysical Research Communications**, 2005.

CHEN, M. et al. Minocycline inhibits caspase-1 and caspase-3 expression and delays mortality in a transgenic mouse model of Huntington disease. **Nature Medicine**, 2000.

CHEN, Y. et al. A non-transgenic mouse model (icv-STZ mouse) of Alzheimer's disease: similarities to and differences from the transgenic model (3xTg-AD mouse). **Molecular neurobiology**, 2013.

CHOI, Y. et al. Minocycline attenuates neuronal cell death and improves cognitive impairment in Alzheimer's disease models. **Neuropsychopharmacology**, 2007.

CHONG, M. S. et al. Continuous positive airway pressure reduces subjective daytime sleepiness in patients with mild to moderate Alzheimer's disease with sleep disordered breathing. **Journal of the American Geriatrics Society**, 2006.

COATES, E. L.; LI, A.; NATTIE, E. E. Widespread sites of brain stem ventilatory chemoreceptors. **Journal of Applied Physiology**, 1993.

CORREIA, S. C. et al. **Insulin-resistant brain state: The culprit in sporadic Alzheimer's disease?Ageing Research Reviews**, 2011.

CUELLO, A. C. et al. **Early-stage inflammation and experimental therapy in transgenic models of the Alzheimer-like amyloid pathology**. Neurodegenerative Diseases. **Anais**...2010

CURRAN, B.; O'CONNOR, J. J. The pro-inflammatory cytokine interleukin-18 impairs long-term potentiation and NMDA receptor-mediated transmission in the rat hippocampus in vitro. **Neuroscience**, 2001.

D., K.; V., S.; R., D. Activation of microglia and astrocytes: a roadway to neuroinflammation and Alzheimer's disease. **Inflammopharmacology**, 2019.

DE CARVALHO, D. et al. Neurochemical and electrical modulation of the Locus coeruleus: Contribution to CO2 drive to breathe. **Frontiers in Physiology**, v. 5 JUL, 2014.

DEAK, M. C.; KIRSCH, D. B. **Sleep-disordered breathing in neurologic conditionsClinics in Chest Medicine**, 2014.

DEL NEGRO, C. A.; FUNK, G. D.; FELDMAN, J. L. **Breathing mattersNature Reviews Neuroscience**, 2018.

DEMPSEY, J. A.; SMITH, C. A. Pathophysiology of human ventilatory control. **European Respiratory Journal**, 2014a.

DEMPSEY, J. A.; SMITH, C. A. **Pathophysiology of human ventilatory control: Number 6 in the series "physiology in respiratory medicine"European Respiratory Journal**, 2014b.

DENG, Y. et al. Dysregulation of insulin signaling, glucose transporters, O-GlcNAcylation, and phosphorylation of tau and neurofilaments in the brain: Implication for Alzheimer's disease. **American Journal of Pathology**, 2009.

DÍAZ-ROMÁN, M. et al. Obstructive sleep apnea and Alzheimer's disease-related cerebrospinal fluid biomarkers in mild cognitive impairment. **Sleep**, 2021.

DICKSON, D. W. Introduction to Neurodegeneration: The Molecular Pathology of Dementia and Movement Disorders. In: **Neurodegeneration: The Molecular Pathology of Dementia and Movement Disorders: Second Edition**. [s.l: s.n.].

DRACHMAN, D. A. The amyloid hypothesis, time to move on: Amyloid is the downstream result, not cause, of Alzheimer's disease. **Alzheimer's and Dementia**, 2014.

DRORBAUGH, J. E.; FENN, W. O. A barometric method for measuring ventilation in newborn infants. **Pediatrics**, 1955.

E., K. et al. Allothetic orientation and sequential ordering of places is impaired in early stages of Alzheimer's disease: Corresponding results in real space tests and computer tests. **Behavioural Brain Research**, 2005.

E.E., N.; A., L. CO2 dialysis in the medullary raphe of the rat increases ventilation in sleep. **Journal of Applied Physiology**, 2001.

EBEL, D. L.; TORKILSEN, C. G.; OSTROWSKI, T. D. Blunted Respiratory Responses in the Streptozotocin-Induced Alzheimer's Disease Rat Model. **Journal of Alzheimer's Disease**, 2017.

EHRENBERG, A. J. et al. Quantifying the accretion of hyperphosphorylated tau in the locus coeruleus and dorsal raphe nucleus: the pathological building blocks of early Alzheimer's disease. **Neuropathology and Applied Neurobiology**, 2017.

ELAM, M. et al. Hypercapnia and hypoxia: Chemoreceptor-mediated control of locus coeruleus neurons and splanchnic, sympathetic nerves. **Brain Research**, 1981.

ESER, R. A. et al. Selective vulnerability of brainstem nuclei in distinct tauopathies: A postmortem study. **Journal of Neuropathology and Experimental Neurology**, 2018.

FAIM, F. et al. Role of ghrelin on growth hormone/insulin-like growth factor-1 axis during endotoxemia. **Growth Hormone and IGF Research**, v. 48–49, n. August, p. 36–44, 2019.

FAMILIAN, A. et al. Inhibitory effect of minocycline on amyloid β fibril formation and human microglial activation. **GLIA**, 2006.

FELDMAN, J. L.; DEL NEGRO, C. A.; GRAY, P. A. **Understanding the rhythm of breathing: So near, yet so farAnnual Review of Physiology**, 2013.

FERRETTI, M. T. et al. Minocycline corrects early, pre-plaque neuroinflammation and inhibits BACE-1 in a transgenic model of Alzheimer's disease-like amyloid pathology. **Journal of Neuroinflammation**, 2012.

FILOSA, J. A.; DEAN, J. B.; PUTNAM, R. W. Role of intracellular and extracellular pH in

the chemosensitive response of rat locus coeruleus neurones. **The Journal of physiology**, v. 541, n. Pt 2, p. 493–509, jun. 2002.

FILOSA, J. A.; PUTNAM, R. W. Multiple targets of chemosensitive signaling in locus coeruleus neurons: Role of K+and Ca2+channels. **American Journal of Physiology - Cell Physiology**, 2003.

FLEMING, W. E.; POLLAK, C. P. **Sleep disorders in multiple sclerosisSeminars in Neurology**, 2005.

FOLCH, J. et al. **Current Research Therapeutic Strategies for Alzheimer's Disease TreatmentNeural Plasticity**, 2016.

FOLEY, D. et al. Daytime sleepiness is associated with 3-year incident dementia and cognitive decline in older Japanese-American men. **Journal of the American Geriatrics Society**, 2001.

FORTIN, G.; CHAMPAGNAT, J. Spontaneous synaptic activities in rat nucleus tractus solitarius neurons in vitro: evidence for re-excitatory processing. **Brain research**, v. 630, n. 1–2, p. 125–35, dez. 1993.

FRAYLING, T. M. et al. An interleukin-18 polymorphism is associated with reduced serum concentrations and better physical functioning in older people. **Journals of Gerontology - Series A Biological Sciences and Medical Sciences**, 2007.

GAIG, C.; IRANZO, A. Sleep-disordered breathing in neurodegenerative diseases. **Current Neurology and Neuroscience Reports**, 2012.

GANNON, M. et al. **Noradrenergic dysfunction in Alzheimer's diseaseFrontiers in Neuroscience**, 2015.

GANNON, M.; WANG, Q. Complex noradrenergic dysfunction in Alzheimer's disease: Low norepinephrine input is not always to blame. **Brain Research**, 2019.

GARCEZ, M. L. et al. Minocycline reduces inflammatory parameters in the brain structures and serum and reverses memory impairment caused by the administration of amyloid β (1-42) in mice. **Progress in Neuro-Psychopharmacology and Biological Psychiatry**, 2017.

GARCIA-ALLOZA, M. et al. A limited role for microglia in antibody mediated plaque clearance in APP mice. **Neurobiology of Disease**, 2007.

GARGAGLIONI, L. H.; HARTZLER, L. K.; PUTNAM, R. W. The locus coeruleus and central chemosensitivity. **Respiratory physiology & neurobiology**, v. 173, n. 3, p. 264–73, out. 2010.

GARRIDO-MESA, N.; ZARZUELO, A.; GÁLVEZ, J. What is behind the non-antibiotic properties of minocycline? **Pharmacological Research**, v. 67, n. 1, p. 18–30, 2013a.

GARRIDO-MESA, N.; ZARZUELO, A.; GÁLVEZ, J. Minocycline: Far beyond an antibiotic. **British Journal of Pharmacology**, v. 169, n. 2, p. 337–352, 2013b.

GEHRMAN, P. R. et al. Sleep-disordered breathing and agitation in institutionalized adults with Alzheimer disease. **American Journal of Geriatric Psychiatry**, 2003.

GHOSH, A. et al. **Locus coeruleus patterns differentially modulate learning and valence in rat via the ventral tegmental area and basolateral amygdala respectivelybioRxiv**,

2020.

GHOVANLOO, M.-R.; PETERS, C. H.; RUBEN, P. C. Effects of acidosis on neuronal voltage-gated sodium channels: Nav1.1 and Nav1.3. **Channels (Austin, Tex.)**, v. 12, n. 1, p. 367–377, 2018.

GLENN, J. A.; BOOTH, P. L.; THOMAS, W. E. Pinocytotic activity in ramified microglia. **Neuroscience Letters**, 1991.

GOLDSTEIN, S. A et al. Potassium leak channels and the KCNK family of two-P-domain subunits. **Nature reviews. Neuroscience**, v. 2, n. 3, p. 175–184, mar. 2001.

GOMOLIN, I. H. et al. Older is colder: Temperature range and variation in older people. **Journal of the American Geriatrics Society**, 2005.

GORDON, S.; MARTINEZ, F. O. **Alternative activation of macrophages: Mechanism and functionsImmunity**, 2010.

GOTTFRIES, C. G. et al. Biochemical changes in Dementia disorders of Alzheimer type (AD/SDAT). **Neurobiology of Aging**, 1983.

GRATHWOHL, S. A. et al. Formation and maintenance of Alzheimer's disease β-amyloid plaques in the absence of microglia. **Nature Neuroscience**, 2009.

GRIEB, P. Intracerebroventricular Streptozotocin Injections as a Model of Alzheimer's Disease: in Search of a Relevant Mechanism. **Molecular Neurobiology**, v. 53, n. 3, p. 1741–1752, 2016.

GRUDZIEN, A. et al. Locus coeruleus neurofibrillary degeneration in aging, mild cognitive

impairment and early Alzheimer's disease. **Neurobiology of Aging**, 2007.

GRÜNBLATT, E. et al. Brain insulin system dysfunction in streptozotocin intracerebroventricularly treated rats generates hyperphosphorylated tau protein. **Journal of Neurochemistry**, 2007.

GRÜNBLATT, E.; HOYER, S.; RIEDERER, P. Gene expression profile in streptozotocin rat model for sporadic Alzheimer's disease. **Journal of Neural Transmission**, 2004.

GRZANNA, R.; MOLLIVER, M. E. The locus coeruleus in the rat: An immunohistochemical delineation. **Neuroscience**, v. 5, n. 1, p. 21–40, 1980.

GUDES, S. et al. The role of slow and persistent ttx-resistant sodium currents in acute tumor necrosis factor- α-mediated increase in nociceptors excitability. **Journal of Neurophysiology**, 2015.

GUERRIERO, F. et al. **Neuroinflammation, immune system and Alzheimer disease: searching for the missing linkAging Clinical and Experimental Research**, 2017.

GUYENET, P. G. et al. **Retrotrapezoid nucleus, respiratory chemosensitivity and breathing automaticityRespiratory Physiology and Neurobiology**, 2009.

HALLIDAY, G. et al. **Alzheimer's disease and inflammation: A review of cellular and therapeutic mechanismsClinical and Experimental Pharmacology and Physiology**, 2000.

HAMMERSCHMIDT, T. et al. Selective Loss of Noradrenaline Exacerbates Early Cognitive Dysfunction and Synaptic Deficits in APP/PS1 Mice. **Biological Psychiatry**, v. 73, n. 5, p.

454–463, mar. 2013.

HANSEN, N.; MANAHAN-VAUGHAN, D. Locus Coeruleus Stimulation Facilitates Long-Term Depression in the Dentate Gyrus That Requires Activation of β-Adrenergic Receptors. **Cerebral Cortex**, 2015.

HARMAN, D. Alzheimer's disease: A hypothesis on pathogenesis. **Journal of the American Aging Association**, 2000.

HARMAN, D. **Alzheimer's disease pathogenesis: Role of aging**. Annals of the New York Academy of Sciences. **Anais**...2006

HARPER, D. G. Disturbance of Endogenous Circadian Rhythm in Aging and Alzheimer Disease. **American Journal of Geriatric Psychiatry**, 2005.

HENDERSON, V. W.; MACK, W.; WILLIAMS, B. W. Spatial Disorientation in Alzheimer's disease. **Archives of Neurology**, 1989.

HENEKA, M. T. et al. **Neuroinflammation in Alzheimer's diseaseThe Lancet Neurology**, 2015.

HENEKA, M. T. Inflammasome activation and innate immunity in Alzheimer's disease. **Brain Pathology**, 2017.

HENSLEY, K. **Neuroinflammation in Alzheimer's disease: Mechanisms, pathologic consequences, and potential for therapeutic manipulationJournal of Alzheimer's Disease**, 2010.

HEPPNER, F. L.; RANSOHOFF, R. M.; BECHER, B. **Immune attack: The role of**

inflammation in Alzheimer diseaseNature Reviews Neuroscience, 2015.

HERREGODTS, P. et al. Monoaminergic neurotransmitters in Alzheimer's disease. An HPLC study comparing presenile familial and sporadic senile cases. **Journal of the Neurological Sciences**, 1989.

HICKMAN, S. E.; ALLISON, E. K.; EL KHOURY, J. Microglial dysfunction and defective β-amyloid clearance pathways in aging alzheimer's disease mice. **Journal of Neuroscience**, 2008.

HILAIRE, G. et al. Modulation of the respiratory rhythm generator by the pontine noradrenergic A5 and A6 groups in rodents. **Respiratory Physiology and Neurobiology**, 2004.

HOBSON, J. A.; MCCARLEY, R. W.; WYZINSKI, P. W. Sleep cycle oscillation: Reciprocal discharge by two brainstem neuronal groups. **Science**, 1975.

HOF, P.; MORRISON, J. Quantitative analysis of a vulnerable subset of pyramidal neurons in Alzheimer's disease. **The Journal of Comparative Neurology**, 1990.

HOOGENDIJK, W. J. G. et al. Increased activity of surviving locus ceruleus neurons in Alzheimer's disease. **Annals of Neurology**, 1999.

HOOZEMANS, J. J. M. et al. **Neuroinflammation and regeneration in the early stages of Alzheimer's disease pathology**. International Journal of Developmental Neuroscience. **Anais**...2006

HOYER, S.; LANNERT, H. Long-term abnormalities in brain glucose/energy metabolism

after inhibition of the neuronal insulin receptor: Implication of tau-protein. **Journal of Neural Transmission, Supplementa**, 2007.

HOYER, S.; MULLER, D.; PLASCHKE, K. **Desensitization of brain insulin receptor. Effect on glucose/energy and related metabolism**. Journal of Neural Transmission, Supplement. **Anais**...1994

HUNTER, C. L. et al. Minocycline protects basal forebrain cholinergic neurons from mu p75-saporin immunotoxic lesioning. **European Journal of Neuroscience**, 2004.

IMAMOTO, K. Origin of microglia: cell transformation from blood monocytes into macrophagic ameboid cells and microglia. **Progress in clinical and biological research**, 1981.

IMBER, A. N. et al. The Role of Ca 2+ and BK Channels of Locus Coeruleus (LC) Neurons as a Brake to the CO 2 Chemosensitivity Response of Rats. **Neuroscience**, 2018.

IQBAL, K. et al. Tau in Alzheimer Disease and Related Tauopathies. **Current Alzheimer Research**, 2010.

J.R., C. et al. Sustained use of CPAP slows deterioration of cognition, sleep, and mood in patients with Alzheimer's disease and obstructive sleep apnea: A preliminary study. **Journal of Clinical Sleep Medicine**, 2009.

JACK, C. R. et al. **NIA-AA Research Framework: Toward a biological definition of Alzheimer's diseaseAlzheimer's and Dementia**, 2018.

JANCZEWSKI, W. A.; FELDMAN, J. L. **Novel data supporting the two respiratory**

rhythm oscillator hypothesis. Focus on "respiration-related rhythmic activity in the rostral medulla of newborn rats"Journal of Neurophysiology, 2006.

JANELSINS, M. C. et al. Early correlation of microglial activation with enhanced tumor necrosis factor-alpha and monocyte chemoattractant protein-1 expression specifically within the entorhinal cortex of triple transgenic Alzheimer's disease mice. **Journal of Neuroinflammation**, 2005.

JAUSSENT, I. et al. Excessive sleepiness is predictive of cognitive decline in the elderly. **Sleep**, 2012.

JENERICK, H. Phase Plane Trajectories of the Muscle Spike Potential. **Biophysical Journal**, 1963.

JOHNSON, S. M.; HAXHIU, M. A.; RICHERSON, G. B. GFP-expressing locus ceruleus neurons from Prp57 transgenic mice exhibit CO2/H+ responses in primary cell culture. **Journal of Applied Physiology**, 2008.

JOHNSTON, J.; FORSYTHE, I. D.; KOPP-SCHEINPFLUG, C. **Going native: Voltage-gated potassium channels controlling neuronal excitability**. Journal of Physiology. **Anais**...2010

JU, Y. E. S. et al. Sleep quality and preclinical Alzheimer disease. **JAMA Neurology**, 2013.

KAR, S. et al. **Interactions between β-amyloid and central cholinergic neurons: Implications for Alzheimer's diseaseJournal of Psychiatry and Neuroscience**, 2004.

KAUR, D.; SHARMA, V.; DESHMUKH, R. **Activation of microglia and astrocytes: a**

roadway to neuroinflammation and Alzheimer's diseaseInflammopharmacology, 2019.

KELLY, S. C. et al. Locus coeruleus cellular and molecular pathology during the progression of Alzheimer's disease. **Acta neuropathologica communications**, 2017.

KIELIAN, T. et al. Minocycline Modulates Neuroinflammation Independently of Its Antimicrobial Activity in Staphylococcus aureus-Induced Brain Abscess. **The American Journal of Pathology**, v. 171, n. 4, p. 1199–1214, out. 2007.

KIM, H. S.; SUH, Y. H. Minocycline and neurodegenerative diseases. **Behavioural Brain Research**, v. 196, n. 2, p. 168–179, 2009.

KIMURA, T. et al. Sequential changes of Tau-Site-Specific phosphorylation during development of paired helical filaments. **Dementia and Geriatric Cognitive Disorders**, 1996.

KLEGERIS, A. et al. Increase in core body temperature of Alzheimer's disease patients as a possible indicator of chronic neuroinflammation: A meta-analysis. **Gerontology**, 2006.

KLINE, D. D. et al. Sensory afferent and hypoxia-mediated activation of nucleus tractus solitarius neurons that project to the rostral ventrolateral medulla. **Neuroscience**, v. 167, n. 2, p. 510–527, maio 2010.

KLUCKEN, J. et al. **Neuritic Alterations and Neural System Dysfunction in Alzheimer's Disease and Dementia with Lewy BodiesNeurochemical Research**, 2003.

KLYUBIN, I. et al. Amyloid β protein immunotherapy neutralizes Aβ oligomers that disrupt synaptic plasticity in vivo. **Nature Medicine**, 2005.

KNEZOVIC, A. et al. Staging of cognitive deficits and neuropathological and ultrastructural changes in streptozotocin-induced rat model of Alzheimer's disease. **Journal of Neural Transmission**, 2015.

KNIGHT, E. M. et al. Age-related changes in core body temperature and activity in triple-transgenic Alzheimer's disease (3xTgAD) mice. **DMM Disease Models and Mechanisms**, 2013.

KORZHEVSKII, D. E.; KIRIK, O. V. Brain Microglia and Microglial Markers. **Neuroscience and Behavioral Physiology**, 2016.

KRASKA, A. et al. In Vivo Cross-sectional Characterization of Cerebral Alterations Induced by Intracerebroventricular Administration of Streptozotocin. **PLoS ONE**, 2012.

KRUEGER, J. The Role of Cytokines in Sleep Regulation. **Current Pharmaceutical Design**, 2008.

KUANG, X. et al. Attenuation of oxidative stress, inflammation and apoptosis by minocycline prevents retrovirus-induced neurodegeneration in mice. **Brain Research**, 2009.

KUMAR, S.; OKELLO, E. J.; HARRIS, J. R. Experimental inhibition of fibrillogenesis and neurotoxicity by amyloid-beta (Aβ) and other disease-related peptides/proteins by plant extracts and herbal compounds. **Subcellular Biochemistry**, 2012.

LAFERLA, F. M.; GREEN, K. N. Animal models of Alzheimer disease. **Cold Spring Harbor Perspectives in Medicine**, 2012.

LANNERT, H.; HOYER, S. Intracerebroventricular administration of streptozotocin causes

long- term diminutions in learning and memory abilities and in cerebral energy metabolism in adult rats. **Behavioral Neuroscience**, 1998a.

LANNERT, H.; HOYER, S. Intracerebroventricular administration of streptozotocin causes long-term diminutions in learning and memory abilities and in cerebral energy metabolism in adult rats. **Behavioral neuroscience**, v. 112, n. 5, p. 1199–1208, out. 1998b.

LASAGNA-REEVES, C. A.; GLABE, C. G.; KAYED, R. Amyloid-β annular protofibrils evade fibrillar fate in Alzheimer disease brain. **Journal of Biological Chemistry**, 2011.

LATTA, C. H. et al. Determining the role of IL-4 induced neuroinflammation in microglial activity and amyloid-β using BV2 microglial cells and APP/PS1 transgenic mice. **Journal of Neuroinflammation**, 2015.

LAURIJSSENS, B.; AUJARD, F.; RAHMAN, A. **Animal models of Alzheimer's disease and drug developmentDrug Discovery Today: Technologies**, 2013.

LEE, J. E. et al. Sleep-disordered breathing and Alzheimer's disease: A nationwide cohort study. **Psychiatry Research**, 2019.

LEE, Y. et al. Insulin/IGF signaling-related gene expression in the Brain of a Sporadic Alzheimer's disease monkey model induced by intracerebroventricular injection of streptozotocin. **Journal of Alzheimer's Disease**, 2014.

LEMON, N. et al. Locus coeruleus activation facilitates memory encoding and induces hippocampal LTD that depends on β-Adrenergic receptor activation. **Cerebral Cortex**, 2009.

LENG, Y. et al. Association of sleep-disordered breathing with cognitive function and risk of cognitive impairment: A systematic review and meta-analysis. **JAMA Neurology**, 2017.

LENZEN, S. **The mechanisms of alloxan- and streptozotocin-induced diabetesDiabetologia**, 2008.

LI, K.-Y.; PUTNAM, R. W. Transient outwardly rectifying A currents are involved in the firing rate response to altered CO2 in chemosensitive locus coeruleus neurons from neonatal rats. **American journal of physiology. Regulatory, integrative and comparative physiology**, v. 305, n. 7, p. R780-92, 1 out. 2013.

LI, N.; LI, A.; NATTIE, E. Focal microdialysis of CO2 in the perifornical-hypothalamic area increases ventilation during wakefulness but not NREM sleep. **Respiratory Physiology and Neurobiology**, 2013.

LI, W. et al. High doses of minocycline may induce delayed activation of microglia in aged rats and thus cannot prevent postoperative cognitive dysfunction. **Journal of International Medical Research**, v. 46, n. 4, p. 1404–1413, 2018.

LIGUORI, C. et al. Obstructive sleep apnea is associated with early but possibly modifiable Alzheimer's disease biomarkers changes. **Sleep**, 2017.

LIGUORI, C. et al. Obstructive sleep apnea may induce orexinergic system and cerebral β-amyloid metabolism dysregulation: is it a further proof for Alzheimer's disease risk? **Sleep Medicine**, 2019.

LIGUORI, C. et al. **Sleep-disordered breathing and the risk of Alzheimer's diseaseSleep Medicine Reviews**, 2021.

LIMA-SILVEIRA, L. et al. Enhancement of excitatory transmission in NTS neurons projecting to ventral medulla of rats exposed to sustained hypoxia is blunted by minocycline. **Journal of Physiology**, 2019.

LINDEBOOM, J.; WEINSTEIN, H. Neuropsychology of cognitive ageing, minimal cognitive impairment, Alzheimer's disease, and vascular cognitive impairment. **European Journal of Pharmacology**, 2004.

LIU, L. H. et al. Degenerative alterations in noradrenergic neurons of the locus coeruleus in Alzheimer's disease. **Neural Regeneration Research**, 2013.

LIU, P. et al. Xanthoceraside attenuates tau hyperphosphorylation and cognitive deficits in intracerebroventricular-streptozotocin injected rats. **Psychopharmacology**, 2014.

LOPES, L. T. et al. Anatomical and functional connections between the locus coeruleus and the nucleus tractus solitarius in neonatal rats. **Neuroscience**, 2016.

MARÍN-TEVA, J. L. et al. Microglia Promote the Death of Developing Purkinje Cells. **Neuron**, 2004.

MARTINEZ, F. O.; HELMING, L.; GORDON, S. **Alternative activation of macrophages: An immunologic functional perspectiveAnnual Review of Immunology**, 2009.

MATCHETT, B. J. et al. **The mechanistic link between selective vulnerability of the locus coeruleus and neurodegeneration in Alzheimer's diseaseActa Neuropathologica**, 2021.

MATHIE, A.; WOOLTORTON, J. R. A.; WATKINS, C. S. **Voltage-activated potassium**

channels in mammalian neurons and their block by novel pharmacological agentsGeneral Pharmacology, 1998.

MATSUZAKI, K. et al. β-amyloid infusion into lateral ventricle alters behavioral thermoregulation and attenuates acquired heat tolerance in rats. **Temperature**, 2015.

MATTHEWS, K. L. et al. Noradrenergic changes, aggressive behavior, and cognition in patients with dementia. **Biological Psychiatry**, 2002.

MAWUENYEGA, K. G. et al. Decreased clearance of CNS β-amyloid in Alzheimer's disease. **Science**, 2010.

MCCURRY, S. M. et al. **Treatment of sleep disturbance in Alzheimer's diseaseSleep Medicine Reviews**, 2000.

MCGEER, P. L.; MCGEER, E. G. **The amyloid cascade-inflammatory hypothesis of Alzheimer disease: Implications for therapyActa Neuropathologica**, 2013.

MELLEN, N. M. et al. Opioid-induced quantal slowing reveals dual networks for respiratory rhythm generation. **Neuron**, 2003.

MENUET, C. et al. Raphé tauopathy alters serotonin metabolism and breathing activity in terminal Tau.P301L mice: Possible implications for tauopathies and Alzheimer's disease. **Respiratory Physiology and Neurobiology**, 2011.

MILÀ-ALOMÀ, M. et al. Amyloid beta, tau, synaptic, neurodegeneration, and glial biomarkers in the preclinical stage of the Alzheimer's continuum. **Alzheimer's and Dementia**, 2020.

MINTER, M. R.; TAYLOR, J. M.; CRACK, P. J. **The contribution of neuroinflammation to amyloid toxicity in Alzheimer's diseaseJournal of Neurochemistry**, 2016.

MIYAMOTO, A. et al. Microglia contact induces synapse formation in developing somatosensory cortex. **Nature Communications**, 2016.

MONACELLI, A. M. et al. Spatial disorientation in Alzheimer's disease: The remembrance of things passed. **Neurology**, 2003.

MORAN, M. et al. Sleep disturbance in mild to moderate Alzheimer's disease. **Sleep Medicine**, 2005.

MORRIS, J. C. **Early-stage and preclinical Alzheimer disease**. Alzheimer Disease and Associated Disorders. **Anais**...2005

MORTOLA, J. P.; REZZONICO, R. Metabolic and ventilatory rates in newborn kittens during acute hypoxia. **Respiration Physiology**, 1988.

MOTZKO-SOARES, A. C. P. et al. Thermoregulatory profile of neurodegeneration-induced dementia of the Alzheimer's type using intracerebroventricular streptozotocin in rats. **Acta Physiologica**, 2018.

MULKEY, D. K. et al. Respiratory control by ventral surface chemoreceptor neurons in rats. **Nature Neuroscience**, 2004.

MULLER, A. P. et al. Physical exercise exacerbates memory deficits induced by intracerebroventricular stz but improves insulin regulation of H 2O2 production in mice synaptosomes. **Journal of Alzheimer's Disease**, 2012.

NAKAHATA, Y.; YASUDA, R. **Plasticity of spine structure: Local signaling, translation and cytoskeletal reorganizationFrontiers in Synaptic Neuroscience**, 2018.

NATTIE, E. **CO2, brainstem chemoreceptors and breathingProgress in Neurobiology**, 1999.

NATTIE, E. E.; LI, A. CO2 dialysis in nucleus tractus solitarius region of rat increases ventilation in sleep and wakefulness. **Journal of Applied Physiology**, 2002.

NATTIE, E.; LI, A. **Central chemoreception in wakefulness and sleep: Evidence for a distributed network and a role for orexinJournal of Applied Physiology**, 2010.

NATTIE, E.; LI, A. Central chemoreceptors: Locations and functions. **Comprehensive Physiology**, 2012.

NICHOLS, N. L. et al. Intrinsic chemosensitivity of individual nucleus tractus solitarius (NTS) and locus coeruleus (LC) neurons from neonatal rats. **Advances in experimental medicine and biology**, v. 605, p. 348–52, 2008.

NIXON, R. A. Amyloid precursor protein & endosomal-lysosomal dysfunction in Alzheimer's disease: Inseparable partners in a multifactorial disease. **FASEB Journal**, 2017.

NIZAMI, S. et al. **Microglial inflammation and phagocytosis in Alzheimer's disease: Potential therapeutic targetsBritish Journal of Pharmacology**, 2019.

NOBLE, W. et al. Minocycline reduces the development of abnormal tau species in models of Alzheimer's disease. **The FASEB Journal**, 2009.

NOGUÉS, M. A.; RONCORONI, A. J.; BENARROCH, E. **Breathing control in**

neurological diseasesClinical Autonomic Research, 2002.

NONAKA, K.; NAKAZAWA, Y.; KOTORII, T. Effects of antibiotics, minocycline and ampicillin, on human sleep. **Brain Research**, 1983.

NORDENGEN, K. et al. Glial activation and inflammation along the Alzheimer's disease continuum. **Journal of Neuroinflammation**, 2019.

O'BRIEN, H. L. et al. Visual mechanisms of spatial disorientation in Alzheimer's disease. **Cerebral Cortex**, 2001.

OBAL, F.; KRUEGER, J. M. **Biochemical regulation of non-rapid-eye-movement sleepFrontiers in Bioscience**, 2003.

ORTEGA-SÁENZ, P. et al. Cellular properties and chemosensory responses of the human carotid body. **Journal of Physiology**, 2013.

OSORIO, R. S. et al. The interaction between sleep-disordered breathing and apolipoprotein E genotype on cerebrospinal fluid biomarkers for Alzheimer's disease in cognitively normal elderly individuals. **Neurobiology of Aging**, 2014.

OSTROWSKI, T. D. et al. H_2O_2 induces delayed hyperexcitability in nucleus tractus solitarii neurons. **Neuroscience**, v. 262, p. 53–69, mar. 2014a.

OSTROWSKI, T. D. et al. Depressed GABA and glutamate synaptic signaling by 5-HT1A receptors in the nucleus tractus solitarii and their role in cardiorespiratory function. **Journal of neurophysiology**, v. 111, n. 12, p. 2493–2504, jun. 2014b.

OYAMADA, Y. et al. Respiration-modulated membrane potential and chemosensitivity of

locus coeruleus neurones in the in vitro brainstem-spinal cord of the neonatal rat. **The Journal of physiology**, v. 513 (Pt 2, n. 2, p. 381–98, dez. 1998.

P., A.-B. et al. Locus coeruleus at asymptomatic early and middle Braak stages of neurofibrillary tangle pathology. **Neuropathology and Applied Neurobiology**, 2017.

PALMER, A. M. et al. Catecholaminergic neurones assessed ante-mortem in Alzheimer's disease. **Brain Research**, 1987.

PAMPHLETT, R.; KUM JEW, S. Different Populations of Human Locus Ceruleus Neurons Contain Heavy Metals or Hyperphosphorylated Tau: Implications for Amyloid-β and Tau Pathology in Alzheimer's Disease. **Journal of Alzheimer's Disease**, 2015.

PAN, Y. et al. Messenger RNA and protein expression analysis of voltage-gated potassium channels in the brain of Aβ 25-35 -treated rats. **Journal of Neuroscience Research**, v. 77, n. 1, p. 94–99, 2004.

PARACHIKOVA, A. et al. Reductions in amyloid-β-derived neuroinflammation, with minocycline, restore cognition but do not significantly affect tau hyperphosphorylation. **Journal of Alzheimer's Disease**, 2010.

PAXINOS, G.; WATSON, C. The Rat Brain in Stereotaxic Coordinates Sixth Edition. **Elsevier Academic Press**, 2007.

PETER-DEREX, L. et al. **Sleep and Alzheimer's diseaseSleep Medicine Reviews**, 2015.

PETERSON, A. C.; LI, C. S. R. **Noradrenergic dysfunction in Alzheimer's and Parkinson's Diseases-An overview of imaging studiesFrontiers in Aging Neuroscience**,

2018.

PEYRON, C. et al. Neurons containing hypocretin (orexin) project to multiple neuronal systems. **Journal of Neuroscience**, 1998.

PICKERING, M.; O'CONNOR, J. J. **Pro-inflammatory cytokines and their effects in the dentate gyrusProgress in Brain Research**, 2007.

PIERCE, A. L.; BULLAIN, S. S.; KAWAS, C. H. **Late-Onset Alzheimer DiseaseNeurologic Clinics**, 2017.

PINEDA, J.; AGHAJANIAN, G. K. Carbon dioxide regulates the tonic activity of locus coeruleus neurons by modulating a proton- and polyamine-sensitive inward rectifier potassium current. **Neuroscience**, 1997.

PUTNAM, R. W. **CO2 chemoreception in cardiorespiratory controlJournal of Applied Physiology**, 2010.

PUTNAM, R. W.; FILOSA, J. A.; RITUCCI, N. A. **Cellular mechanisms involved in CO2 and acid signaling in chemosensitive neuronsAmerican Journal of Physiology - Cell Physiology**, 2004.

QIU, Y. et al. Cognitive heterogeneity in probable Alzheimer disease: Clinical and neuropathologic features. **Neurology**, 2019.

QUERFURTH, H. W.; LAFERLA, F. M. Alzheimer's disease: mechanism of disease. **The New England Journal of Medicine**, 2010.

RAI, S. et al. Glial activation and post-synaptic neurotoxicity: The key events in

Streptozotocin (ICV) induced memory impairment in rats. **Pharmacology Biochemistry and Behavior**, 2014.

RAMIREZ, J. M.; ANDERSON, T. M. **Respiratory rhythm generation: Triple oscillator hypothesisF1000Research**, 2017.

RANSOHOFF, R. M.; PERRY, V. H. **Microglial physiology: Unique stimuli, specialized responsesAnnual Review of Immunology**, 2009.

RASKIND, M. A. et al. Patterns of cerebrospinal fluid catechols support increased central noradrenergic responsiveness in aging and Alzheimer's disease. **Biological Psychiatry**, 1999.

RAVELLI, K. G. et al. Intracerebroventricular Streptozotocin as a Model of Alzheimer's Disease: Neurochemical and Behavioral Characterization in Mice. **Neurotoxicity Research**, 2017.

REITZ, C.; BRAYNE, C.; MAYEUX, R. **Epidemiology of Alzheimer diseaseNature Reviews Neurology**, 2011.

RITUCCI, N. A.; DEAN, J. B.; PUTNAM, R. W. Somatic vs. dendritic responses to hypercapnia in chemosensitive locus coeruleus neurons from neonatal rats. **American journal of physiology. Cell physiology**, v. 289, n. 5, p. C1094-104, nov. 2005.

ROH, J. H. et al. Disruption of the sleep-wake cycle and diurnal fluctuation of amyloid-β in mice with Alzheimer's disease pathology. **Science Translational Medicine**, 2012.

RUBIO-PEREZ, J. M.; MORILLAS-RUIZ, J. M. **A review: Inflammatory process in**

Alzheimer's disease, role of cytokinesThe Scientific World Journal, 2012.

RYU, J. K. et al. Minocycline inhibits neuronal death and glial activation induced by β-amyloid peptide in rat hippocampus. **GLIA**, 2004.

S., A.-I. Sleep and sleep disorders in patients with dementia: Treatable or not? **Sleep and Biological Rhythms**, 2010.

SADOWSKY, C. H.; GALVIN, J. E. **Guidelines for the management of cognitive and behavioral problems in dementiaJournal of the American Board of Family Medicine**, 2012.

SALKOVIC-PETRISIC, M. et al. **What have we learned from the streptozotocin-induced animal model of sporadic Alzheimer's disease, about the therapeutic strategies in Alzheimer's researchJournal of Neural Transmission**, 2013.

SALKOVIC-PETRISIC, M. et al. Multi-target iron-chelators improve memory loss in a rat model of sporadic Alzheimer's disease. **Life Sciences**, 2015.

SANTOS, T. DE O. et al. Early and late neurodegeneration and memory disruption after intracerebroventricular streptozotocin. **Physiology and Behavior**, 2012.

SARDI, F. et al. **Alzheimer's disease, autoimmunity and inflammation. The good, the bad and the uglyAutoimmunity Reviews**, 2011.

SASTRE, M. et al. Nonsteroidal anti-inflammatory drugs repress β-secretase gene promoter activity by the activation of PPARγ. **Proceedings of the National Academy of Sciences of the United States of America**, 2006.

SASTRE, M.; WALTER, J.; GENTLEMAN, S. M. **Interactions between APP secretases and inflammatory mediatorsJournal of Neuroinflammation**, 2008.

SCHIEVEN, G. The Biology of p38 Kinase: A Central Role in Inflammation. **Current Topics in Medicinal Chemistry**, 2005.

SCHIEVEN, G. The p38α Kinase Plays a Central Role In Inflammation. **Current Topics in Medicinal Chemistry**, 2009.

SCHWAB, C.; MCGEER, P. L. Inflammatory aspects of Alzheimer disease and other neurodegenerative disorders. In: **Handbook of Infection and Alzheimer's Disease**. [s.l: s.n.].

SCHWARZACHER, S. W.; RÜB, U.; DELLER, T. Neuroanatomical characteristics of the human pre-Bötzinger complex and its involvement in neurodegenerative brainstem diseases. **Brain**, 2011.

SEABROOK, T. J. et al. Minocycline affects microglia activation, Aβ deposition, and behavior in APP-tg mice. **GLIA**, 2006.

SERRA, L. et al. In vivo mapping of brainstem nuclei functional connectivity disruption in Alzheimer's disease. **Neurobiology of Aging**, 2018.

SERRANO-POZO, A. et al. Neuropathological alterations in Alzheimer disease. **Cold Spring Harbor Perspectives in Medicine**, 2011.

ŠERÝ, O. et al. **Molecular mechanisms of neuropathological changes in Alzheimer's disease: A reviewFolia Neuropathologica**, 2013.

SHADFAR, S. et al. **Involvement of inflammation in Alzheimer's disease pathogenesis and therapeutic potential of anti-inflammatory agentsArchives of Pharmacal Research**, 2015.

SHAMIM, D.; LASKOWSKI, M. Inhibition of Inflammation Mediated Through the Tumor Necrosis Factor α Biochemical Pathway Can Lead to Favorable Outcomes in Alzheimer Disease. **Journal of Central Nervous System Disease**, 2017.

SHANKAR, G. M. et al. Amyloid-β protein dimers isolated directly from Alzheimer's brains impair synaptic plasticity and memory. **Nature Medicine**, 2008.

SHARMA, S.; RAKOCZY, S.; BROWN-BORG, H. **Assessment of spatial memory in miceLife Sciences**, 2010.

SHIN, J. W. et al. α-Asarone ameliorates memory deficit in lipopolysaccharide-treated mice via suppression of pro-inflammatory cytokines and microglial activation. **Biomolecules and Therapeutics**, 2014.

SICA, A.; MANTOVANI, A. **Macrophage plasticity and polarization: In vivo veritasJournal of Clinical Investigation**, 2012.

SILVA, T. M. et al. Minocycline alters expression of inflammatory markers in autonomic brain areas and ventilatory responses induced by acute hypoxia. **Experimental Physiology**, 2018.

SILVESTRELLI, G.; LANARI, A.; DROGHETTI, A. Ventilatory disorders. **Frontiers of Neurology and Neuroscience**, 2012.

SIMIC, G. et al. **Does Alzheimer's disease begin in the brainstem?: AnnotationNeuropathology and Applied Neurobiology**, 2009.

ŠIMIĆ, G. et al. **Monoaminergic neuropathology in Alzheimer's diseaseProgress in Neurobiology**, 2017.

SMITH, J. C. et al. Pre-Bötzinger complex: A brainstem region that may generate respiratory rhythm in mammals. **Science**, 1991.

SMITH, J. C. et al. **Brainstem respiratory networks: Building blocks and microcircuitsTrends in Neurosciences**, 2013.

SMITH, M. DE A. C. Doença de Alzheimer TT - Alzheimer disease. **Rev Bras Psiquiatr**, 1999.

SONG, J. Z. et al. Dysfunction of GABAergic neurons in the parafacial zone mediates sleep disturbances in a streptozotocin-induced rat model of sporadic Alzheimer's disease. **Metabolic Brain Disease**, 2018.

SONNER, P. M.; STERN, J. E. Functional role of A-type potassium currents in rat presympathetic PVN neurones. **The Journal of physiology**, v. 582, n. Pt 3, p. 1219–38, ago. 2007.

SPERLING, R. A.; KARLAWISH, J.; JOHNSON, K. A. **Preclinical Alzheimer disease - The challenges aheadNature Reviews Neurology**, 2013.

SPIRES, T. L.; HYMAN, B. T. **Neuronal structure is altered by amyloid plaquesReviews in the Neurosciences**, 2004.

STANDRIDGE, J. Vicious Cycles Within the Neuropathophysiologic Mechanisms of Alzheimers Disease. **Current Alzheimer Research**, 2006.

STEINER, A. A.; ROCHA, M. J. A.; BRANCO, L. G. S. A neurochemical mechanism for hypoxia-induced anapyrexia. **American Journal of Physiology - Regulatory Integrative and Comparative Physiology**, 2002.

STOKES, J. A. et al. Minocycline blocks glial cell activation and ventilatory acclimatization to hypoxia. **Journal of Neurophysiology**, 2017.

STOWELL, R. D. et al. Cerebellar microglia are dynamically unique and survey Purkinje neurons in vivo. **Developmental Neurobiology**, 2018.

STRUBLE, R. G. et al. **Is brain amyloid production a cause or a result of dementia of the Alzheimer's type?Journal of Alzheimer's Disease**, 2010.

STUNDEN, C. E. et al. Development of in vivo ventilatory and single chemosensitive neuron responses to hypercapnia in rats. **Respiration physiology**, v. 127, n. 2–3, p. 135–55, set. 2001.

SUNYER, B. et al. Barnes maze, a useful task to assess spatial reference memory in the mice. **Protocol Exchange**, 2007.

SZKUDELSKI, T. **The mechanism of alloxan and streptozotocin action in B cells of the rat pancreasPhysiological Research**, 2001.

SZYMUSIAK, R.; MCGINTY, D. **Hypothalamic regulation of sleep and arousal**. Annals of the New York Academy of Sciences. **Anais**...2008

TAN, W. et al. Silencing preBötzinger Complex somatostatin-expressing neurons induces persistent apnea in awake rat. **Nature Neuroscience**, 2008.

TATTERSALL, G. J.; MILSOM, W. K. Hypoxia reduces the hypothalamic thermogenic threshold and thermosensitivity. **Journal of Physiology**, 2009.

TAXINI, C. L. et al. Ionotropic but not metabotropic glutamatergic receptors in the locus coeruleus modulate the hypercapnic ventilatory response in unanaesthetized rats. **Acta Physiologica**, 2013.

TEJERA, D.; T. HENEKA, M. Microglia in Alzheimer's Disease: The Good, the Bad and the Ugly. **Current Alzheimer Research**, 2016.

TENORIO-LOPES, L. et al. Consequences of maternal omega-3 polyunsaturated fatty acid supplementation on respiratory function in rat pups. **Journal of Physiology**, 2017.

TERRY, R. D. et al. Physical basis of cognitive alterations in alzheimer's disease: Synapse loss is the major correlate of cognitive impairment. **Annals of Neurology**, 1991.

THAL, D. R. et al. Phases of Aβ-deposition in the human brain and its relevance for the development of AD. **Neurology**, 2002.

THAMEEM DHEEN, S.; KAUR, C.; LING, E.-A. Microglial Activation and its Implications in the Brain Diseases. **Current Medicinal Chemistry**, 2007.

THEOFILAS, P. et al. Locus coeruleus volume and cell population changes during Alzheimer's disease progression: A stereological study in human postmortem brains with potential implication for early-stage biomarker discovery. **Alzheimer's and Dementia**,

2017.

THEOFILAS, P. et al. Probing the correlation of neuronal loss, neurofibrillary tangles, and cell death markers across the Alzheimer's disease Braak stages: a quantitative study in humans. **Neurobiology of Aging**, 2018.

TING, J. T. et al. Acute brain slice methods for adult and aging animals: Application of targeted patch clamp analysis and optogenetics. **Methods in Molecular Biology**, 2014.

TING, J. T. et al. Preparation of Acute Brain Slices Using an Optimized N-Methyl-D-glucamine Protective Recovery Method. **Journal of visualized experiments : JoVE**, 2018.

TOBINICK, E. **Tumour necrosis factor modulation for treatment of Alzheimer's disease: Rationale and current evidenceCNS Drugs**, 2009.

TOTA, S. et al. Protective effect of quercetin against intracerebral streptozotocin induced reduction in cerebral blood flow and impairment of memory in mice. **Behavioural Brain Research**, 2010.

TOWNSEND, M. et al. Effects of secreted oligomers of amyloid β-protein on hippocampal synaptic plasticity: A potent role for trimers. **Journal of Physiology**, 2006.

TROUSSIÈRE, A. C. et al. Treatment of sleep apnoea syndrome decreases cognitive decline in patients with Alzheimer's disease. **Journal of Neurology, Neurosurgery and Psychiatry**, 2014.

TSAI, M. S. et al. Risk of Alzheimer's Disease in Obstructive Sleep Apnea Patients With or Without Treatment: Real-World Evidence. **Laryngoscope**, 2020.

VAN DAM, D.; DE DEYN, P. P. **Animal models in the drug discovery pipeline for Alzheimer's diseaseBritish Journal of Pharmacology**, 2011.

VERDONK, F. et al. Phenotypic clustering: a novel method for microglial morphology analysis. **Journal of Neuroinflammation**, v. 13, n. 1, p. 153, 17 dez. 2016.

VERRET, L. et al. Inhibitory interneuron deficit links altered network activity and cognitive dysfunction in alzheimer model. **Cell**, 2012.

VICENTE, M. C. et al. Orexinergic system in the locus coeruleus modulates the CO2 ventilatory response. **Pflugers Archiv European Journal of Physiology**, 2016a.

VICENTE, M. C. et al. Orexinergic system in the locus coeruleus modulates the CO<inf>2</inf>ventilatory response. **Pflugers Archiv European Journal of Physiology**, v. 468, n. 5, 2016b.

VICENTE, M. C. et al. Hypercapnic and Hypoxic Respiratory Response During Wakefulness and Sleep in a Streptozotocin Model of Alzheimer's Disease in Rats. **Journal of Alzheimer's Disease**, v. 65, n. 4, p. 1159–1174, 25 set. 2018.

VICENTE, M. C. et al. Decreased excitability of locus coeruleus neurons during hypercapnia is exaggerated in the streptozotocin-model of Alzheimer's disease. **Experimental Neurology**, 2020.

VILLEMAGNE, V. L. et al. **Tau imaging: Early progress and future directionsThe Lancet Neurology**, 2015.

VITIELLO, M. V. et al. Sleep disturbances in patients with mild-stage Alzheimer's disease.

Journals of Gerontology, 1990.

VITVITSKY, V. M. et al. Na + and K + ion imbalances in Alzheimer's disease. **Biochimica et Biophysica Acta - Molecular Basis of Disease**, 2012.

WALSH, D. M.; SELKOE, D. J. **Aβ oligomers - A decade of discoveryJournal of Neurochemistry**, 2007.

WANG, H. L. et al. Minocycline attenuates post-operative cognitive impairment in aged mice by inhibiting microglia activation. **Journal of Cellular and Molecular Medicine**, 2016.

WANG, J. et al. **A systemic view of Alzheimer disease - Insights from amyloid-β metabolism beyond the brainNature Reviews Neurology**, 2017.

WANG, W. Y. et al. **Role of pro-inflammatory cytokines released from microglia in Alzheimer's diseaseAnnals of Translational Medicine**, 2015.

WEAVER, J. D. et al. Interleukin-6 and risk of cognitive decline: Macarthur studies of successful aging. **Neurology**, 2002.

WEINERT, D. **Circadian temperature variation and ageingAgeing Research Reviews**, 2010.

WHITEN, D. R. et al. Tumour necrosis factor induces increased production of extracellular amyloid-β- and α-synuclein-containing aggregates by human Alzheimer's disease neurons. **Brain Communications**, 2020.

WILSON, R. S. et al. The natural history of cognitive decline in Alzheimer's disease.

Psychology and Aging, 2012.

WILSON, R. S. et al. Neural reserve, neuronal density in the locus ceruleus, and cognitive decline. **Neurology**, 2013.

WINER, J. R.; MANDER, B. A. **Waking up to the importance of sleep in the pathogenesis of Alzheimer diseaseJAMA Neurology**, 2018.

WISOR, J. P.; SCHMIDT, M. A.; CLEGERN, W. C. Evidence for neuroinflammatory and microglial changes in the cerebral response to sleep loss. **Sleep**, v. 34, n. 3, p. 261–272, 2011a.

WISOR, J. P.; SCHMIDT, M. A.; CLEGERN, W. C. Evidence for neuroinflammatory and microglial changes in the cerebral response to sleep loss. **Sleep**, 2011b.

WU, D. C. et al. Blockade of microglial activation is neuroprotective in the 1-methyl-4-phenyl-1,2,3,6-tetrahydropyridine mouse model of Parkinson disease. **Journal of Neuroscience**, 2002.

XU, H. et al. Modulation of kir4.1 and kir5.1 by hypercapnia and intracellular acidosis. **The Journal of physiology**, v. 524 Pt 3, p. 725–35, maio 2000.

XU, J. et al. Tetracycline derivatives resist the assembly behavior of human islet amyloid polypeptide. **Biochimie**, 2020.

YAFFE, K. et al. Sleep-disordered breathing, hypoxia, and risk of mild cognitive impairment and dementia in older women. **JAMA - Journal of the American Medical Association**, 2011.

YANG, C. N. et al. Mechanism mediating oligomeric Aβ clearance by naïve primary microglia. **Neurobiology of Disease**, 2011.

YEO, H. G. et al. Characterization of Cerebral Damage in a Monkey Model of Alzheimer's Disease Induced by Intracerebroventricular Injection of Streptozotocin. **Journal of Alzheimer's Disease**, 2015.

YU, S. P. et al. Enhancement of outward potassium current may participate in β-amyloid peptide-induced cortical neuronal death. **Neurobiology of Disease**, 1998.

ZAROW, C. et al. Neuronal loss is greater in the locus coeruleus than nucleus basalis and substantia nigra in Alzheimer and Parkinson diseases. **Archives of Neurology**, 2003.

ZHU, S. et al. Minocycline inhibits cytochrome c release and delays progression of amyotrophic lateral sclerosis in mice. **Nature**, 2002.

Journal of Alzheimer's Disease xx (20xx) x–xx
DOI 10.3233/JAD-180397
IOS Press

Hypercapnic and Hypoxic Respiratory Response During Wakefulness and Sleep in a Streptozotocin Model of Alzheimer's Disease in Rats

Mariane C. Vicente[a], Maria C. Almeida[b], Kênia C. Bícego[a], Daniel C. Carrettiero[b] and Luciane H. Gargaglioni[a,*]
[a]*Department of Animal Morphology and Physiology, Sao Paulo State University–UNESP/FCAV at Jaboticabal, SP, Brazil*
[b]*Center for Natural and Human Sciences; Universidade Federal do ABC (UFABC); São Bernardo do Campo, SP, Brazil*

Accepted 23 July 2018

Abstract. Besides the typical cognitive decline, patients with Alzheimer's disease (AD) develop disorders of the respiratory system, such as sleep apnea, shortness of breath, and arrhythmias. These symptoms are aggravated with the progression of the disease. However, the cause and nature of these disturbances are not well understood. Here, we treated animals with intracerebroventricular streptozotocin (STZ, 2 mg/kg), a drug that has been described to cause Alzheimer-like behavioral and histopathological impairments. We measured ventilation ($\dot{V}_E$), electroencephalography, and electromyography during normocapnia, hypercapnia, and hypoxia in Wistar rats. In addition, we performed western blot analyses for phosphorylated tau, total tau, and amyloid-β (Aβ) peptide in the locus coeruleus (LC), retrotrapezoid nucleus, medullary raphe, pre-Bötzinger/Bötzinger complex, and hippocampus, and evaluated memory and learning acquisition using the Barnes maze. STZ treatment promoted memory and learning deficits and increased the percentage of total wakefulness during normocapnia and hypercapnia due to a reduction in the length of episodes of wakefulness. CO_2-drive to breathe during wakefulness was increased by 26% in STZ-treated rats due to an enhanced tidal volume, but no changes in $\dot{V}_E$ were observed in room air or hypoxic conditions. The STZ group also showed a 70% increase of Aβ in the LC and no change in tau protein phosphorylation. In addition, no alteration in body temperature was observed. Our findings suggest that AD animals present an increased sensitivity to CO_2 during wakefulness, enhanced Aβ in the LC, and sleep disruption.

Keywords: Breathing, chemosensitivity, dementia, hypoxia, locus coeruleus, streptozotocin

Corrected Proof

INTRODUCTION

Alzheimer's disease (AD) is a neurodegenerative disorder, often associated with age, whose cognitive and neuropsychiatric manifestations result in a progressive impairment and eventual disability [1]. AD is the most common cause of dementia, affecting more than 45 million people worldwide [2].

*Correspondence to: Luciane H. Gargaglioni, Via de acesso Paulo Donato Castellane s/n, 14870-000, Departamento de Morfologia e Fisiologia Animal, Faculdade de Ciências Agrárias e Veterinárias, Universidade Estadual Paulista Júlio de Mesquita Filho, Jaboticabal, SP, Brasil. Tel.: +55 16 32092656; Fax: +55 16 32024275; E-mail: luciane.gargaglioni@unesp.br.

ISSN 1387-2877/18/$35.00 © 2018 – IOS Press and the authors. All rights reserved

This disease is characterized by the accumulation of amyloid-β (Aβ) plaques, intracellular neurofibrillary tangles (NFTs) of hyperphosphorylated tau protein, and decreased synaptic density, which eventually leads to widespread neurodegeneration and loss of neurotransmitters [3]. The neurodegeneration occurs in multiple areas of the brain, including the hippocampus, cortex, amygdala, neocortex, and brainstem structures [4–8].

AD is a multifactorial, neurodegenerative, age-related disorder with multiple components involved in its progression [9]. Therefore, the establishment of animal models that reproduce human pathology becomes complex. Despite this, the use of animal models has been crucial in defining critical disease-related mechanisms and has been at the forefront of evaluating novel therapeutic approaches [10]. An animal model that replicates many behavioral and histological aspects of AD was created by the intracerebroventricular (icv) injection of streptozotocin (STZ) [11–14]. This drug promotes a decrement in brain glucose/energy metabolism [11], which is considered an incipient sign of AD [11–14], and have been used to induce AD-like neurodegeneration in rats, since the metabolic abnormalities found in this model resemble those found in sporadic AD. For instance, these animals display progressive loss of memory and learning, increased brain ventricular volume, abnormalities in mitochondrial function, increased tau phosphorylation and increased Aβ peptide in brain areas [15–17]. These morphological changes result in damage and loss of neuronal cells [18]. Therefore, the use of the icv STZ model represents a viable experimental approach to explore changes involved in AD-like neurodegeneration in rats.

Aside from severe cognitive deficits, epidemiological studies have reported that up to 45% of patients with AD have sleep disturbances, such as increasing sleep fragmentation, nighttime awakenings, and a greater tendency for daytime sleep [19, 20]. These symptoms may occur at early stages of AD, but seem to be correlated with a more severe cognitive decline [21, 22]. In addition, it is known that over 70% of institutionalized patients with AD exhibit respiratory changes, and that these problems can contribute to cognitive decline [23–26]. According to Gaig et al. [25], obstructive sleep apnea may worsen or cause cognitive impairment in AD. Furthermore, there is a strong correlation of the severity of sleep-disordered breathing with the severity of AD [26]. The late stages of clinical AD are accompanied by shortness of breath [27]. This evidence shows that regions responsible for respiratory control are possibly changed.

There is a paucity of data in the literature on the study of respiratory control in AD progression. In this scenario, the use of animals as models are valid and essential in AD-related research, as they allow the assessment of early or late pathophysiological processes that are not accessible in human patients. Recently, Ebel et al. [28] demonstrated that icv STZ induces increased respiration at rest and blunted peripheral chemoreflex responses and a small change in the CO_2-drive to breathe. However, the authors did not evaluate the respiratory pattern and ventilatory responses to hypoxic and hypercapnic stimuli during the different phases of the sleep/wake cycle, which was carried out in the present study. This is a crucial point, since the prevalence of sleep apnea in AD patients is high, with 70% to 80% of patients presenting five or more apnea-hypopnea episodes per hour of sleep, and 38% to 48% of individuals with 20 or more episodes of apnea during the sleep phase [27]. Thus, it is quite likely that there is a difference in the chemosensitivity of patients with the AD-dependent phase of the sleep/wake cycle. Therefore, we used the STZ model in order to induce AD-like neurodegeneration in rats to determine the ventilatory response to hypoxia and hypercapnia during wakefulness and non-rapid eye movement (NREM) sleep. In addition, we performed western blot analyses for phosphorylated tau, total tau and amyloid-β peptide (Aβ) in locus coeruleus (LC), retrotrapezoid nucleus (RTN), medullary raphe (Raphe), pre-Bötzinger/Bötzinger complex (PreBötz/BötzC) and hippocampus (HPC), and evaluated memory and learning acquisition using the Barnes maze.

MATERIAL AND METHODS

Animals

Male Wistar rats (3-4 months old; weight 300–350 g) were housed in a temperature-controlled chamber maintained at 24–26°C (ALE 9902001; Alesco Ltda., Monte Mor, SP, Brazil) with a 12:12-h light/dark cycle, and had free access to water and food. The experiments were performed between 08.00 a.m. and 17.00 p.m.

The study was conducted in compliance with the guidelines of the National Council for the Control of Animal Experimentation (CONCEA, MCT, Brazil) and with the approval of the Faculty of Agricultural and Veterinary Sciences and Animal Care and

Corrected Proof

Use Committee (CEUA, FACV-UNESP, Jaboticabal campus; Protocol no. n° 6.030/016).

Surgical procedures

All surgical procedures were performed under anesthesia with an intraperitoneal injection of 100 mg/kg of ketamine (Union National Pharmaceutical Chemistry S/A, Embu-Guaçu, SP, Brazil) and 10 mg/kg of xylazine (Laboratories Calier S/A Barcelona, Spain). Postoperatively, the animals were treated with antibiotic (enrofloxacin, 10 mg/kg, intramuscular) and analgesic (flunixin meglumine, 2.5 mg/kg, subcutaneous) agents.

Intracerebroventricular injection of streptozotocin

The head was shaved and the skin was sterilized with betadine solution and alcohol. The rats were fixed to a Kopf stereotaxic apparatus (David Kopf Instruments, Tujunga, CA, USA). The scalp was incised over the sagittal suture, the periosteum was excised, and two small bilateral orifices were made using a sterilized dental drill to access both lateral ventricles of the brain, where icv injections were to be applied. The following coordinates were used: –0.8 mm posterior, ± 1.4 mm lateral, and –4.4 below bregma [29, 30]. Animals received bilateral icv injections of STZ (2 mg/kg dissolved in 0.05 mol/L citrate buffer, pH 4.5; Sigma, St. Louis, MO) or citrate buffer (2 μL/ventricle) [31]. For the microinjection of drug and vehicle, a 5-μL Hamilton syringe was used, linked to a PE 10 polyethylene tubing, connected to a gengival needle for the application [30]. Thirty days after icv injection, rats were submitted to the behavioral, respiratory, or molecular tests. The respiratory tests were performed in a different group of animals, whereas the behavioral and molecular tests were performed in the same group.

Electroencephalogram (EEG) and electromyogram (EMG) electrodes

Seven days before the beginning of the respiratory tests, EEG and EMG electrodes were implanted in the group that would undergo the respiratory tests. Three EEG electrodes were introduced: the frontal electrode, located 2 mm anterior to bregma and 2 mm lateral to the midline; the parietal electrode, positioned 4 mm anterior to the lambda and 2 mm lateral to the midline; and the electrode "ground" which was inserted between the frontal and parietal electrodes. For EMG recordings, a pair of electrodes were inserted deep into the neck musculature of the rats. These electrodes allowed us to analyze ventilation in the different phases of the sleep/wake cycle.

Body temperature

On the same day as the EEG and EMG surgery, the rats underwent a second surgery for the implantation of a temperature datalogger (SubCue Dataloggers, Calgary, Canada) into the abdominal cavity through a midline laparotomy. The datalogger was programmed to acquire body temperature (Tb) data every 7 min.

Behavioral analysis

Barnes maze

The Barnes maze test was used to assess spatial memory and learning to confirm the success and reliability of the model.

The Barnes maze test consists of a non-aquatic test for memory and spatial learning [32]. The protocol was adapted from Sunyer et al. [33]. The maze was made from a circular, 13-mm thick, white PVC platform (110-cm diameter), which was maintained in the same position throughout the experiment. Twenty holes (10 cm in diameter, 7.5 cm between each hole) were made on the perimeter and the platform was mounted on top of a metal support, 105 cm above the ground. The maze was divided into target hole (T), opposite hole (OP), 9 holes clockwise (1 to 9, counting from T), and 9 holes counterclockwise (–1 to –9, counting from T). The escape cage, below the T hole, had walls covered with black plastic to make the inside dark and attractive to the rats. The platform was also illuminated with a fluorescent white light and visual cues (colored geometric figures) were placed around the labyrinth as points of spatial reference for the animal to escape from the open platform to the "target hole" These clues were not removed throughout the experiment. After testing each rat, as explained below, the whole maze was cleaned using 10% ethanol to avoid olfactory cues and the platform was rotated to avoid intra-maze odor or visual cues. All sessions were recorded by a video camera for further analysis. Prior to testing (probe day), training sessions were performed over 5 days to familiarize the animals with the maze and to allow them learn the location of the escape zone.

Corrected Proof

Acquisition phase

In this stage, spatial learning was evaluated through latency to enter the target hole. From days 1 to 4, each animal was placed in a square start chamber in the center of the maze. After 10 s, the chamber was removed and the animal was allowed to explore the maze for 3 min. The end of the trial was considered when the animal entered the target hole. Therefore, the animal was allowed to stay inside the dark cage for 1 min and, after this period, was returned to its home cage. If the animal had not entered in the target hole after 3 min from the beginning of the test, it was gently coerced to the target hole. These steps were repeated for 4 trials per day with an intertrial interval of 15 min over 4 consecutive days.

Probe trial

On day 5, 24 h after the last training day, the escape cage was removed, while the maze was maintained in the same position as training days. The animal was placed in the start chamber in the center of the maze and, after 10 s, it was removed and the animal was allowed to explore the maze for 90 s. The probe trial was performed in order to determine whether the animals remembered the location of the target hole. The number of times the animal searched for the "target hole" was used as a memory consolidation index [33–35].

Respiration test

Determination of pulmonary ventilation

We used the whole-body plethysmography method to measure of pulmonary ventilation ($\dot{V}_E$) [36, 37], as is commonly used in our laboratory [38–40]. Freely-moving rats were kept in a 5-L chamber ventilated with room air or a hypercapnic gas mixture containing 7% CO_2 (White Martins, Sertãozinho, Brazil) or a hypoxia gas mixture containing 10% O_2 (White Martins, Sertãozinho, Brazil) in low ambient noise conditions. The flow rate of the inflow gas into the animal chamber was monitored by a flowmeter (model 822-13-OV1- PV2-V4, Sierra Instruments, Monterey, CA). During measurements, the flow was interrupted, and the chamber was sealed for short periods of time (approximately 2 min); the pressure oscillations due to respiration were monitored by a differential pressure transducer (TSD 160A, Biopac Systems, Santa Barbara, CA). The signals were fed into a differential pressure transducer (DA 100C, Biopac Systems), passed through an analog-to-digital converter, and digitized on a microcomputer equipped with data acquisition software (MP100A-CE, Biopac Systems). The sampling frequency was 1 kHz. The results were analyzed using the data analysis software Acqknowledge (v. 4.2.3 data acquisition system, Biopac Systems). Tidal volume (V_T) and respiratory frequency (fR) were calculated to estimate ventilation per breath.

V_T was calculated by using an appropriate formula [37]:

$$V_T = V_K \times (P_T/P_K) \times T_b(P_B - P_C)/T_b \times (P_B - P_C) - T_A \times (P_B - P_R)$$

where P_T is the pressure deflection associated with each V_T, P_K is the pressure deflection associated with the injection of the calibration volume (V_K), T_A is the air temperature in the animal chamber, P_B is the barometric pressure, P_C is the water vapor pressure in the animal chamber, Tb is the body temperature, and P_R is the vapor pressure of water at Tb. The $\dot{V}_E$ was calculated as the product of the f_R and the V_T. $\dot{V}_E$ and V_T are presented under conditions of ambient barometric pressure, at Tb and saturated with water vapor (BTPS). Tb was monitored by temperature datalogger (SubCue Dataloggers, Calgary, Canada) and the air temperature in the animal chamber was constantly monitored using a thermoprobe (model 8502-10, Cole Parmer, Chicago, IL, USA). The animal chamber was considered saturated because of a water lane in the bottom separated from the animal by a grid, and so the Pc was calculated indirectly using an appropriate table [41]. The calibration for volume was obtained during each experiment by injecting the animal chamber with 1 mL of room air.

EEG and EMG signals

Similar to other previous studies, the arousal state was determined by analyzing the EEG and EMG records [40, 42]. The signals from the EEG and EMG electrodes were sampled at 1 kHz, filtered at 0.3–50 and 0.1–100 Hz, respectively, and recorded on a computer. Both wakefulness and NREM sleep states were observed consistently through the experiments, but periods of rapid eye movement (REM) sleep were short and were not present in every experiment; thus, REM sleep phases were excluded from the analysis [40].

Experimental protocol

Seven days after implantation of EEG and EMG electrodes, the animals were placed in a

Corrected Proof

plethysmographic chamber and ventilation was measured. The chamber was initially ventilated with moist atmospheric air (21% O_2) for an acclimation phase of at least 30 min. Ventilation control measures were then performed. Ventilation measurements were first made during normocapnia for 63 min. The animals were then submitted to hypercapnia for 63 min, where the chamber was ventilated with a gas mixture containing 7% CO_2, 21% O_2 and balanced with N_2 (White Martins Gases Industriais Ltda, Osasco, SP). After hypercapnia, the chamber was ventilated with atmospheric air again for recovery of baseline ventilation for 60 min. The animals were then submitted to hypoxia for 63 min, where the chamber was ventilated with a gas mixture containing 10% O_2 and equilibrated with N_2 (White Martins Gases Industriais Ltda, Osasco, SP). The order of exposure to hypercapnia and hypoxia was reversed randomly. The ventilatory measures were analyzed at 7, 14, 21, 28, 35, 42, 49, 56, and 63 min after gas exposure. Then, based on the sleep/wake cycle, for the $\dot{V}_E$ measurements, we selected the phases when the animals were either in wakefulness or in sleep.

Neurochemical analysis

Brain area dissection

After each battery of behavioral tests, four rats were randomly selected out of each group and the animals' brains were removed quickly, frozen in liquid nitrogen, and held at –80°C until dissection. In a cryostat at –22°C, the brains were coronary-sectioned to find target areas according to stereotaxic coordinates of the Atlas de Paxinos and Watson [43] as follow: locus coeruleus (LC - distance from bregma: –10.3 mm to –9.3 mm), retrotrapezoid nucleus (RTN, –11.3 mm to –10.3 mm), medullary raphe (–11.6 mm to –10.3 mm); pre-Bötzinger and Bötzinger complex (PreBötz/BötzC, –12.3 mm to –11.8 mm) and hippocampus (HPC, –4.16 mm to –3.16 mm). Samples of 0.7-mm thickness were removed with a 15-gauge needle.

Immunoblotting

Phosphorylated tau protein levels ($Ser^{199/202}$ and Ser^{396}) and Aβ peptide in LC, RTN, Raphe, PreBötzC/BötzC, and HPC were evaluated.

For this procedure, a maceration of the tissue of each corresponding region was performed. This tissue sample was submitted to sonication to promote membrane lysis and eventual release of the intracellular material. The solution containing the lysed cells was collected and transferred to an Eppendorf tube. Then, the quantification of these proteins was performed by the Biochrom UV/Vis spectrophotometer, Biodrop Duo model, UV optical path.

Before running the gel, the samples were denatured at 100°C for 3 min and applied to a polyacrylamide gel (12%) for fractionation. As a control, 8 μL of a molecular weight marker was applied to one well. The samples were applied to the gel, placed in a vial with running buffer and separated by applying 100 V for 2 h. After the run, proteins were transferred to a nitrocellulose membrane (Bio-Rad) using ice-cold transfer buffer for 1 h at 100 V. The membrane was then incubated with non-specific site blocking solution (5% milk in TBS-T) for 1 h at room temperature. After this blocking, the membranes were cut and incubated with the respective primary antibodies, Anti-phospho-Tau (rabbit monoclonal $pSer^{199/202}$, cat. T6819, Sigma,-Aldrich, 1:1000 dilution and rabbit monoclonal $pSer^{396}$, cat. EPR2731-Ab109390, Abcam, 1:1000 dilution), anti-beta-actin (mouse monoclonal beta-actin antibody AC-15, cat. NB600-501, Novus Biological, 1:1000 dilution), anti-beta amyloid (mouse monoclonal β-amyloid B-4, cat. sc-28365, Santa Cruz Biotechnology, 1:500 dilution), and anti-Tau Total (rabbit polyclonal human tau, Ab-356, cat. GWB-ASC840, GenWay, 1:1000 dilution), diluted in the same blocking solution for 24 h at 4°C under constant stirring. The beta-actin antibody was used to normalize the specific labeling values. After washing, the corresponding secondary (anti-mouse IgG and anti-rabbit, 1:1000 dilution, Jackson ImmunoResearch) antibodies were incubated for 2 h at room temperature. The membranes were then washed twice with TBS-T and once with TBS for 10 min each, and the reaction was carried out by incubation with a chemiluminescent reagent for 1 min. The membranes were immediately exposed to chemiluminescence-sensitive film for 30 s to 5 min, as instructed by the manufacturer.

The films were quantified through optical densitometry using a computerized image analysis system (NIH System, ImageJ developed at the US National Institute of Health, available at the website: http://www.rsb.info.nih.gov/nihimage/(ImageJ).

Statistical analyses

Results were expressed as mean ± SEM. The Barnes maze results in the acquisition phase were evaluated by two-way ANOVA, followed by the

Corrected Proof

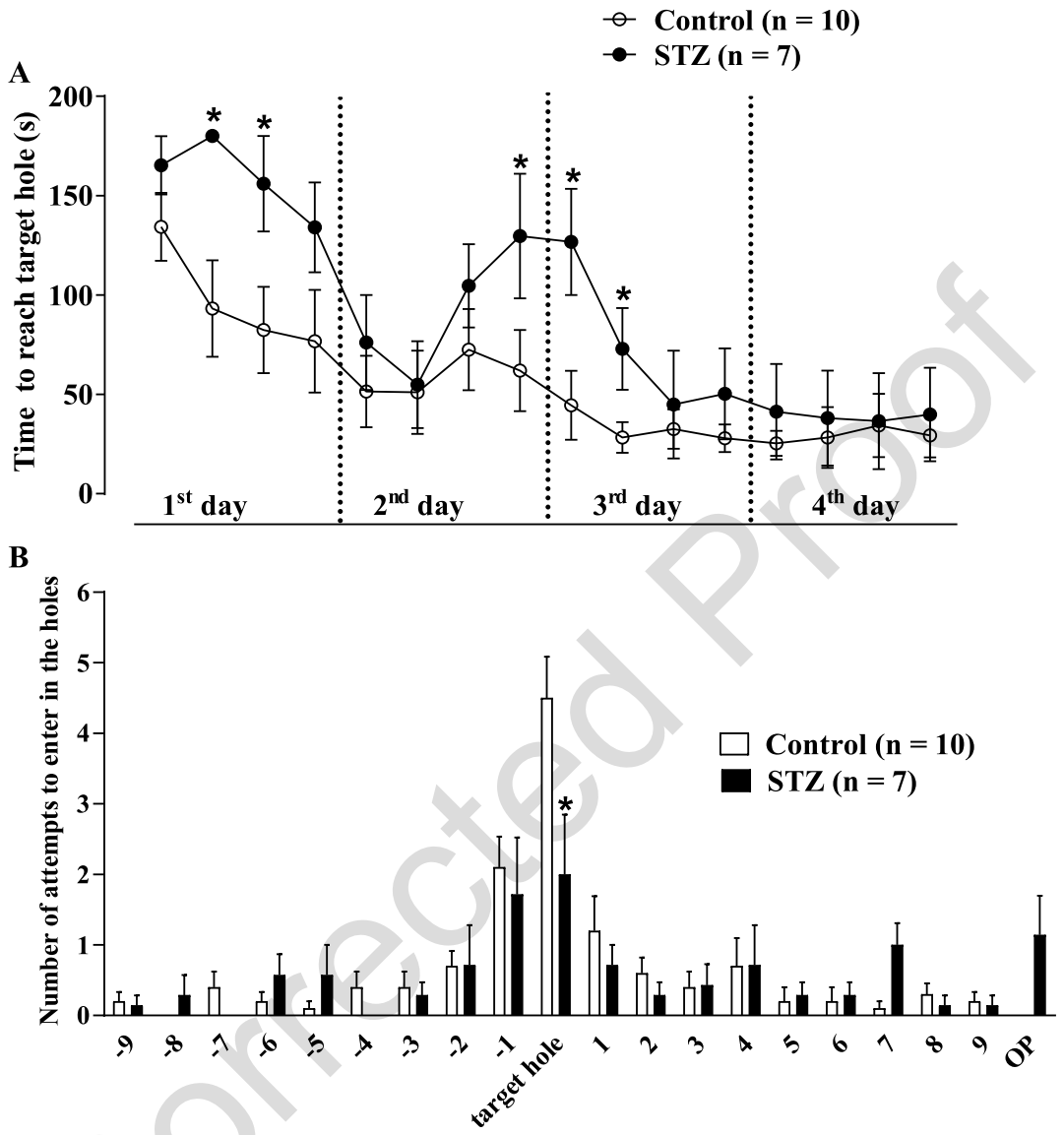

Corrected Proof

Fig. 1. Effect of icv STZ (2 mg/kg) on spatial learning and memory retention in the Barnes maze test. A) Time to reach the target hole in seconds of the control and STZ groups in the 4 training sessions per day (1st to 4th day). B) Number of attempts to enter into the holes in the platform test pattern in the control and STZ group. Values are expressed as mean ± SEM. * indicates a significant difference between the control and STZ groups.

Holm-Sidak post-test. The Barnes maze, on the day of the test, was evaluated by the two-way ANOVA. The results of ventilation, sleep/wake cycle and body temperature in normocapnic, hypercapnic, and hypoxic conditions were evaluated by two-way ANOVA, followed by Bonferroni post-test. The quantification of phosphorylation of tau protein, total tau and Aβ were validated through the *t*-test (Student) for independent samples. The significance level adopted for all results was $p < 0.05$.

RESULTS

Behavioral analysis for model validation

Barnes maze: Acquisition phase

Figure 1A represents the latency value (s) to find the escape box in the target hole in training 4 for 4 days (acquisition phase). We observed that the control group decreased the latency (s) to escape through the target hole as a function of training (day 1: T1

134.3 ± 54.2 versus day 4: T4 29.0 ± 35.1 s, $p < 0.05$; two-way ANOVA). However, the STZ group required more time to find the escape hole compared to the control group on days 1, 2 and 3 ($p < 0.05$; two-way ANOVA). No difference between treatments was observed on the fourth day. On the same day, the STZ group decreased latency, thus improving performance on the platform to find the escape box (day 1: T1 165.8 ± 38.9 versus day 4: T4 39.8 ± 62.4 s, $p < 0.05$; two-way ANOVA).

Barnes maze: Proof test

Figure 1B shows the number of attempts to enter the holes in the platform test pattern. In the Barnes maze test, the STZ-treated group had a lower number of hits in the "target hole" compared to the control group (control: 4.5 ± 1.8 versus STZ: 2.0 ± 2.2, respectively, $p = 0.035$; two-way ANOVA). There was no significant difference between treatments in the other holes of the platform ($p > 0.05$; two-way ANOVA).

Respiration test

During all experimental protocols, the mean chamber temperature was 25.7 ± 0.3°C, and the mean room temperature was 24.6 ± 0.2°C.

Respiration during wakefulness

We observed no difference in respiratory variables in room air conditions in the STZ-treated group compared to the control group during wakefulness (Figs. 3A and 4A). In hypercapnia and hypoxia, all groups showed a significant increase in ventilation when compared to room air conditions ($p < 0.0001$; two-way ANOVA) (Figs. 2A and 3A).

During hypercapnia (Fig. 2A), the increase in $\dot{V}_E$ of the STZ-treated animals was 26% higher compared to the control group (control: 1823.9 ± 457.5 versus STZ: 2481.3 ± 514.2 mL.Kg^{-1}.min^{-1}, $p < 0.05$; two-way ANOVA) due to a higher V_T (vehicle: 13.7 ± 2.9 versus STZ: 17.1 ± 2.7 mL.Kg^{-1}, $p < 0.05$; two-way ANOVA).

Hypoxia caused a similar increase in $\dot{V}_E$ in all groups due to an increase in fR (Fig. 3A). No difference was observed between treatments.

Respiration during NREM sleep

Figures 3B and 4B show the effects of STZ treatment on ventilatory parameters under room air conditions in rats during the sleep cycle. No difference was observed between the control and STZ groups. Both hypercapnia (Fig. 2B) and hypoxia (Fig. 3B) promoted a similar increase in ventilation in both groups, with no difference between them.

Body temperature (Tb)

No significant difference was observed between treatments during room air conditions and hypercapnia (Fig. 4). Hypoxia caused a similar decrease in body Tp of both control and STZ groups (Fig. 4).

Sleep/wakefulness

Under room air condition (Fig. 5A), the rats spent more time awake, but the STZ-treated rats increased the percentage of total wakefulness compared with the control group (control: $73.9 \pm 4.0\%$ versus STZ: $87.0 \pm 3.0\%$, $p < 0.05$; two-way ANOVA). This effect was due to a significant reduction in the length of the episodes of wakefulness (Fig. 5B), while the number of episodes did not change (Fig. 5C). CO_2 exposure and hypoxia significantly increased the time the rats were awake (Fig. 5A), with no difference between treatments during hypoxia. However, under hypercapnic conditions, STZ treatment enhanced the time that the animals spent awake (control: $81.0 \pm 5.7\%$ versus STZ: $93.5 \pm 2.3\%$, $p < 0.05$; two-way ANOVA) due to an increase in episode duration (Fig. 7B) (control: 502.4 ± 179.6 versus STZ: 2096.8 ± 537.9 s, $p < 0.05$; two-way ANOVA) and a reduction in the number of episodes (Fig. 5C) (control: 5.2 ± 1.3 versus STZ: 2.5 ± 0.6, $p < 0.05$; two-way ANOVA).

Neurochemical analysis

Tau protein phosphorylation

In the analysis of tau protein phosphorylation at the $Ser^{199/202}$ and Ser^{396} sites, we evaluated the ratio of phosphorylated tau protein (pTau) levels to total tau protein levels in the regions of interest: LC, RTN, Raphe, PreBötz/BötzC, and HPC.

STZ injection did not alter the levels of phosphorylation of tau protein at $Ser^{199/202}$ site on LC, RTN, Raphe, PreBötz/BötzC, and HPC (Fig. 6). In addition, STZ injection did not alter the levels of phosphorylation of tau protein at the Ser^{396} site in the same regions (Fig. 6).

Aβ protein

Expression analysis of Aβ protein demonstrated a 73% increase in this protein in the LC of the STZ

Corrected Proof

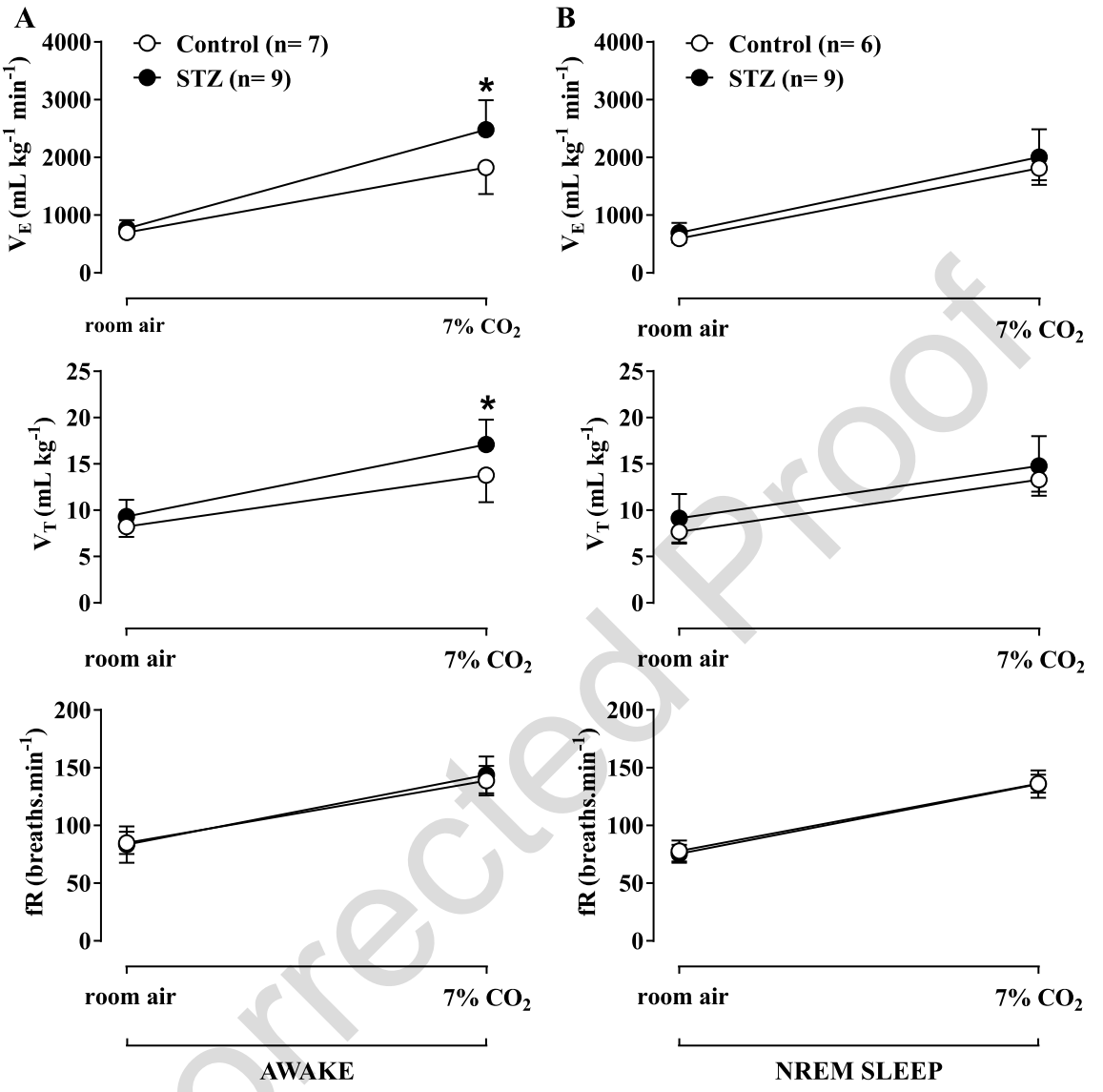

Fig. 2. Effect of icv STZ (2 mg/kg) on ventilation (V_E), tidal volume (V_T) and respiratory frequency (fR) during hypercapnic exposure (7% CO_2) during wakefulness (A) and NREM sleep (B). Values are expressed as mean ± SEM. * indicates a significant difference between the control and STZ groups.

Corrected Proof

group compared to the control ($p = 0.0325$, Student's *t*-test) (Fig. 7). The other structures did not present significant differences between the treatments.

DISCUSSION

In the present study we successfully demonstrated that STZ-treated rats had learning and memory deficits and sleep disturbances, with increase time spent in an awake state. Our main results were that STZ rats showed increased Aβ peptide in the LC region and increased ventilatory response to hypercapnia in wakefulness but not during sleep, with no changes in ventilation during room air conditions and hypoxia. Additionally, no changes were observed in body Tp.

In our study, we were able to reproduce the STZ-induced memory deficits. We showed an impairment in learning and retention of spatial memory (as assessed by a higher latency to find the escape box in the acquisition phase of the Barnes maze), as well as difficulty in maintaining spatial refer-

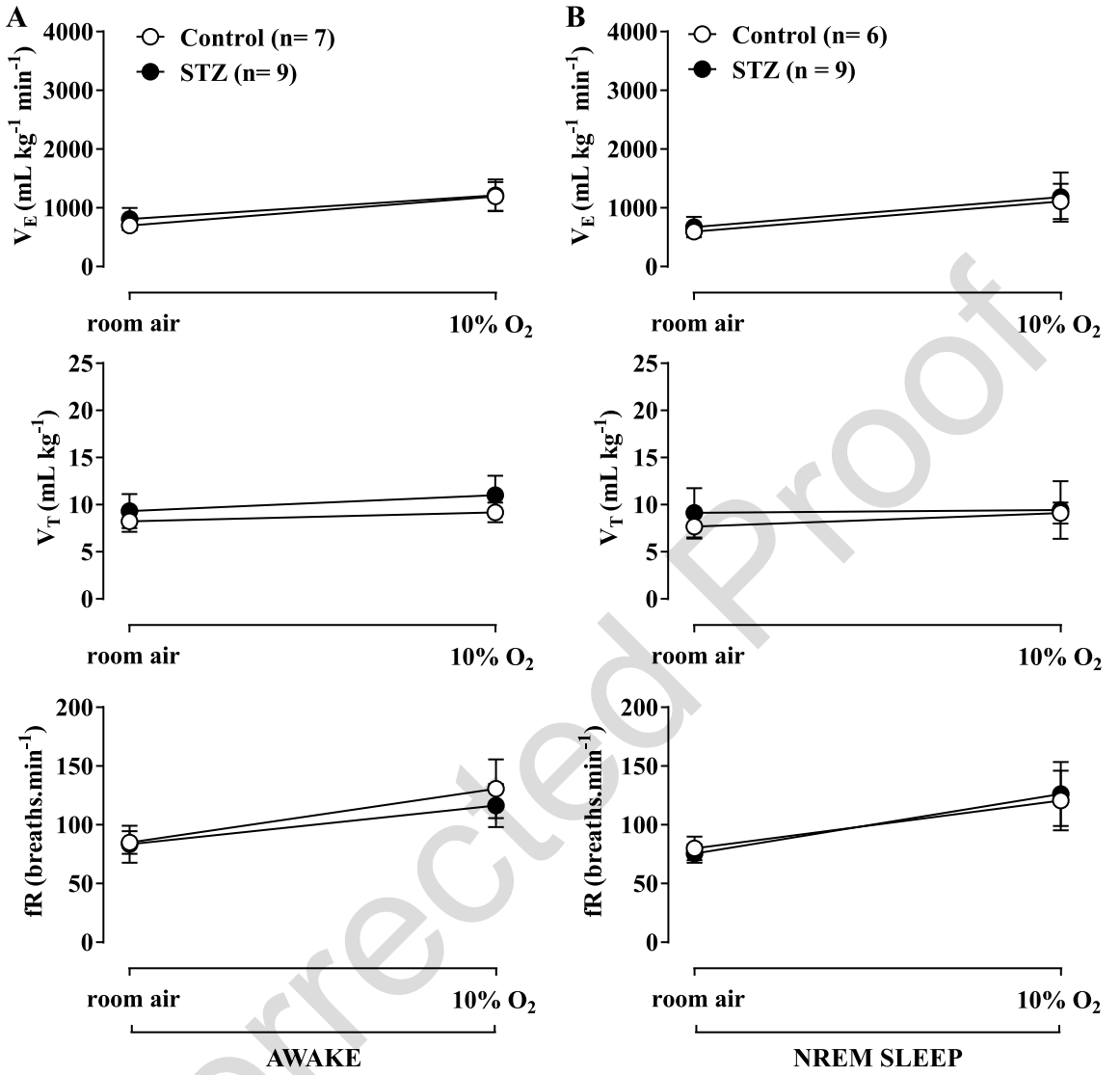

Fig. 3. Effect of icv STZ (2 mg/kg) on ventilation ($\dot{V}_E$), tidal volume (V_T) and respiratory frequency (fR) during hypoxic exposure (10% O_2) during wakefulness (A) and NREM sleep (B). Values are expressed as mean ± SEM.

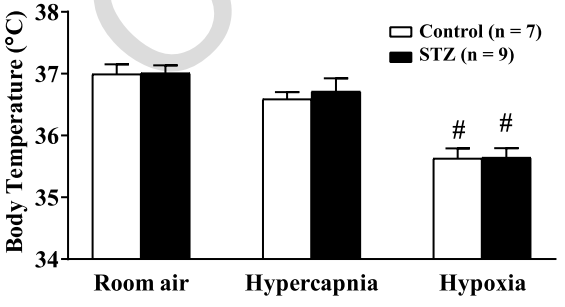

Fig. 4. Effect of icv STZ (2 mg/kg) on body temperature of rats during room air, hypercapnia and hypoxia. Values are expressed as mean ± SEM. # indicates a significant difference from room air and hypercapnia.

ence information (as assessed by the lower number of correct pokes into the target hole of the Barnes maze on the test day). Thus, our results confirm previous studies that have shown that STZ injection causes learning and memory deficits [17, 30, 31, 44, 45]. These findings corroborate the use of STZ in neurodegeneration-induced dementia of the Alzheimer-type in rats, since animals present one of the main cognitive characteristics found in patients with AD [1, 46]. Indeed, evidence that AD patients have problems with spatial orientation—one of the earliest cognitive symptoms—as well as progressive decline in memory, is reported in a number of different studies [47–49].

Corrected Proof

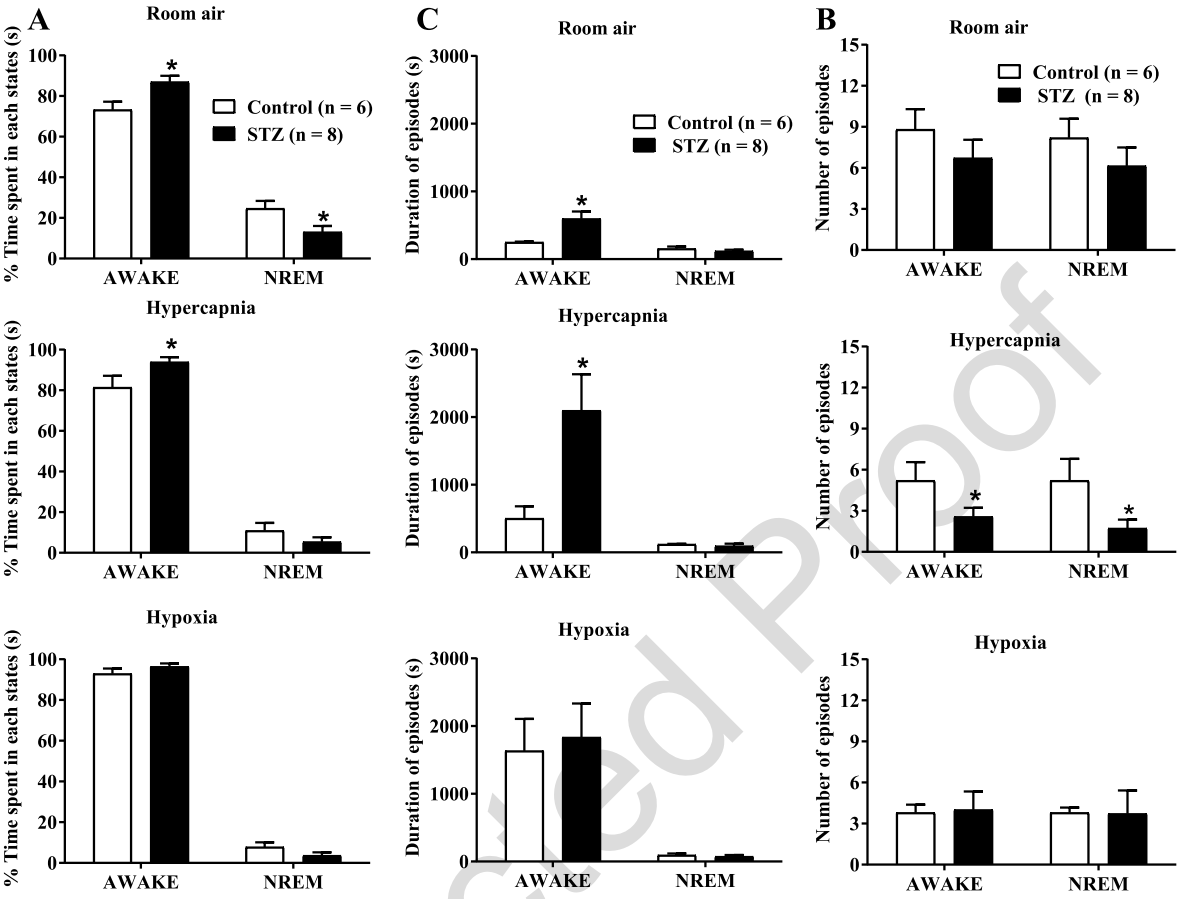

Fig. 5. Effect of icv STZ (2 mg/kg) on the percentage (%) of time spent in each state (A), the duration of episodes in seconds (B) and the number of episodes (C) in control and STZ groups during room air, hypercapnia and hypoxia. Values are expressed as mean ± SEM. *indicates a significant difference between the control and STZ groups.

AD is also characterized by the deposit of extracellular amyloid plaques, composed of Aβ peptide, and intracellular NFTs of hyperphosphorylated tau protein (P-Tau) [3]. In the present study, we did not observe increased phosphorylation of tau protein (Ser^{396} and $Ser^{199/202}$) in the LC, RTN, Raphe, PreBötz/BötzC, and HPC. The absence of increased P-Tau after STZ was also reported previously as P-Tau at Ser $^{199/202}$ in both rats [30] and mice [17] were unaltered in the hippocampus after 30 and 21 days post-STZ, respectively. On the other hand, increases in P-Tau at Ser^{396} and $Ser^{199/202}$ in the hippocampus have been reported after STZ using higher doses (3 mg/kg) than the present study [50] and/or later evaluation [14, 51]. Besides, Grünblatt et al. [31], using lower doses of STZ (1 mg/kg), observed changes in P-Tau protein in the hippocampus, but did not perform a ratio analysis of phosphorylated/total tau; therefore, this may not be considered hyperphosphorylation. In fact, some studies have shown that the onset of NFTs is chronological and hierarchical, since it arises primarily in some regions and late in others [4, 52]. In this sense, it is known that some phosphorylation sites of tau protein hyperphosphorylate at early stages, and other sites in late stages of AD [53, 54], which would also explain the discrepancy in the literature regarding the effects of STZ in P-Tau.

The Aβ peptide in the brain of AD patient was initially considered to be a primary cause of AD dysfunction; however, later studies suggest that the presence of Aβ would be a consequence of early AD events, rather than the cause itself [55, 56]. Similar to what occurs with tau protein phosphorylation, the prevalence of Aβ results from the different stages of AD and different brain regions [57]. In the present study, we observed a 73% increase of Aβ peptide expression in the LC after 30 days of icv administration of STZ. Our data corroborate previ-

Corrected Proof

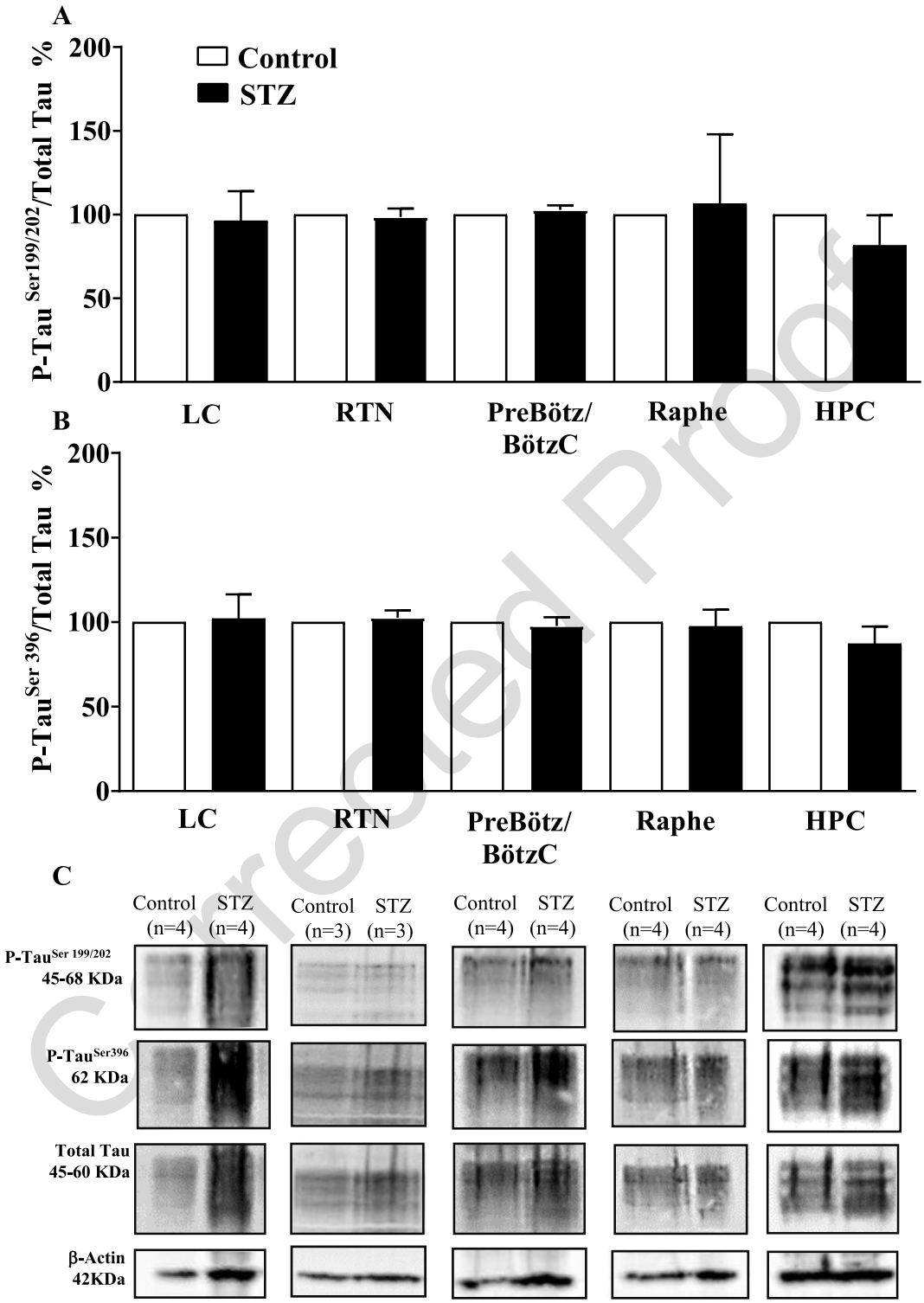

Corrected Proof

Fig. 6. Effect of icv STZ (2 mg/kg) on the phosphorylation levels of tau protein ($Ser^{199/202}$) (A) and the phosphorylation levels of tau protein (Ser^{396}) (B). The graphs represent the mean radius of the phosphorylated tau protein (pTau) relative to total tau protein levels. The values are expressed as percentage values in relation to the control group (100%). Values are expressed as mean ± SEM.

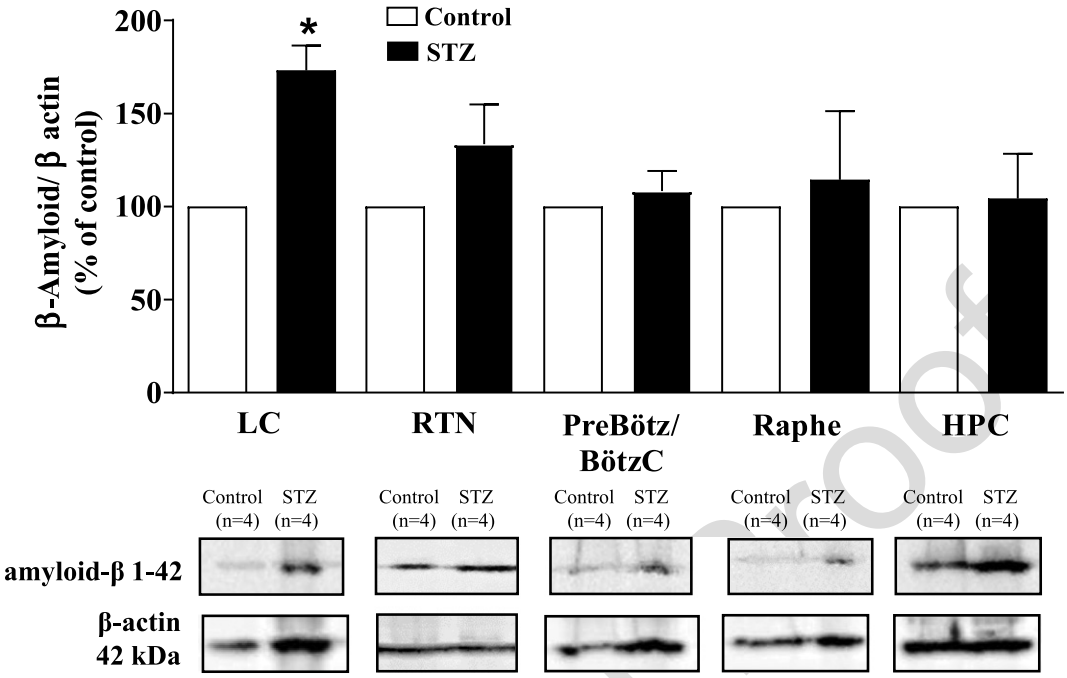

Fig. 7. Effect of icv STZ (2 mg/kg) on the expression of Aβ protein. The values are expressed as percentage values in relation to the control group (100%). Values are expressed as mean ± SEM. * indicates a significant difference between the control and STZ groups.

ous studies showing that central injection of STZ promotes increases in the expression of Aβ peptide [14, 17, 30]. In addition, it is well described that the LC region is affected in AD [58–61]. In this context, we did not observe changes in Aβ peptide expression in the RTN region, Raphe, PreBötz/BötzC, and HPC, which reinforces that the histopathological emergence of AD occurs in a hierarchical and chronological manner [57, 61, 62]. Despite the fact that we did not find histopathological molecular evidence in the present temporal window (30 days after the icv STZ) in the HPC, we observed a cognitive deficit in the model. Therefore, it is possible that other cognitive regions in this temporal window may be affected.

Regarding breathing, STZ treatment did not cause alterations in ventilation under room air conditions and hypoxia during sleep and wakefulness. In the literature, there is a paucity of information on the study of the respiratory system in the progression of AD. Menuet et al. [63], working on a model of taupatia, an important clinical aspect found in AD, observed alterations of the respiratory system, such as upper airway dysfunction, changes in respiratory pattern, and compromised ventilatory response to hypercapnia. However, the authors observed respiratory disfunction in late phases of the disease. In this context, Ebel et al. [28], after 14 days of icv injection of STZ (3 mg/kg), observed respiratory dysfunction in normocapnia, attenuation of the peripheral chemoreflex, as well as a small decrease in respiratory frequency during hypercapnia. Our results differ from those of Ebel et al. [28], as we observed no changes in breathing during room air conditions or hypoxia, and a 26% increase of the ventilatory response to hypercapnia after 30 days of the icv STZ injection (2 mg/kg) only during wakefulness. We believe that these differences may reside in the fact that the authors performed the experiments using a higher dose (3 mg/kg) and a different time window (14 days after the icv injection), whereas in our study, we performed the experiments after 2 mg/kg at 30 days after STZ injection. According to Grieb [64], the neurochemical changes triggered by icv STZ injection(s) follow a time-dependent pattern. Therefore, the effects observed by Ebel et al. [28] may be due to impairment of other brain structures, since they observed a reduction in hypoxic ventilatory response, whereas we showed an exacerbation of the CO_2-drive to breathe. Moreover, higher doses may induce more severe and acute neurodegenerative lesions, which could be associated with inflammation and local oxidative stress, whereas lower doses may lead to less severe but more chronic and widespread effects [64]. In this regard, Kraska et al. [65] stated

Corrected Proof

that doses of 3 mg/kg and higher could be considered a model of very aggressive neurotoxic lesions, rather than subtle alterations due to small mechanistic alterations, as would be expected during the slowly evolving dementia processes or during aging. According to the authors, an intermediate dose, e.g., 2 mg/kg, is more relevant as a sporadic AD model.

The exacerbated CO_2 ventilatory response during wakefulness observed in the present study may result from changes in the central CO_2 chemosensitive areas. In fact, we observed an increase in Aβ peptide expression in the LC region, an important chemosensitive nucleus of the central nervous system [39, 40, 66–68]. We suggest that increased peptide expression may be deregulating the Ca^{2+} channels, increasing their influx within the neuron, which in turn would increase the release of neurotransmitters, such as noradrenaline (NE) [69]. Increased NE in the medullary respiratory neurons would trigger a more pronounced ventilatory response to CO_2. Previous studies have shown that LC/subcoeruleus neurons represent an early starting point for AD pathology, even preceding the occurrence of cortical lesions [70–72]. Measurements of 3-methoxy-4-hydroxyphenylglycol (MHPG), the principal metabolite of noradrenaline (NE), was found to be increased in postmortem brain tissue of AD patients [73–76]. The authors also found an enhanced ratio of MHPG/NE, which indicates that NE metabolism is augmented in these patients, suggesting an increased activity of the remaining LC neurons to compensate for decreased cerebral NE levels in AD [73–75, 77]. As suggested previously [78], enhanced LC activity may occur in the first stages of AD, prior to cell loss or significant reduction in NE neurotransmission, and this would be harmful due to the enhanced spread of P-Tau, whereas at late stages of AD, LC would be degenerating, and NE levels would be low, and tau pathology is already abundant in the forebrain. Therefore, the activity of LC neurons in AD may be dependent on the disease stage.

Around 45% of patients with AD are affected by sleep disturbances [19, 20, 22] and rodent models of AD also show greater sleep fragmentation and shorter amounts of NREM and rapid eye movement sleep [79, 80]. Our data corroborate these previous studies, since STZ-treated rats spent more time in wakefulness than in NREM sleep during the experimental period in normocapnia and hypercapnia. During hypoxia, both groups increased their wakefulness similarly. In fact, high levels of Aβ correlate with sleep deficiencies [81]. In this context, immunization with Aβ prevents amyloid plaque formation in transgenic mice that develop Aβ aggregation and normalizes sleep/wake patterns [79]. Since we found an increase in Aβ in the LC, and since this nucleus is necessary for maintaining normal durations of wakefulness and to promote immediate sleep-to-wake transitions [82], it is likely that the increase in wakefulness in the STZ-treated rats is related to this fact.

Regarding Tb, the main risk factor for sporadic AD is age [83]. In fact, aging alone is associated with a decrease in Tb, a consequence of a deficit in thermoregulation and, in particular, in thermogenesis [84, 85]. However, studies have shown that patients with AD exhibit increased Tb [83, 86]. Interestingly, rats with icv infusion of Aβ select a higher ambient temperature and show a lower heat tolerance compared to control animals [87]. Increased Tb was also shown in a 6 to 10-month-old 3xTg-AD mouse—a transgenic AD animal model [88]. Recently, the thermoregulatory profile of rats injected with 2 mg/kg of STZ was evaluated, and it was shown that STZ-treated rats presented a higher Tb when compared to controls from day 6 to 25 post-STZ injection [89]. Although at later stages, (>30 days post-injection) STZ-treated animals present a cold-avoidance response, and their basal Tb is no longer different from controls [89]. In accordance, in the present report, at 30 days post STZ treatment no differences in Tb of animals treated with STZ under resting conditions were observed. Furthermore, treated animals seem to keep intact the thermal response to hypoxia, which is considered a regulated fall in temperature due to a drop in O_2 consumption during hypoxia [90–92]. Therefore, we suggest that, in the temporal window analyzed in the present study, STZ treatment does not impair thermoregulation in rats.

Conclusion

Our study provides evidence that icv STZ-treated rats present an increased sensitivity to CO_2 during wakefulness, but have no changes in basal ventilation or in the hypoxic chemoreflex. These changes in the CO_2-drive to breathe might be associated with enhanced Aβ in the LC, since this nucleus is highly involved in hypercapnic ventilatory response, mainly during the wake period [40]. Furthermore, STZ animals showed an increase in the percentage of total wakefulness, which correlates with sleep disturbs observed in AD. Therefore, a better comprehension of respiratory alterations in different phases of the sleep/wake cycle, and the role of LC neurons in this

Corrected Proof

modulation in AD models, is needed in order to target novel approaches for the treatment of this disorder.

ACKNOWLEDGMENTS

This work was supported by Fundação de Amparo á Pesquisa do Estado de São Paulo (FAPESP – 2016/24577-3, 2015/02991-0 and 2015/23426-9) and Conselho Nacional de Desenvolvimento Científico e Tecnológico (CNPq - 442560/2014-1 and 449102/2014-9). The authors thank Euclides Seccato for his technical assistance.

Authors' disclosures available online (https://www.j-alz.com/manuscript-disclosures/18-0397r1).

REFERENCES

[1] Harman D (1996) A hypothesis on the pathogenesis of Alzheimer's disease. *Ann N Y Acad Sci* **786**, 152-168.

[2] Wimo A, Guerchet M, Ali GC, Wu YT, Prina MA, Winblad B, Jönsson L, Liu Z, Prince M (2017) The worldwide costs of dementia 2015 and comparisons with 2010. *Alzheimers Dement* **13**, 1-7.

[3] Harris JR (2012) *Protein Aggregation and Fibrillogenesis in Cerebral and Systemic Amyloid Disease*. Springer.

[4] Braak H, Braak E (1991) Neuropathological staging of Alzheimer- related changes. *Acta Neuropathol* **82**, 239-259.

[5] Hof PR, Morrison JH (1999) The cellular basis of cortical disconnection in Alzheimer disease and related dementing conditions. In: *Alzheimer disease*, 2nd edition, Terry R, Katzman R, Bick KL, Sisodia SS, eds. Lippincott Williams & Wilkins, Philadelphia, pp. 207-232.

[6] Klucken J, Mclean PJ, Gomez-Tortosa E, Ingelsson M, Hyman BT (2003) Neuritic alterations and neural system dysfunction in Alzheimer's disease and dementia with Lewy bodies. *Neurochem Res* **28**, 1683-1691.

[7] Spires TL, Hyman BT (2004) Neuronal structure is altered by amyloid plaques. *Rev Neurosci* **5**, 267-278.

[8] Liu L, Luo S, Zeng L, Wang W, Yuan L, Jian X (2013) Degenerative alterations in noradrenergic neurons of the locus coeruleus in Alzheimer's disease. *Neural Regen Res* **24**, 2249-2255.

[9] Nixon RA (2007) Amyloid precursor protein and endosomal-lysosomal dysfunction in Alzheimer's disease: Inseparable partners in a multifactorial disease. *FASEB J* **31**, 2729-2743.

[10] LaFerla FM, Green KN (2012) Animal models of Alzheimer disease. *Cold Spring Harb Perspect Med* **2**(11), a006320.

[11] Hoyer S, Müller D, Plaschke K (1994) Desensitization of brain insulin receptor. Effect on glucose/energy and related metabolism. *J Neural Transm (Suppl)* **44**, 259-268.

[12] Grunblatt E, Hoyer S, Riederer P (2004) Gene expression profile in streptozotocin rat model for sporadic Alzheimer's disease. *J Neural Transm* **111**, 367-386.

[13] Salkovic-Petrisicm M, Knezovic A, Hoyer S, Riederer P (2013) What have we learned from the streptozotocin-induced animal model of sporadic Alzheimer's disease, about the therapeutic strategies in Alzheimer's research. *J Neural Transm* **120**, 233-252.

[14] Salkovic-Petrisicm M, Knezovic A, Barilar JO (2015) Multi-target iron-chelators improve memory loss in rat model of sporadic Alzheimer's disease. *Life Sci* **138**, 108-119.

[15] Lee Y, Kim YH, Park SJ, Huh JW, Kim SH, Kim SU, Kim JS, Jeong KJ, Lee KM, Hong Y, Lee SR, Chang KT (2014) Insulin/IGF signaling-related gene expression in the brain of a sporadic Alzheimer's disease monkey model induced by intracerebroventricular injection of streptozotocin. *J Alzheimers Dis* **38**, 251-267.

[16] Yeo HG, Lee Y, Jeon CY, Jeong KJ, Jin YB, Kan P, Kim SU, Kim JS, Huh JW, Kim YH, Sim BW, Song BS, Park YH, Hong Y, Lee SR, Chang KT (2015) Characterization of cerebral damage in a monkey model of Alzheimer's disease induced by intracerebroventricular injection of streptozotocin. *J Alzheimers Dis* **46**, 989-1005.

[17] Ravelli KG, Rosário BA, Camarini R, Hernandes MS, Britto LR (2017) Intracerebroventricular streptozotocin as a model of Alzheimer's disease: Neurochemical and behavioral characterization in mice. *Neurotox Res* **31**, 327-333.

[18] Correia SC, Santos RX, Perry G, Zhu X, Moreira PI, Smith MA (2011) Insulin-resistant brain state: The culprit in sporadic Alzheimer's disease? *Ageing Res Rev* **10**, 264-273.

[19] Moran M, Lynch CA, Walsh C, Coen R, Coakley D, Lawlor BA (2005) Sleep disturbance in mild to moderate Alzheimer's disease. *Sleep Med* **6**, 347-352.

[20] Peter-Derex L, Yammine P, Bastuji H, Croisile B (2015) Sleep and Alzheimer's disease. *Sleep Med* **19**, 29-38.

[21] Vitiello MV, Prinz PN (1989) Alzheimer's disease. Sleep and sleep/wake patterns. *Clin Geriatr Med* **5**, 289-299.

[22] McCurry SM, Reynolds CF, Ancoli-Israel S, Teri L, Vitiello MV (2000) Treatment of sleep disturbance in Alzheimer's disease. *Sleep Med Rev* **4**, 603-628.

[23] Boeve BF (2008) Update on the diagnosis and management of sleep disturbances in dementia. *Sleep Med Clin* **3**, 347-360.

[24] Schwarzacher SW, Rub U, Deller T (2011) Neuroanatomical characteristics of the human pre-Botzinger complex and its involvement in neurodegenerative brainstem diseases. *Brain* **134**, 24-35.

[25] Gaig C, Iranzo A (2012) Sleep-disordered breathing in neurodegenerative diseases. *Curr Neurol Neurosci Rep* **12**, 205-217.

[26] Deak MC, Kirsch DB (2014) Sleep-disordered breathing in neurologic conditions. *Clin Chest Med* **35**, 547-556.

[27] Ancoli-Israel S, Palmer BW, Cooke JR, Corey-Bloom J, Fiorentino L, Natarajan L, Liu L, Ayalon L, He F, Loredo JS (2008) Cognitive effects of treating obstructive sleep apnea in Alzheimer's disease: A randomized controlled study. *J Am Geriatr Soc* **56**, 2076-2081.

[28] Ebel DL, Torkilsen CG, Ostrowski TD (2017) Blunted respiratory responses in the streptozotocin-induced Alzheimer's disease rat model. *J Alzheimers Dis* **56**, 1197-1211.

[29] Fennell WH, Moore RE (1973) Responses of aged men to passive heating. *J Physiol* **231**, 118P-119.

[30] Santos TO, Mazucanti CH, Xavier GF, Torrão AS (2012) Early and late neurodegeneration and memory disruption after intracerebroventricular streptozotocin. *Physiol Behav* **107**, 401-413.

[31] Grunblatt E, Salkovic-Petrisic M, Osmanovic J, Riederer P, Hoyer S (2007) Brain insulin system dysfunction in streptozotocin intracerebroventricularly treated rats gener-

Corrected Proof

ates hyperphosphorylated tau protein. *J Neurochem* **101**, 757-759.

[32] Sharma S, Rakoczy S, Brown-Borg H (2010) Assessment of spatial memory in mice. *Life Sci* **87**, 521-536.

[33] Sunyer B, Patil S, Hoger H, Lubec G (2007) Barnes maze, a useful task to assess spatial reference memory in the mice. *Protoc Exch,* doi:10.1038/nprot.2007.390

[34] Adams B, Fitch T, Chaney S, Gerlai, R (2002) Altered performance characteristics in cognitive tasks: Comparison of the albino ICR and CD1 mouse strains. *Behav Brain Res* **133**, 351-336.

[35] Chawla A, Cordner ZA, Boersma G, Moran TH (2017) Cognitive impairment and gene expression alterations in a rodent model of binge eating disorder. *Physiol Behav* **180**, 78-90.

[36] Drorbaugh JE, Fenn WO (1955) A barometric method for measuring ventilation in newborn infants. *Pediatrics* **16**, 81-87.

[37] Bartlett D, Tenney SM (1970) Control of breathing in experimental anemia. *Respir Physiol* **10**, 384-395.

[38] Biancardi V, Bícego KC, Almeida MC, Gargaglioni LH (2008) Locus coeruleus noradrenergic neurons and CO_2 drive to breathing. *Pflugers Arch* **6**, 1119-1128.

[39] Patrone LG, Bicego KC, Hartzler LK, Putnam RW, Gargaglioni LH (2014) Cardiorespiratory effects of gap junction blockade in the locus coeruleus in unanesthetized adult rats. *Respir Physiol Neurobiol* **190**, 86-95.

[40] Vicente MC, Dias MB, Fonseca EM, Bícego KC, Gargaglioni LH (2017) Orexinergic system in the locus coeruleus modulates the CO_2 ventilatory response. *Pflugers Arch* **5**, 763-774.

[41] Dejours P (1981) *Principle of comparative respiratory physiology*. 2nd edn. Elsevier, New York.

[42] Nattie EE, Li A (2002) CO_2 dialysis in nucleus tractus solitaries region of rat increases ventilation in sleep and wakefulness. *J Appl Physiol* **92**, 2119-2130.

[43] Paxinos G, Watson C (1998) *The rat brain in stereotaxic coordinates*, 3rd ed. Academic Press. San Diego.

[44] Muller AP (2012) Physical exercise exacerbates memory deficits induced by intracerebroventricular STZ but improves insulin regulation of H_2O_2 production in mice synaptosomes. *J Alzheimers Dis* **30**, 889-898.

[45] Liu P, Zou LB, Wang LH, Jiao Q, Chi TY, Ji XF, Jin G (2014) Xanthoceraside attenuates tau hyperphosphorylation and cognitive deficits in intracerebroventricular-streptozotocin injected rats. *Psychopharmacology (Berl)* **231**, 345-356.

[46] Qiu C, Ronche D, Fratiglioni L (2007) The epidemiology of the dementias: An uptade. *Curr Opin Psychiatry* **20**, 380-385.

[47] Henderson VW, Mack W, Williams BW (1989) Spatial disorientation in Alzheimer's disease. *Arch Neurol* **46**, 391-394.

[48] Kar S, Slowikowski SP, Westaway D, Mount HT (2004) Interactions between beta-amyloid and central cholinergic neurons: Implications for Alzheimer's disease. *J Psychiatry Neurosci* **29**, 427-441.

[49] Kalova E, Vlcek K, Jarolimova E, Bures J (2005) Allothetic orientation and sequential ordering of places is impaired in early stages of Alzheimer's disease: Corresponding results in real space tests and computer tests. *Behav Brain Res* **159**, 175-186.

[50] Deng Y, Li B, Liu Y, Iqbal K, Grundke-Iqbal I, Gong CX (2009) Dysregulation of insulin signaling, glucose transporters, O-GlcNAcylation, and phosphorylation of tau and neurofilaments in the brain: Implication for Alzheimer's disease. *Am J Pathol* **5**, 2089-2098.

[51] Chen Y, Liang Z, Blanchard J, Dai CL, Sun S, Lee MH, Grundke-Iqbal I, Iqbal K, Liu F, Gong CX (2013) A non-transgenic mouse model (icv-STZ mouse) of Alzheimer's disease: Similarities to and differences from the transgenic model (3xTg-AD mouse) *Mol. Neurobiol* **47**, 711-725.

[52] Arnold SE, Hyman BT, Flory J, Damasio AR, Van Hoesen GW (1991) The topographical and neuroanatomical distribution of neurofibrillary tangles and neuritic plaques in the cerebral cortex of patients with Alzheimer's disease. *Cereb Cortex* **1**, 103-116.

[53] Kimura T, Ono T, Takamatsu J, Yamamoto H, Ikegami K, Kondo A, Hasegawa M, Ihara Y, Miyamoto E, Miyakawa T (1996) Sequential changes of tau-site-specific phosphorylation during development of paired helical filaments. *Dementia* **7**, 177-181.

[54] Augustinack JC, Schneider A, Mandelkow EM, Hyman BT (2002) Specific tau phosphorylation sites correlate with severity of neuronal cytopathology in Alzheimer's disease. *Acta Neuropathol* **103**, 26-35.

[55] Struble RG, Ala T, Patrylo PR, Brewer GJ, Yan XX (2010) Is brain amyloid production a cause or a result of dementia of the Alzheimer's type? *J Alzheimers Dis* **2**, 393-399.

[56] Drachman DA (2014) The amyloid hypothesis, time to move on: Amyloid is the downstream result, not cause, of Alzheimer's disease. *Alzheimers Dement* **10**, 372-380.

[57] Alafuzoff I, Thal DR, Arzberger T, Bogdanovic N, Al-Sarraj S, Bodi I, Boluda S, Bugiani O, Duyckaerts C, Gelpi E, Gentleman S, Giaccone G, Graeber M, Hortobagyi T, Höftberger R, Ince P, Ironside JW, Kavantzas N, King A, Korkolopoulou P, Kovács GG, Meyronet D, Monoranu C, Nilsson T, Parchi P, Patsouris E, Pikkarainen M, Revesz T, Rozemuller A, Seilhean D, Schulz-Schaeffer W, Streichenberger N, Wharton SB, Kretzschmar H (2009) Assessment of beta-amyloid deposits in human brain: A study of the BrainNet Europe Consortium. *Acta Neuropathol* **117**, 309-320.

[58] Chan-Palay V, Asan E (1989) Alterations in catecholamine neurons of the locus coeruleus in senile dementia of the Alzheimer type and in Parkinson's disease with and without depression. *J Comp Neurol* **287**, 373-392.

[59] Gannon M, Che P, Chen Y, Jiao K, Roberson ED, Wang Q (2015) Noradrenergic dysfunction in Alzheimer's disease. *Front Neurosci* **9**, 220.

[60] Theofilas P, Ehrenberg AJ, Dunlop S, Lorenzo DI, Alho AT, Nguy A, Leite RE, Rodriguez RD, Mejia MB, Suemoto CK, Ferretti-Rebustini RE, Polichiso L, Nascimento CF, Seeley WW, Nitrini R, Pasqualucci CA, Jacob Filho W, Rueb U, Neuhaus J, Heinsen H, Grinberg LT (2016) Locus coeruleus volume and cell population changes during Alzheimer's disease progression: A stereological study in human postmortem brains with potential implication for early-stage biomarker discovery. *Alzheimers Dement* **13**, 236-246.

[61] Ehrenberg AJ, Nguy AK, Theofilas P, Dunlop S, Suemoto CK, Di Lorenzo Alho AT, Leite RP, Dieh Rodriguez R, Mejia MB, Rüb U, Farfel JM, De Lucena Ferretti-Rebustini RE, Nascimento CF, Nitrini R, Pasquallucci CA, Jacob-Filho W, Miller B, Seeley WW, Heinsen H, Grinberg LT (2017) Quantifying the accretion of hyperphosphorylated tau in the locus coeruleus and dorsal raphe nucleus: The pathological building blocks of early Alzheimer's disease. *Neuropathol Appl Neurobiol* **5**, 393-408.

[62] Wang J, Gu BJ, Masters CL, Wang YJ (2017) A systemic view of Alzheimer disease - insights from amyloid-β metabolism beyond the brain. *Nat Rev Neurol* **10**, 612-623.

Corrected Proof

[63] Menuet C, Borghgraef P, Matarazzo V, Gielis L, Lajard AM, Voituron N, Gestreau C, Dutschmann M, Van Leuven F, Hilaire G (2011) Raphe tauopathy alters serotonin metabolism and breathing activity in terminal Tau.P301L mice: Possible implications for tauopathies and Alzheimer's disease. *Respir Physiol Neurobiol* **178**, 290-303.

[64] Grieb P (2016) Intracerebroventricular streptozotocin injections as a model of Alzheimer's disease: In search of a relevant mechanism. *Mol Neurobiol* **53**, 1741-1752.

[65] Kraska A, Santin MD, Dorieux O, Joseph-Mathurin N, Bourrin E, Petit F, Jan C, Chaigneau M, Hantraye P, Lestage P, Dhenain M (2012) *In vivo* cross-sectional characterization of cerebral alterations induced by intracerebroventricular administration of streptozotocin. *Plos One* **7**, e46196.

[66] Gargaglioni LH, Hartzler LK, Putnam RW (2010) The locus coeruleus and central chemosensitivity. *Respir Physiol Neurobiol* **173**, 264-273.

[67] Taxini CL, Puga CC, Dias MB, Bícego KC, Gargaglioni LH (2013) Ionotropic but not metabotropic glutamatergic receptors in the locus coeruleus modulate the hypercapnic ventilatory response in unanaesthetized rats. *Acta Physiol* **208**, 125-135.

[68] Biancardi V, Bícego KC, Gargaglioni LH (2014) ATP in the locus coeruleus as a modulator of cardiorespiratory control in unanaesthetized male rats. *Exp Physiol* **99**, 232-247.

[69] Bobich JA, Zheng Q, Campbell A (2004) Incubation of nerve endings with a physiological concentration of Abeta1-42 activates CaV2.2(N-Type)-voltage operated calcium channels and acutely increases glutamate and noradrenaline release. *J Alzheimers Dis* **6**, 243-255.

[70] Braak H, Del Tredici K (2011) Alzheimer's pathogenesis: Is there neuron-to-neuron propagation? *Acta Neuropathol* **121**, 589-595.

[71] Attems J, Thal DR, Jellinger KA (2012) The relationship between subcortical tau pathology and Alzheimer's disease. *Biochem Soc Trans* **40**, 711-715.

[72] Braak H, Del Tredici K (2012) Where, when, and in what form does sporadic Alzheimer's disease begin? *Curr Opin Neurol* **25**, 708-714.

[73] Gottfries CG, Adolfsson R, Aquilonius SM, Carlsson A, Eckernäs SA, Nordberg A, Oreland L, Svennerholm L, Wiberg A, Winblad B (1983) Biochemical changes in dementia disorders of Alzheimer type (AD/SDAT) *Neurobiol Aging Winter* **4**, 261-271.

[74] Palmer AM, Francis PT, Bowen DM, Benton JS, Neary D, Mann DM, Snowden JS (1987) Catecholaminergic neurones assessed ante-mortem in Alzheimer's disease. *Brain Res* **30**, 365-375.

[75] Herregodts P, Bruylan M, De Keyser J, Solheid C, Michotte Y, Ebinger G (1989) Monoaminergic neurotransmitters in Alzheimer's disease. An HPLC study comparing presenile familial and sporadic senile cases. *J Neurol Sci* **92**, 101-116.

[76] Hoogendijk WJ, Feenstra MG, Botterblom MH, Gilhuis J, Sommer IE, Kamphorst W, Eikelenboom P, Swaab DF (1999) Increased activity of surviving locus ceruleus neurons in Alzheimer's disease. *Ann Neurol* **45**, 82-91.

[77] Raskind MA, Peskind ER, Holmes C, Goldstein DS (1999) Patterns of cerebrospinal fluid catechols support increased central noradrenergic responsiveness in aging and Alzheimer's disease. *Biol Psychiatry* **15**, 756-765.

[78] Chalermpalanupap T, Schroeder JP, Rorabaugh JM, Liles LC, Lah JJ, Levey AI, Weinshenker D (2017) Locus coeruleus ablation exacerbates cognitive deficits, neuropathology, and lethality in P301S tau transgenic mice. *J Neurosci* **3**, 74-92.

[79] Roh JH, Huang Y, Bero AW, Kasten T, Stewart FR, Bateman RJ, Holtzman DM (2012) Disruption of the sleep-wake cycle and diurnal fluctuation of β-amyloid in mice with Alzheimer's disease pathology. *Sci Transl Med* **4**, 150-122.

[80] Song JZ, Cui SY, Cu XY, Hu X, Ma YN, Ding H, Ye H, Zhang YH (2018) Dysfunction of GABAergic neurons in the parafacial zone mediates sleep disturbances in a streptozotocin-induced rat model of sporadic Alzheimer's disease. *Metab Brain Dis* **33**, 127-137.

[81] Winer JR, Mander BA (2018) Waking up to the importance of sleep in the pathogenesis of Alzheimer disease. *JAMA Neurol* **75**, 654-656.

[82] Carter ME, Yizhar O, Chikahisa S, Nguyen H, Adamantidis A, Nishino S, Deisseroth K, de Lecea L (2010) Tuning arousal with optogenetic modulation of locus coeruleus neurons. *Nat Neurosci* **13**, 1526-1533.

[83] Harper DG, Volicer L, Stopa EG, Mckee AC, Nitta M, Satlin A (2005) Disturbance of endogenous circadian rhythm in aging and Alzheimer disease. *Am J Geriatr Psychiatry* **13**, 359-368.

[84] Gomolin I, Aung MM, Wolf-Klein G, Auerbach C (2005) Older is colder: Temperature range and variation in old people. *J Am Geriatr Soc* **12**, 2170-2172.

[85] Weinert D (2010) Circadian temperature variation and ageing. *Ageing Res Rev* **9**, 51-60.

[86] Klegeris A, Schulzer M, Harper DG, Mcgeer PL (2007) Increase in core body temperature of Alzheimer's disease patients as a possible indicator of chronic neuroinflammation: A meta-analysis. *Gerontology* **53**, 7-11.

[87] Matsuzakia K, Katakuraa M, Sugimotoab N, Haraa T, Hashimotoa M, Shidoa O (2015) β-amyloid infusion into lateral ventricle alters behavioral thermoregulation and attenuates acquired heat tolerance in rats. *Temperature* **3**, 418-24.

[88] Knight EM, Brown TM, Gumusgoz S, Smith JC, Waters EJ, Allan SM, Lawrence CB (2013) Age-related changes in core body temperature and activity in triple-transgenic Alzheimer's disease (3xTgAD) mice. *Dis Model Mech* **6**, 160-170.

[89] Motzko-Soares ACP, Vizin RCL, Martins TMS, Hungaro ARO, Sato JR, Almeida MC, Carrettiero DC (2018) Thermoregulatory profile of neurodegeneration-induced dementia of the Alzheimer's type using intracerebroventricular streptozotocin in rats. *Acta Physiol (Oxf)*, e13084.

[90] Barros RCH, Zimmer ME, Branco LG, Milsom WK (2001) Hypoxic metabolic response of the golden-mantled ground squirrel. *J Appl Physiol* **91**, 603-612.

[91] Bicego KC, Barros RC, Branco LG (2007) Physiology of temperature regulation: Comparative aspects. *Comp Biochem Physiol A Mol Integr Physiol* **147**, 616-639.

[92] Tattersall GJ, Milsom WK (2009) Hypoxia reduces the hypothalamic thermogenic threshold and thermosensitivity. *J Physiol* **587**, 5259-5274.

Corrected Proof

Experimental Neurology 328 (2020) 113250

Contents lists available at ScienceDirect

Experimental Neurology

journal homepage: www.elsevier.com/locate/yexnr

Research paper

Decreased excitability of locus coeruleus neurons during hypercapnia is exaggerated in the streptozotocin-model of Alzheimer's disease

Mariane C. Vicente[a,b], Chuma M. Humphrey[c], Luciane H. Gargaglioni[b], Tim D. Ostrowski[a,*]

[a] Department of Physiology, Kirksville College of Osteopathic Medicine, A.T. Still University of Health Sciences, Kirksville, MO, USA
[b] Department of Animal Morphology and Physiology, Sao Paulo State University–UNESP/FCAV at Jaboticabal, SP, Brazil
[c] Department of Biology, Truman State University, Kirksville, MO, USA

ARTICLE INFO

Keywords:
Brainstem
STZ
Intracerebroventricular
Patch clamp
Brain slice
CO_2
Chemosensitivity
Potassium currents
Neurodegeneration

ABSTRACT

The locus coeruleus (LC) is a pontine nucleus important for respiratory control and central chemoreception. It is affected in Alzheimer's disease (AD) and alteration of LC cell function may account for respiratory problems observed in AD patients. In the current study, we tested the electrophysiological properties and CO_2/pH sensitivity of LC neurons in a model for AD. Sporadic AD was induced in rats by intracerebroventricular injection of 2 mg/kg streptozotocin (STZ), which induces behavioral and molecular impairments found in AD. LC neurons were recorded using the patch clamp technique and tested for responses to CO_2 (10% CO_2, pH = 7.0). The majority (~60%) of noradrenergic LC neurons in adult rats were inhibited by CO_2 exposure as indicated by a significant decrease in action potential (AP) discharge to step depolarizations. The STZ-AD rat model had a greater sensitivity to CO_2 than controls. The increased CO_2-sensitivity was demonstrated by a significantly stronger inhibition of activity during hypercapnia that was in part due to hyperpolarization of the resting membrane potential. Reduction of AP discharge in both groups was generally accompanied by lower LC network activity, depolarized AP threshold, increased AP repolarization, and increased current through a subpopulation of voltage-gated K^+ channels (K_V). The latter was indicated by enhanced transient K_V currents particularly in the STZ-AD group. Interestingly, steady-state K_V currents were reduced under hypercapnia, a change that would favor enhanced AP discharge. However, the collective response of most LC neurons in adult rats, and particularly those in the STZ-AD group, was inhibited by CO_2.

1. Introduction

Alzheimer's disease (AD) is a neurodegenerative disease often associated with aging (Folch et al., 2016; Wilson et al., 2012). In addition to the typical decline in cognition and memory, patients with AD also present with respiratory problems (Deak and Kirsch, 2014; Gaig and Iranzo, 2012; Lee et al., 2019; Liguori et al., 2017). Over 70% of institutionalized AD patients have respiratory disturbances, such as insufficient ventilation during sleep, sleep apnea, and shortness of breath (Deak and Kirsch, 2014; Gaig and Iranzo, 2012; Leng et al., 2017). Recent studies show respiratory problems may lead to cognitive decline and may be a consequence of AD progression (Lee et al., 2019; Liguori et al., 2017; Yaffe et al., 2011). Therefore, respiratory impairment likely reflects alterations in brain areas that control breathing (Deak and Kirsch, 2014; Smith et al., 2013).

The locus coeruleus (LC) is a noradrenergic nucleus of the central nervous system involved in a variety of functions, including wakefulness, learning and memory (Aston-Jones and Cohen, 2005; Aston-Jones and Waterhouse, 2016; Berridge and Waterhouse, 2003), and respiratory function (Biancardi et al., 2008; Gargaglioni et al., 2010; Hilaire et al., 2004; Oyamada et al., 1998; Putnam et al., 2004). Specifically, LC neurons have a vital role in central chemoreception (Biancardi et al., 2008; Filosa and Putnam, 2003; Gargaglioni et al., 2010; Vicente et al., 2016). Previous studies in neonates (postnatal < 10 days) showed CO_2 and pH sensitivity for a high percentage (80%) of LC neurons, thus, making this nucleus important for compensatory responses to CO_2 (Filosa et al., 2002; Johnson et al., 2008; Oyamada et al., 1998; Pineda and Aghajanian, 1997).

The LC of AD patients is severely affected (Andrés-Benito et al., 2017; Arendt et al., 2015; Serra et al., 2018; Wilson et al., 2013) and abnormalities in this chemosensitive area may have direct implications in the respiratory dysfunction with AD. The LC is one of the first regions

* Corresponding author at: Department of Physiology, Kirksville College of Osteopathic Medicine, A.T. Still University of Health Sciences, 800 W. Jefferson St., Kirksville, MO 63501, USA.
E-mail address: tostrowski@atsu.edu (T.D. Ostrowski).

https://doi.org/10.1016/j.expneurol.2020.113250
Received 16 October 2019; Received in revised form 4 February 2020; Accepted 17 February 2020
Available online 20 February 2020
0014-4886/ © 2020 Elsevier Inc. All rights reserved.

that undergoes degeneration in the progression of human AD (Andrés-Benito et al., 2017; Arendt et al., 2015; Braak and Del Tredici, 2011; Peterson and Li, 2018). Postmortem analysis of AD brains indicated cell loss in the LC as high as 50%, which correlated with high levels of hyperphosphorylated tau protein and amyloid beta in this nucleus (Matthews et al., 2002; Pamphlett and Kum Jew, 2015; Šimić et al., 2017; Thal et al., 2002; Zarow et al., 2003). The reduced number of noradrenergic LC cells, in turn, may play a role in the declining level of noradrenaline in the hypothalamus and cortex, contributing to the severity of cognitive impairments. Interestingly, AD damage seems greater in the LC than in any other subcortical nuclei, including the nucleus basalis, that is typically implicated with cholinergic loss in patients with AD (Šimić et al., 2017; Zarow et al., 2003). The collective data suggest an early dysfunctional LC in AD, which may also have an underlying role in breathing dysfunction observed in patients.

To date, there is little data associating LC with respiratory dysfunctions in AD progression. Therefore, we started to focus on the respiratory deficits of the disease using the streptozotocin (STZ)-induced rat model of sporadic AD (Brown et al., 2019; Vicente et al., 2018). Besides progressive deterioration of learning and memory, intracerebroventricular administration of STZ mimics the biochemical and structural changes found in the brains of AD patients. These changes include increased amyloid beta accumulation and tau protein phosphorylation, reduced glucose and energy metabolism, and the typical oxidative stress and neuroinflammation leading to neuronal death (Deng et al., 2009; Grünblatt et al., 2004; Johnston et al., 2010; Knezovic et al., 2015; Lannert and Hoyer, 1998; Rai et al., 2014; Tota et al., 2010), all of which are prominent features of human AD (Ingelsson et al., 2004; Lyness et al., 2003; Milton, 2004; Sato and Morishita, 2015; Zhang et al., 2015). Furthermore, we previously showed that an increase in amyloid beta peptide in the LC region paralleled alterations in the ventilatory responses to hypercapnia. Thus, analyzing the intrinsic activity of LC neurons could provide mechanistic insight into respiratory alterations in this model and in patients with AD. In the current study, we used the patch clamp technique to evaluate the electrophysiological responses of LC neurons to CO_2 in the STZ-AD model.

2. Material and methods

2.1. Animals

The current study used male Sprague-Dawley rats (6–7 weeks; total of 39 rats) that were kept in an AAALAC accredited vivarium at A.T. Still University's Kirksville College of Osteopathic Medicine in Kirksville, Missouri, USA. Rats were maintained on a 12-h day/night cycle at 24 °C and 46% humidity with water and food available ad libitum. All experimental protocols were conducted in accordance with the guidelines of the NIH ("Guide to the Care and Use of Laboratory Animals") and were approved by A.T. Still University's Animal Care and Usage Committee.

2.2. Sporadic Alzheimer's disease model

Similar to our previous studies (Brown et al., 2019; Ebel et al., 2017; Vicente et al., 2018), the typical symptoms of AD were induced by pressure injection of a subdiabetogenic dose of STZ (2 mg/kg, Alfa Aesar, Haverhill, MA) into both lateral ventricles of the brain (5 μL per side). Unlike STZ-AD rats, control (CTL) rats received vehicle only (0.9 mM citrate buffered saline, pH 4.5). For intracerebroventricular injections, rats were anesthetized using isoflurane (5% induction, 2% maintenance, Piramal, Bethlehem, PA) and positioned in a stereotaxic frame (type 68,001, RWD Life Science, San Diego, CA). A sagittal midline incision was made on the scalp to expose the sagittal and coronal suture of the skull. Two holes were drilled into the skull with a rotating tool (Dremel 7300 with engraving cutter 105) to allow access to the lateral ventricles. Injection glass capillaries (type 1B120F-4, World Precision Instruments, Sarasota, FL) were drawn using a P-97 micropipette puller (Sutter Instruments, Novato, CA) and used for intracerebroventricular injections at the following stereotaxic coordinates (Paxinos and Watson, 2007): −0.9 mm AP, ± 1.5 mm ML, and 3.6 mm DV. After surgery, rats received high sugar supplements (Froot Loops, Kellogg's, Battle Creek, MI) in addition to normal rat chow to facilitate weight recovery.

Rats also received 2 mg/kg Dexamethasone (VetOne, Boise, ID) as an immunosuppressant before injections to avoid possible brain swelling. Postoperatively rats were treated with 50 μg/kg buprenorphine hydrochloride (Reckitt Benckiser, Slough, UK) for pain management, 7 mg/kg enrofloxacin (VetOne) for antibiotic treatment, and 3 mL of 0.9% sodium chloride solution (Hospira, Lake Forest, IL) for fluid reconstitution.

2.3. Behavioral test

Eleven days after intracerebroventricular injections, we used the Morris water maze as a positive control to test spatial reference learning and memory in the STZ-AD model (Bao et al., 2017; Bromley-Brits et al., 2011). The apparatus consisted of a 178-cm diameter cylindrical tank filled with water (~730 L, pH = 7.2, 22 °C) that was made opaque with black nontoxic paint (DyeMond pond dye, Airmax, Romeo, MI). The pool was conceptually divided into four equal quadrants, and each quadrant was marked with a visual cue (i.e., yellow star, blue square, red circle, or green triangle). A black platform (10-cm diameter) that was height adjustable was positioned close to the middle of the target quadrant (green triangle).

On day 1, animals were trained during five initial trials to find the raised escape platform (1 cm above water level). Then, the platform was submerged 1 cm below water level and rats were subjected to 15 consecutive trials per day for 3 days (each series was 24 h apart). The rats were placed at randomized starting positions (except the target quadrant) and given 60 s (cutoff time) to find the submerged platform. If the rat was unable to find the hidden escape platform within the cutoff time, it was manually guided to the platform. The time to reach the platform was noted as the escape latency. The swim velocity was recorded using a camera (AW615, Ausdom, City of Industry, CA) positioned above the tank and analyzed using the Animal Tracker plugin in Fiji software (version 1.52i, NIH).

2.4. Patch clamp recordings

2.4.1. In vitro brain slice preparation

Similar to Ting et al. (2014, 2018), rats were anesthetized with isoflurane and transcardially perfused with 60 mL of ice-cold oxygenated *N*-Methyl-D-glucamine (NMDG)-based artificial cerebrospinal fluid (aCSF) with the following composition (in mM): 93 NMDG, 2.5 KCl, 1.2 NaH_2PO_4, 30 $NaHCO_3$, 20 HEPES, 25 glucose, 2 thiourea, 5 sodium ascorbate, 3 sodium pyruvate, 0.5 $CaCl_2{\cdot}2H_2O$, and 10 $MgSO_4{\cdot}7H_2O$, pH 7.4, 300–305 mOsm. NMDG-based solutions were used to better preserve the health of brain tissue from adult rats. Next, the brainstem was rapidly removed and horizontal brain slices (250-μm thick) containing the LC were obtained using a vibratome (7000smz-2, Campden Instruments, Lafayette, IN). Slices were then incubated for 20 min in warm (35 °C) oxygenated (95% O_2–5% CO_2) NMDG aCSF. For patch clamp recordings, tissue sections were placed in a superfusion chamber, secured with a nylon mesh, and superfused at 2–3 mL/min with standard recording aCSF (in mM: 124 NaCl, 3 KCl, 1.2 NaH_2PO_4, 1.2 $MgSO_4$, 25 $NaHCO_3$, 11 D-glucose, and 2 $CaCl_2$, saturated with 95% O_2–5% CO_2, pH 7.4, 300 mOsm) at 35 °C.

2.4.2. Electrophysiological recording

Similar to our previous studies (Ostrowski et al., 2014a, 2014b), LC cell somas were recorded to analyze the electrophysiological properties.

Recordings were primarily obtained from neurons in the dorsal LC because of the greater number of healthy cells. Pipettes (8250, King Precision Glass, Claremont, CA) were made with a Flaming/Brown micropipette puller (Model P-97, Sutter Instruments) and had resistances of 4.5–5 MΩ when filled with standard recording solution (in mM: 130 potassium gluconate, 10 HEPES, 0.4 EGTA, 1 $MgCl_2$, 0.3 Na_2-GTP, and 2 Na_2-ATP, pH 7.45, 280 mOsm) (Nichols et al., 2008). Recording pipettes were guided with a motorized micromanipulator (MP-225, Sutter Instruments). Data were recorded (20 kHz sampling rate) and filtered at 2 kHz using a Patch Clamp EPC 10 USB amplifier/AD converter (HEKA Instruments, Holliston, MA). The liquid junction potential was not corrected and the series resistance was not compensated.

The activity of LC neurons was recorded under normocapnia (baseline: standard 5% CO_2, balanced with O_2) and 5 min into perfusion of hypercapnic aCSF (10% CO_2, balanced with O_2). CO_2 concentrations were achieved by saturating the perfusate using mass flow controllers (MC-5SLPM-D, Alicat Scientific, Tucson, AZ). Increasing CO_2 content from 5% to 10% lowered the pH from an initial 7.4 to 7.0. This drop in pH is sufficient to study the CO_2-induced response of LC neurons (Li and Putnam, 2013; Lopes et al., 2016; Oyamada et al., 1998).

All electrophysiological data were analyzed using Igor Pro 8 (WaveMetrics, Portland, OR), MiniAnalysis (Synaptosoft, Fort Lee, NJ), and Excel (Microsoft, Redmond, WA) software programs.

2.4.3. Current clamp protocol

Criteria for healthy LC neurons under baseline conditions (after establishing whole cell configuration) were a resting membrane potential (RMP) close to −45 to −50 mV and spontaneous spike activity. We used step depolarization (−20 to 100 pA, 10 pA steps, 100-ms duration) to induce action potential (AP) discharge (Kline et al., 2010; Ostrowski et al., 2014a). Because of the heterogeneous response of LC neurons to CO_2 (Lopes et al., 2016; Nichols et al., 2008), we grouped cells according to their change in AP discharge from baseline to hypercapnia. Cells that increased spike activity by 5% (average over all current steps) were categorized as CO_2-activated, those that decreased by 5% as CO_2-inhibited, and those that did not change as non-responder. These classifications do not represent the intrinsic chemosensitivity of LC cells (see Discussion).

Phase plan plots (change of membrane voltage [mV/ms] against the membrane potential [mV]) were generated from an AP elicited during the step depolarizations protocol (first AP to lowest depolarizing current to exclude possible effects from repetitive spiking with stronger stimulation). AP threshold (THR) was identified when the voltage change exceeded 10 mV/ms (Gudes et al., 2015). Other parameters analyzed were AP rising slope (maximal Na^+ conductance) (Jenerick, 1963), AP peak (overshoot), AP falling slope, AP half-width (measured at 50% AP amplitude from RMP), and the afterhyperpolarization (measured from THR). The delay to the first AP in response to 100 pA current is the time from stimulus begin until AP peak. RMP was recorded in the absence of current induction ($I = 0$).

2.4.4. Voltage clamp protocol

All cells were clamped at −60 mV (at the calculated reversal potential for chloride), and the membrane resistance (i.e., input resistance, R_i) was determined from a 5-mV hyperpolarizing step. K^+ conductances were measured using a step protocol between −100 and + 80 mV (+20 mV per step, 400 ms step). Cell capacitance was equal between cells from control and STZ-AD groups (CTL, 104.0 ± 11.0 pF vs STZ-AD, 111.5 ± 7.6; $p = .58$; $n = 13$ in each group). The transient K^+ current was examined by subtracting the steady-state current (near the end of the voltage step) from the initial current to the voltage step (Kline et al., 2010; Ostrowski et al., 2014a). Spontaneous postsynaptic currents (sPSC) were recorded for 1 min in the absence of stimulation and constitute network activity (Fortin and Champagnat, 1993) within the LC.

2.5. Immunohistochemistry

Similar to our previous studies (Brown et al., 2019; Ebel et al., 2017), slices containing the LC (30 μm thick; if previously used for patch clamp recordings, slice thickness was 250 μm) were washed in phosphate buffered saline (PBS) and blocked for 30 min in 10% normal donkey serum (MilliporeSigma, Burlington, MA) with 0.3% Triton-PBS. Next, slices were incubated overnight in 1% normal donkey serum with 0.3% Triton-PBS and primary antibody against tyrosine hydroxylase (TH) (chicken, 1:1000, ab76442, Abcam, Cambridge, MA) and, in some applications, additionally with NeuN (mouse, 1:500, MAB377, MilliporeSigma). The next day, slices were washed and incubated for 2 h in secondary antibody using Alexa Fluor 647 (donkey anti-chicken, 1:200, 703–605–155, Jackson ImmunoResearch, West Grove, PA) or Alexa Fluor 488 (donkey anti-chicken, 1:200, 703–545–155, Jackson ImmunoResearch) and, in some applications, with Alexa Fluor 594 (donkey anti-mouse, 1:200, 715–585–151, Jackson ImmunoResearch). After a final wash, slices were mounted on gelatin-coated glass slides, dried, and cover-slipped using ProLong Diamond (Thermo Fisher Scientific, Waltham, MA). All immunohistochemical steps were performed at room temperature. In a subset of experiments, the patch pipette solution contained 3% Lucifer yellow (LY) (L0259, Sigma-Aldrich, St. Louis, MO) that was ionophoretically injected (negative current for approximately 20 min) into LC neurons after electrophysiological characterization. Patch-slices were then fixed in 4% paraformaldehyde for later immunohistochemical identification of TH. Immunoreactivity was examined on a conventional epifluorescent microscope (Eclipse 80i, Nikon, Tokyo, Japan) with a digital monochrome camera (DS-Qi1Mc, Nikon) and appropriate filter sets or on a confocal microscope (DMI6000 B, Leica, Wetzlar, Germany) using lasers (Argon, HeNe 633) with fluorophore-specific excitation and emission wave length and appropriate filter sets. Confocal images were collected in z-stacks (0.5 μm optical slices). Post-processing of the images (adjustment of contrast and brightness for clarity) was done using the software Fiji.

Schematics of the LC were created with the Inkscape program (version 0.91, http://www.inkscape.org/), and nuclei were identified using Paxinos and Watson's rat brain atlas (Paxinos and Watson, 2007). Analysis of neuron number was completed in representative sections of the LC (Bregma level: from −9.96 to −9.60) and counted blindly by 3 independent persons using Fiji software. Neurons were counted in a 200 × 200 μm box in the dorsal-most portion of the LC excluding spaces that are devoid of cells (e.g., blood vessels). Results of all counters were averaged and compared between groups.

2.6. Statistical analysis

Behavioral, electrophysiological, and immunohistochemical data were analyzed using the *t*-test or two-way repeated measures ANOVA followed by Newman-Keuls post-hoc test where appropriate. All results were considered statistically significantly different at $p \leq .05$. Group data are presented as mean ± SEM.

3. Results

3.1. Diminished memory performance in the streptozotocin-induced Alzheimer's disease (STZ-AD) model

Previous research has shown the STZ-AD rat model results in reduced memory performance (Lannert and Hoyer, 1998; Salkovic-Petrisic et al., 2013). To verify memory dysfunction in our study, we used the Morris water maze. Trial-to-trial performance was compared between groups as measure of spatial memory. Fig. 1A shows the escape latencies for 15 trials on each of the consecutive testing days. During the initial trials (with the visible platform), escape latency of all animals was typically near the cutoff time of 60 s, indicating a similar performance for both groups in the new environment. With an increasing

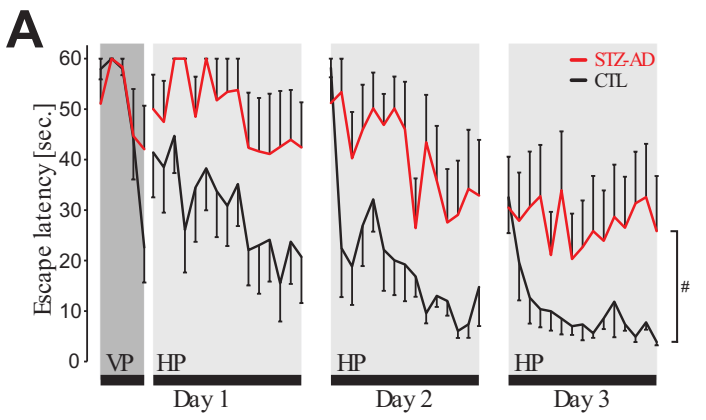

Fig. 1. Spatial learning and memory deficits in the sporadic Alzheimer's disease (AD) animal model.
A) Escape latency to find the hidden platform (HP) in the Morris water maze for the control (CTL) and streptozotocin-induced Alzheimer's disease (STZ-AD) groups during the 3-day testing period with 15 training sessions per day. Cutoff time was 60 s. B) Swim velocity as measure for locomotor function shows no impairment in the STZ-AD group.
Data are reported as mean ± SEM. # $p \leq .05$; 2-way repeated measures ANOVA. n = 6–7 rats per group. VP = visible platform.

number of trials (and a hidden platform), STZ-AD rats spent significantly more time finding the platform than the control group, demonstrating impairment in learning and retention of spatial memory. Both groups had comparable swim velocity (Fig. 1B), indicating motor function of STZ-AD rats was not affected.

3.2. No change in locus coeruleus (LC) neuron number in the STZ-AD model

Because of neurodegeneration of the LC in advanced human AD, we analyzed neuronal number in our STZ-AD model (Fig. 2). We concentrated on three representative regions for the caudal-rostral extent of the LC and immunohistochemically stained for NeuN (neuronal marker) and tyrosine hydroxylase (TH) (typically found in the LC). The numbers of neurons that co-stained for TH and NeuN were compared between the STZ-AD and control group. No difference was found between groups, likely indicating that the AD model of the current study represents an early time point in disease progression (two weeks after AD induction) and that morphological changes in the LC are not (yet) present.

3.3. Spike response of LC neurons during hypercapnia

The LC is located adjacent to the 4th ventricle in the dorsal aspect of the pons. Fig. 3A shows an example of the LC (white dashed line) in a horizontal brainstem slice used for patch clamp recordings. A 40× magnification from a typical cell in the LC with attached patch pipette is shown in Fig. 3B. In a subset of rats and after completion of electrophysiological recordings, we immunohistochemically stained for TH (Fig. 3C). Dense TH is found in the noradrenergic LC (Grzanna and Molliver, 1980) and verified correct placement of our patch pipettes.

The LC is a chemosensitive nucleus with a population of neurons having different response patterns to increased CO_2 conditions. Neurons may show an increase, decrease, or no alteration of activity when exposed to CO_2 (Lopes et al., 2016; Nichols et al., 2008). To test this heterogeneity of neuronal responses to CO_2, we performed a step depolarization protocol (100 ms steps with increasing current, +10 pA/step) to evoke action potential (AP) discharge (Figs. 3D and 4). In the control group (data from 6 rats), the majority of LC neurons (57%, 8 cells from 5 rats) were inhibited by CO_2 (i.e., reduced current-evoked AP discharge) (Fig. 3E). Only a few cells were either activated (increased spiking, 21%, 3 cells from 3 rats) by CO_2 or did not respond (21%, 3 cells from 3 rats). A similar result was obtained for the STZ-AD group (data from 6 rats). The majority of cells (64%, 9 cells from 6 rats) were inhibited by CO_2, only 14% (3 cells from 2 rats) showed activation, and 21% (2 cells from 2 rats) did not change spike discharge to current injections under hypercapnic conditions (Fig. 3F).

Given previous studies that found over 50% of noradrenergic LC neurons in neonatal rats increased firing rate to CO_2 exposure (Berridge and Waterhouse, 2003; Filosa et al., 2002; Johnson et al., 2008), we wanted to confirm the phenotype of LC cells in our preparation using adult rats. A subset of cells (5 cells in uninjected control rats) were

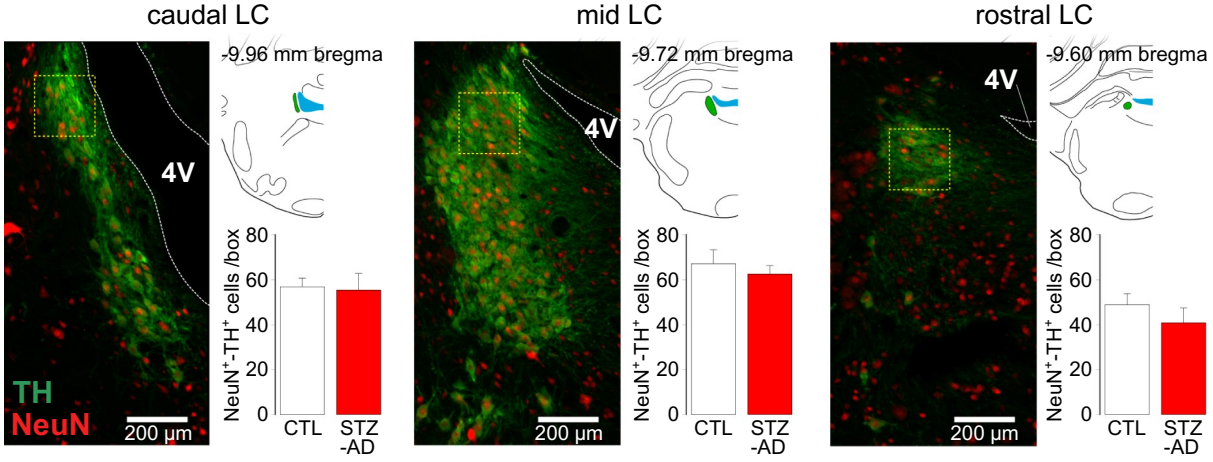

Fig. 2. Unaltered neuronal density in the locus coeruleus (LC) of the streptozotocin-induced Alzheimer's disease (STZ-AD) group.
Three representative coronal sections (30 µm) of the LC with labeling of NeuN-identified neurons (red) and tyrosine hydroxylase (TH) -positive cells (green). Brain schematics illustrate the location and extent of the pontine LC (green area) in relation to bregma. TH^+ neurons were counted in a 200 × 200 µm box (yellow box) in the dorsal-most portion of the LC.
Data are presented as mean ± SEM. n = 6 rats per group. 4 V = 4th ventricle.

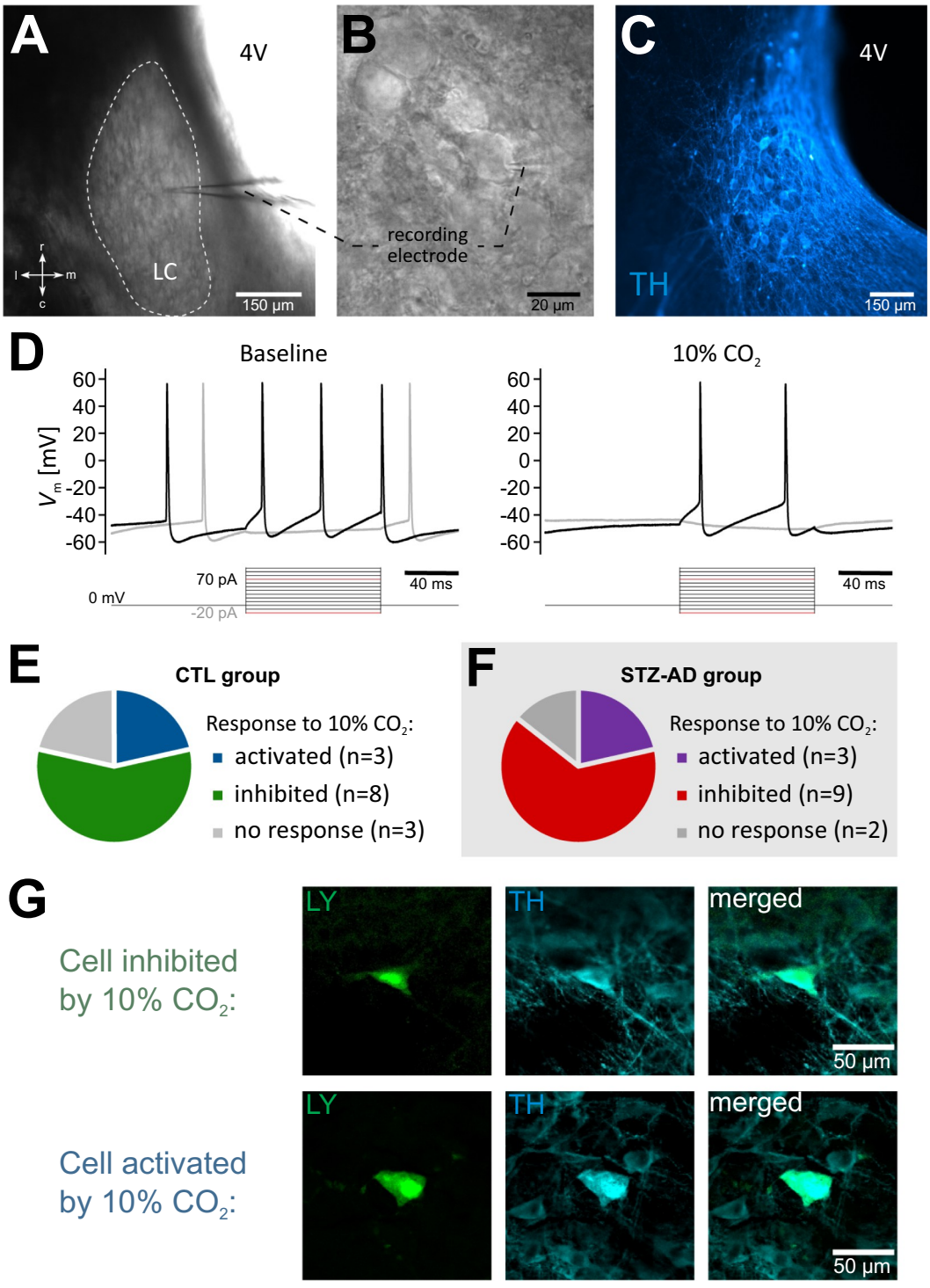

Fig. 3. Response classes of locus coeruleus (LC) neurons to increased CO_2 exposure.
A) Representative horizontal brainstem section (250 µm) illustrating the location of the LC during patch clamp experiments. B) Magnification of a LC neuron with attached glass electrode during the recording. C) Immunohistochemical staining of tyrosine hydroxylase (TH) (blue) in a horizontal brainstem slice subsequent to neuronal recordings in the region of the LC. D) Representative responses of a CO_2-inhibited LC neuron to step depolarization (10 pA steps, 100 ms) at baseline and during the CO_2 condition. Reponses are shown for −20 pA (gray trace) and +70 pA (black trace) only. The stimulus is shown underneath the traces. Note that CO_2 eliminates spontaneous spike activity (before and after the stimulus) and blunts action potential discharge to current injection. E) Response classes of LC neurons to hypercapnia in the control (CTL) group F) Response classes of LC neurons to hypercapnia in the streptozotocin-induced Alzheimer's disease (STZ-AD) group. G) Confocal images (40× oil) of electrophysiologically identified LC neurons that were loaded with Lucifer yellow (LY) (green fluorescence) and stained against tyrosine hydroxylase (TH) (blue). Note the overlap of LY and TH in the merged image, indicating the same LC-specific phenotype for cells that were excited and inhibited by CO_2. All images shown are merged z-stack images from five sections (0.5 µm apart). 4 V = 4th ventricle, r = rostral, c = caudal, m = medial, l = lateral.

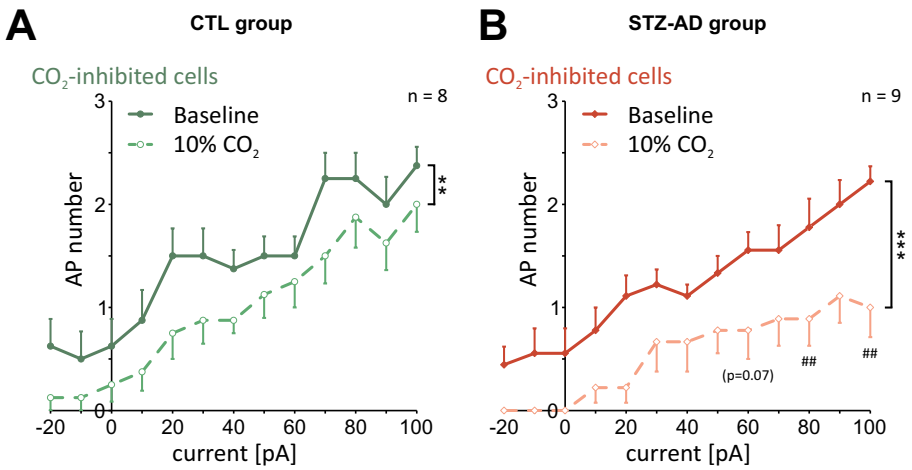

Fig. 4. Spike discharge of locus coeruleus (LC) neurons to current injections at baseline and during increased CO_2.
Action potential (AP) number in response to step depolarization during baseline and hypercapnia (10% CO_2) for cells that were inhibited by CO_2 in the control (CTL) group (A) and the streptozotocin-induced Alzheimer's disease (STZ-AD) group (B).
Data are expressed as mean ± SEM. ** $p \leq .01$ and *** $p \leq .001$ indicated a difference between baseline and the hypercapnia condition. ## $p \leq .01$ indicated a difference between STZ-AD and CTL groups; 2-way repeated measures ANOVA.

loaded with the fluorescent dye Lucifer yellow (LY) during and after electrophysiological characterization. We later co-stained against TH and visualized LY-labeled cells using confocal microscopy (Fig. 3G). Cells that were excited or inhibited by CO_2 expressed the same phenotype for TH. This result furthermore suggests that all neurons recorded in the current study are noradrenergic (see also Fig. 3C). In the following analysis, we concentrated on the majority of LC neurons that were inhibited by CO_2.

3.4. Decreased excitability of LC neurons during hypercapnia is exaggerated in the STZ-AD model

Group data for current-evoked spike discharge in LC neurons that responded to CO_2 is shown in Fig. 4. In the control group, spike discharge of cells inhibited by hypercapnia (Fig. 4A) decreased significantly across all current steps when compared with their baseline response. Spike discharge in the STZ-AD group was also significantly blunted by CO_2 at all current steps (Fig. 4B). This hypercapnic inhibition on discharge was exaggerated in the STZ-AD group when compared with the control group (%change at 100 pA: CTL, 16.7 ± 8.3% vs STZ-AD, 57.4 ± 11.8; $p \leq .01$; $n = 8$–9). Notably, the baseline discharge of both groups reached similar magnitudes. A closer look at the spike discharge in the absence of depolarizing current (−20 to 0 pA in Fig. 4) showed the spontaneous activity of LC cells. Hypercapnia also reduced the spontaneous activity of CO_2-inhibited cells in both groups (Fig. 4A and B), indicating the inhibitory effect of CO_2 was independent of neuronal activity. Together, these data suggest that CO_2 is able to depress activity in a large subgroup of LC cells and that the STZ-AD rat model exhibits an impaired response to hypercapnic conditions.

3.5. CO_2 exposure decreases overall LC network activity

Network activity in the LC can be assessed by analyzing the spontaneous postsynaptic currents (sPSCs) in the absence of stimulation. All cells were clamped at −60 mV (the calculated equilibrium potential for chloride) and sPSCs recorded in this configuration likely represent excitatory inputs. Fig. 5A is a representative example of LC network activity during baseline and at 10% CO_2. CO_2 exposure significantly decreased the number of sPSCs as shown for CO_2-inhibited cells in both groups (Fig. 5B). The magnitude of this reduction was similar between groups (CO_2-induced change in network activity: CTL, −34.3 ± 12.3% vs STZ-AD, −32.1 ± 13.2%; $p > .05$; n = 8–9). The amplitude of sPSCs did not change with exposure to hypercapnia in the control group (baseline, 25.3 ± 3.4 pA vs CO_2, 26.3 ± 2.1 pA; $p > .05$; n = 8) or STZ-AD group (baseline, 27.5 ± 1.9 pA vs CO_2, 26.4 ± 2.8 pA; $p > .05$; $n = 9$).

3.6. CO_2 decreases resting membrane potential (RMP) in the STZ-AD model

To determine whether CO_2 alters basic cell membrane properties, we initially analyzed input resistance (R_i) (resistance across the cell membrane) from a 5 mV step (-60 to -65 mV) in voltage clamp configuration. There was no difference in R_i between groups at baseline and during hypercapnia. However, within the STZ-AD group R_i decrease significantly from baseline to hypercapnia in CO_2-inhibited cells (Table 1). This decrease of R_i is indicative of membrane channel opening. Consistent with this reduction of R_i, RMP was significantly hyperpolarized to more negative potentials in CO_2-inhibited cells from the STZ-AD group. This change indicates alterations of K^+ currents that are important for RMP generation and may contribute to the hypercapnia-induced reduction of AP discharge in the STZ-AD rat model. RMP of CO_2-inhibited cells in the control group did not change.

3.7. CO_2 Depolarizes Spike Threshold (THR) and Increases AP Repolarization in LC Neurons

To identify additional mechanisms for CO_2-induced inhibition of AP discharge in the majority of LC neurons, we closely examined AP properties during our step depolarization protocol. The delay to the first AP in response to 100 pA step depolarization is given in Table 2 and serves as an indicator of neuronal excitation. CO_2-inhibited cells in the STZ-AD group comprised a strong increase in delay of AP discharge, which is consisted with hypercapnia-induced inhibition of the response. This increase in delay is underestimated since three cells (STZ-AD group only) did not elicit spikes at 100 pA under hypercapnia and a higher current step needed to be evaluated. AP delay of CO_2-inhibited cells from the CTL group only showed a small and non-significant increase.

As detailed in Fig. 6A, main AP properties include THR, upstroke, AP peak amplitude, and downstroke. To reliably quantify these parameters, we generated phase plane plots that show the first derivative of membrane voltage against the change in membrane potential. A complete list of all parameters, their changes, and statistical analysis is provided in Table 2. In CO_2-inhibited cells of the CTL and STZ-AD groups, THR increased significantly with hypercapnia (Fig. 6B and 6C, Table 2). The CO_2-induced change in THR also increased the voltage difference from RMP to THR in both groups, making it harder to overcome this voltage difference by a depolarizing stimulus and eliciting AP discharge. The significant hyperpolarization of RMP in the STZ-AD group (Table 1) added to this difference. The STZ-AD group also had a hypercapnia-induced increase in rising slope and peak amplitude of the AP, suggesting alteration of Na^+-dependent inward currents. A prominent change in both groups was the CO_2-induced reduction of half-width resulting from a significantly steeper falling slope of the AP (Fig. 6B and 6C, Table 2). Faster AP repolarization is

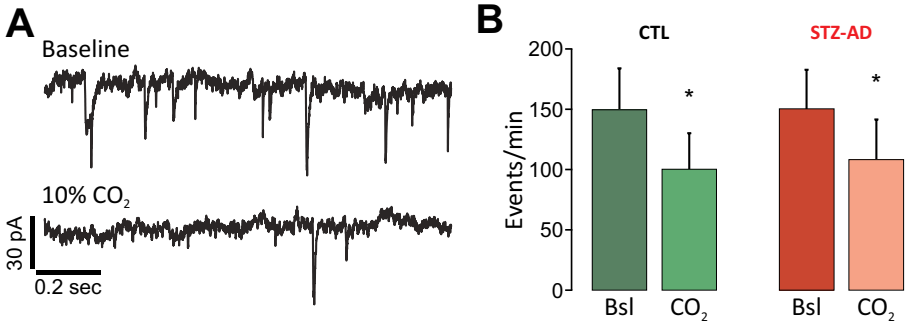

Figure 5. Reduced locus coeruleus (LC) network activity with increased CO_2.
A) Typical example for a reduced number of spontaneous postsynaptic currents (sPSC), representing LC network activity, with 10% CO_2. B) Group data for sPSCs at baseline (Bsl) and at 10% CO_2 for the control (CTL) and streptozotocin-induced Alzheimer's disease (STZ-AD) groups.
Data are expressed as mean ± SEM. * $p \leq .05$; *t*-test. n = 8-9 rats per group.

indicative of increased K^+-dependent outward currents that may contribute to the inhibitory effects of CO_2 observed in the majority of LC neurons.

3.8. CO_2 Modulates Currents Through Voltage-Gated K^+ (K_V) Channels

Because of the CO_2-induced increase of AP repolarization and the reduction of AP discharge in the majority of LC neurons, we analyzed the potential contribution of outward K^+ currents. We used step depolarization of the membrane from −100 to +80 mV (20 mV steps) to elicit outward K^+ currents in LC neurons. Fig. 7A shows representative K^+ currents during baseline and at 10% CO_2 in a LC cell that was inhibited by CO_2. The blue lines depict the time points used to measure the current-voltage (IV) relationship of transient (beginning of the stimulus) and steady-state (end) currents for each voltage step. Results for the steady-state current of CO_2-inhibited cells in the CTL and STZ-AD groups are shown in Fig. 7B. The IV relationship of both groups comprised a significant reduction of steady-state K^+ current with perfusion of 10% CO_2. This decrease of outward K^+ currents occurred at membrane potentials greater than +20 mV, a range that is typically associated with activity of K_V channels (Johnston et al., 2010; Mathie et al., 1998). Interestingly, a reduced steady-state K^+ current with depolarization would facilitate AP discharge. Enhanced AP discharge to CO_2 was not observed in this group of LC neurons, likely indicating a minor role of steady-state K^+ currents on overall neuronal spike activity. While steady-state IV curves at baseline were similar between groups, CO_2 induced a significantly greater reduction of steady-state current in STZ-AD rats than in control animals.

A reliable increase in transient K^+ current (calculated by subtracting the steady-state current from the initial current at the beginning of the voltage step) was seen for CO_2-inhibited cells between -40 to +40 mV under baseline conditions (Fig. 7C), which is consistent with the response typical for A-type K^+ channels (K_A) channels (Sonner and Stern, 2007). Responses of K_A channels became variable at membrane potentials of +40 mV and higher. The transient current increased in CO_2-inhibited cells when exposed to hypercapnia. While this change was only a strong trend in the control group at 0 mV membrane potential and amounted to an increase of ~135% (baseline, 0.142 ± 0.033 nA vs CO_2, 0.337 ± 0.078 nA; $p = .059$; $n = 8$), cells of the STZ-AD group were significantly increased by ~170% (baseline, 0.153 ± 0.054 nA vs CO_2, 0.417 ± 0.045 nA; $p \leq .05$; $n = 9$). The CO_2-dependent increase of K_A current in CO_2-inhibited cells can antagonize AP generation (Li and Putnam, 2013) and may in part explain the observed decrease in AP discharge.

4. DISCUSSION

The current study showed that the majority of noradrenergic LC neurons in adult rats (64% in the STZ-AD group and 57% in the CTL group) were inhibited by CO_2 as indicated by a significant decrease in AP discharge to current injections. The remainder of cells either increased AP discharge (~20%) or did not respond (~20%). The STZ-AD group also had a greater sensitivity to CO_2 than controls as demonstrated by a significantly stronger inhibition of spike discharge during hypercapnia, which was in part from hyperpolarization of the RMP. Reduction of AP discharge in both groups was generally accompanied by lower LC network activity, depolarized AP threshold, increased AP repolarization, and increased current through a subpopulation of K_V channels. The latter result was indicated by enhanced transient K_V currents (strong trend in the control group and significant change in the STZ-AD group). Interestingly, steady-state K_V currents were reduced under hypercapnia, a change that would favor enhanced AP discharge. However, the collective response of most LC neurons in adult rats was inhibited by CO_2.

In the current study, STZ-AD rats had impairment in learning and retention of spatial memory when tested in the Morris water maze. These data corroborate previous studies demonstrating learning and memory deficits with brain-injection of STZ (Ebel et al., 2017; Motzko-Soares et al., 2018; Salkovic-Petrisic et al., 2013; Vicente et al., 2018) and therefore, we were able to reproduce the cognitive alterations found in patients with AD (Kumar et al., 2015; Qiu et al., 2019). It is well known that LC is involved in regulating a broad range of higher cognitive functions, such as working memory, learning and attention (Aston-Jones and Cohen, 2005; Benarroch, 2009; Mather and Harley,

Table 1
Changes of membrane resistance and resting membrane potential to hypercapnia in the STZ-AD animal model. Data are expressed as mean ± SEM. n = 8–9 rats per group.

CO_2-inhibited LC neurons		CTL	STZ-AD
Parameter	**Baseline (bsl)**	**10% CO_2**	***p***, bsl vs. CO_2
Membrane resistance (R_i) [MΩ]	116.1 ± 19.5	113.5 ± 18.7	0.693
	126.5 ± 14.9	98.4 ± 8.2	**0.006**
Resting membrane potential (RMP) [mV]	-46.4 ± 1.4	-47.7 ± 2.1	0.393
	-49.0 ± 1.6	-52.2 ± 1.7	**0.030**

Table 2
Alteration of action potential properties at baseline and increased CO2 in locus coeruleus (LC) neurons of STZ-AD rats. Data are expressed as mean ± SEM. # $p \leq .05$. n = 8–9 rats per group.

CO_2-inhibited LC neurons — CTL | STZ-AD

Parameter	Baseline (bsl)	10% CO_2	*p*, bsl vs. CO_2
Delay to first AP [ms]	15.1 ± 4.3	18.4 ± 4.0	0.164
	18.6 ± 3.7	49.5 ± 10.2#	**0.004**
AP threshold (THR) [mV]	-36.2 ± 3.1	-33.8 ± 3.4	**0.040**
	-38.7 ± 2.7	-34.8 ± 3.4	**0.010**
RMP to THR [mV]	-10.1 ± 1.9	-13.9 ± 2.4	**0.012**
	-10.3 ± 1.9	-17.4 ± 3.3	**0.003**
AP peak [mV]	50.3 ± 2.7	51.0 ± 3.5	0.589
	49.2 ± 1.9	52.2 ± 1.8	**0.038**
Max. AP rising slope [mV/ms]	276.0 ± 24.4	280.1 ± 30.0	0.692
	274.7 ± 15.7	298.9 ± 12.8	**0.049**
Max. AP falling slope [mV/ms]	-83.7 ± 8.4	-107.4 ± 12.4	**0.017**
	-92.2 ± 7.2	-118.8 ± 4.8	**0.001**
AP half-width [ms]	1.19 ± 0.16	0.92 ± 0.12	**0.015**
	1.03 ± 0.08	0.87 ± 0.06	**0.011**
Afterhyperpolarization [mV] from THR	-20.0 ± 3.0	-21.9 ± 2.7	0.142
	-17.4 ± 2.6	-19.1 ± 3.5	0.304

#, vs. CTL

2016; Robbins, 1984), as well as memory consolidation and retrieval (Sara, 2009; Sterpenich et al., 2006). We have previously observed an increase of amyloid beta peptide in the LC of STZ-AD animals (Vicente et al., 2018). In fact, selective lesions of LC neurons exacerbate AD neuropathology and cognitive deficits in both amyloid-based transgenic mouse models and mouse models of tauopathy (Hammerschmidt et al., 2013; Heneka et al., 2010). Therefore, decreased cognitive function in STZ-treated rats may be related to neuronal alterations occurring in the LC–noradrenergic system.

The majority of studies analyzing LC neuron responses to CO_2 were done in neonatal rodents (Filosa et al., 2002; Oyamada et al., 1998; Ritucci et al., 2005; Stunden et al., 2001). In these studies, up to 80% of LC neurons in neonates (postnatal < 10 days) were activated/depolarized by CO_2 in the presence of synaptic blockage (i.e., neurons were intrinsically chemosensitive to CO_2). Studies in older neonates (postnatal > 10 days) showed only 20%–40% of LC neurons were activated/depolarized by hypercapnia (Gargaglioni et al., 2010; Nichols et al., 2008), indicating that the number of CO_2-activated LC neurons is dependent on the age of the animal. Although no synaptic blocker was used in the current study, meaning changes may not exclusively arise from intrinsic chemosensitivity, we also found a low number of activated LC neurons (up to 21%) in 8-9 week old rats (Fig. 3E and 3F). The majority of neurons (more than 57% of cells independent of group) were inhibited by CO_2 exposure as indicated by reduced current-evoked spike discharge (Fig. 4) and overall lower network activity (Fig. 5). These results, in conjunction with the above mentioned previous studies, indicate that inhibition by CO_2 may be unique to LC neurons in adult animals only. Similarly, Lopes et al. (2016) showed a hypercapnia-induced decrease in firing rate of LC neurons projecting to the commissural nucleus tractus solitarii, a brainstem area heavily involved in respiratory control. According to Imber et al. (2018), blunted CO_2-responses of LC neurons in older animals is related to a developmental increase in Ca^{2+}-activated BK channel current. Hypercapnic acidosis raised intracellular Ca^{2+} content and led to BK channel-dependent lowering of spike discharge to CO_2. This process is known as brake phenomenon and appears to be minimally active in the LC neurons of newborn rats, but develops over the first two weeks of life. The influence of such a limiting mechanism may increase with advanced age and result in a general inhibition to hypercapnia as observed in the current study. Additional changes, such as the hypercapnia-induced increase in transient K_V currents (this study), may further contribute to the developmental brake mechanism, ultimately lowering output of LC neurons in adult animals in response to CO_2.

Hypercapnic exposure significantly altered currents through K_V channels. Steady-state K^+ currents, presumably from delayed-rectifying K^+ channels (K_{DR}) (Mathie et al., 1998), were significantly reduced under CO_2 in all LC neurons in the current study. CO_2-sensitivity of K_{DR} in LC neurons has been previously reported in neonates (Filosa and Putnam, 2003; Li and Putnam, 2013). Similar to our data, these studies showed hypercapnia-induced inhibition of K_{DR} currents. A reduction in K_{DR} current likely favors excitatory responses; however, spike discharge to CO_2 was reduced in the majority of LC neurons in our study, suggesting a minor role for decreased steady-state currents at least in adult rats. Conversely, transient K^+ currents from K_A channels (Mathie et al., 1998) may play a greater role whether LC neurons increase or decrease spike discharge in response to CO_2. The strong impact of K_A on spike

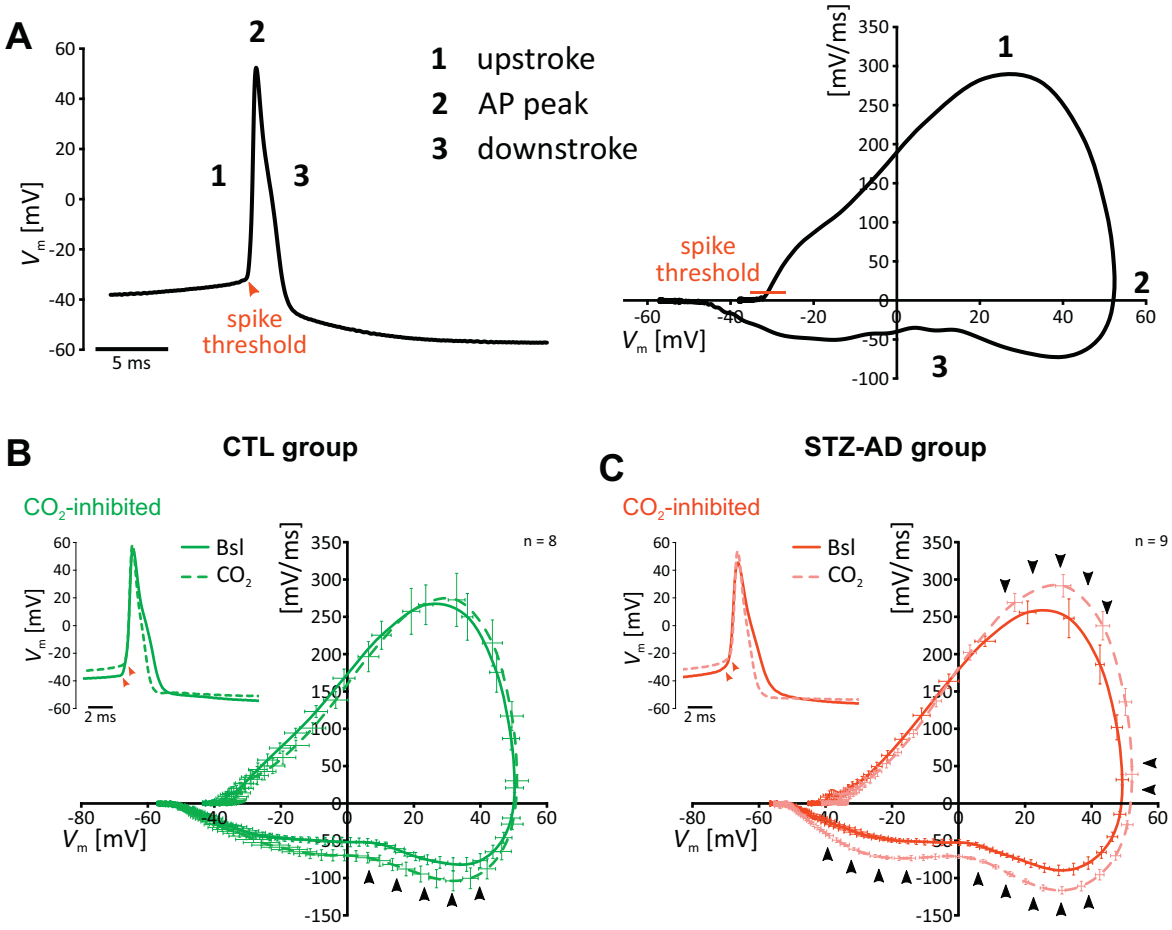

Figure 6. Action potential waveform for locus coeruleus (LC) neurons at baseline and increased CO_2.
A) Representative action potential (AP) with the corresponding phase plane plot. Phase plane plots for CO_2-inhibited LC cells in the control (CTL) group (B) and the streptozotocin-induced Alzheimer's disease (STZ-AD) group (C). Insets show a representative AP at baseline (Bsl) and increased CO_2. Red arrowheads indicate a significant change in spike threshold. Black arrowheads indicate significant changes to baseline (see Table 2).
Data are expressed as mean ± SEM. V_m = membrane potential.

discharge was previously reported in neonatal LC neurons, where blockade of K_A led to increased spike discharge (Li and Putnam, 2013). The opposite may then hold true for the response of LC cells from this study that increased K_A current and decreased AP discharge. Similarly, K_A are well known to modulate AP delay (Dekin and Getting, 1987; Schild et al., 1993). Our data on the delay of the first AP (to 100 pA current injection) is consistent with CO_2-induced modulation of K_A. However, other channels (e.g. those controlling RMP or AP threshold) may change AP delay as well (Corbin-Leftwich et al., 2018; Noble, 1966). K_A also significantly influences AP waveforms (Sonner and Stern, 2007). Blocking K_A resulted in a lower THR and widened APs from delayed repolarization. Enhanced K_A current may then lead to increased THR and reduced AP width. These changes were observed in the majority of LC neurons from the current study and suggest an important role of K_A on the activity of LC neurons during hypercapnic conditions.

Few studies address the CO_2 response of LC neurons in adult rats. Elam et al. (1981) performed extracellular recordings in single LC neurons in intact anesthetized rats (200-300 g, ~7-9 weeks of age), where CO_2 was supplied through the inspired gas mixture. That study reported increased activity of LC neurons in response to hypercapnia, but there was no information about the percentage of cells that responded to activation with CO_2. Similar to our current-evoked AP discharge, increased activation of LC neurons may resemble external inputs that drive neuronal activity of LC neurons to CO_2. In intact animals, such input may stem from other chemosensitive brain regions like the retrotrapezoid nucleus, medullary raphe, and commissural nucleus tractus solitarii (Lopes et al., 2016; Putnam et al., 2004). Thus, whether CO_2 modulates or attenuates spike discharge in LC cannot be concluded from experiments with intact connections to the LC. A study by Pineda and Aghajanian (1997) used slice preparations from adult rats (170-220 g, ~6-7 weeks) and found a depolarizing effect of CO_2 on LC neurons. Their slice thickness was 600 μm and cut in coronal orientation; these two factors allow for intact tracts/inputs coming from more ventral chemosensitive regions in the same slice (e.g., retrotrapezoid nucleus, medullary raphe). Again, in this preparation it cannot be excluded that responses of LC neurons may be driven by input from other centers. We used 250-μm thick horizontal slices containing the dorsal portion of the LC. This preparation excludes respiratory centers that are situated more rostral, ventral, and caudal from the LC and therefore resembles a highly reduced preparation that may reveal responses of LC neurons to CO_2 with very limited external drive.

A direct comparison between our groups showed that the hypercapnia-induced inhibition of LC neurons was exaggerated in the STZ-AD group (Fig. 4B). Mechanisms contributing to this stronger inhibition may be the significantly reduced RMP and associated decrease in R_i (Table 1). Potential candidates for this change are two-pore-domain (Goldstein et al., 2001) and inwardly rectifying K^+ channels (Xu et al., 2000), which have been previously shown to exhibit CO_2/pH-sensitive properties in LC neurons (Filosa and Putnam, 2003; Pineda and Aghajanian, 1997) although with different consequences for the

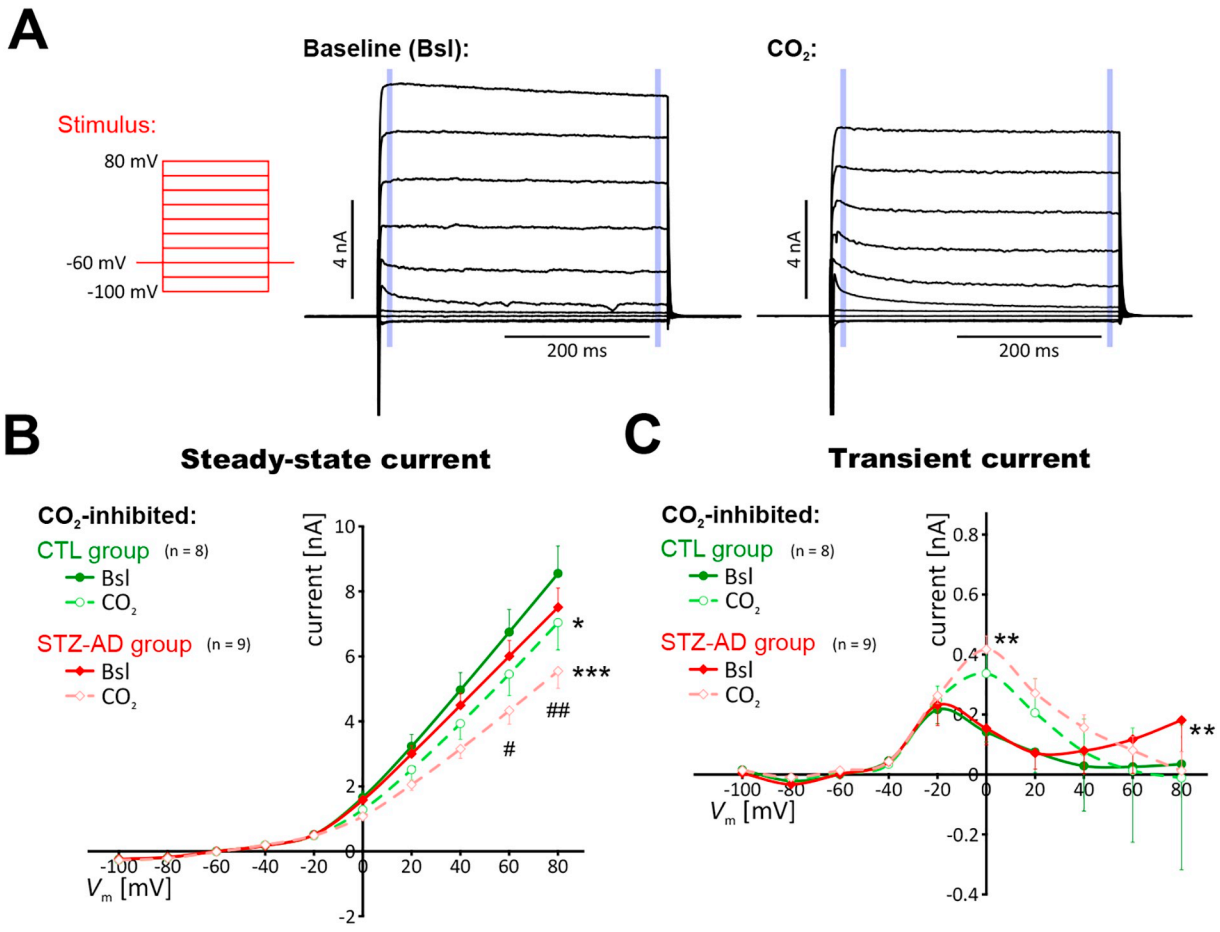

Figure 7. Current-voltage relationship for K^+ channels in locus coeruleus (LC) neurons at baseline and during 10% CO_2.
A) Typical example of currents elicited by step changes of the membrane potential from -100 mV to +80 mV (20 mV step, 400 ms) in a CO_2-inhibited LC neuron at baseline (Bsl) and CO_2. The blue lines describe the time points for measurements of the transient (beginning of stimulus) and steady-state current (end of stimulus) at each voltage step. B) Steady-state K^+ currents of cells inhibited by CO_2 in the control (CTL) and streptozotocin-induced Alzheimer's disease (STZ-AD) groups. C) Transient K^+ currents of cells inhibited by CO_2 in the CTL and STZ-AD groups.
Data are expressed as mean ± SEM. * $p \leq .05$, ** $p \leq .01$, and *** $p \leq .001$ indicated a difference from the Bsl condition. # $p \leq .05$, ## $p \leq .01$ indicated a difference between the STZ-AD and CTL groups; 2-way repeated measures ANOVA. V_m = membrane potential.

cell than observed in the current study. Hyperpolarization of RMP in conjunction with a depolarized THR significantly increased the difference from RMP to THR and, thus, the voltage required for spike generation. This difference in RMP to THR was more pronounced in the STZ-AD model than the CTL group (Table 2). Depolarized THR, reduced AP half-width, and enhanced AP repolarization under CO_2 can be attributed to the increase in K_A currents (see above). This change was significant in the STZ-AD group only (trend in the CTL group). Further, the hypercapnia-induced reduction of K_{DR} was more pronounced in the STZ-AD group than in the control group (Fig. 7B). Given the mainly inhibitory actions of CO_2, the impact of reduced K_{DR} on spike discharge seems minimal. The combined data from the current study indicates an overall increased CO_2-sensitivity of LC neurons in the STZ-AD group, a change that ultimately led to pronounced inhibition of the LC during hypercapnic conditions. We also found a significant increase in AP peak and rising slope. These results (and potentially the changes to THR) may arise from altered voltage-gated Na^+ channels (Ghovanloo et al., 2018); however, specific involvement in the CO_2-response of LC neurons has not yet been reported.

Although responses of LC neurons in the control and STZ-AD groups differed considerably during hypercapnic conditions, baseline responses were similar between groups. These results agree with our previously published in vivo study about respiratory response to high CO_2 conditions (Vicente et al., 2018). In that study, the STZ-AD group had no changes in basal ventilation, but the ventilatory reflex to hypercapnia was significantly stronger than in the control group. Thus, the respiratory response of the STZ-AD rat model to CO_2 exhibited a higher sensitivity to CO_2, which is similar to the responses of LC neurons in the current study. Changes in respiratory function were also correlated with increased amyloid beta protein in the LC region. It has been previously shown that AD modulates K^+ channel expression in humans (Angulo et al., 2004). Amyloid beta also alters currents through K_A, K_{DR}, and voltage-gated Na^+ channels in cortical and hippocampal tissue of AD animal models (Chen, 2005; Pan et al., 2004; Verret et al., 2012; Yu et al., 1998). Although some results from these studies are inconsistent (possibly from tissue-specific effects), it is likely that amyloid beta in the STZ-AD rat model affects the function of K^+ and Na^+ channels in the LC. Furthermore, ion imbalance (increased $[Na^+]$ and $[K^+]$) was shown in the cerebrospinal fluid of AD patients (Vitvitsky et al., 2012). Increased extracellular $[Na^+]$ could also account for the observed increase in AP rising slope and peak in the current study.

Previous studies of AD patients and AD animal models have mainly concentrated on the cortex and hippocampus. AD patients have also been shown to exhibit a high prevalence of breathing problems (Boeve, 2008; Gaig and Iranzo, 2012; Lee et al., 2019; Osorio et al., 2014), but currently there is no information on changes of neuronal activity associated with respiratory dysfunction in AD. To our knowledge, our

study reports the first data on neuronal changes in the LC of the brainstem with abnormal response properties under respiratory stress conditions in an animal model for sporadic AD. We did not observe any changes in LC neuron number in the STZ-AD group, suggesting we were analyzing an early stage of the disease as shown in human patients with successive loss of LC neurons in the course of AD (Kelly et al., 2017; Theofilas et al., 2017). This finding also indicates that AD-induced changes of LC output are not necessarily due to lower neuron number; they may rather be the result of altered intrinsic neuronal properties.

In summary, our study shows that the responses of LC neurons to CO_2 in the STZ-induced model for sporadic Alzheimer's disease is enhanced and potentially involves AD-induced changes in voltage-gated K^+ and Na^+ channels. The exaggerated inhibitory response of the LC to hypercapnia may be an underlying mechanism for the breathing disturbances observed in patients with AD.

AUTHOR CONTRIBUTIONS

MCV, LHGB, and TDO designed the study. MCV performed all experiments. MCV and CMH prepared and analyzed immunohistochemical data. MCV and TDO analyzed the data, prepared figures, and drafted the manuscript. MCV, LHGB, and TDO interpreted the data and edited the manuscript. All authors approved the final manuscript version.

ACKNOWLEDGEMENTS

We thank Dr. D. S. Middlemas (A.T. Still University) for provision of his microscope, Jeong Sook Kim-Han (A.T. Still University) for her help and expertise using the confocal microscope in the university's imaging core, and Deborah Goggin (A.T. Still University) for improving the grammar of the manuscript. This work was supported with the FAPESP stipend 2017/21750-9 to MCV and seed money from A.T. Still University's Kirksville College of Osteopathic Medicine to TDO.

REFERENCES

Andrés-Benito, P., Fernández-Dueñas, V., Carmona, M., Escobar, L.A., Torrejón-Escribano, B., Aso, E., Ciruela, F., Ferrer, I., 2017. Locus coeruleus at asymptomatic early and middle Braak stages of neurofibrillary tangle pathology. Neuropathol. Appl. Neurobiol. 43, 373–392. https://doi.org/10.1111/nan.12386.

Angulo, E., Noé, V., Casadó, V., Mallol, J., Gomez-Isla, T., Lluis, C., Ferrer, I., Ciudad, C.J., Franco, R., 2004. Up-regulation of the Kv3.4 potassium channel subunit in early stages of Alzheimer's disease. J. Neurochem. 91, 547–557. https://doi.org/10.1111/j.1471-4159.2004.02771.x.

Arendt, T., Brückner, M.K., Morawski, M., Jäger, C., Gertz, H.J., 2015. Early neurone loss in Alzheimer's disease: Cortical or subcortical? Acta Neuropathol. Commun. 3, 10. https://doi.org/10.1186/s40478-015-0187-1.

Aston-Jones, G., Cohen, J.D., 2005. An integrative theory of locus coeruleus-norepinephrine function: Adaptive gain and optimal performance. Annu. Rev. Neurosci. 28, 403–450. https://doi.org/10.1146/annurev.neuro.28.061604.135709.

Aston-Jones, G., Waterhouse, B., 2016. Locus coeruleus: From global projection system to adaptive regulation of behavior. Brain Res. 1645, 75–78. https://doi.org/10.1016/j.brainres.2016.03.001.

Bao, J., Mahaman, Y.A.R., Liu, R., Wang, J.Z., Zhang, Z., Zhang, B., Wang, X., 2017. Sex differences in the cognitive and hippocampal effects of streptozotocin in an animal model of sporadic AD. Front. Aging Neurosci. 9, 347. https://doi.org/10.3389/fnagi.2017.00347.

Benarroch, E.E., 2009. The locus ceruleus norepinephrine system: Functional organization and potential clinical significance. Neurology 73, 1699–1704. https://doi.org/10.1212/WNL.0b013e3181c2937c.

Berridge, C.W., Waterhouse, B.D., 2003. The locus coeruleus-noradrenergic system: Modulation of behavioral state and state-dependent cognitive processes. Brain Res. Rev. 42, 33–84. https://doi.org/10.1016/S0165-0173(03)00143-7.

Biancardi, V., Bícego, K.C., Almeida, M.C., Gargaglioni, L.H., 2008. Locus coeruleus noradrenergic neurons and CO_2 drive to breathing. Pflugers Arch. Eur. J. Physiol. 455, 1119–1128. https://doi.org/10.1007/s00424-007-0338-8.

Boeve, B.F., 2008. Update on the diagnosis and management of sleep disturbances in dementia. Sleep Med. Clin. 3, 347–360. https://doi.org/10.1016/j.jsmc.2008.04.010.

Braak, H., Del Tredici, K., 2011. The pathological process underlying Alzheimer's disease in individuals under thirty. Acta Neuropathol. 121, 171–181. https://doi.org/10.1007/s00401-010-0789-4.

Bromley-Brits, K., Deng, Y., Song, W., 2011. Morris water maze test for learning and memory deficits in Alzheimer's disease model mice. J. Vis. Exp. 53, 2920. https://doi.org/10.3791/2920.

Brown, A.G., Thapa, M., Hooker 4th, J.W., Ostrowski, T.D., 2019. Impaired chemoreflex correlates with decreased c-Fos in respiratory brainstem centers of the streptozotocin-induced Alzheimer's disease rat model. Exp. Neurol. 311, 285–292. https://doi.org/10.1016/j.expneurol.2018.10.012.

Chen, C., 2005. β-amyloid increases dendritic Ca^{2+} influx by inhibiting the A-type K+ current in hippocampal CA1 pyramidal neurons. Biochem. Biophys. Res. Commun. 338, 1913–1919. https://doi.org/10.1016/j.bbrc.2005.10.169.

Corbin-Leftwich, A., Small, H.E., Robinson, H.H., Villalba-Galea, C.A., Boland, L.M., 2018. A Xenopus oocyte model system to study action potentials. J. Gen. Physiol. 150, 1583–1593. https://doi.org/10.1085/jgp.201812146.

Deak, M.C., Kirsch, D.B., 2014. Sleep-disordered breathing in neurologic conditions. Clin. Chest Med. 35, 547–556. https://doi.org/10.1016/j.ccm.2014.06.009.

Dekin, M.S., Getting, P.A., 1987. In vitro characterization of neurons in the ventral part of the nucleus tractus solitarius. II. Ionic basis for repetitive firing patterns. J. Neurophysiol. 58, 215–229. https://doi.org/10.1152/jn.1987.58.1.215.

Deng, Y., Li, B., Liu, Y., Iqbal, K., Grundke-Iqbal, I., Gong, C.X., 2009. Dysregulation of insulin signaling, glucose transporters, O-GlcNAcylation, and phosphorylation of tau and neurofilaments in the brain: Implication for Alzheimer's disease. Am. J. Pathol. 175, 2089–2098. https://doi.org/10.2353/ajpath.2009.090157.

Ebel, D.L., Torkilsen, C.G., Ostrowski, T.D., 2017. Blunted respiratory responses in the streptozotocin-induced Alzheimer's disease rat model. J. Alzheimers. Dis. 56, 1197–1211. https://doi.org/10.3233/JAD-160974.

Elam, M., Yao, T., Thorén, P., Svensson, T.H., 1981. Hypercapnia and hypoxia: chemoreceptor-mediated control of locus coeruleus neurons and splanchnic, sympathetic nerves. Brain Res. 222, 373–381. https://doi.org/10.1016/0006-8993(81)91040-4.

Filosa, J.A., Putnam, R.W., 2003. Multiple targets of chemosensitive signaling in locus coeruleus neurons: Role of K^+ and Ca^{2+} channels. Am. J. Physiol. Cell Physiol. 284, C145–155. https://doi.org/10.1152/ajpcell.00346.2002.

Filosa, J.A., Dean, J.B., Putnam, R.W., 2002. Role of intracellular and extracellular pH in the chemosensitive response of rat locus coeruleus neurones. J. Physiol. 541, 493–509. https://doi.org/10.1113/jphysiol.2001.014142.

Folch, J., Petrov, D., Ettcheto, M., Abad, S., Sánchez-López, E., García, M.L., Olloquequi, J., Beas-Zarate, C., Auladell, C., Camins, A., 2016. Current research therapeutic strategies for Alzheimer's disease treatment. Neural Plast. 2016, 8501693. https://doi.org/10.1155/2016/8501693.

Fortin, G., Champagnat, J., 1993. Spontaneous synaptic activities in rat nucleus tractus solitarius neurons in vitro: evidence for re-excitatory processing. Brain Res. 630, 125–135. https://doi.org/10.1016/0006-8993(93)990650-C.

Gaig, C., Iranzo, A., 2012. Sleep-disordered breathing in neurodegenerative diseases. Curr. Neurol. Neurosci. Rep. 12, 205–217. https://doi.org/10.1007/s11910-011-0248-1.

Gargaglioni, L.H., Hartzler, L.K., Putnam, R.W., 2010. The locus coeruleus and central chemosensitivity. Respir. Physiol. Neurobiol. 173, 264–273. https://doi.org/10.1016/j.resp.2010.04.024.

Ghovanloo, M.R., Peters, C.H., Ruben, P.C., 2018. Effects of acidosis on neuronal voltage-gated sodium channels: Nav1.1 and Nav1.3. Channels (Austin). 12, 367–377. https://doi.org/10.1080/19336950.2018.1539611.

Goldstein, S.A., Bockenhauer, D., O'Kelly, I., Zilberberg, N., 2001. Potassium leak channels and the KCNK family of two-P-domain subunits. Nat. Rev. Neurosci. 2, 175–184. https://doi.org/10.1038/35058574.

Grünblatt, E., Hoyer, S., Riederer, P., 2004. Gene expression profile in streptozotocin rat model for sporadic Alzheimer's disease. J. Neural Transm. (Vienna) 111, 367–386. https://doi.org/10.1007/s00702-003-0030-x.

Grzanna, R., Molliver, M.E., 1980. The locus coeruleus in the rat: An immunohistochemical delineation. Neuroscience 5, 21–40. https://doi.org/10.1016/0306-4522(80)90068-8.

Gudes, S., Barkai, O., Caspi, Y., Katz, B., Lev, S., Binshtok, A.M., 2015. The role of slow and persistent TTX-resistant sodium currents in acute tumor necrosis factor- α-mediated increase in nociceptors excitability. J. Neurophysiol. 113, 601–619. https://doi.org/10.1152/jn.00652.2014.

Hammerschmidt, T., Kummer, M.P., Terwel, D., Martinez, A., Gorji, A., Pape, H.-C., Rommelfanger, K.S., Schroeder, J.P., Stoll, M., Schultze, J., Weinshenker, D., Heneka, M.T., 2013. Selective loss of noradrenaline exacerbates early cognitive dysfunction and synaptic deficits in APP/PS1 mice. Biol. Psychiatry 73, 454–463. https://doi.org/10.1016/j.biopsych.2012.06.013.

Heneka, M.T., Nadrigny, F., Regen, T., Martinez-Hernandez, A., Dumitrescu-Ozimek, L., Terwel, D., Jardanhazi-Kurutz, D., Walter, J., Kirchhoff, F., Hanisch, U.-K., Kummer, M.P., 2010. Locus ceruleus controls Alzheimer's disease pathology by modulating microglial functions through norepinephrine. Proc. Natl. Acad. Sci. U. S. A. 107, 6058–6063. https://doi.org/10.1073/pnas.0909586107.

Hilaire, G., Viemari, J.C., Coulon, P., Simonneau, M., Bévengut, M., 2004. Modulation of the respiratory rhythm generator by the pontine noradrenergic A5 and A6 groups in rodents. Respir. Physiol 143, 187–197. Neurobiol. https://doi.org/10.1016/j.resp.2004.04.016.

Imber, A.N., Patrone, L.G.A., Li, K.Y., Gargaglioni, L.H., Putnam, R.W., 2018. The role of Ca^{2+} and BK channels of locus coeruleus (LC) neurons as a brake to the CO_2 chemosensitivity response of rats. Neuroscience. 381, 59–78. https://doi.org/10.1016/j.neuroscience.2018.03.031.

Ingelsson, M., Fukumoto, H., Newell, K.L., Growdon, J.H., Hedley-Whyte, E.T., Frosch, M.P., Albert, M.S., Hyman, B.T., Irizarry, M.C., 2004. Early Abeta accumulation and progressive synaptic loss, gliosis, and tangle formation in AD brain. Neurology. 62, 925–931. https://doi.org/10.1212/01.wnl.0000115115.98960.37.

Jenerick, H., 1963. Phase plane trajectories of the muscle spike potential. Biophys. J. 3, 363–377. https://doi.org/10.1016/S0006-3495(63)86827-7.

Johnson, S.M., Haxhiu, M.A., Richerson, G.B., 2008. GFP-expressing locus ceruleus

neurons from Prp57 transgenic mice exhibit CO_2/H^+ responses in primary cell culture. J. Appl. Physiol. 105, 1301–1311. https://doi.org/10.1152/japplphysiol.90414.2008.
Johnston, J., Forsythe, I.D., Kopp-Scheinpflug, C., 2010. Going native: Voltage-gated potassium channels controlling neuronal excitability. J. Physiol. 588, 3187–3200. https://doi.org/10.1113/jphysiol.2010.191973.
Kelly, S.C., He, B., Perez, S.E., Ginsberg, S.D., Mufson, E.J., Counts, S.E., 2017. Locus coeruleus cellular and molecular pathology during the progression of Alzheimer's disease. Acta Neuropathol. Commun. 5, 8. https://doi.org/10.1186/s40478-017-0411-2.
Kline, D.D., King, T.L., Austgen, J.R., Heesch, C.M., Hasser, E.M., 2010. Sensory afferent and hypoxia-mediated activation of nucleus tractus solitarius neurons that project to the rostral ventrolateral medulla. Neuroscience 167, 510–527. https://doi.org/10.1016/j.neuroscience.2010.02.012.
Knezovic, A., Osmanovic-Barilar, J., Curlin, M., Hof, P.R., Simic, G., Riederer, P., Salkovic-Petrisic, M., 2015. Staging of cognitive deficits and neuropathological and ultrastructural changes in streptozotocin-induced rat model of Alzheimer's disease. J. Neural Transm. (Vienna) 122, 577–592. https://doi.org/10.1007/s00702-015-1394-4.
Kumar, A., Singh, A., Ekavali, 2015. A review on Alzheimer's disease pathophysiology and its management: An update. Pharmacol. Rep. 67, 195–203. https://doi.org/10.1016/j.pharep.2014.09.004.
Lannert, H., Hoyer, S., 1998. Intracerebroventricular administration of streptozotocin causes long-term diminutions in learning and memory abilities and in cerebral energy metabolism in adult rats. Behav. Neurosci. 112, 1199–1208. https://doi.org/10.1037/0735-7044.112.5.1199.
Lee, J.E., Yang, S.W., Ju, Y.J., Ki, S.K., Chun, K.H., 2019. Sleep-disordered breathing and Alzheimer's disease: A nationwide cohort study. Psychiatry Res. 273, 624–630. https://doi.org/10.1016/j.psychres.2019.01.086.
Leng, Y., McEvoy, C.T., Allen, I.E., Yaffe, K., 2017. Association of sleep-disordered breathing with cognitive function and risk of cognitive impairment: A systematic review and meta-analysis. JAMA Neurol. 74, 1237–1245. https://doi.org/10.1001/jamaneurol.2017.2180.
Li, K.Y., Putnam, R.W., 2013. Transient outwardly rectifying AA currents are involved in the firing rate response to altered CO_2 in chemosensitive locus coeruleus neurons from neonatal rats. Am. J. Physiol. Regul. Integr. Comp. Physiol. 305, R780–792. https://doi.org/10.1152/ajpregu.00029.2013.
Liguori, C., Mercuri, N.B., Izzi, F., Romigi, A., Cordella, A., Sancesario, G., Placidi, F., 2017. Obstructive sleep apnea is associated with early but possibly modifiable Alzheimer's disease biomarkers changes. Sleep 40, zsx011. https://doi.org/10.1093/sleep/zsx011.
Lopes, L.T., Patrone, L.G.A., Li, K.Y., Imber, A.N., Graham, C.D., Gargaglioni, L.H., Putnam, R.W., 2016. Anatomical and functional connections between the locus coeruleus and the nucleus tractus solitarius in neonatal rats. Neuroscience 324, 446–468. https://doi.org/10.1016/j.neuroscience.2016.03.036.
Lyness, S.A., Zarow, C., Chui, H.C., 2003. Neuron loss in key cholinergic and aminergic nuclei in Alzheimer disease: a meta-analysis. Neurobiol. Aging 24, 1–23. https://doi.org/10.1016/s0197-4580(02)00057-x.
Mather, M., Harley, C.W., 2016. The Locus coeruleus: EEssential for Maintaining Cognitive Function and the Aging Brain. Trends Cogn. Sci. 20, 214–226. https://doi.org/10.1016/j.tics.2016.01.001.
Mathie, A., Wooltorton, J.R.A., Watkins, C.S., 1998. Voltage-activated potassium channels in mammalian neurons and their block by novel pharmacological agents. Gen. Pharmacol. 30, 13–24. https://doi.org/10.1016/S0306-3623(97)00034-7.
Matthews, K.L., Chen, C.P.L.H., Esiri, M.M., Keene, J., Minger, S.L., Francis, P.T., 2002. Noradrenergic changes, aggressive behavior, and cognition in patients with dementia. Biol. Psychiatry 51, 407–416. https://doi.org/10.1016/S0006-3223(01)01235-5.
Milton, N.G.N., 2004. Role of Hydrogen Peroxide in the aetiology of Alzheimer's Disease Implications for Treatment. Drugs Aging 21, 81–100. https://doi.org/10.2165/00002512-200421020-00002.
Motzko-Soares, A.C.P., Vizin, R.C.L., Martins, T.M.S., Hungaro, A.R.O., Sato, J.R., Almeida, M.C., Carrettiero, D.C., 2018. Thermoregulatory profile of neurodegeneration-induced dementia of the Alzheimer's type using intracerebroventricular streptozotocin in rats. Acta Physiol. (Oxf). 224, e13084. https://doi.org/10.1111/apha.13084.
Nichols, N.L., Hartzler, L.K., Conrad, S.C., Dean, J.B., Putnam, R.W., 2008. Intrinsic chemosensitivity of individual nucleus tractus solitarius (NTS) and locus coeruleus (LC) neurons from neonatal rats. Adv. Exp. Med. Biol. 605, 348–352. https://doi.org/10.1007/978-0-387-73693-8_61.
Noble, D., 1966. Applications of Hodgkin-Huxley equations to excitable tissues. Physiol. Rev. 46, 1–50. https://doi.org/10.1152/physrev.1966.46.1.1.
Osorio, R.S., Ayappa, I., Mantua, J., Gumb, T., Varga, A., Mooney, A.M., Burschtin, O.E., Taxin, Z., During, E., Spector, N., Biagioni, M., Pirraglia, E., Lau, H., Zetterberg, H., Blennow, K., Lu, S.E., Mosconi, L., Glodzik, L., Rapoport, D.M., de Leon, M.J., 2014. The interaction between sleep-disordered breathing and apolipoprotein E genotype on cerebrospinal fluid biomarkers for Alzheimer's disease in cognitively normal elderly individuals. Neurobiol. Aging. 35, 1318–1324. https://doi.org/10.1016/j.neurobiolaging.2013.12.030.
Ostrowski, T.D., Hasser, E.M., Heesch, C.M., Kline, D.D., 2014a. H_2O_2 induces delayed hyperexcitability in nucleus tractus solitarii neurons. Neuroscience 262, 53–69. https://doi.org/10.1016/j.neuroscience.2013.12.055.
Ostrowski, T.D., Ostrowski, D., Hasser, E.M., Kline, D.D., 2014b. Depressed GABA and glutamate synaptic signaling by 5-HT1A receptors in the nucleus tractus solitarii and their role in cardiorespiratory function. J. Neurophysiol. 111, 2493–2504. https://doi.org/10.1152/jn.00764.2013.
Oyamada, Y., Ballantyne, D., Mückenhoff, K., Scheid, P., 1998. Respiration-modulated membrane potential and chemosensitivity of locus coeruleus neurones in the in vitro brainstem-spinal cord of the neonatal rat. J. Physiol. 513, 381–398. https://doi.org/10.1111/j.1469-7793.1998.381bb.x.
Pamphlett, R., Kum Jew, S., 2015. Different populations of human locus ceruleus neurons contain heavy metals or hyperphosphorylated tau: implications for amyloid-β and tau pathology in Alzheimer's disease. J. Alzheimers. Dis. 45, 437–447. https://doi.org/10.3233/JAD-142445.
Pan, Y., Xu, X., Tong, X., Wang, X., 2004. Messenger RNA and protein expression analysis of voltage-gated potassium channels in the brain of $A\beta_{25-35}$-treated rats. J. Neurosci. Res. 77, 94–99. https://doi.org/10.1002/jnr.20134.
Paxinos, G., Watson, C., 2007. The Rat Brain in Stereotaxic Coordinates, sixth ed. Elsevier Academic Press, Cambridge, Massachusetts.
Peterson, A.C., Li, C.R., 2018. Noradrenergic dysfunction in Alzheimer's and Parkinson's diseases: An overview of imaging studies. Front. Aging Neurosci. 10, 127. https://doi.org/10.3389/fnagi.2018.00127.
Pineda, J., Aghajanian, G.K., 1997. Carbon dioxide regulates the tonic activity of locus coeruleus neurons by modulating a proton- and polyamine-sensitive inward rectifier potassium current. Neuroscience 77, 723–743. https://doi.org/10.1016/S0306-4522(96)00485-X.
Putnam, R.W., Filosa, J.A., Ritucci, N.A., 2004. Cellular mechanisms involved in CO_2 and acid signaling in chemosensitive neurons. Am. J. Physiol. Cell Physiol. 287, C1493–1526. https://doi.org/10.1152/ajpcell.00282.2004.
Qiu, Y., Jacobs, D.M., Messer, K., Salmon, D.P., Feldman, H.H., 2019. Cognitive heterogeneity in probable Alzheimer disease: CClinical and neuropathologic features. Neurology 93, e778–e790. https://doi.org/10.1212/WNL.0000000000007967.
Rai, S., Kamat, P.K., Nath, C., Shukla, R., 2014. Glial activation and post-synaptic neurotoxicity: The key events in Streptozotocin (ICV) induced memory impairment in rats. Pharmacol. Biochem. Behav. 117, 104–117. https://doi.org/10.1016/j.pbb.2013.11.035.
Ritucci, N.A., Dean, J.B., Putnam, R.W., 2005. Somatic vs. dendritic responses to hypercapnia in chemosensitive locus coeruleus neurons from neonatal rats. Am. J. Physiol. Cell Physiol. 289, C1094–1104. https://doi.org/10.1152/ajpcell.00329.2004.
Robbins, T.W., 1984. Cortical noradrenaline, attention and arousal. Psychol. Med. 14, 13–21. https://doi.org/10.1017/s0033291700003032.
Salkovic-Petrisic, M., Knezovic, A., Hoyer, S., Riederer, P., 2013. What have we learned from the streptozotocin-induced animal model of sporadic Alzheimer's disease, about the therapeutic strategies in Alzheimer's research. J. Neural Transm. (Vienna) 120, 233–252. https://doi.org/10.1007/s00702-012-0877-9.
Sara, S.J., 2009. The locus coeruleus and noradrenergic modulation of cognition. Nat. Rev. Neurosci. 10, 211–223. https://doi.org/10.1038/nrn2573.
Sato, N., Morishita, R., 2015. The roles of lipid and glucose metabolism in modulation of β-amyloid, tau, and neurodegeneration in the pathogenesis of Alzheimer disease. Front. Aging Neurosci. 7, 1–9. https://doi.org/10.3389/fnagi.2015.00199.
Schild, J.H., Khushalani, S., Clark, J.W., Andresen, M.C., Kunze, D.L., Yang, M., 1993. An ionic current model for neurons in the rat medial nucleus tractus solitarii receiving sensory afferent input. J. Physiol. 469, 341–363. https://doi.org/10.1113/jphysiol.1993.sp019817.
Serra, L., D'Amelio, M., Di Domenico, C., Dipasquale, O., Marra, C., Mercuri, N.B., Caltagirone, C., Cercignani, M., Bozzali, M., 2018. In vivo mapping of brainstem nuclei functional connectivity disruption in Alzheimer's disease. Neurobiol. Aging 72, 72–82. https://doi.org/10.1016/j.neurobiolaging.2018.08.012.
Šimić, G., Babić Leko, M., Wray, S., Harrington, C.R., Delalle, I., Jovanov-Milošević, N., Bažadona, D., Buée, L., de Silva, R., Di Giovanni, G., Wischik, C.M., Hof, P.R., 2017. Monoaminergic neuropathology in Alzheimer's disease. Prog. Neurobiol. 151, 101–138. https://doi.org/10.1016/j.pneurobio.2016.04.001.
Smith, J.C., Abdala, A.P.L., Borgmann, A., Rybak, I.A., Paton, J.F.R., 2013. Brainstem respiratory networks: building blocks and microcircuits. Trends Neurosci. 36, 152–162. https://doi.org/10.1016/j.tins.2012.11.004.
Sonner, P.M., Stern, J.E., 2007. Functional role of A-type potassium currents in rat presympathetic PVN neurones. J. Physiol. 582, 1219–1238. https://doi.org/10.1113/jphysiol.2007.134379.
Sterpenich, V., D'Argembeau, A., Desseilles, M., Balteau, E., Albouy, G., Vandewalle, G., Degueldre, C., Luxen, A., Collette, F., Maquet, P., 2006. The locus ceruleus is involved in the successful retrieval of emotional memories in humans. J. Neurosci. 26, 7416–7423. https://doi.org/10.1523/JNEUROSCI.1001-06.2006.
Stunden, C.E., Filosa, J.A., Garcia, A.J., Dean, J.B., Putnam, R.W., 2001. Development of in vivo ventilatory and single chemosensitive neuron responses to hypercapnia in rats. Respir. Physiol. 127, 135–155. https://doi.org/10.1016/S0034-5687(01)00242-0.
Thal, D.R., Rüb, U., Orantes, M., Braak, H., 2002. Phases of Aβ-deposition in the human brain and its relevance for the development of AD. Neurology. 58, 1791–1800. https://doi.org/10.1212/WNL.58.12.1791.
Theofilas, P., Ehrenberg, A.J., Dunlop, S., Di Lorenzo Alho, A.T., Nguy, A., Leite, R.E.P., Rodriguez, R.D., Mejia, M.B., Suemoto, C.K., Ferretti-Rebustini, R.E.L., Polichiso, L., Nascimento, C.F., Seeley, W.W., Nitrini, R., Pasqualucci, C.A., Jacob Filho, W., Rueb, U., Neuhaus, J., Heinsen, H., Grinberg, L.T., 2017. Locus coeruleus volume and cell population changes during Alzheimer's disease progression: A stereological study in human postmortem brains with potential implication for early-stage biomarker discovery. Alzheimers Dement. 13, 236–246. https://doi.org/10.1016/j.jalz.2016.06.2362.
Ting, J.T., Daigle, T.L., Chen, Q., Feng, G., 2014. Acute brain slice methods for adult and aging animals: application of targeted patch clamp analysis and optogenetics. Methods Mol. Biol. 1183, 221–242. https://doi.org/10.1007/978-1-4939-1096-0_14.
Ting, J.T., Lee, B.R., Chong, P., Soler-Llavina, G., Cobbs, C., Koch, C., Zeng, H., Lein, E.,

2018. Preparation of acute brain slices using an optimized N-methyl-D-glucamine protective recovery method. J. Vis. Exp. 132, 53825. https://doi.org/10.3791/53825.

Tota, S., Awasthi, H., Kamat, P.K., Nath, C., Hanif, K., 2010. Protective effect of quercetin against intracerebral streptozotocin induced reduction in cerebral blood flow and impairment of memory in mice. Behav. Brain Res. 209, 73–79. https://doi.org/10.1016/j.bbr.2010.01.017.

Verret, L., Mann, E.O., Hang, G.B., Barth, A.M.I., Cobos, I., Ho, K., Devidze, N., Masliah, E., Kreitzer, A.C., Mody, I., Mucke, L., Palop, J.J., 2012. Inhibitory interneuron deficit links altered network activity and cognitive dysfunction in Alzheimer model. Cell. 149, 708–721. https://doi.org/10.1016/j.cell.2012.02.046.

Vicente, M.C., Dias, M.B., Fonseca, E.M., Bícego, K.C., Gargaglioni, L.H., 2016. Orexinergic system in the locus coeruleus modulates the CO_2 ventilatory response. Pflugers Arch. Eur. J. Physiol. 468, 763–774. https://doi.org/10.1007/s00424-016-1793-x.

Vicente, M.C., Almeida, M.C., Bícego, K.C., Carrettiero, D.C., Gargaglioni, L.H., 2018. Hypercapnic and hypoxic respiratory response during wakefulness and sleep in a streptozotocin model of Alzheimer's disease in rats. J. Alzheimers. Dis. 65, 1159–1174. https://doi.org/10.3233/JAD-180397.

Vitvitsky, V.M., Garg, S.K., Keep, R.F., Albin, R.L., Banerjee, R., 2012. Na + and K + ion imbalances in Alzheimer's disease. Biochim. Biophys. Acta. 1822, 1671–1681. https://doi.org/10.1016/j.bbadis.2012.07.004.

Wilson, R.S., Segawa, E., Boyle, P.A., Anagnos, S.E., Hizel, L.P., Bennett, D.A., 2012. The natural history of cognitive decline in Alzheimer's disease. Psychol. Aging 27, 1008–1017. https://doi.org/10.1037/a0029857.

Wilson, R.S., Nag, S., Boyle, P.A., Hizel, L.P., Yu, L., Buchman, A.S., Schneider, J.A., Bennett, D.A., 2013. Neural reserve, neuronal density in the locus ceruleus, and cognitive decline. Neurology. 80, 1202–1208. https://doi.org/10.1212/WNL.0b013e3182897103.

Xu, H., Cui, N., Yang, Z., Qu, Z., Jiang, C., 2000. Modulation of kir4.1 and kir5.1 by hypercapnia and intracellular acidosis. J. Physiol. 524, 725–735. https://doi.org/10.1111/j.1469-7793.2000.00725.x.

Yaffe, K., Laffan, A.M., Harrison, S.L., Redline, S., Spira, A.P., Ensrud, K.E., Ancoli-Israel, S., Stone, K.L., 2011. Sleep-disordered breathing, hypoxia, and risk of mild cognitive impairment and dementia in older women. JAMA 306, 613–619. https://doi.org/10.1001/jama.2011.1115.

Yu, S.P., Farhangrazi, Z.S., Ying, H.S., Yeh, C.H., Choi, D.W., 1998. Enhancement of outward potassium current may participate in β-amyloid peptide-induced cortical neuronal death. Neurobiol. Dis. 5, 81–88. https://doi.org/10.1006/nbdi.1998.0186.

Zarow, C., Lyness, S.A., Mortimer, J.A., Chui, H.C., 2003. Neuronal loss is greater in the locus coeruleus than nucleus basalis and substantia nigra in Alzheimer and Parkinson diseases. Arch. Neurol. 60, 337–341. https://doi.org/10.1001/archneur.60.3.337.

Zhang, Z.-G., Li, Y., Ng, C.T., Song, Y.-Q., 2015. Inflammation in Alzheimer's Disease and Molecular Genetics: RRecent Update. Arch. Immunol. Ther. Exp. (Warsz) 63, 333–344. https://doi.org/10.1007/s00005-015-0351-0.